

UNIVERSITÄT  
BAYREUTH

**The role of retinoic acid  
in the development of  
pelvic fins in *Danio rerio***

Doctoral Thesis

submitted to obtain the academic degree of Doctor of Natural Sciences

(Dr. rer. nat.)

of the Bayreuth Graduate School of Mathematical and Natural Sciences

(BayNAT)

of the University of Bayreuth

**Heidrun Draut**

from Pegnitz

Bayreuth, 2020

This doctoral thesis was prepared at the department of Developmental Biology at the University of Bayreuth from 07.2016 until 11.2020 and was supervised by Prof. Dr. Gerrit Begemann.

This is a full reprint of the thesis submitted to obtain the academic degree of Doctor of Natural Sciences (Dr. rer. nat.) and approved by the Bayreuth Graduate School of Mathematical and Natural Sciences (BayNAT) of the University of Bayreuth.

Date of submission: 26.11.2020

Date of approval: 07.12.2020

Date of defence: 08.04.2021

Acting director: Prof. Dr. Markus Lippitz

Doctoral committee:

Prof. Dr. Gerrit Begemann	(reviewer)
Prof. Dr. Stefan Schuster	(reviewer)
Prof. Dr. Andreas Möglich	(chairman)
Prof. Dr. Stefan Heidmann	

## Summary

The molecular mechanisms that control the development of paired extremities are broadly conserved among vertebrate species. The paired fins of fish - pectoral and pelvic fins - are homologous to the fore- and hindlimbs of land vertebrates. Consequently, a fundamental knowledge about signalling processes in zebrafish paired fin development might help to understand limb patterning and congenital limb defects in humans. All-trans-retinoic acid (RA) is a key factor in many developmental processes including limb development. The current model for forelimb development was predominantly determined from studies in mice (Cunningham et al., 2013; Mic et al., 2002, 2004; Sandell et al., 2007; Zhao et al., 2009), chicken (Nishimoto et al., 2015) and zebrafish (Begemann et al., 2001; Gibert et al., 2006; Grandel & Brand, 2011; Grandel et al., 2002). It suggests an antagonism between RA and fibroblast growth factors (FGFs) along the anteroposterior axis, which mediates the correct positioning of the limb field and establishes a permissive environment for the induction of limb budding (Cunningham et al., 2013; Zhao et al., 2009). Moreover, RA cooperatively interacts with  $\beta$ -catenin signalling and *Hox* genes to control *Tbx5* expression during forelimb development in chicks (Nishimoto et al., 2015). Examinations in zebrafish agree with the requirement of RA for pectoral fin induction (Gibert et al., 2006). For hindlimb development, however, the roles of RA are still controversial. The idea of a similar role for RA in fore- and hindlimb development (Nishimoto et al., 2015) contrasts with the opinion that RA is dispensable for hindlimb development (Zhao et al., 2009). In the zebrafish model, comparable studies investigating the role of RA on pelvic fin development are missing, which is why this thesis focused on this particular question.

Gene expression analysis on zebrafish larvae revealed the presence of *Rdh10a*, *Aldh1a2*, *Cyp26b1* and *Cyp26c1* transcripts during the early stages of pelvic fin bud formation. The expression pattern of these genes, which are involved in RA synthesis and metabolism, indicated the establishment of an anteroposterior RA gradient in the early pelvic fin bud. Later, activity of RA signalling associated genes was detected along the forming fin rays. Based on heat-shock treatments of transgenic *Hsp70l:Cyp26a1* zebrafish larvae, overexpression of *Cyp26a1* and thus a reduction of the RA level was achieved during pelvic fin formation. From the obtained results an important role of RA in the development of pelvic fins during early stages of fin bud formation was concluded. A complete inhibition of

the formation of endo- and exoskeletal pelvic fin structures could be achieved if the heat-shock treatment was started before the first signs of a morphological fin bud appeared. After the onset of fin bud formation, *Cyp26a1* overexpression resulted in the reduction of the overall length of the pelvic girdle accompanied by the lack of diverse skeletal elements, mostly the posterior process and the radials. These results indicate a putative role of RA in the pelvic fin initiation process, which seems to occur during a limited time frame. Moreover, they suggest a role of RA in pelvic girdle patterning and chondrogenesis. Additionally, a participation in fin ray formation and growth is likely. However, since the entire organism is affected in these experiments, unspecific effects cannot be ruled out. Therefore, the main focus of this work was to establish the binary Gal4-UAS system with the aim to manipulate RA signalling in a spatially and temporally controlled manner. On the one hand, driver lines provide the expression of either a hormone- or light-inducible Gal4 variant under the control of tissue-specific enhancers. Here, three Gal4 variations - ERT2-Gal4-VP16, KalTA4-ERT2 and GAVPO (Akerberg et al., 2014; Distel et al., 2009; Gerety et al., 2013; Kajita et al., 2014; Wang et al., 2012) - were investigated and considered suitable for the use in zebrafish. Tissue-specificity was achieved by selecting enhancers of the genes *Prrx1a*, *Prrx1b* and *Pitx1*, which are active specifically in pectoral and/or pelvic fins (Chan et al., 2010; Hernández-Vega & Minguillón, 2011). On the other hand, effector lines express genes encoding either a dominant-negative retinoic acid receptor (*dnRara2a*) (Stafford et al., 2006) or the RA metabolizing enzyme *Cyp26a1* under the control of five repetitive (5x) or four non-repetitive (4xnr) upstream activating sequences (UAS) (Akitake et al., 2011; Goll et al., 2009). Driver and effector constructs are equipped with minimal Tol2 *cis* sequences mediating transgene integration into the genome by Tol2 transposase activity. Moreover, different marker genes facilitate the identification of single or multiple transgenic zebrafish. As a proof-of-principle, the activation of *dnRara2a* expression in F3 embryos of *5xUAS:dnRara2a-IRES-eGFP* zebrafish by injection of *KalTA4-ERT2-GI* mRNA, followed by induction with 4-hydroxy-tamoxifen (4-OHT) was demonstrated. Altogether, the basis for a valuable genetic tool was created, that combines several advantages: a simple and practical application, a simplified screening process, the visualisation of transgene activity and the optimization for the zebrafish model organism.

## Zusammenfassung

Die molekularen Mechanismen, welche die Entwicklung von paarigen Extremitäten kontrollieren, sind unter Vertebraten weitreichend konserviert. Die paarigen Flossen von Fischen - die Brust- und Bauchflossen - sind homolog zu den vorderen und hinteren Extremitäten von Landwirbeltieren. Demnach kann ein fundiertes Wissen über die ablaufenden Signalwege während der Entwicklung paariger Flossen im Zebrafisch möglicherweise Aufschluss geben über angeborene Defekte der Extremitäten beim Menschen. Das aktuelle Modell zur Entwicklung von Extremitäten basiert überwiegend auf Studien an Mäusen (Cunningham et al., 2013; Mic et al., 2002, 2004; Sandell et al., 2007; Zhao et al., 2009), Hühnern (Nishimoto et al., 2015) und Zebrafischen (Begemann et al., 2001; Gibert et al., 2006; Grandel & Brand, 2011; Grandel et al., 2002). Es beschreibt unter anderem einen Antagonismus zwischen Retinsäure und Fibroblasten-Wachstumsfaktoren entlang der anteroposterioren Achse, welcher die Positionierung der Extremität festlegt und die Voraussetzung für die Induktion der Extremitäten-Knospe schafft (Cunningham et al., 2013; Zhao et al., 2009). Zur Aktivierung der *Tbx5*-Expression in Hühnern, interagiert Retinsäure zudem in kooperativer Art und Weise mit Komponenten des  $\beta$ -Catenin Signalweges sowie mit *Hox* Genen (Nishimoto et al., 2015). Untersuchungen an Embryonen des Zebrafisches deuten ebenfalls auf eine Funktion von Retinsäure bei der frühen Induktion der Brustflosse hin (Gibert et al., 2006). In Bezug auf die Entwicklung der hinteren Extremitäten sind die Funktionen von Retinsäure bisher noch widersprüchlich. Hierbei steht die Idee einer ähnlichen Rolle von Retinsäure in vorderen und hinteren Extremitäten (Nishimoto et al., 2015) der Meinung gegenüber, dass Retinsäure für die Entwicklung hinterer Gliedmaßen nicht notwendig ist (Zhao et al., 2009). Vergleichbare Studien im Zebrafisch fehlen in diesem Zusammenhang noch, weshalb sich diese Arbeit auf die Aufklärung ebendieser Fragestellung fokussiert.

Eine Analyse der Genexpression von *Rdh10a*, *Aldh1a2*, *Cyp26b1* und *Cyp26c1* an Larven des Zebrafisches bestätigte die Aktivität dieser Gene, welche Teil der Retinsäure-Synthese sowie ihres Metabolismus sind, während der frühen Entwicklung der Bauchflosse. Ihr Expressionsmuster deutet auf die Bildung eines anteroposterioren Retinsäure-Gradienten in den frühen Stadien der Flossenknospe hin. Später wurde die Aktivität von Genen des Retinsäure-Signalweges entlang der sich bildenden Flossenstrahlen nachgewiesen.

Ausgehend von Hitzebehandlungen transgener *Hsp70l:Cyp26a1* Larven des Zebraärblings wurde während der Bauchflossenentwicklung eine Überexpression von *Cyp26a1* und damit eine Verringerung des Retinsäure-Pegels hervorgerufen. Aus den erhaltenen Ergebnissen wurde eine wichtige Rolle von Retinsäure während der Bauchflossenentwicklung abgeleitet. Die Bildung von Elementen des Endo- und Exo-Skelettes konnte bei Beginn der Hitzebehandlung vor dem Auftreten erster morphologischer Anzeichen einer Bauchflossenknospe vollständig unterdrückt werden. Nach dem Einsetzen der Flossenknospenbildung führte die Überexpression von *Cyp26a1* zu einer Verringerung der Gesamtlänge des Beckengürtels sowie zum Verschwinden verschiedener Skelettelemente, wobei hier in erster Linie die posterioren Prozesse und die Radiale betroffen waren. Diese Ergebnisse deuten auf eine Rolle von Retinsäure beim Initiierungsprozess der Bauchflossen hin, welche scheinbar auf einen eng limitierten Zeitrahmen beschränkt ist. Weiterhin legen sie eine Rolle bei der Strukturierung des Beckengürtels sowie der Chondrogenese nahe. Eine Beteiligung von Retinsäure an der Formierung und dem Wachstum der Flossenstrahlen ist ebenfalls wahrscheinlich. Da diese Experimente aber den gesamten Organismus betreffen, können unspezifische Effekte nicht ausgeschlossen werden.

Der Schwerpunkt dieser Arbeit lag daher auf der Etablierung des binären Gal4-UAS Systems mit dem Ziel, eine räumlich und zeitlich gesteuerte Manipulation des Retinsäure-Signalweges zu ermöglichen. Hierbei dienen die Treiber-Linien der Expression von hormon- oder light-induzierbaren Gal4-Varianten, welche unter der Kontrolle von gewebe-spezifischen regulatorischen Elementen erfolgt. In diesem Zusammenhang wurden drei verschiedene Gal4-Varianten - ERT2-Gal4-VP16, KalTA4-ERT2 und GAVPO (Akerberg et al., 2014; Distel et al., 2009; Gerety et al., 2013; Kajita et al., 2014; Wang et al., 2012) - getestet und für das Modellsystem Zebraärbling als geeignet eingestuft. Die Gewebespezifität wurde durch die Wahl von regulatorischen Elementen der Gene *Prrx1a*, *Prrx1b* und *Pitx1* ermöglicht, welche spezifisch in Brust- und/oder Bauchflossen aktiv sind (Chan et al., 2010; Hernández-Vega & Minguillón, 2011). Die Effektor-Linien sind für die Expression von Genen verantwortlich, welche den Retinsäure-Signalweg inhibieren. Diese kodieren entweder für eine dominant-negative Version des Retinsäure-Rezeptors *Rarα2a* (*dnRarα2a*) (Stafford et al., 2006) oder *Cyp26a1*. Ihre Expression wird durch fünf repetitive (5x) oder vier nicht-repetitive (4xnr) vorgeschaltete Aktivator-Sequenzen (UAS) gesteuert (Akitake et al., 2011; Goll et al., 2009). Treiber- und Effektor-Linien sind mit Tol2 *cis* Sequenzen ausgestattet,

anhand derer aktive Tol2 Transposase die Integration des Transgens in das Genom ermöglicht. Zudem erleichtern verschiedene Marker-Gene die Identifizierung einfach oder mehrfach transgener Zebrabärblinge. Zur Bestätigung des Funktionsprinzips wurde die Aktivierung der *dnRara2a*-Expression in F3-Embryonen der Linie *5xUAS:dnRara2a-IRES-eGFP*, nach Injektion von *KalTA4-ERT2-GI*-mRNA und anschließender Induktion mit 4-Hydroxytamoxifen (4-OHT), demonstriert. Insgesamt wurde somit die Basis für ein wertvolles genetisches Werkzeug geschaffen, welches mehrere Vorteile ineinander vereint: eine einfache und praktische Anwendung, eine vereinfachte Identifizierung von transgenen Nachkommen, die Visualisierung der Transgenaktivität sowie die Optimierung für das Modellsystem Zebrabärbling.

## Table of contents

Summary .....	3
Zusammenfassung .....	5
Table of contents .....	8
<b>1 Introduction.....</b>	<b>12</b>
1.1 The retinoic acid pathway and its key functions in development.....	12
1.2 <i>Danio rerio</i> as a model organism in developmental biology.....	17
1.3 The development of paired fins in zebrafish with focus on pelvic fins.....	18
1.3.1 Anatomical description .....	18
1.3.2 Molecular processes .....	20
1.3.2.1 Positioning.....	21
1.3.2.2 Induction and initiation .....	23
1.3.2.3 Outgrowth .....	28
1.3.2.4 The role of RA in the development of paired fins/limbs .....	30
1.4 Molecular systems for the genetic manipulation of zebrafish.....	32
1.4.1 The Tol2-Transposon system .....	32
1.4.2 The Gal4-UAS system.....	34
1.4.3 The CRISPR/Cas9 system .....	38
1.5 Previous results on the role of RA in pelvic fin development .....	40
1.6 Goal of this study .....	47
<b>2 Results .....</b>	<b>49</b>
2.1 Gene expression in the pelvic fin bud during early development.....	49
2.2 Manipulation of the retinoic acid pathway during pelvic fin development .....	54
2.2.1 Overexpression of <i>Cyp26a1</i> using a transgenic zebrafish line.....	54
2.2.2 Analysis of the expression pattern in the pelvic fin bud after <i>Cyp26a1</i> overexpression	62
2.3 Establishment of the Gal4-UAS system in zebrafish .....	63
2.3.1 Establishment of UAS effector lines to manipulate RA signalling.....	63
2.3.1.1 <i>5xUAS:Cyp26a1-eGFP</i> .....	64
2.3.1.2 <i>5xUAS:dnRara2a-IRES-eGFP</i> .....	68
2.3.1.3 Variations of UAS sequences, reporter genes and fusion constructs.....	70
2.3.2 Evaluation of fin specific enhancers and establishment of reporter lines.....	77
2.3.2.1 <i>Tbx4</i> enhancers .....	78
2.3.2.2 <i>Pitx1</i> enhancers .....	79
2.3.2.3 <i>Prrx1</i> enhancers.....	81
2.3.3 Establishment of ERT2-Gal4 driver lines.....	84
2.3.3.1 <i>Pel2.5kb:ERT2-Gal4</i> .....	85
2.3.3.2 <i>Prrx1:ERT2-Gal4</i> .....	87

---

2.3.4	Functionality tests of driver plasmids containing Gal4 derivatives .....	89
2.3.4.1	KalTA4.....	90
2.3.4.2	GAVPO .....	95
2.3.5	Crossing driver and effector lines to manipulate retinoic acid signalling .....	98
<b>2.4</b>	<b>Creation and testing of dnRar<math>\alpha</math>2a/ERT2 fusion constructs .....</b>	<b>101</b>
<b>2.5</b>	<b>Establishment of a <i>Pitx1</i> Knock-out line using the CRISPR/Cas9 system .....</b>	<b>106</b>
2.5.1	Design of sgRNAs .....	106
2.5.2	Functionality tests of sgRNAs .....	108
2.5.2.1	CRISPR Somatic Tissue Activity Test (CRISPR-STAT) .....	109
2.5.2.2	Tracking of Indels by DEcomposition (TIDE) .....	111
2.5.2.3	T7 Endonuclease 1 Assay.....	113
2.5.3	Identification of F0 founder fish .....	115
2.5.4	Identification of heterozygous F1 fish .....	115
2.5.5	Identification of homozygous F2 fish.....	118
<b>3</b>	<b>Discussion .....</b>	<b>121</b>
<b>3.1</b>	<b>Signalling pathways in the early zebrafish pelvic fin bud .....</b>	<b>121</b>
3.1.1	General overview.....	121
3.1.2	Fgf signalling .....	122
3.1.3	RA signalling.....	126
<b>3.2</b>	<b>The role of RA in zebrafish pelvic fin development .....</b>	<b>130</b>
<b>3.3</b>	<b>Prospects and limitations of the Gal4-UAS system .....</b>	<b>134</b>
3.3.1	Prospects .....	135
3.3.2	Limitations .....	137
<b>3.4</b>	<b>Establishment of a zebrafish <i>Pitx1</i> knockout mutant .....</b>	<b>140</b>
<b>4</b>	<b>Material and Methods .....</b>	<b>143</b>
<b>4.1</b>	<b>Material.....</b>	<b>143</b>
4.1.1	Hard- and Software.....	143
4.1.2	Chemicals and reagents.....	143
4.1.3	Buffers and solutions .....	144
4.1.4	Plasmids.....	145
4.1.5	DNA oligonucleotides .....	151
4.1.6	RNA antisense probes.....	157
4.1.7	Single-guided RNAs (sgRNAs).....	159
<b>4.2</b>	<b>Molecular biological methods .....</b>	<b>159</b>
4.2.1	Polymerase chain reaction (PCR).....	159
4.2.2	PCR purification .....	160
4.2.3	Restriction digest.....	160

---

4.2.4	Dephosphorylation .....	161
4.2.5	Ligation .....	162
4.2.6	Gibson Assembly.....	163
4.2.7	Aqua Cloning.....	163
4.2.8	Agarose gel electrophoresis .....	164
4.2.9	Capillary electrophoresis .....	164
4.2.10	Isolation of plasmid DNA from <i>E. coli</i> .....	164
4.2.11	Measurement of DNA/RNA concentration.....	164
4.2.12	Extraction of genomic DNA.....	165
4.2.13	T7 Endonuclease 1 Assay.....	165
4.2.14	Sequencing .....	166
4.2.15	Synthesis of sgRNA .....	166
4.2.16	<i>In vitro</i> transcription of mRNA.....	168
4.2.17	Synthesis of cDNA.....	169
4.2.18	<i>In vitro</i> transcription of DIG-labelled RNA antisense probes .....	170
4.2.19	Whole-mount <i>in situ</i> Hybridisation (WISH) .....	171
4.2.20	Fluorescent immunostaining .....	172
<b>4.3</b>	<b>Microbiological methods.....</b>	<b>173</b>
4.3.1	<i>E. coli</i> strains .....	173
4.3.2	Cultivation and storage of <i>E. coli</i> .....	173
4.3.3	Transformation of <i>E. coli</i> .....	174
4.3.4	Preparation of chemical competent cells .....	174
<b>4.4</b>	<b>Zebrafish techniques.....</b>	<b>175</b>
4.4.1	Maintenance.....	175
4.4.2	Zebrafish strains .....	175
4.4.3	Mating fish and collection of eggs .....	176
4.4.4	Microinjection of zebrafish eggs.....	176
4.4.5	Chemical fixation of zebrafish .....	177
4.4.6	Sorting of zebrafish based on their pelvic fin developmental stage.....	177
4.4.7	Heat-shock treatment of zebrafish.....	177
4.4.8	Pharmacological treatment of zebrafish .....	178
4.4.9	Anesthetization of zebrafish .....	178
4.4.10	Fin clips of adult zebrafish .....	179
4.4.11	Skeletal staining.....	179
4.4.12	Microscopy of zebrafish.....	180
<b>5</b>	<b>Literature.....</b>	<b>181</b>

<b>6</b>	<b>List of abbreviations.....</b>	<b>199</b>
<b>7</b>	<b>Supplementary data.....</b>	<b>204</b>
<b>8</b>	<b>Acknowledgements.....</b>	<b>233</b>
<b>9</b>	<b>(Eidesstattliche) Versicherung und Erklärung .....</b>	<b>235</b>

# 1 Introduction

## 1.1 The retinoic acid pathway and its key functions in development

All-*trans*-retinoic acid (RA) has been identified as the biologically active form of vitamin A more than 70 years ago (Arens & van Dorp, 1946c, 1946b, 1946a). The small, lipophilic molecule, consisting of a  $\beta$ -ionone ring and a polyene hydrocarbon chain, is functioning as a diffusible morphogen and is a key player in vertebrate embryonic development (Dubey, et al., 2018; Thaller & Eichele, 1987) (Fig. 1A). It is crucial that RA acts in exactly the right places and in the appropriate concentration, which is why a precise regulation of RA signalling is indispensable. During critical developmental stages, vitamin A deficiency (VAD) (Maden et al., 1996; Wilson et al., 1953) as well as an excess of vitamin A have teratogenic effects and cause a wide range of malformations, for example in the facial region, the eyes, inner ear, heart, lungs and the forelimbs (Kam et al., 2012; Niederreither & Dollé, 2008; Rhinn & Dollé, 2012).

The uptake of RA into the body occurs with the diet in the form of retinol (ROL, vitamin A), retinyl esters or carotenoids that are found in animal sources and in diverse vegetables and fruits (Fig. 1A). RA itself is only found in very low concentrations or even in traces in animal or plant sources, respectively. The *de novo* synthesis of retinoids and carotenoids is only possible in plants and certain microorganisms (Asson-Batres & Rochette-Egly, 2016; IARC Handbooks of Cancer Prevention, 1998; Rhinn & Dollé, 2012).

In the organism, RA storage takes place as ROL or retinyl esters in the liver. To mobilize it, ROL is bound by retinol binding protein 4 (Rbp4), which mediates the transport to the target tissues. In birds and mammals, holo-Rbp additionally forms a complex with transthyretin (TTR) to stabilize the complex and to prevent degradation of retinol by the kidney (Bellovino et al., 2003; Rhinn & Dollé, 2012). Holo-Rbp then binds to the membrane-bound receptor protein Stra6, which catalyses the release of retinol into the cytoplasm where it is complexed by cellular retinoid binding proteins (Crpb) (Kawaguchi et al., 2007; Kawaguchi et al., 2015) (Fig. 1B). During early development, a mammalian embryo is provided with maternal ROL and in case of birds or fish, the embryo draws it from the supply of the yolk (Niederreither & Dollé, 2008).

Subsequently, ROL is oxidized to RA in two sequential steps. The first, reversible step is catalysed by alcohol dehydrogenases (Adh) or retinol dehydrogenases (Rdh), mainly Rdh10, and produces retinaldehyde (retinal, RAL) (Fig. 1). Interestingly, studies in mice suggest that the main function of Adhs might not be the participation in RA synthesis but the removal of excess ROL (Molotkov et al., 2002). In contrast to that, Rdh10 is essential for RA synthesis and embryonic development. Knockout of *Rdh10* in mice results in severe defects, which are for example reduced forelimbs, impaired organogenesis and facial malformations, especially concerning the eyes and the nose (Rhinn et al., 2011; Sandell et al., 2007). In the second step, RAL is irreversibly oxidized to RA by retinaldehyde dehydrogenases (Raldh1-3, also known as Aldh1a1-a3). The main RA producing enzyme in embryonic development is Aldh1a2. The mouse knockout mutant for *Aldh1a2* dies at mid-gestation and shows a truncation of the body axis, defects in the hindbrain, the heart and other organs as well as absence of limb buds (Niederreither et al., 1999; Rhinn & Dollé, 2012). The zebrafish *Aldh1a2* loss-of-function mutant *neckless (nls)* shows similar defects. The larvae survive for a maximum of 4-6 days post fertilization (dpf) and fail to form the hindbrain, neural crest cells and pectoral fins (Begemann et al., 2001).

Apart from the synthesis, the regulation of the RA level occurs via metabolism, degradation and excretion of RA. RA is converted to more polar compounds by the enzymes Cyp26a1/b1/c1 from the cytochrome P450 family. Cyp26 enzymes are heme-containing 4-hydroxylases, modifying RA at the C-4 or C-18 of the  $\beta$ -ionone ring, to create 4- and 18-hydroxy-RA. Further conversion by oxidoreductases results in the production of 4-oxo-RA or 5,6-epoxy-RA (Fig. 1). For the latter, some bioactivity similar to RA was shown in VAD quails and *Xenopus* embryos. However, the fast degradation of these metabolites is believed to prevent their action in RA signalling under normal circumstances (Chithalen et al., 2002; Dubey et al., 2018; Pijnappel et al., 1993; Reijntjes et al., 2005). *In vitro*, Cyp26a1 shows the highest catalytic efficiency, indicating that this might be the major RA metabolizing enzyme (Lutz et al., 2009). All three *Cyp26* genes are conserved among species and show a differential expression during embryonic development, with *Cyp26a1* being extensively expressed in the tailbud of both mouse and zebrafish embryos and *Cyp26b1* particularly in the distal limb bud mesenchyme (Yashiro et al., 2004). Moreover, *Cyp26* genes show a specific expression pattern during hindbrain development (Sirbu et al., 2005). It is often observed that the expression domains of *Cyp26* genes are in the immediate vicinity of the

areas of RA synthesis. This is of major importance to establish RA gradients, which are an essential prerequisite for normal development and organogenesis (Dubey et al., 2018).

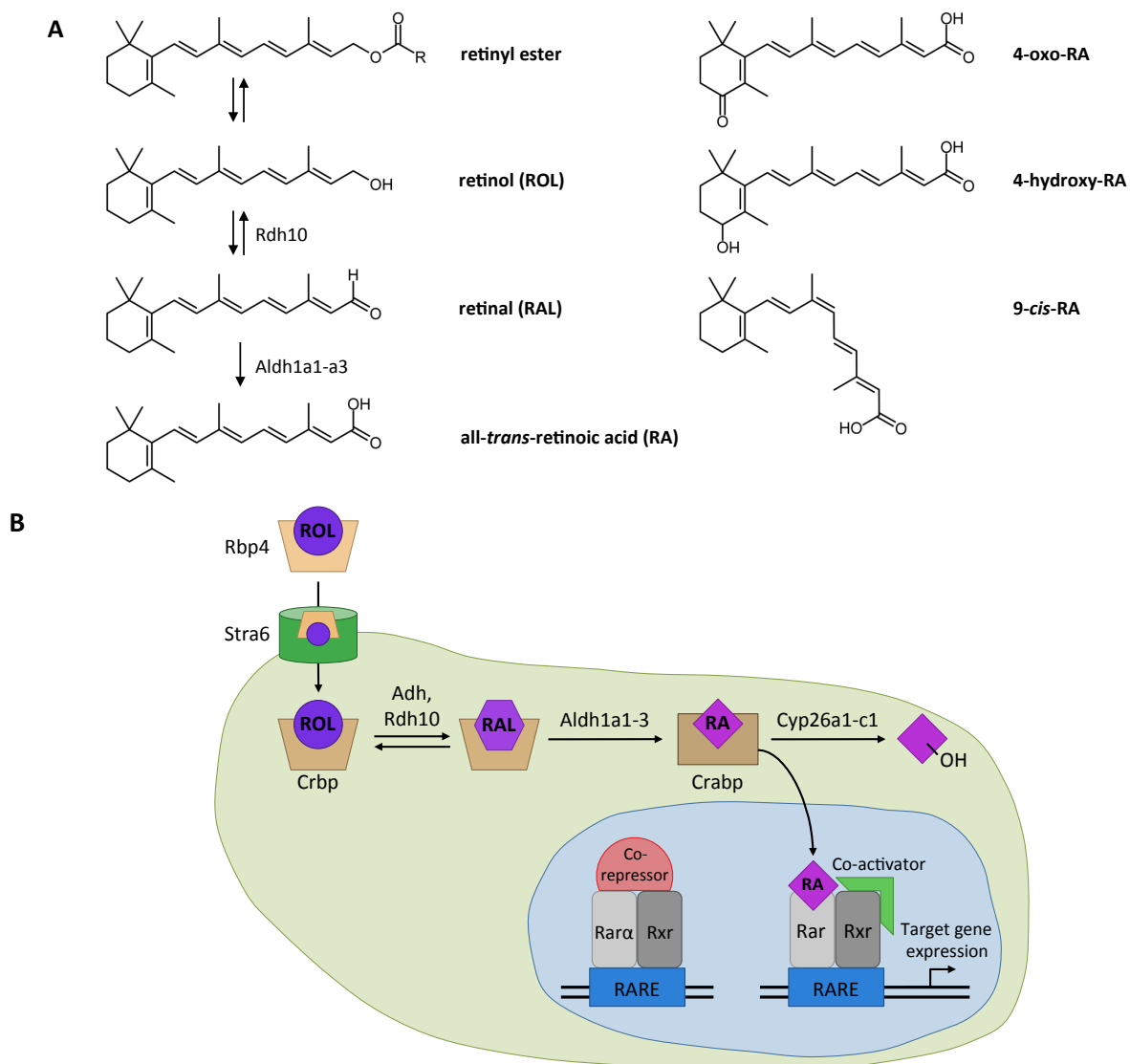


**Fig. 1 The RA signalling pathway** **A:** Chemical structures of the major retinoids relevant in the RA pathway. **B:** Schematic representation of the retinoic acid (RA) signalling pathway. Maternal or yolk derived retinol, bound to retinol binding protein 4 (Rbp4), is internalized via the receptor protein Stra6. In the cell, it is bound by a cellular Rbp (Crbp). The oxidation to RA takes place in two steps. First, retinol (ROL) is reversibly transformed to retinal (RAL) by alcohol dehydrogenases (Adh) or retinol dehydrogenases (Rdh), especially Rdh10. In the second step, catalysed by retinaldehyde dehydrogenases 1-3 (Aldh1a1-a3), RAL is irreversibly oxidized to RA. When RA enters the nucleus, it binds to its nuclear receptor, retinoic acid receptor (Rar), which forms a heterodimer with retinoid X receptor (Rxr). The heterodimeric receptor complex is bound to RA response elements (RAREs). In case of Rar $\alpha$ , it is associated with co-repressors in absence of RA, preventing target gene expression. RA binding results in dissociation of the repressive factors and the recruitment of co-activators, which in turn activate target gene expression. RA conversion into the more polar derivatives 4-hydroxy-RA and 4-oxo-RA is executed by Cyp26a1-c1. Crabbp: cellular retinoic acid binding protein. Figure inspired by Niederreither & Dollé, 2008; Rhinn & Dollé, 2012; Hauksdottir et al., 2003; Kawaguchi et al., 2015.

Further on in the RA signalling pathway, RA is transported into the nucleus, where it binds to its nuclear receptor, the retinoic acid receptor (Rar). This in turn forms a heterodimer with the retinoid X receptor (Rxr) (Fig. 1B). There are three receptor isoforms each, which are Rar $\alpha$ , Rar $\beta$ , Rar $\gamma$  and Rxr $\alpha$ , Rxr $\beta$ , Rxr $\gamma$ , respectively. Each of them is highly conserved throughout vertebrate species and shows a differential expression pattern during development, indicating individual functions for each receptor isoform (Dollé, 2009). All Rars have a high affinity for all-*trans*-RA, but can also be activated by the stereoisomer 9-*cis*-RA (Fig. 1A). In contrast to that, Rxrs exclusively bind 9-*cis*-RA, which is however barely detected in the living organism (Bourguet et al., 2000; Chambon, 1996; Mic et al., 2003). Both, Rars and Rxrs exhibit a modular structure, consisting of six conserved regions referred to as A - F with the DNA binding domain being located in region C (Chambon, 1996; Rochette-Egly & Germain, 2009) (Fig. 2B). The heterodimeric Rar/Rxr complex is bound to specific regions of the DNA, called RA response elements (RAREs). This binding occurs even in the absence of RA (Duester, 2008; Rhinn & Dollé, 2012) (Fig. 1B). Whether downstream-located target genes are actively transcribed or kept inactive is, at least in case of Rar $\alpha$ , depending on the C-terminal helix 12 (H12) with its ligand dependent transcription activation function and the C-terminal F domain. In absence of RA, H12 is in a protruding position that is stabilized by the F domain (Farboud & Privalsky, 2004). In this form, Rar $\alpha$  exposes a hydrophobic pocket, formed by the helices 3 and 4 (H3, H4), to which co-repressors like SMRT and N-CoR can attach. The co-repressors then block the docking surface of H12 thus inhibiting its interaction with co-activators (Fig. 2A). The binding of RA causes a conformational change in the receptor that results in the repositioning of H12, which subsequently caps the ligand-binding pocket (LBP) and in this way stabilizes the ligand-bound state. Dissociation of repressive factors follows and H3, H4 and H12, which are now located in close proximity, generate a new interaction interface that triggers the recruitment of co-activators (Fig. 2A). This finally leads to the transcription of corresponding target genes (Bourguet et al., 2000; Egea et al., 2001; Renaud et al., 1995; Rochette-Egly & Germain, 2009; Steinmetz et al., 2001). In contrast to that, Rar $\beta$  and Rar $\gamma$  are able to activate modest target gene transcription also in the absence of RA and show barely any interaction with co-repressors. The reasons for this phenomenon are differences in the amino acid sequence of H3. It is assumed that there is a constant interaction of H3 and H12 in these receptor subtypes,

which enables co-activator recruitment even in a ligand-free surrounding (Farboud & Privalsky, 2004; Hauksdottir et al., 2003; Privalsky, 2004).

As most components of the RA signalling pathway, Rars and Rxrs are highly conserved throughout vertebrates. Each receptor-encoding gene shows an individual expression pattern during development that is either widespread ( $Rar\alpha$ ,  $Rxr\alpha$ ,  $Rxr\beta$ ) or locally restricted to defined cells or tissues ( $Rar\beta$ ,  $Rary$ ,  $Rxry$ ) (Dollé, 2009). Prominent target genes of Rars are among others *Cyp26a1-c1*. The fact that RA up-regulates genes that are responsible for its own metabolism ensures the equilibrium between RA synthesis and degradation, which is essential for the control of this signalling pathway.

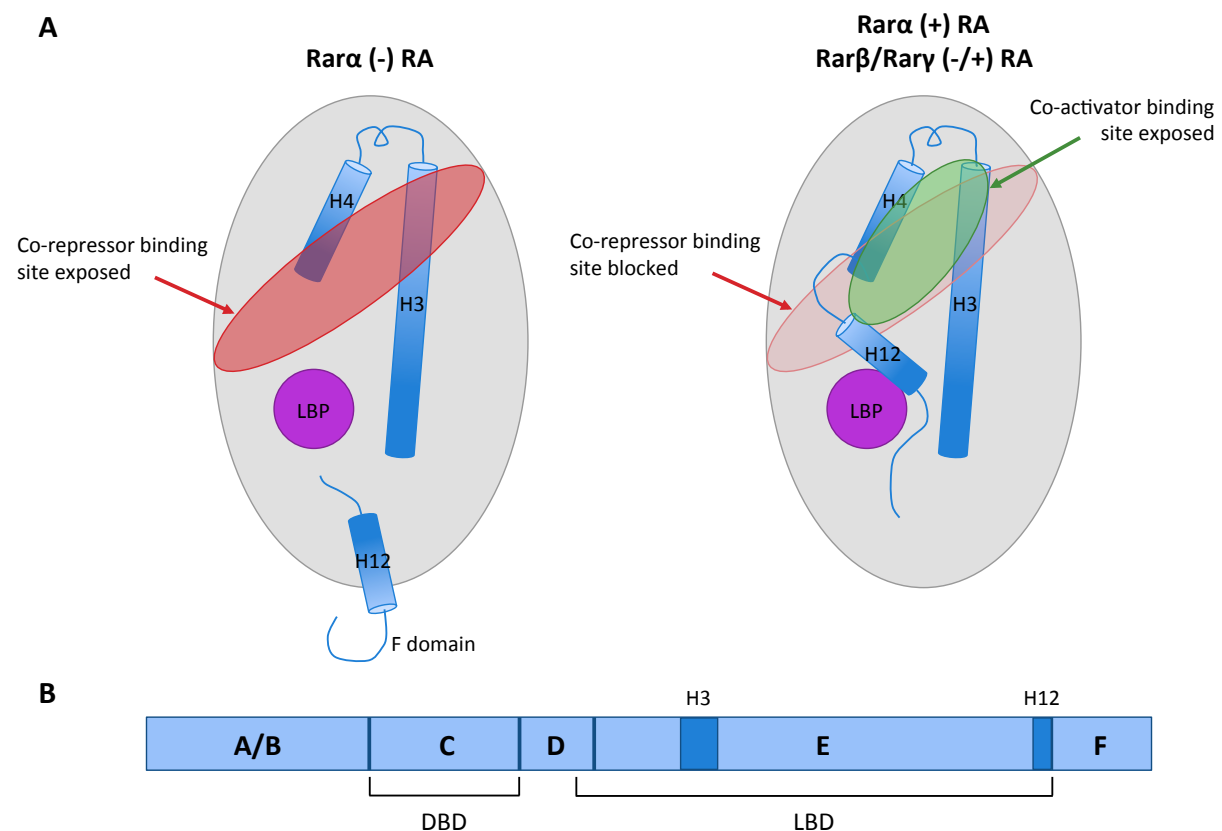


**Fig. 2 Mechanism of Rar mediated target gene repression and activation.** **A:** Model showing the structural alternations in  $Rar\alpha$  upon ligand binding. In absence of RA, the helix 12 (H12) protrudes from the rest of the protein, exposing the free hydrophobic ligand-binding pocket (LBP). At the same time, H3 and H4 create an interaction site recognized by co-repressors. RA binding results in a conformational change, whereby H12 folds over the LBP and stabilizes the bound ligand. Moreover, H12 now locates in proximity to H3 and H4. Thus, it partially blocks the co-repressor binding site and, together with H3 and H4, creates a surface for co-activator recruitment. In case of  $Rar\beta$  and  $Rary$ , this conformation is adopted even in the absence of RA; however, the binding of RA enhances co-activator recruitment. **B:** Schematic representation of Rar or Rxr protein with subdomains A - F. The DNA binding domain (DBD) is located in subdomain C. The ligand-binding domain (LBD) stretches over domain E, with the hinge region in domain D. The position of the helices H3 and H12 is indicated in dark blue. Figure inspired by Bourguet et al., 2000; Farboud & Privalsky, 2004; Privalsky, 2004; Rochette-Egly & Germain, 2009; Steinmetz et al., 2001.

## 1.2 *Danio rerio* as a model organism in developmental biology

The zebrafish, *Danio rerio*, has been established as a powerful model organism in biological and medicinal research during the last decades. The small teleost fish of the Cyprinidae family is typically habituated in slow moving streams or still pools throughout India and its neighbouring countries like Pakistan, Nepal or Bangladesh (Engeszer et al., 2007; Parichy, 2015). In its natural environment it was first described in 1822 by the Scottish physician Francis Hamilton (Hamilton, 1822). Its career as a model organism in life science started in the mid-1960s when George Streisinger decided to investigate the embryonic development of the vertebrate nervous system. To fully understand these complex mechanisms he needed a vertebrate model system. Due to its external fertilization, fast development and transparency during early embryonic stadia, zebrafish turned out to be particularly suitable (Varga, 2018). Streisinger's motivation to concentrate his studies on mutant strains resulted in the cloning of zebrafish (Streisinger, 1984; Streisinger et al., 1981) and led to one of the first zebrafish mutagenesis screens (Kimmel, 1989; Meyers, 2018), qualifying zebrafish as a model organism for forward genetic applications. Two large scaled mutagenesis screens followed in the 1990s and brought about more than 4000 recessive mutant phenotypes that exhibit developmental defects in diverse organ systems (Driever et al., 1996; Haffter et al., 1996). The sequencing of the zebrafish genome (Howe et al., 2013) enabled the use of zebrafish not only in forward but also in reverse genetic approaches. Moreover, it revealed that 70 % of all human genes have at least one orthologue in zebrafish, making it an valuable model organism for studying human diseases (Howe et al., 2013).

Due to its excellent genetic accessibility and its various other advantages, like the high reproductive rate, relatively short generation time and the comparatively simple husbandry, the zebrafish is justifiably one of the most popular model organisms in developmental biology today.

### **1.3 The development of paired fins in zebrafish with focus on pelvic fins**

Paired appendages are a basic feature of all vertebrates. They are fore- and hindlimbs in land vertebrates and pelvic and pectoral fins in fish, respectively. Both structures, forelimbs and pectoral fins as well as hindlimbs and pelvic fins are homologous to each other. Most current knowledge on limb formation was obtained from studies on chick and mouse embryos, however, the molecular mechanisms that control the development of paired extremities are broadly conserved among vertebrate species. Only recently, the zebrafish came into focus for investigation of pectoral and, to a lesser extent, pelvic fin development.

Pectoral fin development commences very early in embryonic development, with the first signs of a fin bud appearing at 28 hours post fertilization (hpf). The pectoral fin is initially built as a larval form consisting of a single cartilaginous endoskeletal disc that undergoes a conversion to the adult form after three weeks of development (Dewit et al., 2011; Grandel & Schulte-Merker, 1998). This early outgrowth reflects the important function of pectoral fins being required for speeding up and braking during prey hunt (McClenahan et al., 2012) and also a supporting function in respiration was postulated (Green et al., 2011). In contrast to that, pelvic fin development does not begin until an age of 3 - 4 weeks post fertilization (wpf), which makes researching them more challenging and time-consuming. These fins develop their adult structure directly (Grandel & Schulte-Merker, 1998). Their function is rather passive and not as crucial as that of pectoral fins. They likely are responsible for stabilization and fine-tuning during swimming manoeuvres (Don et al., 2013; Harris, 1938) .

#### **1.3.1 Anatomical description**

The pectoral fins are located lateral of the fish's body, at the transition from the head to the trunk, while the pelvic fins are located ventrally, in the middle of the body at the level of the ninth and tenth myotome, right in front of the anus (Don et al., 2013; Grandel & Schulte-Merker, 1998). Both fin structures are build of endo- and exoskeletal parts, which will be described for the pelvic fin in more detail in the following.

In case of the pelvic fins, the endoskeletal part is referred to as pelvic girdle and consists of the anterior process, the fin base and the posterior process. The fin base designates a thickened part of the pelvic girdle that is associated with several radials and anchors the lepidotrichs (Fig. 3A-C). The posterior process is located posterior to the fin base and is joined with its counterpart on the other side via a ligament. The exoskeletal part, forming the fin, is made of the lepidotrichs with the first one being referred to as marginal ray. Their number is variable among individuals, with an average number of 7 - 8. They are embedded in the dermal fin fold, which is serving as a web for the entire fin (Grandel & Schulte-Merker, 1998) (Fig. 3A-C).

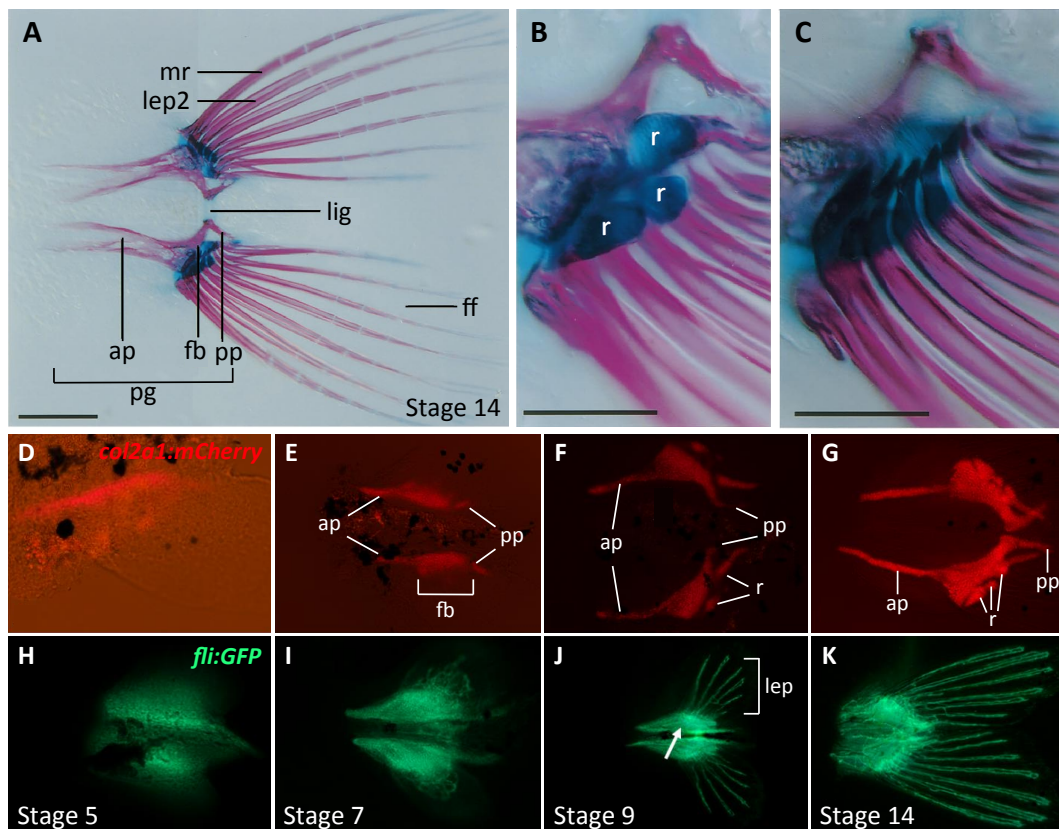


**Fig. 3 Anatomy of the pelvic girdle and fin in larval and juvenile state.** A-C: Alcian blue and alizarin red double stained pelvic girdle and fin of a 17 mm juvenile zebrafish (corresponds to Stage 14). A: Ventral overview of the pelvic girdle and fin. B: Magnification of A showing the fin base with radials in detail. C: Magnification of A showing fin base with focus on lepidotrich insertion. D-K: Dissected pelvic girdles and fins of *fli:eGFP;col2a1:mCherry* double transgenic zebrafish larvae and juveniles of pelvic fin developmental Stages 5, 7, 9 and 14. The *col2a1* marker stains chondrocytes (D-G) while the *fli* marker visualizes chondrocytes, chondrocyte precursor cells (arrows) and endothelial cells (H-K). All structures are shown with anterior to the left. mr: marginal ray; lep: lepidotrich; lig: ligament; ap: anterior process; fb: fin base; pp: posterior process; ff: fin fold; r: radial. Scale bars: A = 500  $\mu$ m, B/C = 200  $\mu$ m. Pictures taken and modified from Grandel & Schulte-Merker, 1998 (A-C) and from Marzi, 2015 (D-K).

Previously, pelvic fin outgrowth was structured in defined developmental stages, beginning at Stage 1 with no visible fin bud yet and finishing at Stage 14 with all endo- and exoskeletal structures formed (Marzi, 2015; for a more detailed description see 1.5) (Fig. 3D-K).

Fin formation begins with a thin layer of mesenchymal cells assembling in the prospective region of the pelvic fin (Stage 1-2). Upon proliferation, these are forming a clearly visible bulge termed the pelvic fin bud (Stage 2) (Grandel & Schulte-Merker, 1998). Subsequently, the ectodermal cells, covering the mesenchyme, are forming an apical thickening that edges the pelvic fin bud from anterior to posterior. Invasion of the mesenchymal cells results in the transformation of the apical endodermal thickening to the fin fold (Stage 3-4) (Grandel & Schulte-Merker, 1998). Soon after, the first endoskeletal structures arise (Fig. 3D, Stage 5), which then grow on both sides in anteroposterior direction, forming the anterior and posterior process as well as the first indications of the fin base (Fig. 3E, Stage 7). After the fin base is established, two or three radials form via condensation of chondrocytes (Fig. 3F-G, Stage 9-14) (Grandel & Schulte-Merker, 1998). Meanwhile, in the fin fold, sequential formation of lepidotrichs takes place in mediolateral direction (Fig. 3I-K, Stage 8-14). On the cellular level, this happens through a stepwise reorientation of extracellular matrix components, which first leads to the bulging of the basement membrane and later to its ossification. This way, the lepidotrichs end up completely embedded in the fin fold providing form and stability for the complete fin (Grandel & Schulte-Merker, 1998).

### **1.3.2 Molecular processes**

The visible developmental process starts with the formation of the fin buds from the lateral plate mesoderm (LPM). However, molecular settings are established much earlier in development. Generally, the underlying processes can be divided into four basic phases: positioning, induction, initiation and outgrowth (Don et al., 2013; Feneck & Logan, 2020; Nishimoto et al., 2015; Tanaka, 2013) (Fig. 4).

### 1.3.2.1 Positioning

All gnathostomes possess a particular stripe along the lateral trunk that has the competency to develop paired appendages upon receiving the appropriate signals (Yonei-Tamura et al., 2008). Within this competent stripe, the positioning of the extremities is mainly regulated by the expression of *Hox* genes in a specific, staggered pattern (Fig. 4). *Hox* genes encode homeobox transcription factors and are organized in four clusters, A-D. These reflect their sequential timing of expression and their defined expression patterns along the anteroposterior axis (Burke et al., 1995).

Functional studies in chick embryos revealed that the forelimb position is defined through *Hoxb4* expression during gastrulation (Moreau et al., 2019). In zebrafish embryos, the anterior border of the *Hoxb4* expression domain also coincides with the site of pectoral fin formation (Thisse et al., 2004). Additionally, in mouse, chick and zebrafish embryos, the forelimbs or pectoral fins align with the anterior border of the *Hoxc6* expression domain, which extents almost exactly to the middle of the developing limb or fin bud (Burke et al., 1995; Molven et al., 1990; Muto et al., 2014).

The positioning of hindlimbs or pelvic fins is defined by the expression of *Hoxb9*, *Hoxc9* and *Hoxd9* (Cohn et al., 1997; Moreau et al., 2019; Tanaka et al., 2005). These three genes are simultaneously expressed in the prospective forelimb, interlimb and hindlimb regions during early development of chick embryos. Later, *Hoxd9* withdraws from the interlimb region, while expression in fore- and hindlimb forming regions persists (Cohn et al., 1997). In three-spine sticklebacks (*Gasterosteus aculeatus*), *Hoxd9* expression appears during metamorphosis (21-25 dpf) laterally and central of the fish's body, marking the position of pelvic apparatus formation (Tanaka et al., 2005). Correspondingly, the lack of pelvic fins in puffer fish (*Takifugu rupripes*) was attributed to the missing of *Hoxd9* expression in the prospective pelvic fin region (Tanaka et al., 2005). Apart from this, a role for *Hoxc10a* in pelvic fin positioning was postulated. This was based on the fact that the cell population of the LPM that eventually will form the pelvic fin bud directly locates next to the region of *Hoxc10a* expression during somitogenesis, before the protrusion of the trunk-tail (Murata et al., 2010). The *Hox* gene expression in the pelvic fin region itself is, in turn, regulated by *Gdf11*, a member of the transforming growth factor  $\beta$  (Tgf $\beta$ ) superfamily. This was demonstrated with knockout and knockdown experiments in mice and zebrafish,

respectively, which resulted in a caudal shift of *Hoxc10* and *Hoxc11* expression domains (McPherron et al., 1999; Murata et al., 2010).

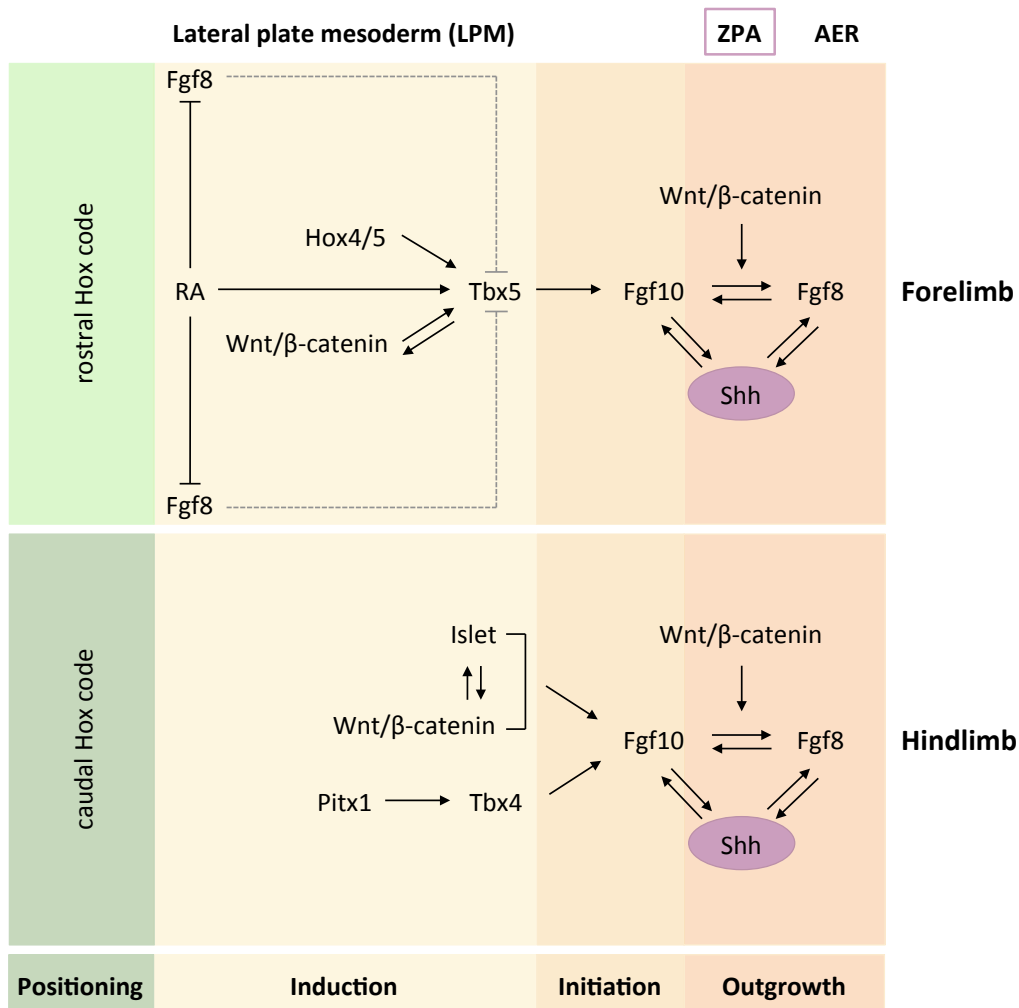


**Fig. 4 Key factors of limb development.** Schematic representation of the basic interactions regulating limb development, which is divided into four phases: positioning, induction, initiation and outgrowth. The correct positions of fore- and hindlimbs are set by several defined *Hox* genes, expressed in the lateral plate mesoderm (LPM). Afterwards, limb bud formation is induced by the homeobox transcription factors *Tbx5*, *Tbx4* and *Pitx1*. *Tbx5* is thought to be activated via a coherent feed-forward mechanism by *Hox4/5*, Wnt/ $\beta$ -catenin and RA, originating from the somites. Moreover, it was demonstrated that a negative interaction between RA and *Fgf8* keeps the limb field free of *Fgf8* expression, in this way providing a permissive environment for *Tbx5* activation. In hindlimb development, *Pitx1* directly induces *Tbx4* expression via conserved binding sites in its regulatory elements. The action of *Tbx4/5* then initiates *Fgf10* expression, which in turn activates, via Wnt/ $\beta$ -catenin signalling, *Fgf8* in the ectoderm, now preconditioned to form the apical ectodermal ridge (AER). In mice, also the factors *Islet1* and Wnt/ $\beta$ -catenin were demonstrated to be crucial for *Fgf10* initiation. A positive feedback loop between *Fgf8* and *Fgf10* maintains their expression levels, which is essential for limb outgrowth. An additional player in limb formation and patterning is *Shh*, signalling from the zone of polarizing activity (ZPA) in the most posterior margin of the limb bud, interacting with both, *Fgf8* and *Fgf10*. It must be noted that most of these mechanisms have been demonstrated in mouse or chick embryos, whereas corresponding studies in zebrafish are often lacking, particularly with regard to pelvic fins. Figure inspired by Feneck & Logan, 2020; Nishimoto et al., 2014; Nishimoto et al., 2015; Tanaka et al., 2005; Zhao et al., 2009.

### 1.3.2.2 Induction and initiation

#### Limb specification

In the next step, limb formation is initiated and the limb-type is specified. The key players in this phase are the homeobox transcription factors (TFs) *Tbx5* and *Tbx4*, which are specifically expressed in pectoral and pelvic fins, respectively, as well as the hindlimb-specific homeobox transcription factor *Pitx1* (paired-like homeodomain 1) (Fig. 4). Because of their distinct expression, *Tbx4* and *Tbx5* were thought to be responsible for specifying limb-type (Don et al., 2013; Gibson-brown et al., 2014; Ruvinsky et al., 2000; Tamura et al., 1999). However, genetic studies in mice suggest a role for *Tbx4* and *Tbx5* only in limb initiation but not in limb specification (Minguillon et al., 2005; Naiche & Papaioannou, 2007). It was demonstrated that *Tbx4* expression in *Tbx5*-depleted forelimbs compensates its function, resulting in the formation of a normal limb with forelimb-character (Minguillon et al., 2005). An unambiguously limb-specifying function was observed *Pitx1*. Upon misexpression in the forelimb field, *Pitx1* is able to influence forelimb development in a way that hindlimb characteristics are established (DeLaurier et al., 2006; Logan & Tabin, 1999; Minguillon et al., 2005). Interestingly, the compensating function of *Tbx* genes does not work the other way round as in *Pitx1* knockout mice, *Tbx4* was able to rescue most hindlimb features, while *Tbx5* was not (Ouimette et al., 2010).

#### Induction and initiation of pectoral fins/forelimbs

Diverse signalling cascades regulate the expression of *Tbx4* and *Tbx5*. Regarding *Tbx5*, Hox and Tcf/Lef (Wnt/ $\beta$ -catenin) binding sites as well as RA response elements (RAREs) were detected in a regulatory element located in its intron 2, which is conserved in amniotes (Minguillon et al., 2012; Nishimoto et al., 2014; Nishimoto et al., 2015) (Fig. 5). Moreover, a second enhancer region, referred to as CNS12sh, was discovered downstream of the *Tbx5* coding sequence showing a high conservation throughout gnathostomes (Fig. 5). Accordingly, CNS12sh from mouse and gar were successfully used to drive transgene expression in pectoral fins of zebrafish larvae. Though, no specific binding sites in CNS12sh for transcription factors or other regulatory elements were revealed so far (Adachi et al., 2016).

In accordance with this findings, one current view postulates that *Tbx5* expression is induced by three components, Hox4 and Hox5,  $\beta$ -catenin/Wnt signalling and RA that act together in a coherent feed-forward mechanism (Nishimoto et al., 2015) (Fig. 4). A prominent candidate for Wnt participation might be *Wnt2b* as it is strongly expressed in the intermediate mesoderm and LPM (Kawakami et al., 2001). Mutation of either all Hox binding sites, the RAREs or the Tcf/Lef site destroys enhancer activity and prevents *Tbx5* activation or strongly reduces it, giving evidence for the necessity of each element (Minguillon et al., 2012; Nishimoto et al., 2015). Interestingly, a recent genomic knockout study demonstrated that, upon deletion of either one or both enhancers, neither the regulatory elements in intron 2 nor CNS12sh are essential for *Tbx5* expression initiation or forelimb bud formation. This undoubtedly indicates that additional enhancers must exist that still need to be identified and functionally examined (Cunningham et al., 2018).

Once initiated, *Tbx5* acts cooperatively with RA to activate *Fgf10* expression (Agarwal, 2003; Ng et al., 2002; Nishimoto et al., 2015), which is mediated directly through a conserved *Tbx5* binding site located in the promoter region of *Fgf10* (Agarwal, 2003). Loss-of function of either *Tbx5* or *Fgf10* results in the absence of forelimbs or pectoral fins, proving the central role of both factors for forelimb or pectoral fin induction (Ng et al., 2002; Sekine et al., 1999). *Tbx5* was also shown to activate *Wnt2b*. Reverse signalling from this gene is involved in maintaining *Tbx5* and *Fgf10* expression levels to promote further limb/fin development and initiate outgrowth (Kawakami et al., 2001; Ng et al., 2002; Takeuchi et al., 2003) (Fig. 4). In a second model, an antagonism between RA and fibroblast growth factor 8 (*Fgf8*) along the anteroposterior axis that mediates the correct positioning of the limb field and establishes a permissive environment for the induction of limb budding is postulated. Hereby, RA restricts the *Fgf8* expression domains in two directions, anterior to the heart forming field and posterior to the primitive streak and epiblast, thus keeping the forelimb field free of *Fgf8* to allow *Tbx5* induction (Cunningham et al., 2013; Zhao et al., 2009) (Fig. 4). This idea is supported by the fact that a conserved RARE was detected near the *Fgf8* promoter indicating a direct regulation of *Fgf8* expression by RA (Zhao et al., 2009). Moreover, the pectoral finless phenotype of zebrafish *nls* mutants could be rescued by additional suppression of Fgf signalling. For this, *nls* fish were crossed with a strain, which expresses a dominant negative form of the Fgf receptor 1 upon heat-shock treatment (*Hsp70:dn-Fgfr1-eGFP*) (Cunningham et al., 2013). Similar antagonistic RA-Fgf-interactions

were observed for example in the patterning of the retina of chick embryos or in the regulation of body axis extension (da Silva & Cepko, 2017; Diez del Corral et al., 2003). Interestingly, in these cases, RA binding to the Rar/Rxr heterodimer results in the recruitment of repressing factors leading to the silencing of target genes (Cunningham & Duester, 2015; Kumar & Duester, 2014; Studer et al., 1994).

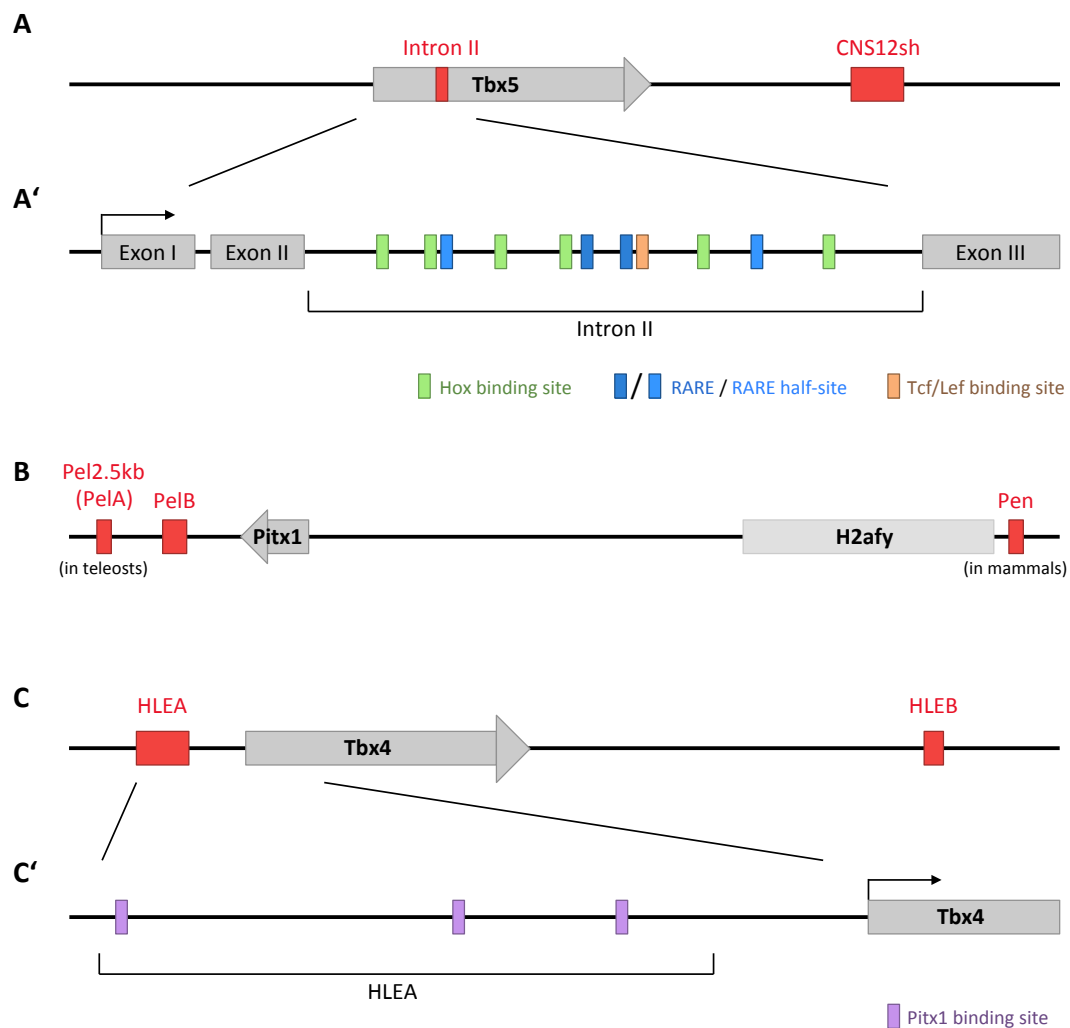


**Fig. 5 Regulatory elements controlling expression of limb specific transcription factors.** Schematic representation of gene architectures of *Tbx5* (A), *Pitx1* (B) and *Tbx4* (C) with A' and C' showing detailed maps to point out specific binding sites for regulators. A: There are two known regulatory regions for *Tbx5* activity, intron II and CNS12sh enhancer, whereby the intron II region contains RAREs, Tcf/Lef and Hox binding sites (A'). B: For *Pitx1*, three limb enhancers have been identified so far: Pel2.5kb (PelA), PelB and the pan-limb enhancer Pen. The promoter region of the housekeeping gene *H2afy* is indispensable for the coordination of the hindlimb specific activity of Pen. It should be emphasized that Pel2.5kb (PelA) and Pen do not appear together as Pel2.5kb is conserved only in teleosts and Pen only in mammals and that the common representation is just for completeness. C: The hindlimb enhancers HLEA and HLEB are both required for stable *Tbx4* expression. Three Pitx1 binding sites in HLEA demonstrate the role of Pitx1 in *Tbx4* activation (C'). Enhancers are depicted in red, genes in grey. Figure inspired by Chan et al., 2010; Cunningham et al., 2018; Kragestein et al., 2018; Menke et al., 2008; Minguillon et al., 2012; Nishimoto et al., 2014, 2015; Thompson et al., 2018.

### Induction and initiation of pelvic fins/hindlimbs

Concerning the development of pelvic fins, the homeobox transcription factor *Pitx1* plays a key role. Its expression is regulated by several enhancers, discovered in mice and stickleback (Chan et al., 2010; Kragesteen et al., 2018; Sarro et al., 2018; Thompson et al., 2018). First of all, a region upstream of the *Pitx1* locus, with conservation throughout teleosts, was found in stickleback and defined as enhancer, henceforth referred to as Pel2.5kb according to its size or as PelA (Chan et al., 2010; Thompson et al., 2018) (Fig. 5). Interestingly, various stickleback populations exist that exhibit a partial or complete loss of their pelvic structures - an adaptive feature established during evolution that could be attributed to different deletions of the Pel2.5kb enhancer, which all overlap in its 501bp core regulatory fragment (Chan et al., 2010). Recently, further investigations revealed molecular features of the *Pitx1* locus that lead to an increased fragility of the DNA and therefore raise the probability of DNA damage and mutations, explaining the repeated occurrence of this natural stickleback phenotype (Xie et al., 2019). Furthermore, another BAC screen in mouse directed to the enhancer PelB, located downstream of *Pitx1* and bearing one subregion that is conserved in vertebrates (Thompson et al., 2018) (Fig. 5). A CRISPR/Cas9 mediated deletion of PelB slightly decreased *Pitx1* expression in hindlimb buds and caused a reduction of foot bones, suggesting that this enhancer acts cooperatively with other regulatory elements rather than independently (Thompson et al., 2018). Thirdly, an interesting regulatory mechanism controlling hindlimb specific *Pitx1* expression was recently identified in mice (Kragesteen et al., 2018) (Fig. 5). The pan-limb enhancer Pen drives strong expression in both, fore- and hindlimbs upon combination with a *lacZ* reporter gene in transgenic mice. However, differences in the chromatin structure in the respective limb types make the *Pitx1* promoter accessible for interaction with Pen only in hindlimbs, while in forelimbs promoter and enhancer are spatially separated from each other, unable to interact (Kragesteen et al., 2018). In this mechanism, the promoter region of the adjacent housekeeping gene *H2afy* plays a decisive role (Kragesteen et al., 2018, 2019). Deletion of Pen reduced *Pitx1* expression by 35 - 50 % and partially resulted in hindlimb malformations in adult mice (Kragesteen et al., 2018).

*Pitx1* then directly initiates the expression of *Tbx4* (Duboc & Logan, 2011; Logan & Tabin, 1999) (Fig. 4). This happens via two regulatory elements, referred to as hindlimb enhancer A and B (HLEA and HLEB, respectively) that were identified up- and downstream of the coding

region of *Tbx4* in mice and are both required for a stable *Tbx4* expression (Menke et al., 2008). While HLEB shows a strong conservation from fish to mammals, HLEA is conserved only in mammals and contains three putative Pitx1 binding sites (Fig. 5). Mutation of one single, perfectly conserved site results in significant reduction of enhancer activity in hindlimbs. A targeted knockout of HLEA diminishes *Tbx4* expression and causes significant shortening of hindlimb bones. In a subsequent study, Pitx1 has also been shown to bind to HLEB, however to a lesser extent in comparison to HLEA (Infante et al., 2013).

Subsequently, *Tbx4* activates *Fgf10* to promote further pelvic fin development (Fig. 4). Conditional knockout studies in mice, inactivating the whole *Tbx4* gene before the onset of hindlimb formation, describe minor expression of *Fgf10* in early limb buds, which is completely lost when embryos develop further and finally leads to premature termination of limb formation (Naiche & Papaioannou, 2003, 2007). Moreover, *Tbx4*<sup>-/-</sup> is embryonic lethal in mice due to a failure of chorioallantoic fusion (Naiche & Papaioannou, 2003). This suggests a central role of *Tbx4* in *Fgf10* activation, yet demonstrates that additional factors must be involved. Two prominent candidates in this context are the LIM-homeobox transcription factor *Islet1* and the signalling factor  $\beta$ -catenin. Knockout of either gene results in the absence of hindlimb budding and loss of *Fgf10* initiation in mouse embryos. This strongly suggests that both genes are crucial for hindlimb induction and demonstrates that their activity precedes that of *Fgf10* (Kawakami et al., 2011; Narkis et al., 2012; Yang et al., 2006). A mutation in the *Tbx4* nuclear localisation signal (NLS) in a natural occurring zebrafish mutant named *pelvic finless (pfl)*, completely suppresses *Fgf10* expression, which likewise results in failure of pelvic fin formation. This neither indicates any involvement of further activators, nor excludes it (Don et al., 2016). In zebrafish, *Islet2a* has been shown to be expressed in the presumptive pelvic fin field at specific time points during zebrafish development, including the embryonic, larval and metamorphic state. It was postulated to be involved in a mechanism that controls the fate of the cells of the presumptive pelvic fin field, from their positional determination in early somitogenesis to their differentiation in metamorphosis (Moriyama et al., 2019; Murata et al., 2010). However, whether *Islet2a* also functions in pelvic fin induction still remains elusive. Comparable to forelimbs, *Tbx4* activates *Wnt8c*, a *Wnt* gene family specifically expressed in hindlimbs, which signals back to maintain *Tbx4* and *Fgf10* expression levels and drives limb outgrowth (Kawakami et al., 2001; Ng et al., 2002; Takeuchi et al., 2003) (Fig. 4).

### 1.3.2.3 Outgrowth

After induction, *Tbx5/Wnt2b/Fgf10* and *Tbx4/Wnt8c/Fgf10* maintain each others expression levels via positive feedback loops in fore- and hindlimbs, respectively (Takeuchi et al., 2003). Constant *Fgf10* activity subsequently leads to the expression of *Fgf8* in the prospective limb bud ectoderm, where the apical ectodermal ridge (AER) will form shortly after (Boulet et al., 2004; Ohuchi et al., 1997; Xu et al., 1998). Hereby, activation of *Fgf8* is mediated via  $\beta$ -catenin dependent *Wnt3a* signalling in mice and chicks (Barrow et al., 2003; Kawakami et al., 2001; Narita et al., 2007) (Fig. 4). While emerging *Fgf8* expression first occupies a broad area in the ectoderm, it becomes precisely defined upon AER formation (Fernandez-Teran & Ros, 2008). Then, a positive feedback loop between *Fgf10* and *Fgf8* is established, which mutually maintains their activity and whose essential function for the outgrowth of paired extremities has been demonstrated, at least in mice (Lewandoski et al., 2000; Moon & Capecchi, 2000; Ohuchi et al., 1997; Xu et al., 1998) (Fig. 4). *Fgf4*, likewise expressed in the AER, also contributes to limb outgrowth, among other things by partially compensating for the function of *Fgf8* in case of its loss (Boulet et al., 2004).

In zebrafish, there is evidence that paired fins develop slightly different (Don et al., 2013). Although *Fgf8* similarly seems to have an important function, it could be dispensable for the outgrowth of pectoral fins, which is clear from the *Fgf8* mutant *acerebellar (ace)*, whose pectoral fins are almost unaffected (Reifers et al., 1998). Additionally, unlike in mice, the first appearance of *Fgf8* coincides with the formation of the AER (Reifers et al., 1998). Furthermore, other *Fgf* genes were reported to be involved in pectoral fin formation, which are *Fgf24* and *Fgf16* (Fischer et al., 2003; Nomura et al., 2006). *Fgf24* was shown to act downstream of *Tbx5* and *Wnt2b*, but upstream of *Fgf10* (Fischer et al., 2003). *Ikarus (ika)* mutants, defective for *Fgf24*, are viable in a homozygous state, but completely lack pectoral fins, even as adults. Interestingly, the pelvic fins are present and of normal morphology, indicating that different signalling factors and regulations are responsible for the development of each type of paired fin (Fischer et al., 2003; van Eeden et al., 1996).

Outgrowth as well as anterior-posterior patterning of the pectoral and pelvic fin buds are additionally controlled via a gradient of the signalling molecule *Shh*, emerging from the zone of polarizing activity (ZPA), which is located at the posterior margin of the fin bud (Riddle et al., 1993). *Shh* expression is induced by *Fgf8* from the AER and then maintained by mutual interactions between *Fgf8*, *Fgf10* and *Shh* (Ohuchi et al., 1997; Tickle & Towers, 2017)

(Fig. 4). The morphogen Shh has a special function in digit formation, which is based on both, a concentration and a temporal gradient. This means that for each of the five digits a well-defined amount and duration of Shh exposure is required to enable development (Harfe et al., 2004; Tickle & Towers, 2017). In zebrafish, pectoral and pelvic fins establish the ZPA and *Shh* expression during early fin bud development, similar to mice. Later the *Shh* expression is shifted to the forming lepidotrichs and fin rays, which share a common developmental history with digits (Nakamura et al., 2016). In pectoral fins this shift occurs with a time delay, during morphogenesis of the larval into the adult fin form (Laforest et al., 1998).

Furthermore, a role for RA is postulated in AER establishment. In mouse embryos a gradual RARE activity is observed in forelimb buds, generated by proximal *Aldh1a2* and distal *Cyp26b1* activity, which is believed to participate in outgrowth and proximodistal patterning (Mic et al., 2004; Yashiro et al., 2004). Depletion of endogenous RA signalling leads to a significant reduction of the AER to a minimal, centrally oriented spot and to an anterior shift of *Shh* expression, eventually resulting in a slowed outgrowth and a smaller limb bud size (Mic et al., 2004). The major players for hindlimb initiation, *Pitx1* and *Tbx4*, are still present in the limb mesenchyme after budding (Gibson-Brown et al., 1996; Szeto et al., 1999). However, in spite of its prominent function during initiation, *Tbx4* seems to play a minor function in limb outgrowth, as its knockout after bud formation does neither affect *Fgf10* expression nor limb outgrowth in mouse embryos. However, defects of the skeletal structures are observed (Naiche & Papaioannou, 2007). *Pitx1* acts, during later stages of mouse hindlimb formation, independently of *Tbx4*. In this process, it regulates the accurate formation of skeletal structures, muscles and tendons, based on a direct interaction with genes of the respective underlying signalling networks (Duboc & Logan, 2011; Nemeč et al., 2017; Wang et al., 2018). Knockout of *Pitx1* in mice results in neonatal lethality accompanied with severe malformations or reductions of the hindlimb bones, including the long bones (femur, tibia, fibula), pelvis, tarsus and patella, while digits are unaffected (Lanctôt et al., 1999; Szeto et al., 1999). It is noteworthy that this phenotype is always more pronounced on the right side of the animal's body, which might be attributed to a partial compensation by the paralogue *Pitx2*, which is involved in establishment of left-right asymmetry (Piedra et al., 1998; Ryan et al., 1998). As *Pitx1* is also expressed in the pituitary gland and the jaw, it is not surprising that in *Pitx1*<sup>-/-</sup> mice, serious defects are noted in these structures as well (Lanctôt et al., 1999; Szeto et al., 1999).

#### 1.3.2.4 The role of RA in the development of paired fins/limbs

Several studies point out a role of RA in limb/fin development. For example, the two zebrafish mutants *neckless (nls)* and *no-fin (nof)*, both defective for the RA synthesizing enzyme *Aldh1a2*, do not develop pectoral fins and correspondingly lack *Tbx5* and *Fgf10* expression (Begemann et al., 2001; Grandel et al., 2002). Further studies in zebrafish were based on the inhibition of RA synthesis using the Aldh inhibitor 4-diethylaminobenzaldehyde (DEAB) in varying concentrations and during diverse time frames throughout gastrulation and somitogenesis with the intention to determine the exact timing of RA signalling (Gibert et al., 2006; Grandel & Brand, 2011; Grandel et al., 2002). Summarized, a dual role of RA during early zebrafish development is postulated. It is suggested that RA is first involved in the determination of fin precursor cells during gastrulation and later, during somitogenesis, RA signalling is necessary for the maintenance of the precursor cells (Grandel & Brand, 2011). Thus, DEAB treatment during somitogenesis enables the establishment of *Tbx5* expression but restrains fin bud formation (Grandel & Brand, 2011). Accordingly, the pectoral finless phenotype of *nls* or *nof* mutants can only be effectively rescued by the end of gastrulation by application of exogenous RA (Begemann et al., 2001; Grandel et al., 2002). Unfortunately, as *nls* and *nof* are embryonic lethal, these mutants cannot be used for the investigation of the role of RA in pelvic fin development.

The role of RA was also verified in early chick embryos by studies that were based on barrier insertions to prevent diffusion of signalling molecules between tissues. They were placed either between the presomitic mesoderm and LPM during early development or between the somites and LPM in slightly older embryos. Early interference blocked *Tbx5* or *Tbx4* activation and limb bud formation, whereas later manipulations resulted in the loss of *Fgf10*, *Fgf8* and *Shh* domains while *Tbx5* or *Tbx4* were detectable. It was possible to rescue limb bud formation and restore *Fgf10*, *Fgf8* and *Shh* expression by insertion of a RA-soaked bead in the LPM. Together, this indicates that RA signals from the somites and is necessary for both, induction of *Tbx4* or *Tbx5* as well as participation in *Fgf10* activation (Nishimoto et al., 2015). The observations upon late barrier insertions are in conformity with the results obtained by Grandel & Brand (2011), describing normal *Tbx5* expression upon DEAB treatment of zebrafish embryos during somitogenesis. Moreover, in case of hindlimbs, the involvement of RA was additionally confirmed by insertion of beads in the LPM soaked with the pan-Rar inverse agonist BMS493, which inhibits RA signal transduction, and resulted in a

significant reduction of *Fgf10* expression and a diminution of limb bud size (Nishimoto et al., 2015).

While these studies in chicken suggest a similar role for RA in fore- and hindlimb development, studies in mice indicate a different mode of action in each limb type (Cunningham et al., 2013; Mic et al., 2002, 2004; Sandell et al., 2007; Zhao et al., 2009). In these studies, mouse embryos deficient for the RA synthesizing enzyme *Raldh2* were used. Low doses of RA were maternally applied for a short, defined timespan to rescue the embryonic lethality of this mutation. Rescued *Raldh2*<sup>-/-</sup> mouse embryos developed smaller forelimbs, but normal hindlimbs (Mic et al., 2002, 2004). A similar phenotype was observed in *Rdh10*<sup>-/-</sup> mutant mice (Sandell et al., 2007). The difference was attributed to remaining RARE activity in the mesonephros, which is located in close proximity to the developing hindlimb bud, likely due to RA production by *Raldh3* (Mic et al., 2004). Consequently, *Raldh2*<sup>-/-</sup>;*Raldh3*<sup>-/-</sup> double mutants were generated, exhibiting no further RARE activity in the mesonephros. However, rescue with maternal RA supply, likewise resulted in formation of normal sized hindlimb buds, while the size of forelimb buds was decreased (Zhao et al., 2009). It was concluded, that RA is only necessary in forelimb, but not in hindlimb development. This matches the model of RA acting permissive in forelimb induction by antagonizing *Fgf8* expression in axial structures. As hindlimb induction occurs later in development, during a time when RA is not present in the axial structures next to the presumptive hindlimb field, it seems plausible that is not needed for hindlimb development (Cunningham et al., 2013; Zhao et al., 2009). However, it cannot definitely be excluded that the short RA pulse that is necessary in these experiments to overcome embryonic lethality of *Raldh2*<sup>-/-</sup>;*Raldh3*<sup>-/-</sup> mutants, is already sufficient to reach the RA threshold required for limb bud formation, but too little to be detected by the used RARE-lacZ reporter constructs (Nishimoto & Logan, 2016; Rosello-Diez et al., 2014).

Taken together, it is well established that RA plays a key role in forelimb or pectoral fin development, although the exact mechanism - inductive or permissive function - is still under debate. In case of hindlimbs or pelvic fins, the results are contradictory and further research is needed to obtain reproducible and consistent results that unequivocally confirm the involvement of RA and reveal its potential target genes (Duester, 2017).

## 1.4 Molecular systems for the genetic manipulation of zebrafish

In the course of establishing zebrafish as a model system for reverse genetic approaches, several methods were developed to disrupt the function of a particular gene of interest. For example, using modified antisense oligonucleotides (morpholinos), a transient knockdown of gene activity can be achieved by blocking the procession or translation of RNAs. However, this method works only efficiently during the first two to three days of zebrafish embryonic development (Nasevicius & Ekker, 2000). But there are also molecular mechanisms that enable the generation of stable transgenic lines. To be mentioned is the Tol2 transposon system, which enables the random integration of diverse genetic constructs into the zebrafish genome (Kawakami et al., 2000). In addition to the generation of reporter lines, this allows the establishment of genetic tools like the Cre-loxP or the Gal4-UAS system to specifically and locally manipulate gene expression in zebrafish. An editing at exactly defined sites in the genome, either by inducing indel mutations or by insertion of transgenes, is made possible by nucleases like zinc-finger nucleases (ZFNs) (Doyon et al., 2008; Meng et al., 2008), transcription activator-like effector nucleases (TALENs) (Huang et al., 2011) and the CRISPR/Cas9 system (Cong et al., 2013; Varshney et al., 2016). Techniques used in this study are described in more detail below.

### 1.4.1 The Tol2-Transposon system

The Tol2-Transposon system is based on the autonomous Tol2 transposable element originating in the genome of the medaka fish (*Oryzias latipes*). It has been discovered more than twenty years ago by the working group around Koichi Kawakami, and since then was extensively studied, optimized and established in various model organisms, including zebrafish (Kawakami, 2007; Kawakami et al., 1998, 2000a, 2000b, 2004; Kawakami & Shima, 1999; Nagayoshi et al., 2008; Urasaki et al., 2006). Upon microinjection into fertilized zebrafish eggs, *in vitro* transcribed Tol2 mRNA is translated into active Tol2 transposase, which is able to mediate the transposition of basically any gene of interest into a random area of the host genome. The prerequisites for effective integration are minimal Tol2 *cis* sequences with a length of 200 bp at the 5' end and 150 bp at the 3' end that flank the construct to be transferred (Kawakami et al., 1998, 2000a; Kawakami & Shima, 1999) (Fig. 6). By inversion of these sequences (150 bp at the 5' end and 200 bp at the 3' end), efficiency

could be additionally enhanced (Suster et al., 2009; 2011). A size limit for Tol2 mediated genomic integration is currently not known and successful transgenesis has already been carried out even with large sized bacterial artificial chromosomes (BACs) up to 230 kb (Suster et al., 2011). Transient transgenesis is observed in about 20 % of the injected embryos via detectable mosaic expression of the foreign gene. The percentage of manipulated F0 fish that transmit the transgene via the germline to the F1 generation can be as high as 50 - 70 % of injected fish (Lieschke et al., 2009; Suster et al., 2011).

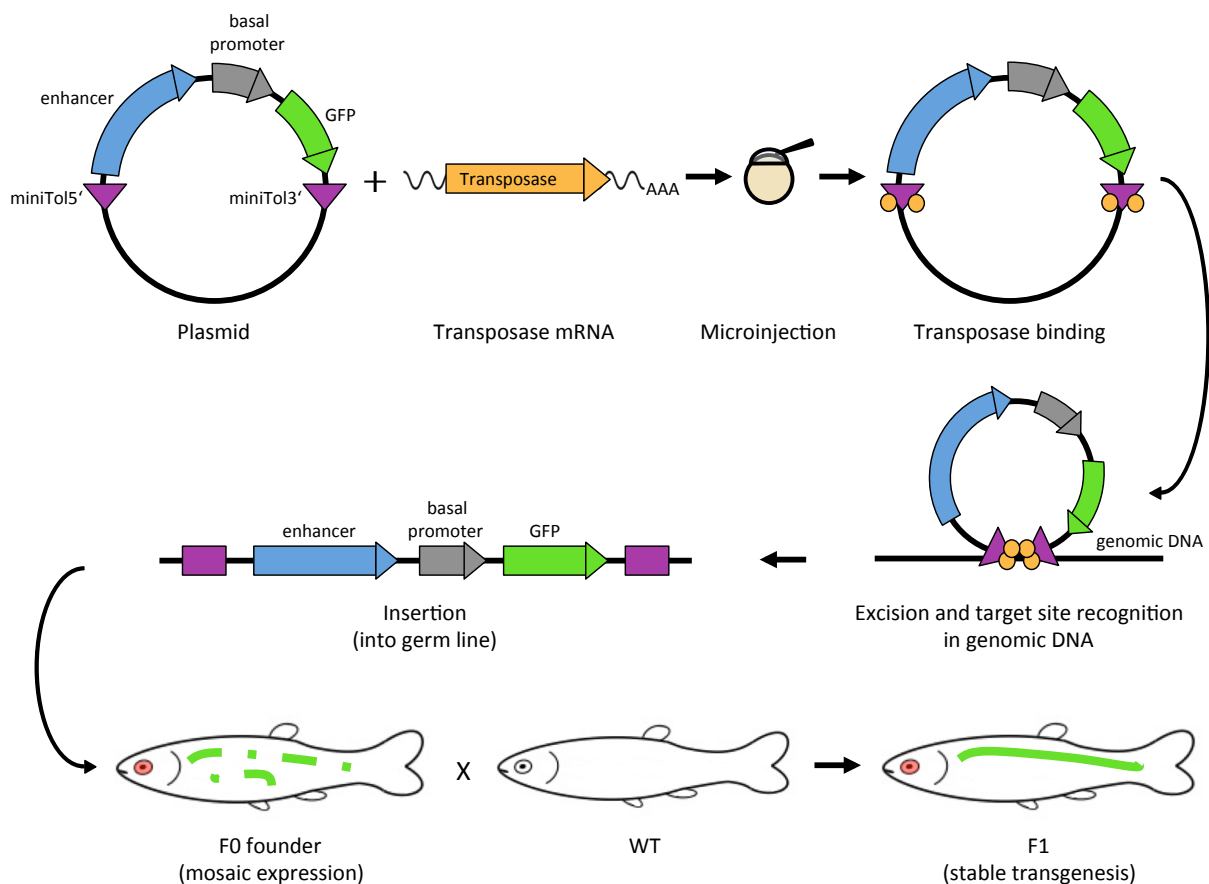


**Fig. 6 The Tol2 transposon system.** Schematic representation of components and mode of action of the Tol2 transposon system. A plasmid containing 5' and 3' mini Tol2 *cis* sequences is co-injected with *Tol2 transposase* mRNA into fertilized zebrafish eggs (one-cell stage). Following translation into active protein, transposase binds to its *cis* elements, excises the flanked DNA construct and integrates it into the genomic DNA of the organism at a random target site. Growing fish of the F0 generation frequently show mosaic expression of the transgene in diverse parts of the body. Crossing them with wild type (WT) fish generates heterozygous F1 fish that exhibit stable transgene expression in defined tissue or organs. Figure designed by Amelie Mück. Taken and modified from Mück, 2019, with inspiration from Creative-biolabs, 2020; Suster et al., 2009.

Due to its high capability to generate stable transgenes, the Tol2 transposon system has evolved as a powerful tool in developmental biology to study gene activity and regulation, for example via gene or enhancer trap methods. For this, Tol2 donor vectors are created that combine green fluorescent protein (GFP) with a splice acceptor or a basal promoter, so that GFP is expressed after genomic integration within a gene or in the reach of a chromosomal enhancer, respectively (Kawakami et al., 2004; Lieschke et al., 2009). Additionally, creating reporter lines in which a putative enhancer region is linked to a basal promoter and GFP enables activity and specificity tests of newly identified enhancers *in vivo* (Adachi et al., 2016; Chan et al., 2010; Hernández-Vega & Minguillón, 2011).

#### **1.4.2 The Gal4-UAS system**

The Gal4-UAS-system originates in yeast and has been established in various vertebrate and non-vertebrate model organisms since it was first described in the 1980s (Brand & Perrimon, 1993; Giniger et al., 1985; Kakidani & Ptashne, 1988; Scheer & Campos-Ortega, 1999; Webster et al., 1988). Its mechanism is based on Gal4, a transcriptional activator, binding to a specific upstream activating sequence (UAS) and thereby inducing the expression of any downstream located gene of interest. To use this feature in order to achieve a tissue-specific gene expression, the generation of two stable transgenic lines is required. The driver line expresses *Gal4* under the control of a tissue specific enhancer or promoter and the effector line contains any gene of interest under the control of UAS (Fig. 7A) (Asakawa & Kawakami, 2008). The development of the Tol2 transposon system was therefore an important milestone in the implementation of the Gal4-UAS system to facilitate the production of transgenes (Asakawa & Kawakami, 2008; Kawakami, 2007).

The minimal region of Gal4 needed for DNA binding is the Gal4 DNA binding domain (DBD) consisting of the N-terminal 74 amino acids (Keegan et al., 1986). Based on this, diverse constructs were generated to optimize the handling, functionality and efficiency of the Gal4-UAS system. First, the Gal4 DBD was fused to the strong transcriptional activation domain from the VP16 protein isolated from the *Herpes simplex* virus, in order to enhance the transcriptional activator potential, which is now even exceeding the original (Köster & Fraser, 2001; Sadowski et al., 1988).

To enable temporal regulation of transgene expression in addition to a local restriction, inducible Gal4 variants were designed (Akerberg et al., 2014; Gerety et al., 2013; Wang et al., 2012). In one variant, the Gal4-VP16 was fused to the hormone-binding domain of the human estrogen receptor 2 (ERT2), which has an especially high affinity for the estrogen receptor modulator 4-hydroxy-tamoxifen (4-OHT) (Akerberg et al., 2014; Gerety et al., 2013). After the addition of 4-OHT, ERT2-Gal4-VP16 enters the cell nucleus, binds to UAS and activates target gene expression, whereas in absence of 4-OHT, no UAS binding takes place, which ensures rapid reversibility of this system upon drug washout. The level of expression can furthermore be controlled via the dose of 4-OHT (Akerberg et al., 2014; Gerety et al., 2013) (Fig. 7B).

A second variant, GAVPO, is a light-inducible version of Gal4, consisting of the Gal4 DBD connected to the smallest light-oxygen-voltage (LOV) domain Vivid (vvd) from *N. crassa* and the p65 transactivation domain (AD) isolated from human cells (Wang et al., 2012). The Vivid domain includes a flavin co-factor that forms a cystein-flavin adduct with Cystein(108) upon blue-light activation. This in turn leads to a conformational change that results in dimerization of GAVPO and its binding to UAS (Fig. 7C). This process is reversible as soon as illumination is switched off (Wang et al., 2012; Zoltowski et al., 2007). Using GAVPO in driver lines circumvents the treatment with 4-OHT, which always must be handled carefully, because of its toxicity and its instability upon light-exposure.

Further modifications were introduced to adapt the Gal4-UAS system to certain model organisms. To be named is the variant *KalTA4*, which is a *Gal4* version optimized for the use in zebrafish. *KalTA4* consists of a Kozak sequence and a codon usage optimized for zebrafish, thus significantly enhancing transcriptional efficiency in this species (Distel et al., 2009). In addition, only the minimal, but potent TA4 core region from the VP16 transactivation domain was integrated in this construct. Due to the modification of the transcriptional activator, *KalTA4* is still able to activate UAS in the same manner as *Gal4*, but is less toxic to the organism. Toxicity of Gal4 is a consequence of a squelching effect, meaning that the activation regions of Gal4 interact with the intrinsic transcriptional machinery of the organism, although UAS are absent, resulting in the inhibition of numerous genes (Gill & Ptashne, 1988). Similar to Gal4, the combination of *KalTA4* with ERT2 has already been proven to be effective (Kajita et al., 2014) (Fig. 7B).

The effector lines possess multiple upstream activating sequences as a rising level of activation has been demonstrated with increasing number of sequences, up to a certain threshold of consecutive UAS, until a plateau is reached (Distel et al., 2009). In this work, five repetitive UAS (5xUAS) as well as four non-repetitive UAS (4xnrUAS) were used (Akitake et al., 2011; Goll et al., 2009). The latter exhibit a difference in their sequence of 50% and are said to be less susceptible to methylation and subsequent transcriptional silencing while the activation of downstream genes is just as good. This was verified in comparison to the frequently used 14xUAS construct, composed of repetitive sequences (Akitake et al., 2011).

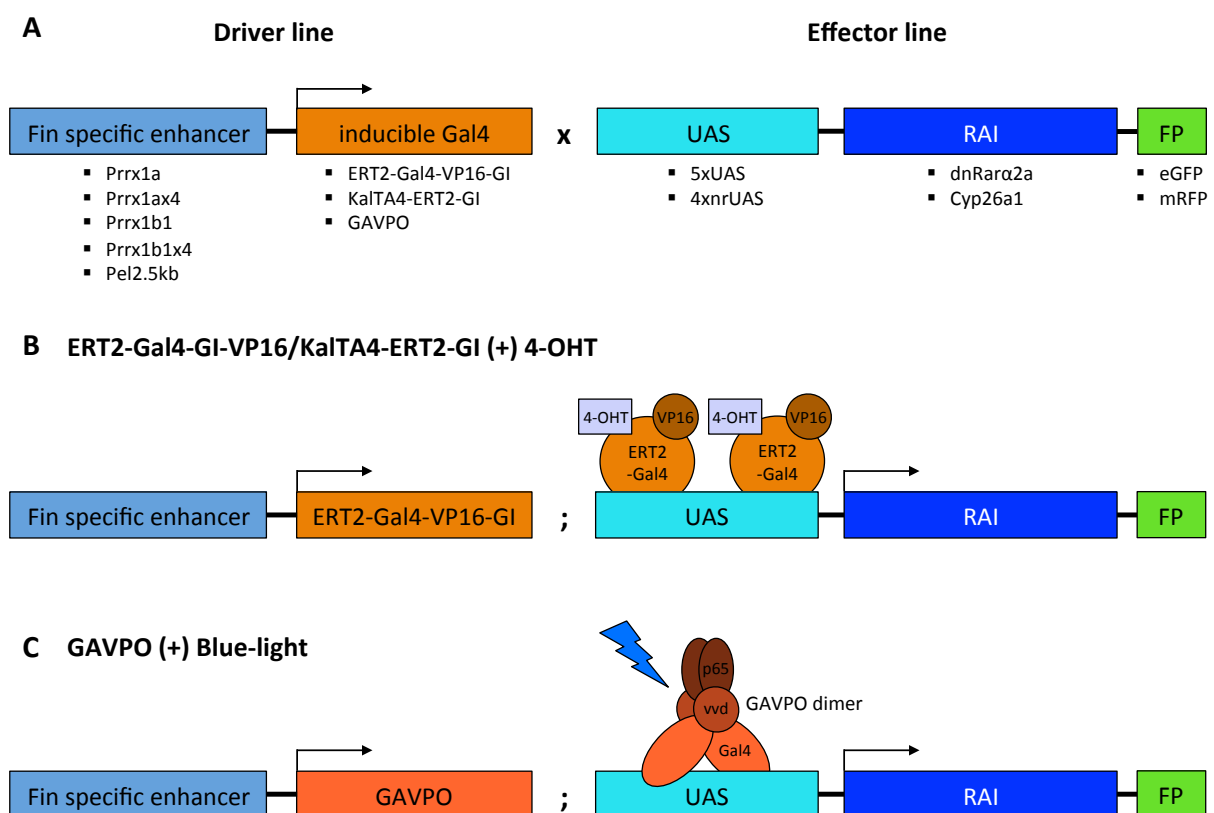


**Fig. 7 The Gal4-UAS system.** **A:** Schematic representation of the binary Gal4-UAS system as applied in the study of the role of RA in pelvic fin development. The driver lines provide expression of an oestrogen- or light-inducible *Gal4* derivative under the control of enhancer sequences specific for pelvic and/or pectoral fins. In the effector lines, upstream activating sequences (UAS) control the activity of genes that encode RA signalling inhibitors (RAI) in combination with fluorescing proteins (FP). All used components are listed below the respective bar. **B-C:** Crossing of driver and effector lines generates double transgenic fish that possess both parts of the system, which enables a spatial disruption of RA signalling exclusively in pelvic and/or pectoral fins. Additionally, a temporal control is mediated by the selection of the starting point of 4-hydroxy-tamoxifen (4-OHT) treatment, in case of ERT2-Gal4-VP16-GI and KalTA4-ERT2-GI (**B**), or blue-light irradiation, in terms of GAVPO (**C**). Figure inspired by Akerberg et al., 2014; Mruk et al., 2020; Wang et al., 2012.

To apply this system for the study of the role of RA in pelvic fin development in zebrafish, the genes *Cyp26a1* and *zfdnRara2a*, whose proteins are associated with the RA signalling pathway, are selected for creating the effector lines. Via overexpression of each of the two genes, a disruption of the RA signalling is intended. *Cyp26a1* metabolizes RA to more polar and less biologically active compounds that are subject to further degradation, which ultimately leads to a pronounced RA deficiency in the organism (Niederreither & Dollé, 2008). The gene *zfdnRara2a* encodes a dominant negative version of the zebrafish *Rara2a*, which is shortened at the C-terminus of the protein after amino acid 403, whereby the activation domain consisting of Helix 12 is missing (Stafford et al., 2006) (Fig. 2). Thus this receptor variant is still able to heterodimerize with Rxr and to bind RAREs, but is unable to activate associated target genes, resulting in an interruption of RA signal transmission. The effectiveness of the dominant-negative action of corresponding receptor variants has already been demonstrated in human cells, *Xenopus* larvae and zebrafish (Blumberg, 1997; Damm et al., 1993; Pratt et al., 1990; Sharpe & Goldstone, 1997; Stafford et al., 2006).

For the creation of the driver lines, the enhancers of the limb and fin specific genes *Pitx1* and *Prrx1* were chosen. The first chosen enhancer is the *Pitx1* enhancer Pel2.5kb from the three-spine stickleback (Chan et al., 2010) (Fig. 5). The 2.5 kb enhancer fragment is conserved in zebrafish and other teleost fish and was already used to drive *eGFP* expression in the pelvic region of sticklebacks as well as in the pelvic fin bud mesenchyme of zebrafish (Chan et al., 2010; Don, 2013). The identification of the corresponding regulatory elements of *Pitx1* in the zebrafish genome is however still pending.

In addition, the regulatory elements of the paired-related homeobox gene 1 (*Prx1* / *Prrx1*) were utilized. *Prx1* is expressed, among others, in the mesenchymal tissue of the early limb bud and is therefore serving as a marker of the lateral plate and limb bud mesoderm (Cserjesi et al., 1992; Kuratani et al., 1994; Leussink et al., 1995). It has a central role in coordinating the morphogenesis of the handplate and the zeugopod in both, fore- and hindlimbs. This was concluded from the phenotype of mice carrying mutations in *Prx1* and its homologue *Prx2*, which were showing severe disorders in digit number and placement (Lu et al., 1999). The *Prx1* limb enhancer was originally identified in mice (Martin & Olson, 2000). Obviously, it also has influence on limb bone growth, which has been visualized in transgenic mice, whose *Prx1* enhancer was exchanged with the corresponding regulatory element from bats, whereby these animals consequently developed significantly enlarged

forelimbs (Cretekos et al., 2008). Zebrafish possess two orthologs of the *Prx1* gene, *Prrx1a* and *Prrx1b*, whose expressions are regulated by three non-coding enhancer sequences, *Prrx1a*, *Prrx1b1* and *Prrx1b2*. All three sequences were reported to drive *eGFP* expression in transgenic zebrafish reporter lines (Hernández-Vega & Minguillón, 2011). For this study, the two enhancers *Prrx1a* and *Prrx1b1* were chosen to generate the Gal4 driver lines.

### 1.4.3 The CRISPR/Cas9 system

The term CRISPR/Cas refers to an unique adaptive immune response mechanism commonly observed in bacteria and archaea. It is based on clustered regulatory interspaced short palindromic repeat (CRISPR) loci in the genome that act in combination with CRISPR-associated (Cas) elements. After a microorganism has first come into contact with a viral pathogen, the absorbed foreign DNA (protospacer sequence) is cut and incorporated as spacer into the CRISPR locus. In the case of a subsequent infection, the corresponding CRISPR loci are transcribed and the raw RNA processed into CRISPR RNA (crRNA). This hybridizes with another short RNA termed the transactivating RNA (tracrRNA) and both form the endoribonuclease surveillance complexes upon recruitment of one or several Cas proteins, like Cas9 (Gonzales & Yeh, 2014; Jinek et al., 2012; Sander & Joung, 2014).

The derived CRISPR-Cas technique was developed to enable a specific and precise editing of the genome with the possibility to knockout genes or insert sequences at exactly defined loci. Numerous protocols were designed to establish this system in diverse model systems (Cong et al., 2013; Kraft et al., 2015; Varshney et al., 2016). Generally, the methods are based on the induction of a double-strand break (DSB) in the genomic DNA, mediated by a chimeric single-guided RNA (sgRNA), which combines the features of crRNA and tracrRNA, and the Cas9 endonuclease. The sgRNA possesses a specific sequence and secondary structure that enable it to recruit the Cas9 endonuclease and, following complex formation, to hybridize with its target sequences. Subsequently, Cas9 induces the DSB three bases upstream of the protospacer adjacent motif (PAM) (Gonzales & Yeh, 2014; Sander & Joung, 2014) (Fig. 8). Cellular mechanisms discover this defect and activate one of two possible repair mechanisms: homology directed repair (HDR) or non-homologous end joining (NHEJ). HDR fixes the cutting site by homologous recombination using a donor DNA with a homologous sequence. This repair mechanism enables the insertion of DNA pieces or even whole genes in the target region. In contrast to that, NHEJ repairs the DSB by direct ligation,

a process that is very error-prone and often leads to insertions or deletions (indels) of a few nucleotides. These indel mutations can on the one hand affect only few amino acids, which, depending on the relevance of the residues, might deplete the protein function. On the other hand, indels can cause reading frame shifts resulting in a completely different translation or the translation of a truncated protein in case a premature stop codon is created (Gonzales & Yeh, 2014; Sander & Joung, 2014) (Fig. 8).

There are numerous practical applications for the CRISPR/Cas9 technology. Targeted knockouts can be used for functional studies of a specific gene or enhancer of interest. New insertions allow, among other things, the creation of precisely defined point mutations. The utilization of two different sgRNAs enables the introduction of larger rearrangements in the genome. Combinations of the CRISPR/Cas9 machinery with activation or effector domains, make it possible to manipulate the expression of selected genes or to introduce certain modifications that change, for example, the chromatin state (Sander & Joung, 2014).

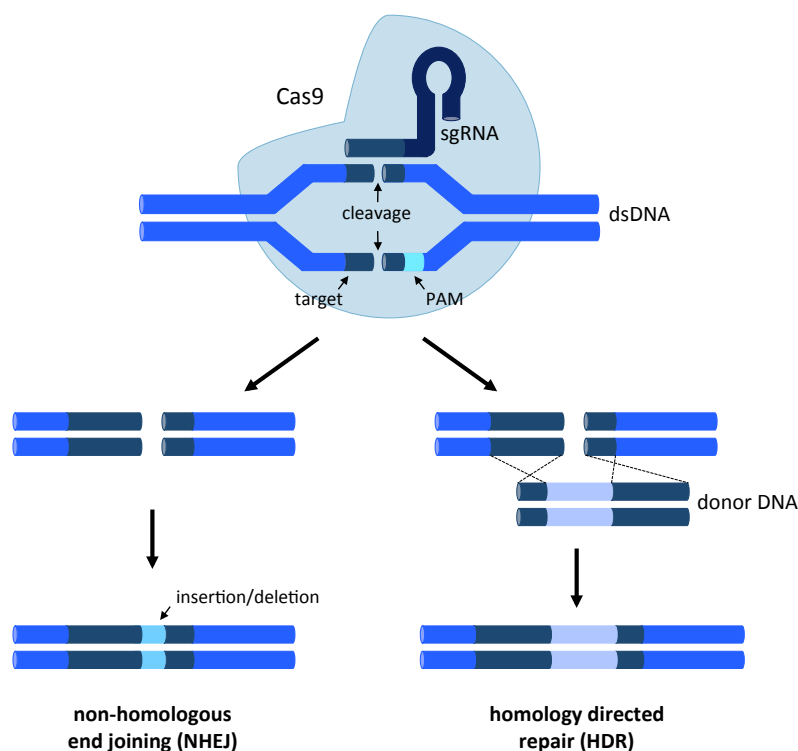


**Fig. 8 The CRISPR/Cas9 system.** The chimeric sgRNA recruits the Cas9 endonuclease and hybridizes with the endogenous target sequence. Cas9 then introduces a double strand break (DSB) three bases upstream of the PAM. As a consequence, cellular mechanisms activate one of two possible repair mechanisms: NHEJ or HDR. The error-prone NHEJ often results in indel mutations that can cause point mutations, reading frame shifts or generate premature stop codons. In contrast to that, HDR uses homologous recombination to repair the DSB and in this way allows the insertion of new DNA sequences in the target site. Figure inspired by Ersgenomics, 2020.

## 1.5 Previous results on the role of RA in pelvic fin development

The zebrafish loss-of-function mutants *nls* and *nof*, that are lacking an essential component of the RA signalling pathway already die in early embryonic stages, long before the onset of pelvic fin development (Begemann et al., 2001; Grandel et al., 2002). Therefore, traditional forward genetics are hard to use regarding the study of the role of RA during pelvic fin formation so that other methods must be applied that enable the manipulation of RA signalling during later stages of larval development. These could be, for example, pharmacological treatments to specifically target RA synthesis or its signal transduction or the overexpression of RA signalling activating or repressing genes using transgenic zebrafish lines. In this way, previous master and bachelor theses already investigated the role of RA in pelvic fin development (Breu, 2017; Marzi, 2015; Welte, 2011). In two different experimental setups, zebrafish larvae were treated with 4-diethylaminobenzaldehyde (DEAB), a potent inhibitor of aldehyde dehydrogenases (Aldhs) that suppresses the synthesis of RA. Published experiments with DEAB on zebrafish embryos confirmed the suitability of a concentration of 10  $\mu$ M (Perz-Edwards et al., 2001; Russo et al., 1988).

First, the larvae were sorted based on their standard length (SL), which is defined as the distance from the head to the beginning of the caudal fin, and the respective groups were treated with 10  $\mu$ M DEAB for up to 18 days (Fig. 9). Subsequent Alcian Blue staining to label cartilage structures allowed the evaluation of RA deficiency on pelvic girdle and fin formation (Welte, 2011). Starting this experiment from a SL of 5.6 mm completely inhibited pelvic fin outgrowth in all DEAB treated larvae (Fig. 9B-C). In the case that DEAB was added at a SL of 6.1 mm, a complete lack of pelvic fins was observed in 14 % of the larvae. 77 % of the other individuals showed diverse severe malformations of the pelvic girdle cartilage, partly in combination with asymmetric outgrowth of the pelvic fins (Fig. 9D-H). Frequently observed deformations were misshaped and bend anterior processes (Fig. 9E), formation of additional cartilage structures like a mirror-image duplication of the posterior process (Fig. 9F), cleavage of the fin base (Fig. 9G, only observed when treated from a SL of 7.1 mm) as well as a reduced number of fin rays. These defects were seen on both sides of the pelvic girdle, however, in some cases one side was more affected than the other (Fig. 9H) (Welte, 2011). These results suggested that RA is needed in two ways and at two distinct time points, early for the induction of pelvic fin formation and later for the patterning of the pelvic girdle skeleton (Welte, 2011).

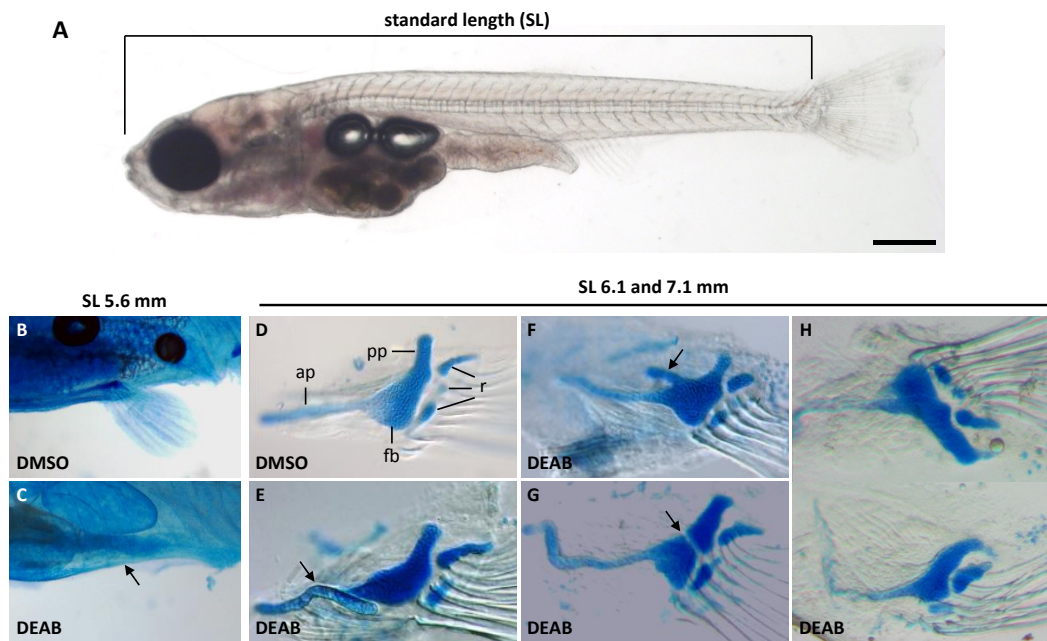


**Fig. 9 Early inhibition of RA synthesis suppresses pelvic fin outgrowth and causes severe malformation of the pelvic girdle.** **A:** Lateral view of a 23 dpf zebrafish larva short before pelvic fin bud formation to illustrate the determination of the standard length (SL). Anterior is left. **B-H:** Alcian Blue cartilage staining of zebrafish larvae treated with 10  $\mu$ M DEAB or equivalent volume of DMSO (control; **B,D**) from the reaching of the stated SL for up to 18 days. Arrows point to missing or malformed structures of the pelvic girdle. A complete hindrance of pelvic fin outgrowth is observed when DEAB treatment started at a SL of 5.6 mm (**C**). Starting at a SL of 6.1 or 7.1 mm results in malformations of the pelvic girdle cartilage, like bend anterior processes (**E**), formation of additional cartilage elements (**F**), cleavage of the fin base (**G**) or asymmetric pelvic girdle growth (**H**). ap: anterior process; pp: posterior process; fb: fin base; r: radials. Scale bar: 1 mm. Pictures B-H taken and modified from Welte, 2011, inspired by Breu, 2017.

More detailed observations of the process of pelvic fin outgrowth revealed that the standard length is not a reliable benchmark for the determination of the exact developmental stage (Marzi, 2015). To obtain a reproducible experimental setup for future investigations, a staging system for pelvic fin development was created. This classification is based on the transgenic zebrafish reporter line *Tg(fli:EGFP)<sup>y1</sup>*, which labels, among others, chondrocytes, chondrocyte precursor cells and mesenchymal condensations. It includes different characteristics of the larval development and thus allows the determination of reproducible starting points for the pharmacological treatments (Fig. 10 and Fig. S1) (Marzi, 2015). The definition starts with Stage 1, characterized by the first appearance of ventral *fli:eGFP* signal in the prospective pelvic fin region. Stage 2 is defined by lateral eGFP fluorescence in the same area and the first visibility of the pelvic fin bud. For the later stages, the size of the outgrowing pelvic fin is set into relation to the progressive decrease of the minor lobe. Additionally, the numbers of the parallel developing radials and rays of dorsal and anal fin were counted (Fig. 10 and S1) (Marzi, 2015).

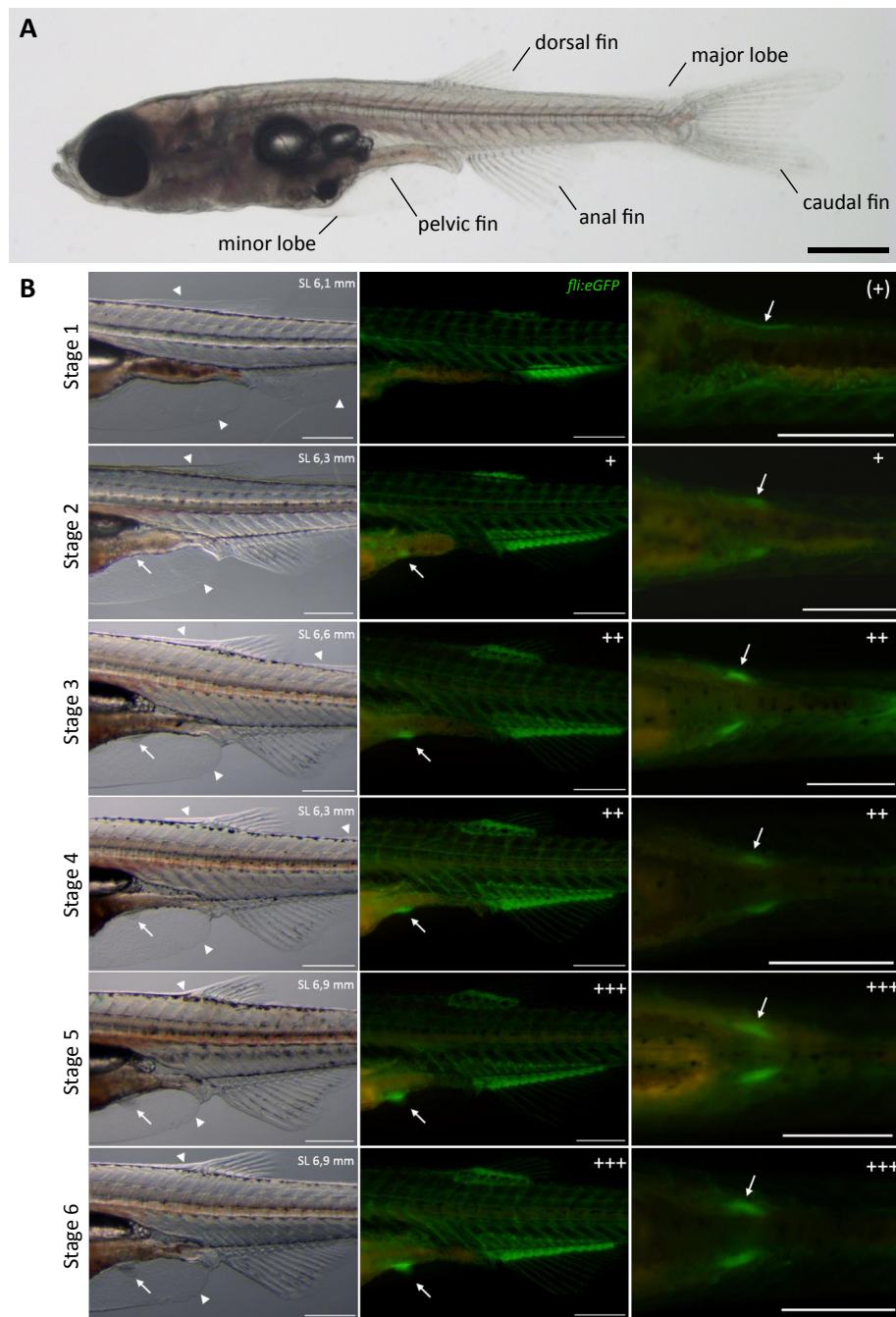


**Fig. 10 Definition of stages of pelvic fin development based on  $Tg(fli:EGFP)^{Y1}$  reporter line. A:** Lateral view of a zebrafish larva in pelvic fin developmental Stage 4 with designation of the structures used for the classification. The size of the growing pelvic fin was mainly compared to the progressive decrease of the distal margin of the minor lobe, but also the decrease of the major lobe as well as the number of the parallel developing radials and rays of dorsal and anal fin were included. **B:** Lateral view (left and middle column) and ventral view (right column) of the pelvic region of zebrafish larvae during pelvic fin development. Indication of increasing eGFP fluorescence intensity ventrally: (+), +, ++, +++. Arrows point to pelvic fin bud, arrowheads mark decline of larval fin lobe. SL: standard length. **Stage 1:** No pelvic fin bud, weak ventral eGFP fluorescence. **Stage 2:** Lateral pelvic fin bud, lateral and ventral eGFP fluorescence. **Stage 3:** Size of pelvic fin bud is 1/8 of the minor lobe. **Stage 4:** Size of pelvic fin bud is 1/6 of the minor lobe. **Stage 5:** Size of pelvic fin bud is 1/4 of the minor lobe. **Stage 6:** Size of pelvic fin bud is 1/3 of the minor lobe. Anterior is to the left. Scale bars: A, 1 mm; B, 500  $\mu$ M. Figure B: Pictures and caption taken and modified from Marzi, 2015.

The subsequently performed experiments were based on long-term pharmacological treatments of double transgenic zebrafish larvae expressing the fluorescence markers *fli:eGFP* and *col2a1:mCherry* with DEAB (Breu, 2017). The *fli:eGFP* fluorescence marker is a prerequisite for the usage of the pelvic staging system by Marzi, 2015 (Fig. 10), while in *Tg(col2a1BAC:mCherry)<sup>hu5900</sup>* zebrafish chondrocytes are labelled, visualizing skeletal structures (Hammond & Moro, 2012; Lawson & Weinstein, 2002). Briefly, the fish were sorted at the age of 3 wpf according to their pelvic fin developmental stage, whereby only the earliest stages were chosen (S1 - S6). Fish that, at the time of staging, did not show ventral eGFP fluorescence at the prospective site of pelvic fin formation were referred to as S<1 and also added to the experiment. Afterwards the fish of each group were transferred to 100 ml Petri dishes and treated with 10 µM DEAB for 45 days on average. An equivalent amount of pure DMSO was used as control, whereby DMSO control groups contained larvae ranging from S<1 to S6 (Fig. 11A) (Breu, 2017).

Severe malformations up to the complete lack of pelvic girdle and fins were observed. The various malformations were classified in six skeletal malformation categories, termed SM0 - SM5 and three fin malformation categories, FM1 - FM3 (Fig. 11; Breu, 2017). In SM0, a wild type appearance of the pelvic girdle is observed (Fig. 11G). SM1, SM2 and SM3 refer to mild, medium or severe loss or reduction of skeletal substructures, which often occur in combination with asymmetry as well as lateral and/or anterioposterior dislocations (Fig. 11F,E,D). SM4 fish possess a very basic pelvic girdle, as it is normally observed much earlier in development (Fig. 11C), while the category SM5 is defined by a complete loss of pelvic girdle skeleton (Fig. 11B). In case of the formation of the exoskeletal fin part, FM1 is defined as wild type appearance (Fig. 11J). Fish assigned to FM2 exhibit a (one-sided) loss or reduction of the pelvic fins, frequently combined with a differing number of fin rays on each side (Fig. 11I). FM3 refers to a complete loss of both pelvic fins in combination with only weak remaining *fli:eGFP* signal, resembling a much earlier developmental stage (Fig. 11H).

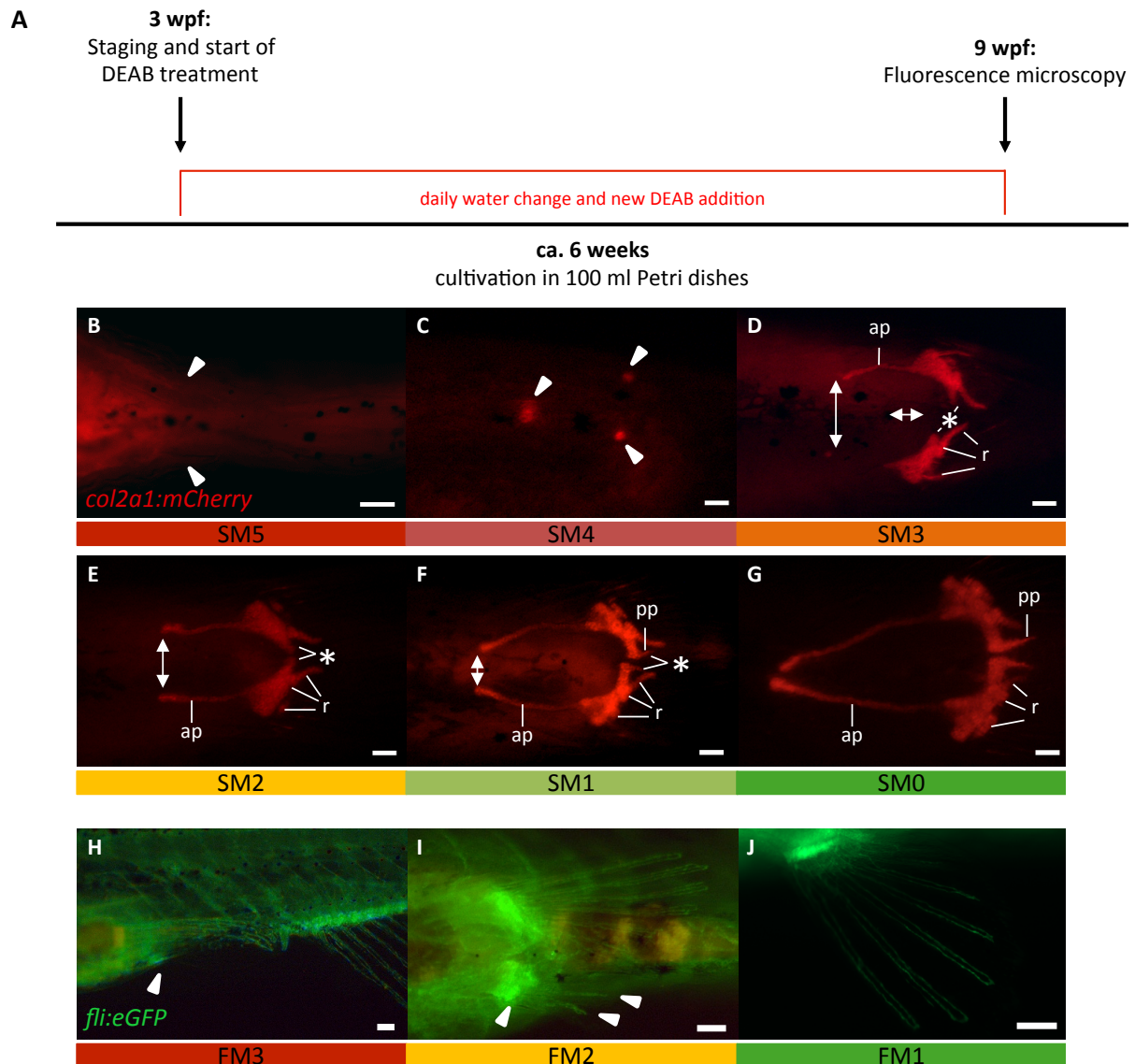


**Fig. 11 Inhibition of RA synthesis during early stages of pelvic fin development results in severe malformations of the pelvic girdle and fin, up to a complete reduction.** **A:** Workflow of long-term DEAB treatments of double-transgenic zebrafish larvae starting with the sorting of larvae based on their pelvic fin developmental stage (Marzi, 2015) followed by the treatment with 10  $\mu$ M DEAB or an equivalent amount of DMSO (control) for 45 days on average. Formed skeletal structures of the pelvic girdle and fins were then documented using *fli:eGFP* and *col2a1:mCherry* marker genes. **B-J:** Endo- (B-G) and exoskeletal (H-J) parts of the pelvic fins of juvenile zebrafish (ca. 9 wpf) after long-term DEAB treatment. Different degrees of skeletal and fin malformations (SM and FM) were observed and categories defined, SM0 - SM5 and FM1 -FM3, respectively. **B: SM5**, no skeletal elements at  $S \geq 14$ , no chondrocyte precursors (*fli:eGFP*) or chondrocytes (*col2a1:mCherry*), white arrows indicate missing pelvic girdle skeleton and fins. **C: SM4**, one- or two-sided minimal/primitive skeletal pelvic girdle element/s (represented by *fli:eGFP* and *col2a1:mCherry* signal, white arrows) with the appearance/shape of an early pelvic girdle developmental stage ( $S \leq 5$ ) present at  $S \geq 14$ . **D: SM3**, basic pelvic girdle skeletal structures present at  $S \geq 14$ , strong expression of at least one of the following criteria: complete loss (\*) and/or reductions of cartilage substructures, cartilage deformations, asymmetry, anteroposterior and/or lateral dislocation of the anterior process and/or the fin base (double arrows). **E: SM2**, Majority of the pelvic girdle cartilage structure present at  $S \geq 14$ , medium expression of at least one of the following criteria: complete loss (\*) and/or reductions of cartilage substructures, cartilage deformations, asymmetry, anteroposterior and/or

lateral dislocation of the anterior process (double arrow) and/or the fin base. **F: SM1**, Almost complete pelvic girdle cartilage structures present at  $S \geq 14$ , mild expression of at least one of the following criteria: complete loss and/or reductions (\*) of cartilage substructures, cartilage deformations, asymmetry, anteroposterior and/or lateral dislocation of the anterior process (double arrow) and/or the fin base, appearance of the pelvic girdle cartilage close to wild type condition. **G: SM0**, Complete pelvic girdle cartilage structures with wild type like appearance present at  $S \geq 14$ , undistinguishable from DMSO control, none of the above malformation criteria complied. **H: FM3**, No pelvic fins and fin rays are present on both sides at  $S \geq 14$ , no pelvic chondrocyte precursors (*fli:eGFP* signal) in most larvae, some fish exhibit a one or two sided, primitive *fli:eGFP* signal (equivalent to an early ( $S \geq 5$ ) fin developmental stage). **I: FM2**, At least one-sided basic fin structure is present at  $S \geq 14$ . Malformation, reduction or even complete loss of one fin. Asymmetric (difference between right and left fin) fin length and/or different (difference  $\geq 2$ ) number of fin rays. **J: FM1**, Two completely developed fins with wild type like morphology (undistinguishable from DMSO control), maximum difference in number of rays = 1, no difference in number of fin rays in most larvae, both fins have (almost) the same size. ap: anterior process; pp: posterior process; r: radials. Pictures B-J and capture taken with minor modifications from Breu, 2017.

The most severe categories of skeletal (SM5, SM4, SM3) and fin malformation (FM3, FM2) were mainly observed when larvae were treated with DEAB beginning from  $S < 1$ , S1 and, to a lesser extend, S2. Starting DEAB treatment at S3 or later had little or no effect on pelvic girdle and fin formation, strongly suggesting a role of RA in early pelvic fin development (Fig. 12) (Breu, 2017).

A detailed analysis of the pelvic girdle malformations revealed a significant reduction of its total length in DEAB treatment groups S1 and S2, while the total width generally was unaffected. Dislocations and asymmetries within the pelvic girdle also occurred more frequently in the groups  $S < 1$ , S1 and S2 as well as a reduction of the fin length and number of fin rays. Moreover, the overall development of the zebrafish larvae was strongly affected by DEAB, which is reflected in a significant reduction of the standard length of fish treated from  $S < 1$ , S1 and S2 (Breu, 2017).

The obtained results are in conformity with the observations of Welte, 2011 and indicate that RA plays an important role in the development of pelvic fins. It was assumed that RA acts in a very limited time frame during the early stages of fin bud formation and consequently might be involved in the initiation process. However, no influence of RA on the expression levels of the major players of pelvic fin initiation, *Pitx1* and *Tbx4*, could be proven by means of a short-time (48 h) DEAB treatment and subsequent whole-mount *in situ* hybridisation (WISH), leaving the question about potential RA targets open (Breu, 2017).

The high degree of skeletal malformations and dislocations additionally suggests a role for RA in the correct formation and positioning of the pelvic girdle skeletal structures, which also was postulated by Welte, 2011, yet.

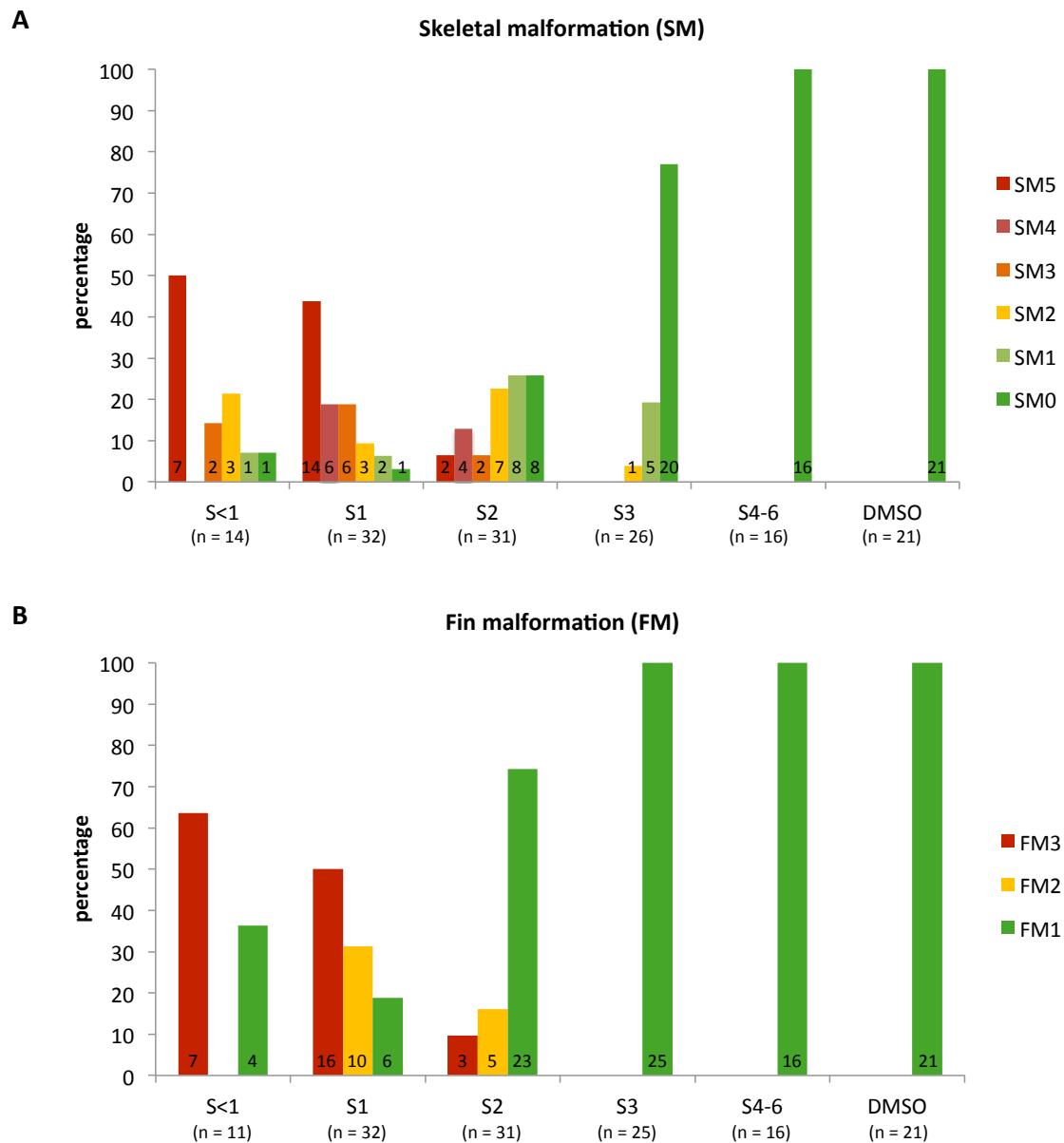


**Fig. 12** Percentage of zebrafish juveniles (ca. 9 wpf) that were assigned to the stated classes of skeletal and fin malformations (SM and FM, respectively) after long-term DEAB treatment. DMSO treatment was used as control. The numbers on the bars indicate the amount of zebrafish in the respective SM/FM class, n is the total amount of zebrafish in the respective treatment group. **A:** Skeletal malformation (SM) classification. The earlier in pelvic fin development the DEAB treatment was started, the more severe malformations were observed in the skeletal structures of the pelvic girdle, especially in treatment groups S<1 and S1. Treatment from S3 or later had only minor or no effects on pelvic girdle formation. **B:** Fin malformation (FM) classification. Similarly, the earlier in pelvic fin development the DEAB treatment was started, the more severe malformations of the pelvic fin were observed, especially in treatment groups S<1 and S1. Treatment from S3 or later no effects on pelvic fin outgrowth, resulting in phenotypes comparable to DMSO treated fish. Graphs taken and modified from Breu, 2017.

## 1.6 Goal of this study

The general aim of this study was to further investigate the exact role of RA in pelvic fin development.

For this, additional experiments that reproduce the results obtained in the Master thesis of Mike Breu (2017) and the Bachelor thesis of Cornelia Welte (2011) were performed (Breu, 2017; Welte, 2011). These were based on long-term heat-shock experiments using triple transgenic *fli:GFP;col2a1:mCherry;Hsp70l:Cyp26a1* fish. The use of transgenic zebrafish lines containing the heat-shock promoter Hsp70l enables a stable overexpression of the downstream located gene, in this case the RA-metabolizing enzyme Cyp26a1 to achieve a condition resembling a RA deficiency. This approach was already tested by Lisa Marzi in the course of her Master thesis, however toxicity of repeated heat-shock treatments hindered further investigations (Marzi, 2015). This protocol was now optimized to achieve a continuous *Cyp26a1* overexpression during the whole time span of normal pelvic fin outgrowth.

Moreover, the aim was to investigate the role of RA in zebrafish pelvic fin development via a reverse genetic approach using the Gal4-UAS system. In contrast to pharmacological or heat-shock treatments that, due to methodical limits, always affect the entire organism, this approach aimed the spatially and temporally restricted manipulation of RA signalling. Therefore, driver plasmids were created that mediate the expression of inducible *Gal4* variants (*ERT2-Gal4*, *KalTA4-ERT2* and *GAVPO*) under the control of different fin specific enhancers. In the corresponding effector plasmids the genes *Cyp26a1* and *dnRara2a* are regulated by either repetitive or non-repetitive upstream activating sequences (UAS). Following a proof-of-principle, the generation of transgenic zebrafish lines with this vector constructs was performed using the Tol2 transposon system. Eventually, crossing fish of driver and effector lines will facilitate a tissue specific disruption of RA signalling, in addition to a temporal control by the selection of the starting point of Gal4 induction.

In the course of a further project, the CRISPR/Cas system was established in the working group with the aim to create a zebrafish *Pitx1* knockout mutant for the characterization of the corresponding loss-of function phenotype in this model organism. The consequences of a functional *Pitx1* knockout were so far studied only in mice, describing severe impairments of, among others, the hindlimbs, the pelvis and the jaw (Lanctôt et al., 1999; Szeto et al., 1999). In stickleback, regulatory *Pitx1* mutations result in reduction or complete loss of the

pelvic apparatus, while other organs are unaffected (Chan et al., 2010; Sarro et al., 2018). After proving the functionality of the CRISPR/Cas9 system via a knockout of the gene *Tyrosinase* (*Tyr*), being involved in zebrafish pigmentation, short insertions and deletions (indel mutations) were introduced in the *Pitx1* gene by co-injection of target specific sgRNA and *Cas9* mRNA. Using Polymerase chain reaction (PCR) with subsequent T7 Endonuclease 1 (T7E1) assay, F0 founder fish carrying the indel mutation in the germ line, as well as heterozygous F1 fish were identified and afterwards the mutated *Pitx1* locus examined by sequencing.

## 2 Results

### 2.1 Gene expression in the pelvic fin bud during early development

In the first part of this thesis, the expression patterns of selected genes were analysed during the early stages of pelvic fin development. The aim of the project was to get an overview of the most important signalling pathways taking part in this developmental process and to map the expression domains of the respective genes. Most of the molecular processes in hindlimb development, explained in the introduction, are based on studies in mice or chicken embryos and it is not known if these findings are transferable to zebrafish. Previous expression studies on zebrafish pelvic fins were carried out by Emily Don, investigating the genes *Pitx1*, *Tbx4*, *Tbx5*, *Fgf10a*, *Fgf8a*, *Sp8* and *Shh* in larvae aged 21 and 28 dpf (Don, 2013). Here in this study, the scope was expanded and based on the classification of the pelvic fin developmental stages, defined by Lisa Marzi (Marzi, 2015) (Fig. 10, Fig. S1).

For this, *fli:eGFP* larvae were grown until an age of 3 - 4 weeks and then sorted according to their current pelvic fin developmental stage. The focus was on the Stages 1 - 6. Thereafter, whole-mount *in situ* hybridisation (WISH) was performed using specific RNA antisense probes detecting transcripts of *Pitx1*, *Tbx4*, *Prrx1a*, *Prrx1b*, *Rdh10a*, *Aldh1a2*, *Aldh1a3*, *Cyp26a1*, *Cyp26b1*, *Cyp26c1*, *Fgf8a*, *Fgf10a* and *Shh*. For a high-resolution imaging of the expression site, the stained pelvic fin buds were dissected (Fig. 13 - 15) (Eberlein, 2018a; Weber, 2020).

First of all, the fin-specific genes *Pitx1*, *Tbx4* as well as *Prrx1a* and *Prrx1b* were examined (Fig. 13). *Pitx1* expression was observed from S2 - S6 (Fig. 13A-E). In the early Stages 2, 3 and 4, the WISH staining extended over almost the entire fin bud, with exception of the most distal edge (Fig. 13A-C). Later, as the fin edge elongates, the expression area was restricted to the proximal part of the outgrowing pelvic fin bud, leaving the fin edge clear of *Pitx1* transcripts (Fig. 13D,E) (Weber, 2020). WISH staining for *Tbx4* was obtained from Stages 2 - 5. It was located in the mesenchymal area of the pelvic fin bud, excepting the most distal edge and the most proximal region (Fig. 13F-I). Consequently, it is overlapping with the *Pitx1* expression domain. In S2, *Tbx4* expression was evenly distributed over this area, while from S3 - S5 a concentration to the posterior region of the fin bud was observed (Fig. 13G-I). The

staining got more faint in Stage 5 and was no longer detectable in Stage 6 (Weber, 2020). For the two homologous genes *Prrx1a* and *Prrx1b*, intense WISH staining was detected from S2 - S6 (Fig. 13J-N and 13O-S, respectively). The expression patterns of these two genes were very similar, expanding over the entire pelvic fin bud, except of the most distal edge. The intensity of WISH staining increased from S2 to S3 and remained at this level in all developmental stages that were further examined. In addition, it was observed in S6 that the edges of *Prrx1a* and *Prrx1b* expression domains in the anterior half of the fin bud were clearly defined, while in contrast to that, in the posterior fin bud, the transition of the stained mesenchymal area to the clear fin edge was blurred (Fig. 13N,S) (Eberlein, 2018a).

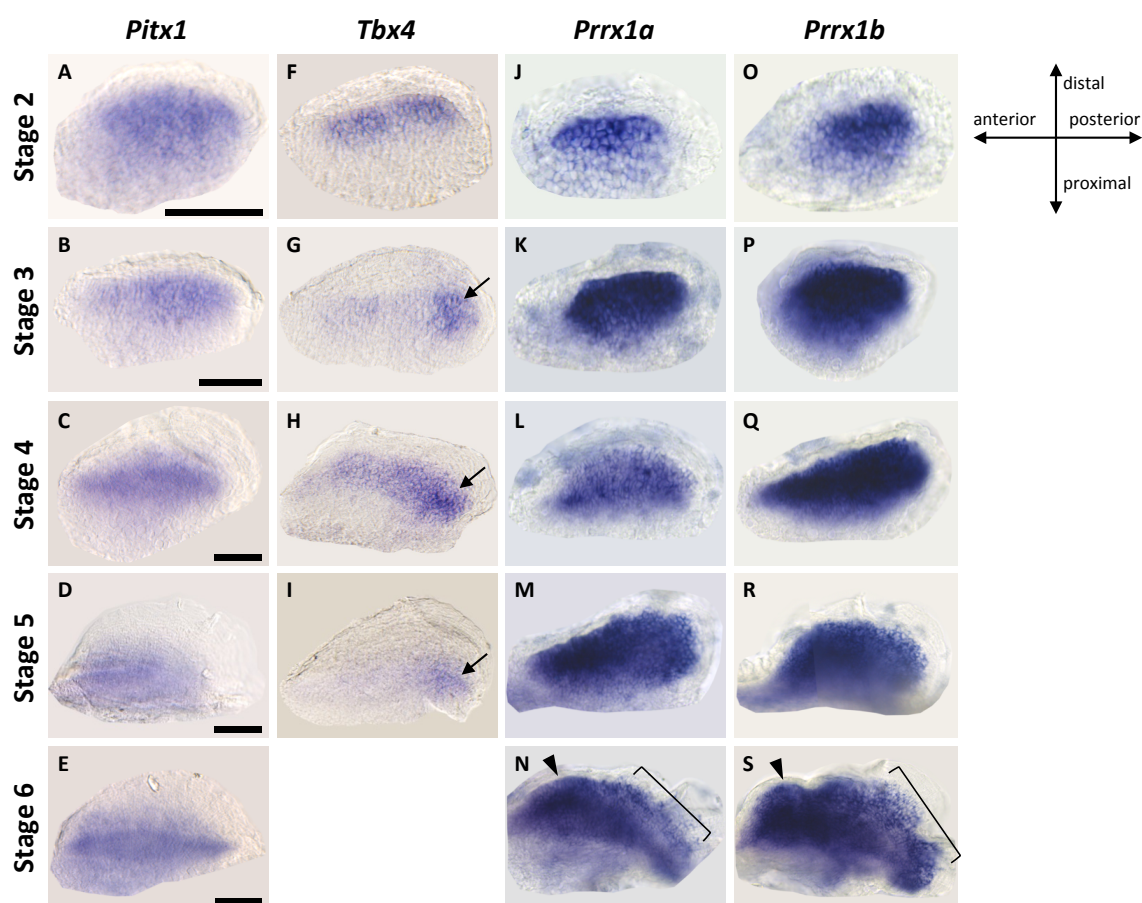


**Fig. 13 Expression patterns of *Pitx1*, *Tbx4*, *Prrx1a* and *Prrx1b* during the early stages of pelvic fin development.** WISH was performed on *fli:eGFP* zebrafish larvae of pelvic fin developmental stages 2 - 6 at an age of approximately 3 - 4 wpf. Stained pelvic fin buds were dissected and subsequently imaged by means of bright field microscopy. **A-E:** *Pitx1*. Expression from S2 - S6 in the fin bud mesenchyme. **F-I:** *Tbx4*. Expression from S2 - S5 in the fin bud mesenchyme, excepting the most proximal part. From S3 - S6 it concentrates in the posterior region (arrows). **J-N:** *Prrx1a*. **O-S:** *Prrx1b*. Strong expression of both *Prrx1* genes in the fin bud mesenchyme in all stages. Arrowheads are pointing to the sharp border between the *Prrx1a/1b* expression domain and the fin fold, while brackets indicate an area of blurred transition. The cross on the right shows the orientation of the pelvic fin buds. Scale bars: 50  $\mu$ m. Pictures A-I by Sophia Weber, J-S by Jean Eberlein. Taken and modified from Weber, 2020 and Eberlein, 2018a.

Next, important genes of the RA signalling pathway - *Rdh10a*, *Aldh1a2*, *Aldh1a3*, *Cyp26a1*, *Cyp26b1* and *Cyp26c1* - were examined for their expression during early pelvic fin development. *Rdh10a*, encoding the enzyme that transforms ROL to RAL, was detected earliest at S2, showing weak WISH staining in the posterior pelvic fin bud. The staining intensity increased steadily as the bud grows out, while the expression area remained restricted to the proximal, mesenchymal region (Fig. 14A-E) (Weber, 2020).

The expression of *Aldh1a2* was detected from S3 - S6 (Fig. 14F-I). It showed a conspicuous expression pattern, which was restricted to a certain area in the posterior part of the outgrowing pelvic fin bud. In S5, the *Aldh1a2* expression domain began to expand anteriorly (Fig. 14H). In S6, it extended over the entire length of the pelvic fin bud, with the area of highest expression still localizing posteriorly (Fig. 14I). Across all examined developmental stages, *Aldh1a2* expression was limited to the proximal region of the fin bud (Weber, 2020).

Similarly, *Cyp26b1* expression first occurred at S3 and localized in a defined spot in the centre of the pelvic fin bud, with a slight tendency to the posterior region (Fig. 14J). Consequently, it localizes right next to the *Aldh1a2* expression domain in this developmental stage. In the following Stages 4 and 5, WISH staining of *Cyp26b1* expanded more anteriorly, always being limited to the fin bud mesenchyme. Additionally, high *Cyp26b1* expression was detected in the lateral plate mesoderm just beneath the outgrowing fin bud, which is seen in the preparations of the S4 and S5 fin buds (Fig. 14K,L) (Eberlein, 2018a; Weber, 2020).

In contrast to that, *Cyp26c1* showed a completely different expression pattern. This gene was detected only in Stages 2 and 3. The WISH staining localized in the most distal part of the pelvic fin bud, extending in anteroposterior orientation along the entire fin edge (Fig. 14M,N) (Weber, 2020). For the remaining two genes, *Aldh1a3* and *Cyp26a1*, no expression could be detected in the pelvic fin bud in any of the investigated developmental stages (Weber, 2020) (data not shown).

The next genes to be examined were *Fgf8a*, *Fgf10a* and *Shh* that are all known to play a key role during limb development. The gene *Shh* is expressed in a defined area in the posterior margin of the pelvic fin bud from S2 - S4 (Fig. 15K-M). In S5, the expression pattern changes completely and WISH staining is now found in five distinct stripes, orientated proximodistally, presumably defining the places of fin ray formation (Fig. 15N). The expression pattern of *Shh* in S6 was not determined (Eberlein, 2018a).

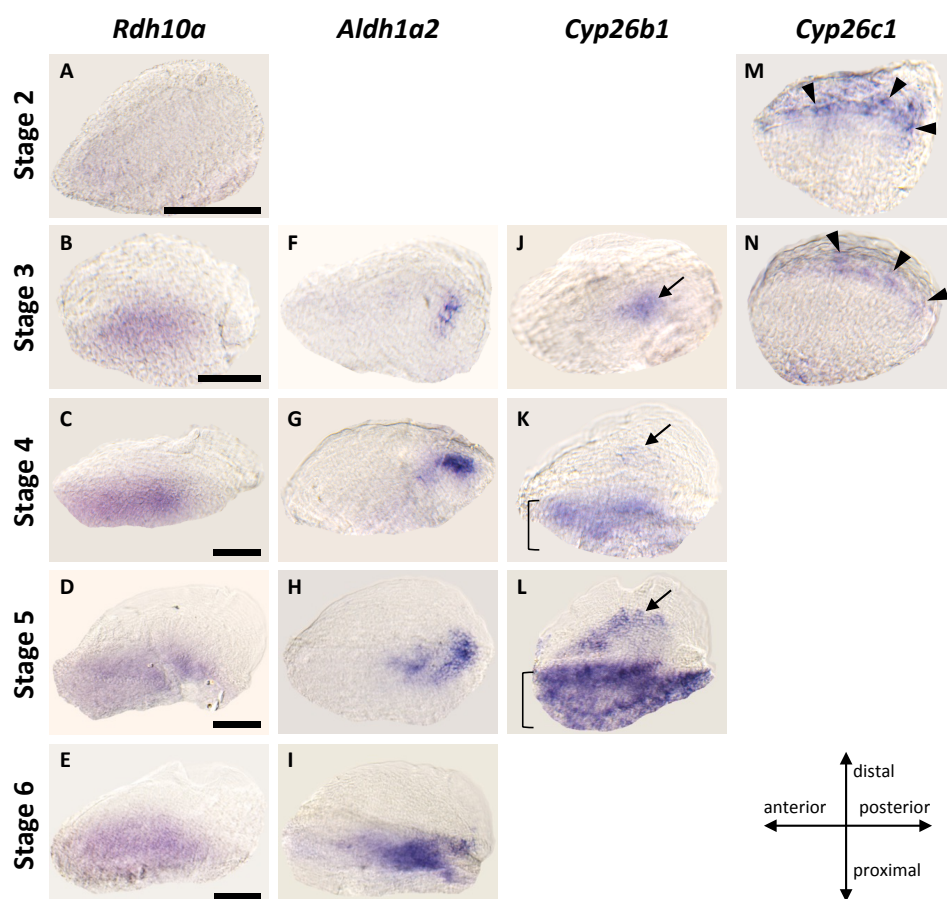


**Fig. 14 Expression patterns of *Rdh10a*, *Aldh1a2*, *Cyp26b1* and *Cyp26c1* during the early stages of pelvic fin development.** WISH was performed on *fli:eGFP* zebrafish larvae of pelvic fin developmental stages 2 - 6 at an age of approximately 3 - 4 wpf. Stained pelvic fin buds were dissected and subsequently imaged by means of bright field microscopy. **A-E: *Rdh10a*.** Expression from S2 - S6 in the fin bud mesenchyme. **F-I: *Aldh1a2*.** Expression from S3 - S6, localized posteriorly in S3 and S4, from S5 on it expanded in anterior direction. **J-L: *Cyp26b1*.** Expression from S3 - S5 in the fin bud mesenchyme (arrows), in S3 restricted to a distinct spot in the centre of the fin bud. Brackets mark the tissue of the LPM beneath the fin bud showing *Cyp26b1* expression. **M-N: *Cyp26c1*.** Expression in S2 and S3, restricted to the most distal fin edge (arrowheads). The cross shows the orientation of the pelvic fin buds. Scale bars: 50  $\mu$ m. All pictures by Sophia Weber, taken and modified from Weber, 2020.

Surprisingly, *Fgf8a* expression was detected in the fin bud mesenchyme, right in the centre of the outgrowing fin bud (Fig. 15A-E). The intense WISH staining was first detected in S2 and remained at least until S6. These observations were made twice, in two independent WISH experiments, carried out by two different students (Eberlein, 2018a; Weber, 2020). These results are contradictory to the knowledge gained from studies on mouse and chicken embryos that unanimously identified *Fgf8* as a marker for the apical ectodermal ridge (see Fig. 4; Fernandez-Teran & Ros, 2008). Moreover, they do not reproduce the data of Don, 2013, where an expression along the distal edge of the pelvic fin bud was described. Therefore the identity of the WISH probe was additionally checked by Sanger sequencing

and confirmed as *Fgf8a* (Fig. S2). The expression pattern of *Fgf10a* is very similar to that of *Fgf8a*. *Fgf10a* is expressed from S2 - S6 in the fin bud mesenchyme. However, unlike than *Fgf8a*, it expands more distally, forming a defined border to the overlying ectoderm (Fig. 15F-J) (Eberlein, 2018a). The *Fgf10a* probe was also checked by sequencing to avoid confusion (Fig. S3). These results on the expression of *Fgf8a* and *Fgf10a* suggest a completely different mechanism for the outgrowth of pelvic fins compared to what is known from the hindlimbs of mice or chickens.

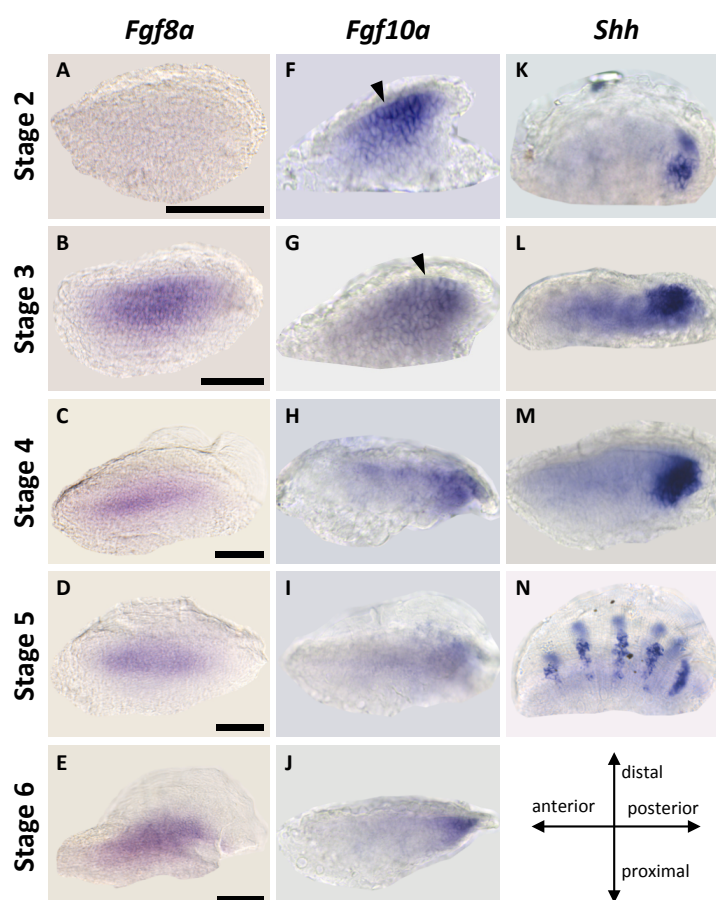


**Fig. 15 Expression patterns of *Fgf8a*, *Fgf10a* and *Shh* during the early stages of pelvic fin development.**

WISH was performed on *fli:eGFP* zebrafish larvae of pelvic fin developmental stages 2 - 6 at an age of approximately 3 - 4 wpf. Stained pelvic fin buds were dissected and subsequently imaged by means of bright field microscopy. **A-E:** *Fgf8a*. Expression in the fin bud mesenchyme from S3 - S6. No WISH staining was detected in the distal edge of the fin bud. **F-J:** *Fgf10a*. Expression in the fin bud mesenchyme from S2 - S6, forming a defined border to the overlying ectoderm in S2 and S3 (arrowheads). **K-N:** *Shh*. Expression in a defined posterior area from S2 - S4; in S5 in five separate, proximodistally orientated stripes. The cross shows the orientation of the pelvic fin buds. Scale bars: 50  $\mu$ m. Pictures A-E by Sophia Weber, F-N by Jean Eberlein. Taken and modified from Weber, 2020 and Eberlein, 2018a.

## 2.2 Manipulation of the retinoic acid pathway during pelvic fin development

In order to gain an expanded view of the consequences that manipulation of the RA signalling pathway has on the development of zebrafish pelvic fins, further experiments were performed to complement those carried out by Breu, 2017 and Welte, 2011.

### 2.2.1 Overexpression of *Cyp26a1* using a transgenic zebrafish line

The strategy focused on the transgenic zebrafish line *Hsp70l:Cyp26a1*, which stably overexpresses *Cyp26a1* upon heat-shock treatment (Blum & Begemann, 2012; Kikuchi et al., 2011). Regularly repeated heat-shocks were performed to achieve and maintain a RA-deficiency situation during the entire time span, in which normally pelvic fin formation takes place. After approximately four weeks of treatment, the effects on pelvic girdle and fins were examined using fluorescence microscopy, as previously described (Breu, 2017).

The heterozygous *Hsp70l:Cyp26a1* fish were first mated with *fli:eGFP;col2a1:mCherry* double transgenic fish and the larvae identified for both fluorescence markers. At an age of 3 - 4 weeks, the larvae were sorted depending on their stage of pelvic fin development, whereby only individuals of Stages S<1, S1 and S2 were included in the experiment. Using this setup, each treatment group automatically contains *Hsp70l:Cyp26a1*<sup>+/-</sup> and *Hsp70l:Cyp26a1*<sup>-/-</sup> fish, providing an internal control and ensuring an identical treatment of all animals. Only at the end of the experiment, each individual was genotyped by PCR.

A total of five runs were carried out to determine the optimal heat-shock conditions that cause an effect, but are not fatal for the larvae. These runs differed in terms of temperature, number of heat-shocks as well as time span between subsequent treatments. On the one hand, it turned out that temperatures of 37 °C and 38 °C are not sufficient to achieve an effective level of *Cyp26a1* overexpression in larvae of this age. On the other hand, it was observed that heat-shocks at 38.5 °C have an effect, but result in a high mortality rate if performed too frequently (Draut, 2020; Mayer, 2020, with additional support by Lina Stacker). The final experimental workflow combines the experience from these preliminary experiments and is visualized in Fig. 16A. The successful overexpression was confirmed by performing one single heat-shock treatment at 38.5 °C for 1.5 h with subsequent WISH against *Cyp26a1* 48 h thereafter (Fig. S4).

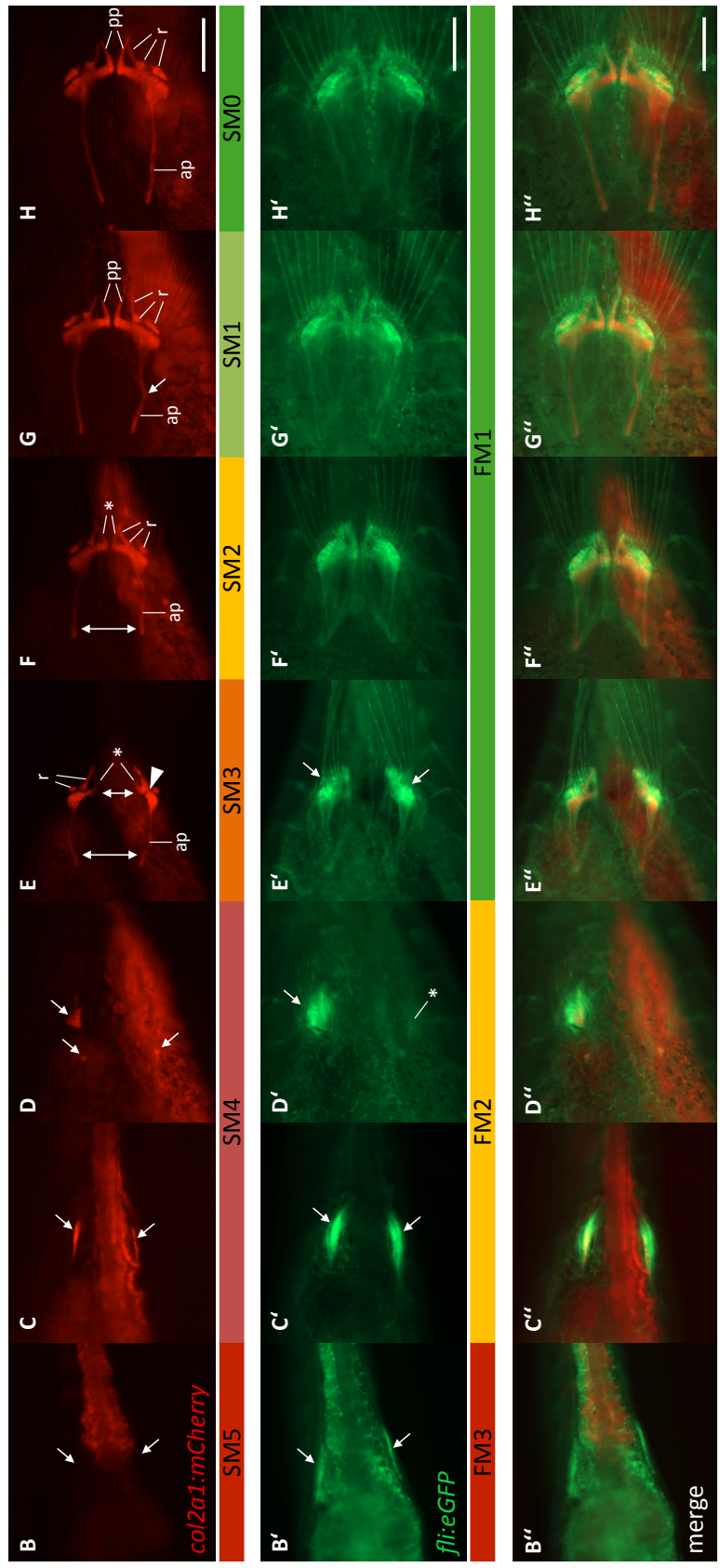
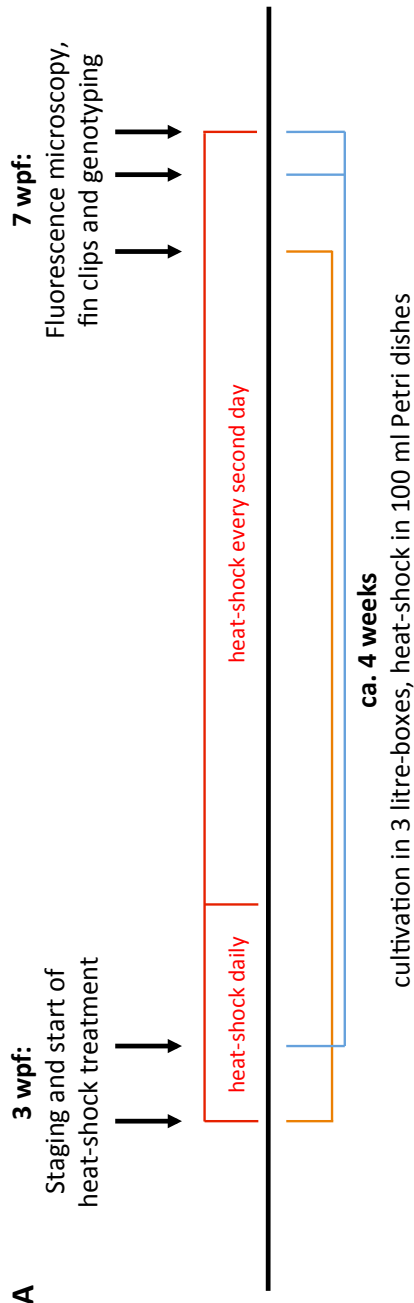


**Fig. 16 Increased RA metabolism due to *Cyp26a1* overexpression during early stages of pelvic fin development results in severe malformations of the pelvic girdle and fin, up to a complete reduction.**

**A:** Workflow of long-term heat-shock treatments of double-transgenic (*Hsp70l:Cyp26a1*<sup>-/-</sup>;*fli:eGFP*<sup>+/-</sup>;*col2a1:mCherry*<sup>+/-</sup>) or triple-transgenic (*Hsp70l:Cyp26a1*<sup>+/-</sup>;*fli:eGFP*<sup>+/-</sup>;*col2a1:mCherry*<sup>+/-</sup>) zebrafish larvae. The experiment started with the sorting of larvae based on their pelvic fin developmental stage (Marzi, 2015) followed by repeated heat-shock treatments for ca. 4 weeks. Skeletal structures of the pelvic girdle and fins were then documented based on *fli:eGFP* and *col2a1:mCherry* marker genes. Arrows indicate days of staging and microscopy. The red bracket relates to the entire experiment, the blue and orange brackets to individual treatment periods. **B-H:** Pelvic girdles and fins (ventral view) of juvenile zebrafish (ca. 7 wpf) after long-term heat-shock treatment. Different degrees of skeletal and fin malformations (SM and FM, respectively) were observed and the individuals sorted into the classes SM0 - SM5 (**B-H**) and FM1 - FM3 (**B'-H'**), according to Breu, 2017 (see Fig. 11). **B:** **SM5**, no skeletal elements (arrows). **C/D:** **SM4**, minimal pelvic girdle structures (arrows). **E:** **SM3**, severe loss or reduction of skeletal substructures, asymmetry, lateral and/or anterioposteror dislocations. **F:** **SM2**, medium loss or reduction of skeletal substructures, asymmetry, lateral and/or anterioposteror dislocations. **G:** **SM1**, minimal reduction of skeletal substructures, asymmetry, lateral and/or anterioposteror dislocations. **H:** **SM0**, complete pelvic girdle structures. **B':** **FM3**, no pelvic fins on both sides, only weak eGFP signal (arrows). **C'/D':** **FM2**, basic pelvic fin structure (at least on one side), asymmetric fin length and/or different number of fin rays (arrows). **E'-H':** **FM1**, two complete developed fins. Malformed pelvic girdle might impair attachment of fins (arrows in E'). Double arrows indicate asymmetry or dislocations, asterisks mark reduced or missing structures. The arrowhead points to a cleaved fin base. ap: anterior process; pp: posterior process; r: radials. B''-H'' show merged images. Scale bars: 100 µm. The workflow was established in collaboration with Anna-Maria Mayer (Mayer, 2020), the classification was adapted from Breu, 2017.

Three days apart, two separate staging procedures were performed with siblings from the same clutch. Thereafter, the individual groups (S<1, S1 and S2) were kept in 3 litre-boxes for the duration of the entire experiment. Only for the heat-shocks, the larvae were transferred into 100 ml Petri dishes and put back immediately after the treatment. The first heat-shock was carried out the subsequent day after the staging procedure at a temperature of 38.5 °C for 1.5 h. During the first week, the heat-shock was repeated daily, whereby the larvae from the first staging date received seven subsequent treatments, and the larvae from the second staging date four. For the next three weeks, the heat-shock was carried out every other day under the same conditions (Fig. 16A). The microscopy took place after a period of four weeks; at this point 81 % of the treated fish had developed a complete pelvic fin (Fig. 17B). Compared to the long-term DEAB treatments performed by Breu, 2017, the treatment period was relatively short, however the keeping conditions in 3 litre-boxes, instead of 100 ml Petri dishes, enabled the fish to grow significantly faster during this time, thus making up for this difference. The overall survival rate was 66 % for treatment group S<1 (38/57), 80 % for S1 (25/31) and 100 % for S2 (5/5). This includes both, *Hsp70l:Cyp26a1*<sup>-/-</sup> and *Hsp70l:Cyp26a1*<sup>+/-</sup> fish as this value was determined before genotyping. The significant

mortality might be related to a serious side effect that was noted in some *Hsp70l:Cyp26a1<sup>+/-</sup>* fish, which is a destruction of the eye lenses (Fig. S5); a phenotype that was already documented previously (Nicola Blum, unpublished).

Regarding the pelvic girdle and the exoskeletal fin part, phenotypes of various degrees of severity were obtained that could be assigned to the malformation classes defined by Breu, 2017 (Fig. 16B-H and 16B'-H'; compare to Fig. 11B-G and 11H-J, respectively). Fig. 17 shows the distribution of these different phenotypes among the individual treatment groups. There was an obvious difference between *Hsp70l:Cyp26a1<sup>+/-</sup>* and *Hsp70l:Cyp26a1<sup>-/-</sup>* fish with the most severe phenotypes generally being found in treatment groups S<1 and S1.

A total of 24 % of *Hsp70l:Cyp26a1<sup>+/-</sup>* fish in group S<1 (4/17) and 7 % in S1 (1/14) were classified as SM5 since they developed no pelvic girdle skeletal structures at all (Fig. 16B; Fig. 17A). The phenotype of SM5 per definition resembles the phenotype of the pelvic fin developmental Stage 1. Further 18 % (3/17) of the larvae from group S<1 and 21 % (3/14) from group S1 were assigned to the malformation class SM4 since their pelvic phenotype at 7 wpf corresponds still to an early developmental stage ranging between S6 - S9 (Fig. 16C,D). Hereby, 4 of the 6 *Hsp70l:Cyp26a1<sup>+/-</sup>* fish, classified as SM4, exhibited an asymmetric pelvic girdle, with one side corresponding to the appearance of an early developmental stage and the counterpart on the opposite side missing completely (Fig. 16D). Phenotypes of class SM3 were also found with high frequencies in all treatment groups of *Hsp70l:Cyp26a1<sup>+/-</sup>* fish (S<1: 29 %; S1: 64 %; S2: 33 %) (Fig. 16E; Fig. 17A). These are defined as severe loss or reduction of skeletal substructures, frequently appearing together with asymmetry, lateral and/or anterioposterior dislocations. Only a minor number of all treated *Hsp70l:Cyp26a1<sup>+/-</sup>* fish developed a pelvic girdle that resembles (almost) the wild type (SM1 and SM0; a total of 5/34; 15 %; originating from groups S<1 and S2) (Fig. 16G-H; Fig. 17A).

In contrast to that, the majority of all *Hsp70l:Cyp26a1<sup>-/-</sup>* control fish show a correctly developed pelvic girdle skeleton (SM0; 14/34; 41 %; originating from groups S<1 and S1) (Fig. 16H; Fig. 17A) or exhibit at least minimal malformations (SM1; 7/34; 21 %; originating from groups S<1 - S2) (Fig. 16G; Fig. 17A). Moderate malformations of class SM2 (Fig. 16F) were found with a total frequency of 29 % (10/34; originating from groups S<1 - S2) (Fig. 17A). Only 2 of 21 individuals (10 %) of the *Hsp70l:Cyp26a1<sup>-/-</sup>* fish in group S<1 showed a significant reduction of the pelvic girdle to minimal remaining skeletal structures (SM4) (Fig. 16C-D; Fig. 17A). A false negative PCR result for these two individuals can be excluded,

as the PCR was repeated three times using two independently prepared extracts of genomic DNA from fin tissue, always giving the same outcome.

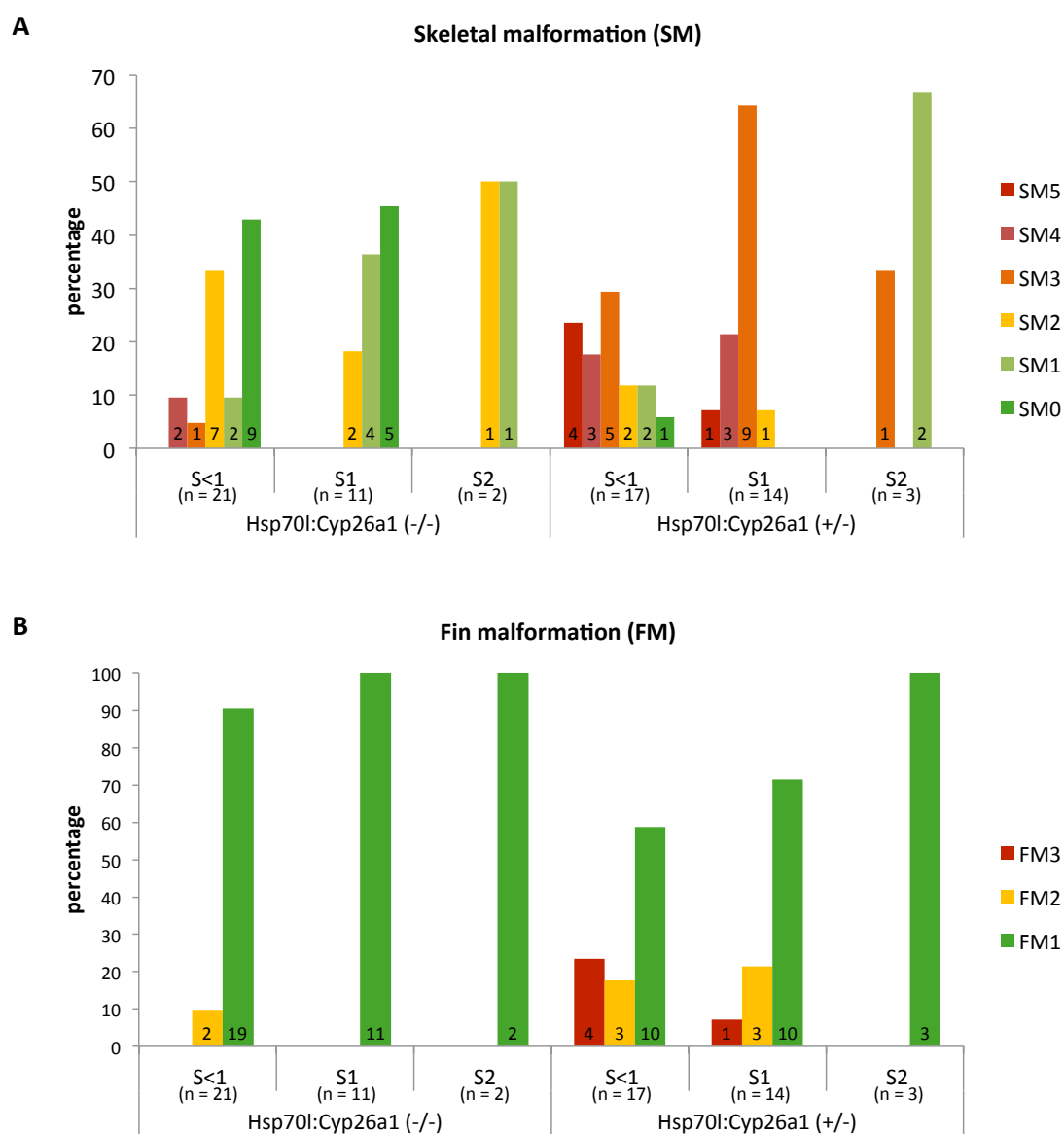


**Fig. 17** Percentage of zebrafish juveniles (ca. 7 wpf) that were assigned to the stated classes of skeletal and fin malformations (SM and FM, respectively) after long-term heat-shock treatment. The numbers on the bars represent the numbers of zebrafish in the respective SM/FM class; n is total number of zebrafish in the respective treatment group. There is an unambiguous difference between *Hsp70l:Cyp26a1*<sup>+/+</sup> fish and *Hsp70l:Cyp26a1*<sup>-/-</sup> control fish. Fish treated from S<1 were generally affected the most. The later in development the heat-shock-treatment started the less pronounced are the malformations and reductions of pelvic girdle and fin. **A:** Skeletal malformation (SM) classification. In *Hsp70l:Cyp26a1*<sup>+/+</sup> fish, severe malformations and reductions of the pelvic girdle skeletal structures (SM5, SM4, SM3) were observed in 76 % of the individuals (26/34), originating almost exclusively in treatment groups S<1 and S1. In *Hsp70l:Cyp26a1*<sup>-/-</sup> control fish only 9 % of all fish were classified as SM4 or SM3 (3/34), whereby these were from group S<1. SM5 fish were not found. **B:** Fin malformation (FM) classification. Similarly, the most severe malformations and reductions of the pelvic fin (FM3, FM2) were observed in *Hsp70l:Cyp26a1*<sup>+/+</sup> fish, exclusively in treatment groups S<1 and S1. Thereby, a total of 15 % (5/34) were classified FM3 and 18 % FM2 (6/34). The classification was adapted from Breu, 2017.

In case of the exoskeletal part of the pelvic fin, normal outgrowth was observed in 81 % of all treated fish (55/68) (Fig. 16E'-H'; Fig. 17B). An amount of 24 % of all *Hsp70l:Cyp26a1*<sup>+/-</sup> fish in treatment group S<1 (4/17) and 7 % in group S1 (1/14) were assigned FM3 due to their failure to develop any exterior pelvic fin structures (Fig. 16B'; Fig. 17B). In the same two groups (S<1, S1), a total of six fish developed only small pelvic fin buds during the treatment period, classified as FM2. Those are representing a phenotype comparable to the pelvic fin appearance of much earlier developmental stages between S6 - S9 (Fig. 16C',D'; Fig. 17B). Four of these FM2 fish exhibited this phenotype only on one side, while the fin on the opposite side was reduced completely (Fig. 16D').

Of the *Hsp70l:Cyp26a1*<sup>-/-</sup> control fish almost all individuals, with the exception of two fish in treatment group S<1 that were assigned to FM2, exhibited a normal sized, symmetrical pair of pelvic fins (FM1, 32/34, 94 %) (Fig. 16 E'-H'; Fig. 17B).

To gain a deeper understanding of the exact consequences that RA-deficiency has on pelvic girdle and fin formation, a quantification of defined distances within the pelvic girdle (Fig. 18A,A') as well as general features of the juvenile zebrafish was done, accordingly to previous work (Breu, 2017). It was observed that throughout all treatment groups (S<1, S1, S2) the standard length of *Hsp70l:Cyp26a1*<sup>+/-</sup> fish was significantly reduced compared to their *Hsp70l:Cyp26a1*<sup>-/-</sup> siblings (Fig. 18B). Furthermore, also the fin or fin bud length showed a significant reduction in all treatment groups (Fig. 18C). This value was calculated as percentage of the standard length for a better comparison of the data based on the assumption that generally larger fish exhibit larger pelvic fins / fin buds. This phenotype is accompanied by a reduced number of fin rays, which is significantly differing from the control fish at least in treatment groups S1 and S2 (Fig. 18D). Thus, overexpression of *Cyp26a1* negatively impaired the overall growth of zebrafish larvae, which is reflected in a significant reduction of the standard length, the length of the fin (bud) as well as the number of fin rays, in case fish were treated beginning from stages S<1, S1 or S2.

Next, the length and width of the pelvic girdle itself and distances within this structure were quantified based on a measurement method established previously (Breu, 2017). Fig. 18A shows the pelvic girdle of a *Hsp70l:Cyp26a1*<sup>-/-</sup> control fish in SM0 and Fig. 18A' the pelvic girdle of a *Hsp70l:Cyp26a1*<sup>+/-</sup> fish in SM3 to illustrate the distances taken into account. The total length and width of the pelvic girdle were calculated as percentage to the standard length. In case of the total length, a significant reduction compared to the control data was

observed in treatment groups S<1 and S1 (Fig. 18E). For the total width similar values were measured in all three groups, independently of the genotype, indicating RA signalling has no influence on this feature (Fig. 18E). The evaluated distances within the pelvic girdle were determined from four specific points in the pelvic girdle: a1, a2, b1 and b2 and henceforth referred to as AL, BL, AW and BW (Fig. 18A,A') (Breu, 2017). Distances between these points were calculated as percentage to the total length or width of the respective individual. Generally, throughout all treatment groups, larger values were measured for *Hsp70l:Cyp26a<sup>+/-</sup>* fish, compared to control fish (Fig. 18F,G). However, the distances AL and BL are quite variable, which resulted in enormous standard deviations, which in turn are the reason for lower levels of significance. Nevertheless, significant higher values, in comparison to control data, were obtained for the distance AL in treatment groups S<1 and for distance BL in groups S<1 and S1 (Fig. 18F). Considering the lateral distance AW and BW, significant enlargements in *Hsp70l:Cyp26a<sup>+/-</sup>* fish were observed for both values throughout all three treatment groups, with the exception of distance AW in the group treated from S2 onwards (Fig. 18G).

Summarizing these heat-shock experiments, increasingly severe reductions and malformations of the exo- and endoskeletal parts of the pelvic fin were obtained the earlier in development the heat-shock treatment was started (Fig. 16,17). The overall developments of the entire larvae as well as the pelvic girdle and fin were affected the most when *Cyp26a1* overexpression was started from S<1 and S1. With the start of the heat-shock-treatment in developmental Stage 2 the effect is decreasing, albeit still measurable (Fig. 17,18). This strongly suggests that RA acts during the short time period between S<1 to S1 and that its influence on outgrowth and the development of relevant pelvic fin features decreases in S2. On the other hand, considering the generally delayed growth of the larvae (Fig. 18B) and other severe side effects (Fig. S5), which are caused by *Cyp26a1* overexpression, the total or partial absence of pelvic fin structures could also be attributed to this circumstance and not to a specific effect of RA signalling on pelvic fin formation. If the phenotypes obtained in the heat-shock experiments (Fig. 16) are compared to the appearance of the pelvic fins in untreated fish of diverse developmental stages (Fig. 3), this seems likely. The pelvic phenotype of the individuals assigned to SM4 (Fig. 16C) resembles a normal pelvic girdle skeleton of a larva in developmental Stage 7 (Fig. 3E) and similarly the SM3 phenotype (Fig. 16E) is comparable to the developmental Stage 9 (Fig. 3F).

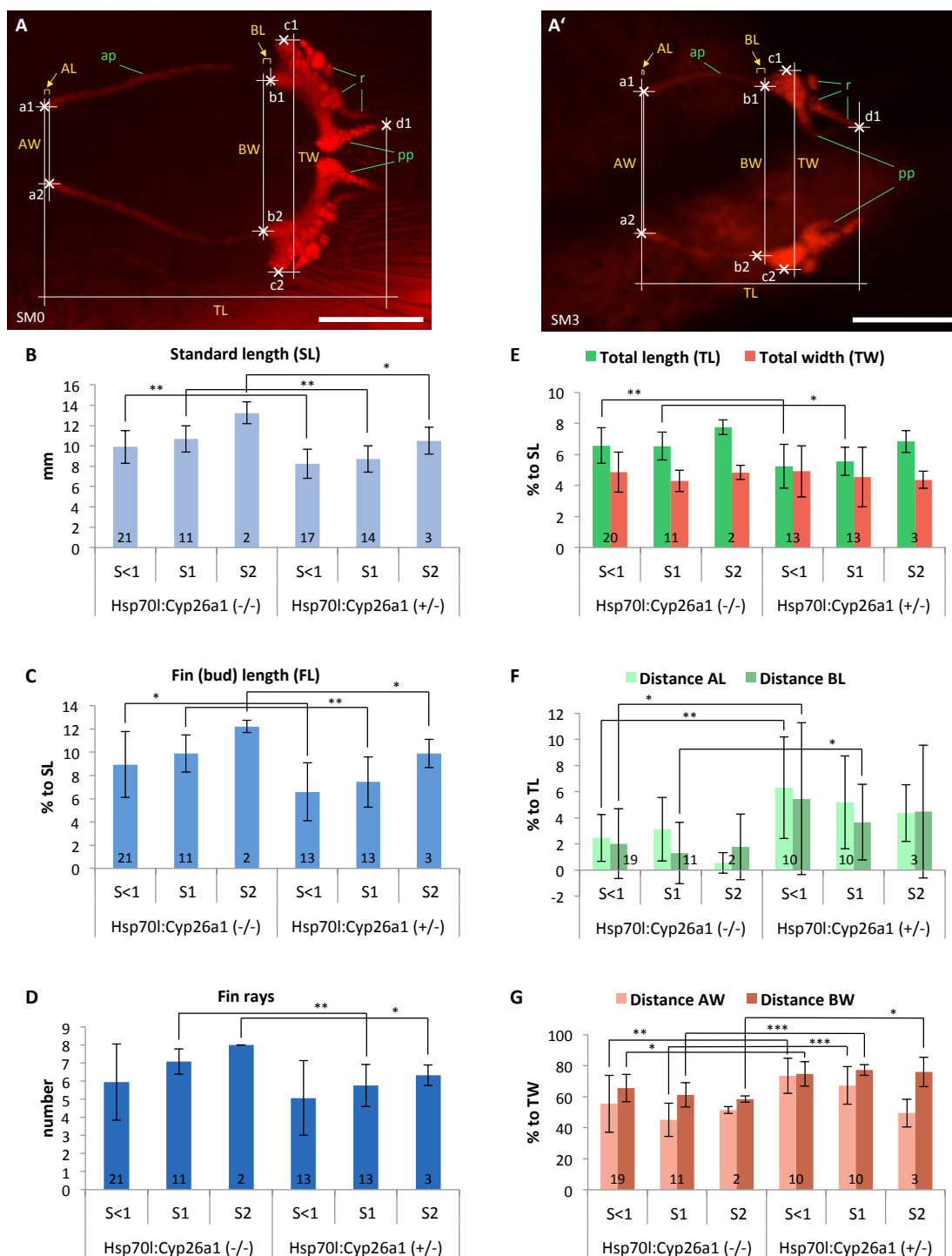


**Fig. 18 Quantification of pelvic girdle dislocations caused by *Cyp26a1* overexpression.** A/A': Zebrafish pelvic girdle assigned to SM0 (A) and SM3 (A') to illustrate the distances measured for quantification of malformations caused by *Cyp26a1* overexpression. Measurement points are marked white, structures of the pelvic girdle are labelled in green and distances in yellow. ap: anterior process, pp: posterior process, r: radials. TL: total length. TW: total width. AL: anteroposterior distance between a1 and a2. AW: lateral distance between a1 and a2. BL: anteroposterior distance between b1 and b2. BW: lateral distance between b1 and b2. Pictures are taken from ventral view with anterior to the left. Scale bar: 200  $\mu$ m. B-D: Quantification of changes in general features of the larvae - standard length (B), length of fin (bud) (C) and number of fin rays (D). E-G: Quantification of certain distances within the pelvic girdle depicted in A and A'. The numbers on the bars represent the number of zebrafish individuals taken into account for the respective evaluation. Significant deviations from the control data were determined using a t-test. \*:  $p < 0,05$ ; \*\*:  $p < 0,005$ ; \*\*\*:  $p < 0,0005$ . The measurement method and the quantification was adapted from Breu, 2017.

### 2.2.2 Analysis of the expression pattern in the pelvic fin bud after *Cyp26a1* overexpression

In a further experiment, the focus was laid on the investigation of potential target genes during pelvic fin development, which are responsive to RA signalling. For this, short-term heat-shock treatments using the same *fli:eGFP;col2a1:mCherry;Hsp70l:Cyp26a1* fish were conducted. These were based on one single heat-shock treatment for 1.5 h at 38.5 °C. It was performed on larvae of 3 - 4 wpf that were sorted, immediately before, according to their pelvic fin development and divided into groups S<1, S1, S2 and S4-6. Then, 24 h after the treatment, the larvae were fixed and whole-mount *in situ* hybridisation (WISH) was conducted. The focus was on the genes *Pitx1*, *Tbx4*, *Fgf10a*, *Fgf8a* and *Aldh1a2* to detect potentially changed expression patterns in response to decreased RA signalling. As a control for an effective heat-shock, the increase of *Cyp26a1* expression was examined. The genotyping of *Hsp70l:Cyp26a1*<sup>-/-</sup> fish and *Hsp70l:Cyp26a1*<sup>+/-</sup> fish was done by means of PCR at the end of the experiment, following the WISH staining (Weber, 2020).

At the first view, for neither gene, except *Cyp26a1*, a difference of the expression patterns or intensities was observed, when comparing *Hsp70l:Cyp26a1*<sup>-/-</sup> fish to *Hsp70l:Cyp26a1*<sup>+/-</sup> fish. To quantify this data, the larvae were sorted according to their intensity of the WISH staining and divided into categories of strong gene expression, weak or none. Representative images for the three categories in each developmental stage and a graphical representation of the numbers of larvae assigned to these are shown in Fig. S6 - S11. For each of the investigated genes, larvae exhibiting different intensities of WISH staining in pelvic fin buds were found throughout all developmental stages, independently of the genotype. However, this observation cannot be attributed to a deficient heat-shock treatment, since a significantly increased *Cyp26a1* expression was found in the pelvic region (Fig. S11) (Weber, 2020). Interestingly, in contrast to the expression studies described in section 2.1, *Aldh1a2* expression was detected also in S1 and S2 in this experimental series (Fig. S10) (Weber, 2020). These results therefore do not allow a statement about possible target genes that are sensitive to altered RA concentrations. Possibly the experimental was not suitable or the actual target genes were not among those examined. This brings about the necessity of further experiments that need to be performed to elucidate the underlying mechanisms, which are responsible for the reduction of pelvic fin structures following impairment of RA signalling.

## 2.3 Establishment of the Gal4-UAS system in zebrafish

In the main project of this study, the GAL4-UAS system was established to achieve a targeted disruption of RA signalling specifically in pelvic fins of zebrafish without affecting the entire organism. Fin specific enhancers are chosen to mediate a tissue specific *Gal4* expression. Via simultaneous application of inducible Gal4 variants, additionally a temporal control is provided by the selection of the starting point of Gal4 induction.

### 2.3.1 Establishment of UAS effector lines to manipulate RA signalling

To investigate the role of RA in pelvic fin development, the genes *Cyp26a1* and *dnRara2a*, whose proteins play an essential role in the RA signalling pathway, were selected. To clone the first series of effector plasmids, the basic vector pSELF (p347) was used, which is characterized by 5' and 3' minimal Tol2 *cis* sequences (miniTol5' and miniTol3') that flank the insert to be integrated in the genome by Tol2 Transposase activity. Further, it contains a transcriptional start site (TSS), five repetitive upstream activating sequences (5xUAS) and an  $\alpha$ -crystallin-promoter connected to *mRFP* (Fig. 19). The latter construct facilitates the identification of successfully generated transgenic larvae. It provides a visual marker, in which a red fluorescence of the eye lenses is mediated by the activity of the  $\alpha$ -crystallin-promoter (Runkle et al., 2002). The genes *dnRara2a* and *Cyp26a1* were linked to the reporter gene *eGFP* in two different ways. *Cyp26a1* was connected to *eGFP* via a short sequence encoding a linker peptide consisting of three consecutive Glycine residues (3xGly). This construct produces a fusion protein (Fig. 19A). In contrast to that, in the *dnRara2a* construct, an internal ribosomal entry site (IRES) was used (Fig. 19B). IRESs can be found in many pathogenic viruses. They mediate an RNA-dependent recruitment mechanism of the ribosome to the start codon, working without the necessity of a 5' Cap structure and most of the associated proteins. This advantage is transferred to bicistronic vectors, in which IRESs enable the expression of multiple genes from the same mRNA (Fahrenkrug et al., 1999; Kieft, 2008). The IRES used in this study originates from the encephalomyocarditis virus (EMCV). As a cloning method, Gibson assembly was used. Finished constructs were validated by Sanger sequencing and co-injected together with *Tol2* mRNA in the one-cell stage of zebrafish embryos to generate stable transgenic lines. A summary of all created constructs and the current status of the zebrafish lines is given in Table 1.

**Table 1. 5xUAS effector plasmids to manipulate RA signalling.** Summary of cloned 5xUAS vectors, containing five repetitive UAS sequences to control transgene expression. Stable transgenic lines were established using the *Cyp26a1-eGFP* and the *dnRara2a-IRES-eGFP* construct.

Effector plasmid	Stable transgenic zebrafish line
<i>pTol2_5xUAS:eGFP-Cyp26a1_α-crystallin:mRFP</i>	-
<i>pTol2_5xUAS:Cyp26a1-eGFP_α-crystallin:mRFP</i>	2 lines in F2 generation
<i>pTol2_5xUAS:dnRara2a-IRES-eGFP_α-crystallin:mRFP</i>	5 lines in F2 or F3 generation

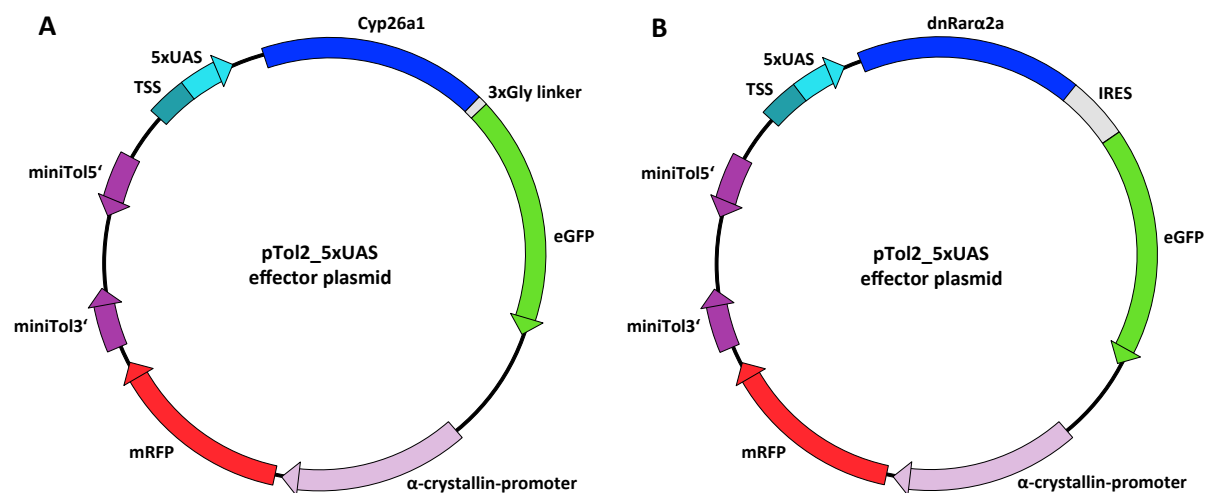


**Fig. 19 Schematic representation of the effector plasmids.** The basic vector pTol2 (pSELF/p347) contained a transcriptional start site (TSS), five repetitive upstream activating sequences (5xUAS) and an  $\alpha$ -crystallin-promoter connected to *mRFP*. The genes *dnRara2a* and *Cyp26a1* were linked to the reporter gene *eGFP* either via a 3xGly linker (**A**) or via an internal ribosomal entry site (IRES) (**B**).

### 2.3.1.1 5xUAS:Cyp26a1-eGFP

Previous to the design of the C-terminal fusion construct, an N-terminal eGFP-Cyp26a1 variant was designed and assembled by Fabian Merkel (Merkel, 2016). In this variant, *Cyp26a1* and *eGFP* were also connected with a sequence encoding a 3xGly linker peptide. For a preliminary functionality test of the Gal4-UAS system and this construct, co-injections of the plasmid *pTol2\_5xUAS:eGFP-Cyp26a1* together with *in vitro* transcribed *Gal4-VP16* mRNA were performed in the one-cell stage of zebrafish embryos (Merkel, 2016). Fabian Merkel documented a green fluorescence, visible from 7 hpf to at least 24 hpf, with a distribution in a mosaic pattern. At 24 hpf, embryos exhibited severe malformations, particularly affecting the head and the eyes, which led to their death around 30 - 40 hpf. However, a direct connection between this phenotype and RA signalling was not evident and it could also be attributed to excessively high concentrations of injected nucleic acids.

Moreover it was suggested that incorrect folding of the fusion protein might have led to protein aggregates that are toxic to the organism (Merkel, 2016) (data not shown).

Therefore, the C-terminal version Cyp26a1-eGFP was designed and constructed (Fig. 19A) (Eberlein, 2018b). Sanger sequencing revealed a point mutation in the *Cyp26a1* sequence changing the amino acid Alanin(143) to Valin(143). However, since both amino acids are small and hydrophobic and combined with the fact that the mutation was noticed before (Merkel, 2016), the construct was used for further experiments. Co-injection of the plasmid *pTol2\_5xUAS:Cyp26a1-eGFP* together with *Gal4-VP16* mRNA (40 ng/μl each) in the one-cell stage of zebrafish embryos led to mosaic-like eGFP fluorescence at 24 hpf accompanied by various deformities, including missing eyes, truncated tails and malformed heads (Fig. S12C,D). Double whole-mount *in situ* hybridisation (WISH) against *Epha4a* and *MyoD* additionally demonstrated a hindbrain defect, characterized by a shortening of the distance between rhombomere 5 and somite 1 (Fig. S12E) (Eberlein, 2018b). The latter is a significant feature of the *Aldh1a2* mutant *neckless (nls)* and might indicate a state of RA deficiency (Begemann et al., 2001). However, also control embryos injected with *Gal4-VP16* mRNA alone exhibited this phenotype (Fig. S12B), strongly suggesting an unspecific, toxic effect, whereupon an adjustment of the injected plasmid and mRNA concentration was made to 40 ng/μl and 20 ng/μl, respectively. This amount of mRNA did not impair the appearance of control embryos (Fig. S12H,I), whereas co-injected embryos still exhibited a moderate *nls*-like phenotype (Fig. S12L) (Eberlein, 2018b).

These proof-of-principle experiments clearly demonstrated that the Gal4-UAS system is basically working and the eGFP part of the fusion constructs is functional. Similarities to the *nls* phenotype in co-injected embryos at 24 hpf also indicated an activity of *Cyp26a1*.

Based on these results a stable transgenic *5xUAS:Cyp26a1-eGFP* zebrafish line was established. For this, the plasmid *pTol2\_5xUAS:Cyp26a1-eGFP* was co-injected with *Tol2* mRNA in the one-cell stage of zebrafish embryos of the *Casper* strain (40 ng/μl each). At 5 dpf, transgenic larvae were identified based on the red fluorescence of the *α-crystallin:mRFP* lens marker and raised to adulthood (F0 generation). Upon reaching sexual maturity, F0 fish were mated with wild type fish (*Casper*) and their progeny (F1 generation) examined for expression of the lens marker. For each F0 fish at least 100 offspring were considered. Positively identified F1 larvae were raised to adulthood and represent the stable transgenic line. The transgenic parents are referred to as the founder fish.

For *5xUAS:Cyp26a1-eGFP* zebrafish line, transgenic F1 larvae could be obtained from crossings of the F0 pair ♂8 and ♀8 and of the F0 fish ♀7 with a wild type male (Eberlein, 2018a). The functionality of the transgenic line was examined by injecting *in vitro* transcribed *ERT2-Gal4-VP16* mRNA in zygotes of the F2 generation (obtained either from F1 incross or outcross with *Casper*). *ERT2-Gal4-VP16* is the Gal4 variant, inducible by addition of 4-hydroxy-tamoxifen (4-OHT) (Fig. 7B). In previous test series, the functionality of *ERT2-Gal4-VP16* was proven via injection of *ERT2-Gal4-VP16* mRNA in one-cell stage embryos of the transgenic *UAS:GFP* zebrafish line followed by induction with 4-OHT in concentration of 1, 2 and 5  $\mu$ M. Strong eGFP fluorescence was obtained with all three concentrations, documented until 5 dpf (Fig. S13).

Upon injection of *ERT2-Gal4-VP16* mRNA (40 ng/ $\mu$ l) in F2 zygotes of *5xUAS:Cyp26a1-eGFP* and subsequent induction with 2  $\mu$ M 4-OHT at a developmental stage of 50 % epiboly, expression of eGFP could be effectively induced, which was visible throughout the entire embryo at 24 hpf (Fig. 20D). Embryos treated with pure EtOH as control showed no eGFP fluorescence (Fig. 20C) (Eberlein, 2018a). However, hindbrain defects, which are expected from reduced RA signalling, could not be observed at 24 hpf (Fig. 20F). Therefore, embryos were examined again at 72 hpf, where they were still showing intense eGFP fluorescence, restricted to the trunk and tail (Fig. 20J). This time the focus was on the appearance of the pectoral fins, due to the fact that their formation is completely suppressed in the *nls* mutant (Begemann et al., 2001). However, the pectoral fins in 4-OHT-induced larvae had a normal size and shape with no obvious functional impairments. Minor size variations of the fins were attributed to natural fluctuation (Fig. 20K,L) (Eberlein, 2018a). Corresponding experiments with F2 offspring of founder ♀7 led to comparable results (data not shown).

This strongly suggests that the C-terminal *Cyp26a1-eGFP* fusion protein is inactive. Most likely the function of *Cyp26a1* is disturbed due to the linkage to eGFP via a 3xGly linker peptide. This connection might either influence the folding process of *Cyp26a1* or cause steric hindrances due to the eGFP part, negatively impairing the catalytic activity of *Cyp26a1* (Chen et al., 2013). The missing activity is probably not due to the *Cyp26a1* sequence since the previously established *Hsp70l:Cyp26a1* zebrafish line, based on the same sequence, is working well (see 2.2.2 and Blum & Begemann, 2012).

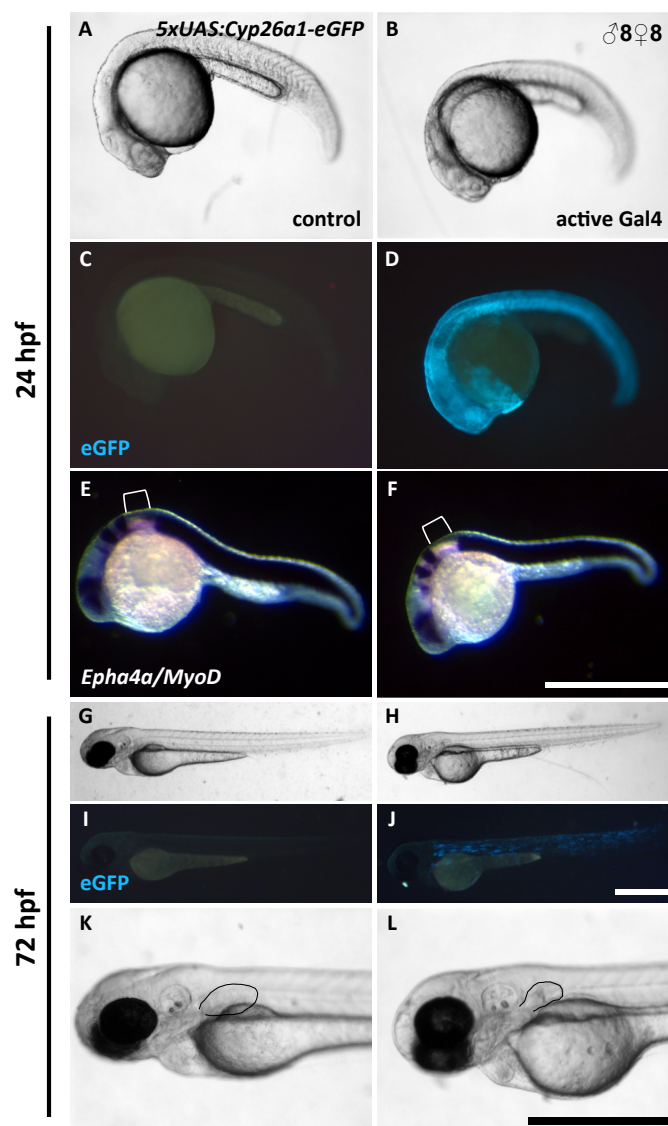


**Fig. 20** Active Gal4 results in transgene expression in the *5xUAS:Cyp26a1-eGFP* effector line. F2 zygotes of the *5xUAS:Cyp26a1-eGFP* zebrafish line from founder pair ♂8 and ♀8 were injected with *ERT2-Gal4-VP16* mRNA (40 ng/μl) and the embryos subsequently treated with 2 μM 4-OHT or EtOH (control) at 50 % epiboly. At 24 hpf, eGFP fluorescence is visible only in induced embryos throughout the whole body (C,D). Embryos seem normally developed and healthy; there are no signs of RA-deficiency (A,B). Whole-mount *in situ* hybridisation against *Epha4a* and *MyoD* mRNA does not reveal any truncation of the anteroposterior axis anterior to the somites. The distance between rhombomere 5 and somite 1 is indicated with brackets (E,F). At 72 hpf eGFP fluorescence is visible only in induced larvae in a stripe pattern in the trunk and tail (I,J). K,L: magnifications of the anterior body half of larvae shown in G,H. There is only a slight reduction of pectoral fin size that might be a morphological variation and does not confirm the RA-deficiency-phenotype. Black lines in K and L highlight outlines of pectoral fins. All embryos are shown in lateral view with anterior to the left. Scale bars: 500 μm. Pictures by Jean Eberlein; taken and modified from (Eberlein, 2018a).

### 2.3.1.2 *5xUAS:dnRara2a-IRES-eGFP*

For the second UAS effector line, a dominant-negative allele of *Rara2a* from zebrafish was connected with *eGFP* via an IRES and put under the control of *5xUAS*. This was done by Marlene Schmidt as part of her Master thesis (Fig. 19B) (Schmidt, 2017). Marlene Schmidt additionally performed preliminary activity test with the newly assembled plasmid, that were based on co-injections of *5xUAS:dnRara2a-IRES-eGFP* in one-cell stage embryos together with *Gal4-VP16* mRNA using 40 ng/ $\mu$ l DNA and 50 ng/ $\mu$ l mRNA. At 24 hpf, a tessellated eGFP fluorescence was documented in 7 % of the co-injected embryos (Schmidt, 2017) (data not shown).

In this study, similar injections were performed with a lower concentration of nucleic acids, resulting in eGFP fluorescence in 47 % of co-injected embryos at 24 hpf. This fluorescence was mainly restricted to the yolk, which is most likely due to the process of microinjection (Fig. S12N). Injections are, whenever possible, performed directly into the cell, however, a distribution of the injected nucleic acid mixture into the yolk cannot be excluded. The results proved the efficient expression of the second gene on this bicistronic mRNA, indicating a properly integrated IRES and a functional eGFP protein. Subsequent WISH against *Epha4a* and *MyoD* revealed only a minor shortening of the anteroposterior axis anterior to the somites, which however corresponds to expectations based on the poor distribution of transgene activity in the bodies of the embryos (Fig. S12O) (Eberlein, 2018b).

From this test series, the functionality of the *dnRara2a* component of the construct could neither be unambiguously proven nor refuted, thus it was proceeded with the establishment of a stable transgenic line. Following co-injection of the plasmid *pTol2\_5xUAS:dnRara2a-IRES-eGFP* together with *Tol2* mRNA, five different F0 founder fish ( $\delta$ 4,  $\delta$ 5,  $\delta$ 10,  $\delta$ 11 and  $\delta$ 13) could be identified from which stable F1 generations were bred. The presence of *dnRara2a* and *eGFP* sequences was confirmed by PCR for all five independent lines (Nardini, 2018) (data not shown).

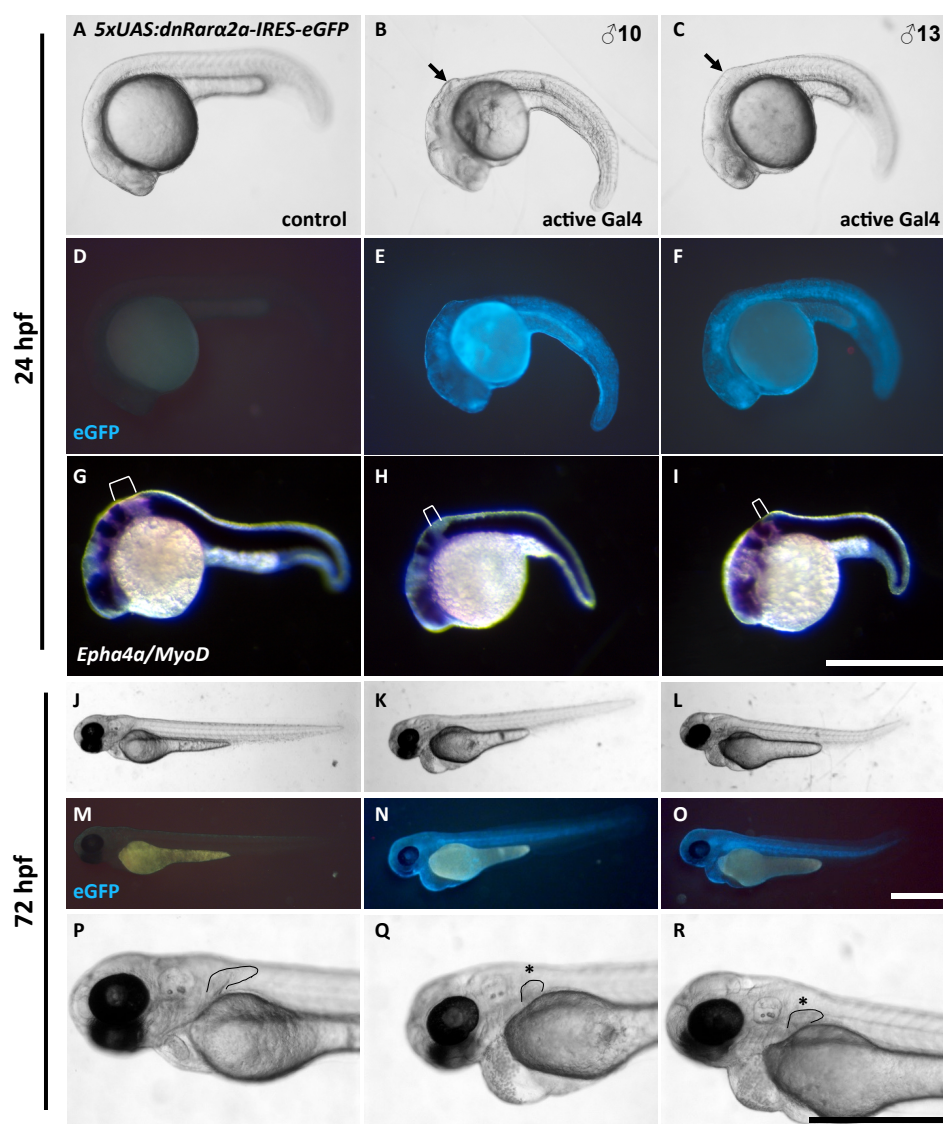


**Fig. 21 Active Gal4 causes a RA-deficiency phenotype in the *5xUAS:dnRara2a-IRES-eGFP* effector line.** *ERT2-Gal4-VP16* mRNA (40 ng/ $\mu$ l) was injected in zebrafish eggs of the *5xUAS:dnRara2a-IRES-eGFP* effector line (F2 generation) at the one-cell stage and the embryos were subsequently treated with 2  $\mu$ M 4-OHT or EtOH (control) at 50 % epiboly. The results of the lines founded by  $\sigma$  10 and  $\sigma$  13 are shown. At 24 hpf only induced embryos show the characteristic bulge in the 'neck' of the RA-deficiency-phenotype (A-C, arrows). Intense eGFP fluorescence is visible in these embryos throughout the whole body (D-F). Whole-mount *in situ* hybridisation against *Epha4a* and *MyoD* mRNA shows a truncation of the anteroposterior axis anterior to the somites. The distance between rhombomere 5 and somite 1 is indicated with brackets (G-I). At 72 hpf eGFP fluorescence is visible only in induced larvae throughout the whole body (M-O). P-R: magnifications of the anterior body half of larvae shown in J-L. Reduction of pectoral fin size indicates the RA deficiency phenotype (asterisks). Black lines in P-R highlight outlines of pectoral fins. All embryos are shown in lateral view with anterior to the left. Scale bars: 500  $\mu$ m. Pictures by Jean Eberlein; taken and modified from Eberlein, 2018.

To evaluate the inhibitory activity of *dnRara2a* on RA signalling, injection of *ERT2-Gal4-VP16* mRNA were performed in F2 zygotes of each *5xUAS:dnRara2a-IRES-eGFP* zebrafish line and embryos were subsequently treated with 2  $\mu$ M 4-OHT from 50 % epiboly onwards. The control groups were treated with equivalent amounts of EtOH (Eberlein, 2018a). At 24 hpf, induced embryos exhibited a strong eGFP fluorescence, that was never seen in the control (Fig. 21D-F; Fig. S14E-H). Moreover, embryos of all five lines developed the expected RA deficiency (*nls*) phenotype to varying extends. The specific bulge in the neck is clearly visible at 24 hpf (Fig. 21A-C; Fig. S14A-D), while WISH against *Epha4a* and *MyoD* demonstrated the hindbrain defects, characterized by an approximation of rhombomere 5 to somite 1 (Fig. 21G-I; Fig. S14I-L). Later, at 72 hpf, a significant reduction of the pectoral fins was observed in induced embryos, compared to the control (Fig. 21P-R; Fig. S14U-X). A complete reduction of the pectoral fins was not observed. However, this was not to be expected, since after a single microinjection, an increasing dilution of the *ERT2-Gal4-VP16* mRNA must be assumed, which lowers effectiveness of Gal4 induced transgene activation. At this point, some of the embryos also showed other severe impairments, among others pericardial edema (Fig. S14V,W) (Eberlein, 2018a). In summary, these results suggests, that all five transgenic *5xUAS:dnRara2a-IRES-eGFP* lines are indeed able to block RA signalling at the presence of active Gal4. Hereby the most convincing results were obtained for the lines founded by ♂ 10 and ♂ 13, why these were further bred to F2 and F3 generations.

### 2.3.1.3 Variations of UAS sequences, reporter genes and fusion constructs

In further projects, various modifications of the effector constructs, used so far, were tested and evaluated, in order to optimize this system and improve long-term stability of transgenic lines (Mück, 2019). In this context, the functionality of four non-repetitive upstream activator sequences (*4xnrUAS*) instead of *5xUAS* was tested. These four distinct sequences are less susceptible to methylation while their ability to activate downstream genes is on the same level (Akitake et al., 2011; Goll et al., 2009). Moreover, different marker genes were selected and evaluated for applicability in the Gal4-UAS system. The intention was to establish a set of vectors, expressing different fluorescence markers that label distinct structures within the zebrafish larvae. Ultimately this will facilitate the identification of double transgenic individuals emerging from a crossing of effector and driver lines. The reporter constructs  *$\alpha$ -crystallin:Citrine* and *cmlc2:mCherry* ('bleeding heart') were

considered, which mediate a green labelling of the eye lenses or a red labelling of the myocardium, respectively (Huang et al., 2003; Runkle et al., 2002).

The plasmids used for these projects were based on 'zero-background' Tol2 vectors designed by David Richter (University of Bayreuth) as part of the further development of his ZeBRα DNA-assembly system (Richter et al., 2019, Fig. S15A,B). Again, the whole expression cassette is flanked by minimal Tol2 *cis* sequences that enable random integration into the zebrafish genome, mediated by Tol2 transposase activity (Fig. S15A,B; Fig. 22).

To test the functionality of the *4xnrUAS* and the two marker genes, several plasmids were cloned, which contained these components, together with various combinations of either *Cyp26a1* or *dnRara2a* constructs (Table 2) (Mück, 2019). In this context, the functionality of both RAI genes was to be tested as fusion construct or with an intermediate IRES between the coding sequence and the reporter gene. For *Cyp26a1*, this strategy build upon previous findings that indicated the inactivity of *Cyp26a1* as a fusion protein (see 2.3.1.1 and Eberlein, 2018a; Merkel, 2016). In general, the fusion construct has the advantage that the exact location of *Cyp26a1* or *dnRara2a* activity is reflected. In contrast to that, in the case of IRES constructs, diffusion is possible due to the formation of two individual proteins. Thus the fluorescence can be present at a location other than the place of *Cyp26a1* or *dnRara2a* activity (Snapp, 2005).

As another variation, *Cyp26a1* or *dnRara2a* were connected with *mRFP* instead of *eGFP*. The red fluorescence marker will allow an additional crossing of either the effector or the driver line to the *fli:eGFP* zebrafish line for the application of the pelvic fin staging system (Marzi, 2015) in advance of the 4-OHT-treatments. In this way, corresponding experiments to the DEAB and heat-shock treatments, described previously (see 1.5 and 2.2.2), are enabled.

The cloning strategy for the generation of the *4xnrUAS* plasmids started by removing the toxic *ccdB* part of the 'zero-background' vector by means of restriction digest with *AgeI* (Fig. S15A,B). Then, the linearized vector and the PCR amplified inserts were combined using Gibson assembly or Aqua cloning. Test digestion and Sanger sequencing were performed to confirm the correct assembly of each plasmid (data not shown).

**Table 2. 4xnrUAS effector plasmids to manipulate RA signalling.** Summary of cloned 4xnrUAS vectors, containing four non-repetitive UAS sequences to control transgene expression. Vectors are further composed of different combinations of marker genes (*α-crystallin:Citrine* and *cmlc2:mCherry*) and the RA signalling inhibiting genes *Cyp26a1* and *dnRara2a*, either as a fusion or IRES constructs with *eGFP* or *mRFP*. So far, no stable transgenic zebrafish lines have been established yet.

Effector plasmid	Stable transgenic zebrafish line
<i>pTol2_4xnrUAS:dnRara2a-IRES-eGFP_α-crystallin:Citrine</i>	-
<i>pTol2_4xnrUAS: dnRara2a-mRFP_α-crystallin:Citrine</i>	-
<i>pTol2_4xnrUAS:Cyp26a1-mRFP_α-crystallin:Citrine</i>	-
<i>pTol2_4xnrUAS: dnRara2a-mRFP_cmlc2:mCherry</i>	-
<i>pTol2_4xnrUAS:Cyp26a1-mRFP_cmlc2:mCherry</i>	-
<i>pTol2_4xnrUAS: dnRara2a-IRES-mRFP_cmlc2:mCherry</i>	-
<i>pTol2_4xnrUAS:Cyp26a1-IRES-mRFP_cmlc2:mCherry</i>	-

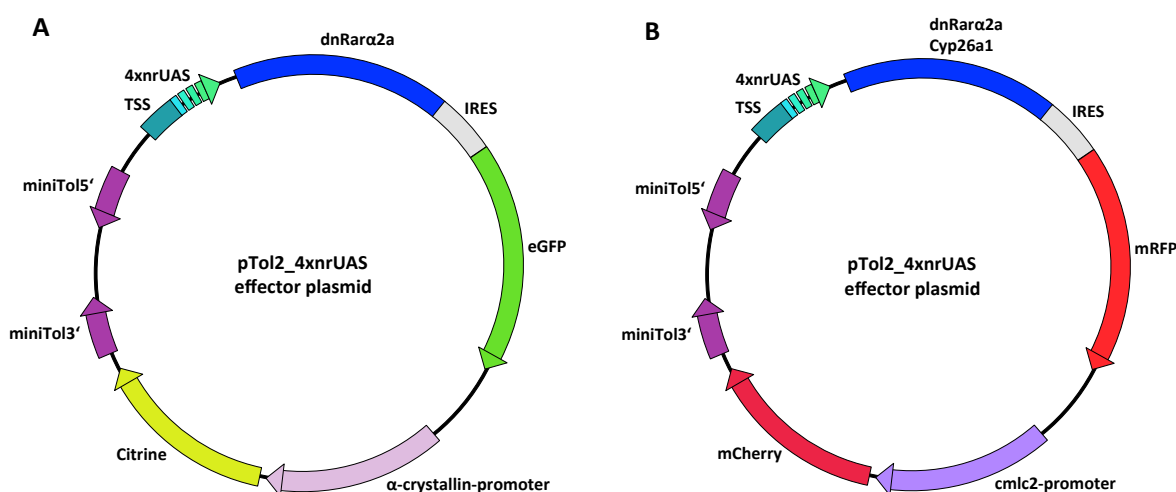


**Fig. 22 Schematic representation of the 4xnrUAS effector plasmids.** The basic vectors pTol2 (p403, p404) contained a transcriptional start site (TSS), four non-repetitive upstream activating sequences (4xnrUAS) and either an *α-crystallin-promoter* connected to *Citrine* (A) or a *cmlc2-promoter* connected to *mCherry*. The genes *dnRara2a* and *Cyp26a1* were linked to the reporter gene *mRFP* or *eGFP* either via a 3xGly linker or via an internal ribosomal entry site (IRES) (B).

First of all, the *dnRara2a-IRES-eGFP* construct, which was already proven to effectively inhibit RA signalling in transgenic zebrafish (Fig. 21; Fig. S14), was cloned into the 4xnrUAS vector containing the *α-crystallin:Citrine* reporter gene. For a preliminary test of the functionality of the 4xnrUAS, co-injection of *pTol2\_4xnrUAS:dnRara2a-IRES-eGFP\_α-crystallin:Citrine* and *Gal4-VP16* mRNA were carried out in the one-cell stage of embryos of the *Casper* strain. At 24 hpf, intense eGFP fluorescence was detected in a mosaic pattern throughout the embryo's body in 75 % of the individuals (64/86) (Fig. 23B) (Mück, 2019). A

comparison with the fluorescence pattern that arose after the injection of the corresponding 5xUAS plasmid (Fig. 23A) (Eberlein, 2018b), revealed an improved distribution over the body cells, while almost no fluorescence localized in the yolk. The green fluorescence of the *α-crystallin:Citrine* marker was observed at 72 hpf, specifically in the eye lens (Fig. 23C). Control injections with *Gal4-VP16* mRNA alone did not result in any fluorescence or phenotype (data not shown) (Mück, 2019). These results demonstrate the successful activation of 4xnrUAS by *Gal4-VP16* and confirm the functionality of the *α-crystallin:Citrine* lens marker (Mück, 2019).

Next, the focus was on the plasmids carrying the *cm1c2:mCherry* marker (Fig. S15B). In order to evaluate the effectiveness of *dnRara2a* and *Cyp26a1* as a fusion or an IRES construct in parallel, both variants were created for each of the two genes together with the fluorescence marker gene *mRFP*. For the fusion constructs, the same sequence, encoding the 3xGly linker peptide, was used to connect the RAI genes with *mRFP* (Table 2) (Mück, 2019). Afterwards, each correctly assembled plasmid (40 ng/μl) was co-injected with *Gal4-VP16* mRNA (20 ng/μl) in the one-cell stage of zebrafish embryos (*Casper* strain). At 24 hpf, mosaic-like fluorescence was observed for all four constructs in different intensities and frequencies. An amount of 20 % (10/50) of the *dnRara2a-mRFP*-injected embryos exhibited weak *mRFP* fluorescence (Fig. 23E). In case of *dnRara2a-IRES-mRFP*, *mRFP* fluorescence was relatively difficult to detect, since it was present only in few cells and was blurred in the rest of the embryo (Fig. 23H). Regarding *Cyp26a1-mRFP*, 8 % (5/65) of injected embryos were identified for present *mRFP* fluorescence (Fig. 23K), while for the *Cyp26a1-IRES-mRFP* construct, fluorescence was barely visible (Fig. 23N) (Mück, 2019). For all tested constructs, the cardiac tissue specific *cm1c2:mCherry* marker was visible at 72 hpf in a mosaic-like pattern in the heart of the embryos (Fig. 23F,I,L,O) (Mück, 2019). Consequently, the fusion constructs yielded more intense *mRFP* fluorescence than the corresponding IRES constructs. This is not unexpected, as normally the second reading frame on the bicistronic mRNA is translated to a lesser extent compared to the first one, ranging in most cases between 20 - 50 % (Mizuguchi et al., 2000). Moreover, in comparison to eGFP, *mRFP* seems to have a lower detection sensitivity while bearing a higher stability at the same time (Wan et al., 2002). This is reflected in the plasmid functionality tests, since the observed red fluorescence was often weak and very difficult to detect, which is accordingly not directly attributable to a lower expression level.

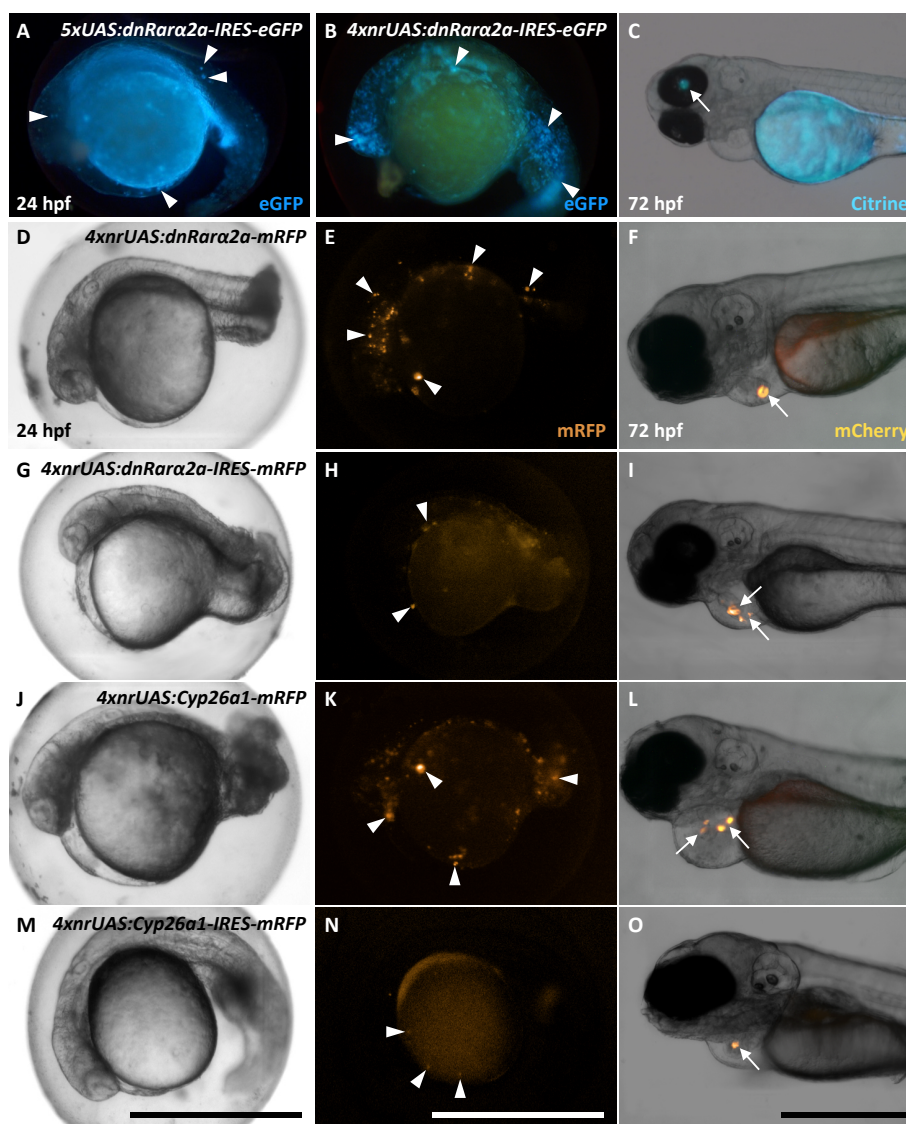


**Fig. 23 Gal4-VP16 induces transgene expression in zebrafish larvae upon co-injection with *4xnrUAS* effector plasmids.** **A:** Injection of *pTol2\_5xUAS:dnRara2a-IRES-eGFP\_α-crystallin:mRFP* (40 ng/μl), containing 5 repetitive UAS, together with *Gal4-VP16* mRNA (20 ng/μl) into the one-cell stage of embryos of the *Casper* strain shows tessellated eGFP fluorescence at 24 hpf (arrowheads). **B/C:** Injection of *pTol2\_4xnrUAS:dnRara2a-IRES-eGFP\_α-crystallin:Citrine*, containing 4 non-repetitive UAS, together with *Gal4-VP16* mRNA shows intense expression of eGFP at 24 hpf in a mosaic pattern (**B**, arrowheads). *Citrine* expression is observed at 72 hpf specifically in the eye lenses (**C**, arrow). **D-O:** Different effector plasmids (40 ng/μl), containing *dnRara2a* or *Cyp26a1* and *mRFP* either as a fusion construct (with a 3xGlycin linker) or as IRES construct, were co-injected with *Gal4-VP16* mRNA (20 ng/μl) in the one-cell-stage of zebrafish embryos. **D-F:** *pTol2\_4xnrUAS:dnRara2a-mRFP\_cmlc2:mCherry*, **G-I:** *pTol2\_4xnrUAS: dnRara2a-IRES-mRFP\_cmlc2:mCherry*, **J-L:** *pTol2\_4xnrUAS:Cyp26a1-mRFP\_cmlc2:mCherry*, **M-O:** *pTol2\_4xnrUAS: Cyp26a1-IRES-mRFP\_cmlc2:mCherry*. Mosaic mRFP fluorescence is observed at 24 hpf in injected embryos (**E,H,K,N**, arrowheads). Specific mosaic expression of *mCherry* in the myocardium is seen at 72 hpf (**F,I,L,O**, arrows). Embryos are shown in lateral view with anterior to the left. Scale bars: 500 μm. Picture A by Jean Eberlein, pictures B-O by Amelie Mück, taken and modified from Eberlein, 2018b and Mück, 2019.

Concerning the phenotypic effect of the *4xnrUAS:Cyp26a1* and *4xnrUAS:dnRara2a* plasmids, diverse malformations were observed following co-injection with *Gal4-VP16* mRNA. This includes deformed heads, truncated tails (Fig. 23G,J) and reduced or missing eyes; the same effects that were observed previously, in course of testing the corresponding 5xUAS plasmids (Fig. S12). They had been attributed to a toxic effect due to excessively high nucleic acid concentrations. Although here, lower concentrations of plasmid and *Gal4-VP16* mRNA of 40 ng/μl and 20 ng/μl, respectively, were used, the effects were still present, which suggests that an even lower concentration would be useful.

In order to determine the inhibiting effect of the constructs on RA signalling, WISH against *Epha4a* and *MyoD* was performed on co-injected embryos at an age of 24 hpf. All injected embryos were used for this, meaning that they were not pre-sorted according to their mRFP fluorescence. Un-injected embryos were used as negative control. Progeny of the *Hsp70l:Cyp26a1* line that were heat-shocked at 30 - 50 % epiboly for 2.5 h at 38.5 °C served as a positive control (Fig. 24) (Mück, 2019). The co-injection of all four constructs with *Gal4-VP16* mRNA resulted in a reduction of the anteroposterior axis, which is visualized by a shortening of the distance between rhombomere 5 and somite 1 (Fig. 24C-F). The un-injected embryos exhibited a normal spacing between these two structures (Fig. 24A), while in the *Hsp70l:Cyp26a1* embryos the effect is so pronounced that rhombomere 5 fused with the somites (Fig. 24B) (Mück, 2019). For the quantification of the data, these distances were measured for each embryo and the mean values calculated. This revealed a gradation of the phenotypic expression among the various constructs (Fig. 24G). The measured distances for *dnRara2a-mRFP* and *dnRara2a-IRES-mRFP* were approximately the same. In case of *Cyp26a1-mRFP* and *Cyp26a1-IRES-mRFP* the differences were more striking. Here, significantly lower values were obtained for *Cyp26a1-IRES-mRFP* (Mück, 2019). This again indicated that Cyp26a1 is inactive as a fusion protein, regardless of its combination with eGFP or mRFP (see Fig. 20 and Fig. 24) (Eberlein, 2018a; Mück, 2019). However, the *Cyp26a1-IRES-mRFP* construct gave the lowest values apart from the positive control, suggesting that the single Cyp26a1 protein is active. In case of *dnRara2a*, both versions - fusion and IRES construct - seem to be equally effective in hindering RA signalling. The reason for different effectiveness of Cyp26a1 and dnRara2a as a fusion protein with mRFP is most likely based on their different nature and mode of action, with dnRara2a being a DNA

bound RA-receptor protein and Cyp26a1 a heme-containing RA-metabolizing enzyme (Awadalla et al., 2016; Bourguet et al., 2000).

Alltogether, *pTol2\_4xnrUAS:Cyp26a1-IRES-mRFP\_cmlc2:mCherry* and *pTol2\_4xnrUAS:dnRara2a-IRES-mRFP\_cmlc2:mCherry* turned out to be the most promising constructs to manipulate RA signalling and in addition have most benefits for practical use in terms of reporter genes and fluorescence markers.

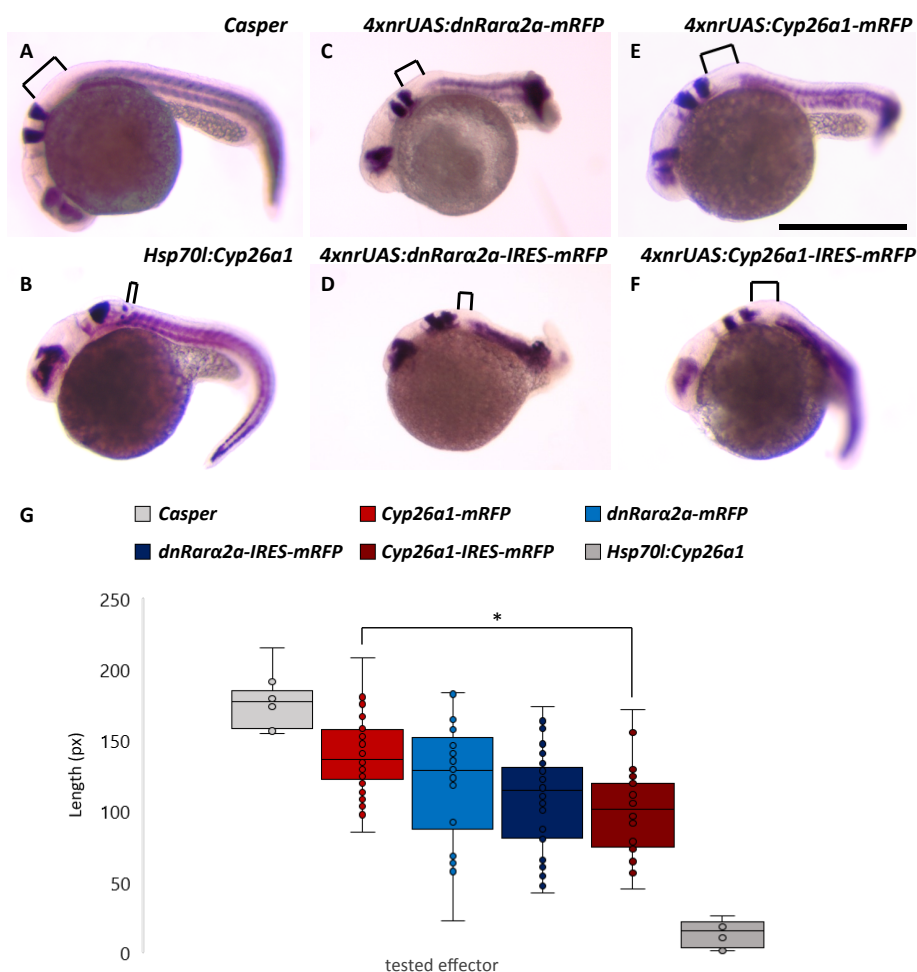


**Fig. 24 Evaluation of the RA deficiency phenotype of zebrafish larvae co-injected with *Gal4-VP16* mRNA and various *4xnrUAS* effector plasmids. A-F:** Indicated effector plasmids (40 ng/ $\mu$ l) were injected together with *Gal4-VP16* mRNA (20 ng/ $\mu$ l) in the one-cell stage of zebrafish embryos of the *Casper* strain. This leads to a RA-deficiency phenotype at 24 hpf visualized by WISH against *Epha4a* and *MyoD*. The distance between rhombomere 5 and somite 1 is indicated with brackets. **A:** Un-injected control embryos of the *Casper* strain. **B:** *Hsp70l:Cyp26a1* embryos that were heat-shocked at 30 - 50% epiboly for 2.5 h at 38.5 °C as a positive control. **G:** The average distance between rhombomere 5 and the first somite is significantly reduced after co-injection of different *4xnrUAS* effector plasmids and *Gal4-VP16* mRNA. Significant deviations were calculated using a t-test. \*:  $p < 0.05$ . Embryos are shown in lateral view with anterior to the left. Scale bar: 300  $\mu$ m. Pictures and statistical analysis by Amelie Mück; taken and modified from Mück, 2019.

### 2.3.2 Evaluation of fin specific enhancers and establishment of reporter lines

Parallel to the effector lines, the second part of the Gal4-UAS system consisting of the Gal4 driver lines was established. As preliminary work, transgenic zebrafish reporter lines were generated, with the intention to functionally evaluate different fin specific enhancers. For this purpose, the enhancer detection plasmid pTol2 was used, which was obtained from Reinhard Köster (TU Braunschweig). It provides 5' and 3' minimal Tol2 *cis* sequences and is therefore suitable for the generation of new zebrafish transgenic lines. The respective enhancer fragments were PCR-amplified either from zebrafish genomic DNA or from plasmid and placed in pTol2 upstream of the  $\beta$ -actin basal promoter and the *eGFP* derived marker gene *mClover* (Fig. 25). If necessary, some plasmids were later expanded to include a further reporter gene, the eye lens marker  *$\alpha$ -crystallin:mRFP* (Runkle et al., 2002).

Under consideration were the *Tbx4* enhancers HLEA from mouse and HLEB from stickleback (Menke et al., 2008). Moreover, the *Pitx1* enhancer Pel2.5kb (PelA) was investigated (Chan et al., 2010). In this context, a screen for corresponding regulatory sequences of *Pitx1* in the zebrafish genome was carried out as well (Merkel, 2016) and the two detected, putative enhancer sequences PPE1 and PPE2 tested for activity. Last, the *Prrx1* enhancers *Prrx1a* and *Prrx1b1*, specifically active in zebrafish pectoral and pelvic fins, were chosen (Hernández-Vega & Minguillón, 2011).

**Table 3. Reporter constructs to visualize enhancer activity in pelvic fins.** Summary of all reporter constructs tested for enhancer activity in zebrafish. Stable transgenic lines were established for both *Prrx1* enhancer constructs.

Reporter plasmid	Stable transgenic zebrafish line
<i>pTol2_HLEA:mClover</i>	-
<i>pTol2_HLEA:mClover_α-crystallin:mRFP</i>	-
<i>pTol2_2xHLEB:mClover</i>	-
<i>pTol2_Pel2.5kb:mClover</i>	-
<i>pTol2_Pel2.5kb:mClover_α-crystallin:mRFP</i>	-
<i>pTol2_PPE1:mClover</i>	-
<i>pTol2_PPE1:mClover_α-crystallin:mRFP</i>	-
<i>pTol2_PPE2:mClover</i>	-
<i>pTol2_PPE2:mClover_α-crystallin:mRFP</i>	-
<i>pTol2_Prrx1a:mClover</i>	3 lines in F3 generation
<i>pTol2_Prrx1b1:mClover</i>	1 line in F3 generation

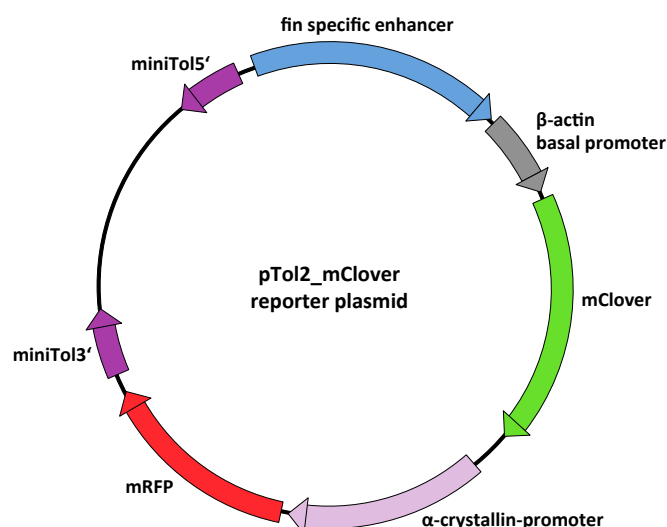


**Fig. 25 Schematic representation of the enhancer detection plasmid pTol2\_mClover. A:** In the reporter constructs, the fin specific enhancers are located upstream of a  $\beta$ -actin basal promoter, driving the expression of the reporter gene *mClover*. In some constructs, an  $\alpha$ -crystallin-promoter connected to mRFP was added additionally, driving *mRFP* expression in the eye lenses from 4 dpf onwards for easier identification of transgenic zebrafish larvae. Minimal Tol2 *cis* sequences (MiniTol) flank the whole cassette. They enable the integration of the foreign DNA into the zebrafish genome by Tol2 transposase activity. Tol2 is injected as mRNA into zebrafish zygotes.

Successfully assembled *pTol2\_mClover* reporter plasmids were confirmed by Sanger sequencing and subsequently co-injected with *Tol2* mRNA (40 ng/ $\mu$ l each) in the one-cell stage of zebrafish eggs of the *Casper* strain. All reporter plasmids that were created and tested are listed in Table 3, together with information concerning the current status of the associated zebrafish line.

### 2.3.2.1 *Tbx4* enhancers

First, the hindlimb specific *Tbx4* enhancers HLEA and HLEB (hindlimb enhancer A and B) (Menke et al., 2008) were tested for driving *mClover* expression in transgenic zebrafish. The vectors *pDBM7*, containing the full-length 1.1 kb HLEA fragment from mouse, and *pDBM20*, including four consecutive repeats of the stickleback HLEB enhancer (4xHLEB) with a total length of 3.5 kb, were generously provided by Douglas Menke (University of Georgia).

In case of 4xHLEB, the cloning of the four tandem repeats in the enhancer detection plasmid pTol2 turned out to be problematic. As part of his master thesis, Fabian Merkel succeeded in constructing a *pTol2\_2xHLEB:mClover* vector, containing two consecutive HLEB sequences instead of the originally four (Merkel, 2016). In addition, he assembled the *pTol2\_HLEA:mClover* construct (Table 3). Injecting either of these two plasmids together

with *Tol2* mRNA in fertilized zebrafish eggs generated several F0 fish (Merkel, 2016). However, as the plasmids were lacking an additional marker gene for easier identification of transgenic fish, the identification of founder fish, which inherited the transgene to their progeny, turned out to be difficult. Therefore the *pTol2\_HLEA:mClover* plasmid was modified, by adding an additional *α-crystallin:mRFP* reporter construct, driving *mRFP* expression in the eye lenses (Table 3). Injections of the newly created *pTol2\_mHLEA:mClover\_α-crystallin:mRFP* vector together with *Tol2* mRNA in zebrafish zygotes were conducted and larvae screened for red fluorescence in the eyes at 5 dpf. After approximately four months, sexually mature F0 fish were crossed with wild type zebrafish of the *Casper* strain and the progeny screened for expression of the lens marker. This resulted in the identification of one founder fish (♂9). Further observations of F1 progeny of ♂9, however, revealed no mClover fluorescence in the pelvic fin region at an age of 3 - 4 wpf (data not shown), suggesting that HLEA from mouse is likely to be non-functional in zebrafish. The work on the 2xHLEB construct was not further continued and the focus was laid on other pelvic enhancers.

### 2.3.2.2 *Pitx1* enhancers

Next, the 2.5 kb *Pitx1* enhancer sequence (Pel2.5kb, PelA) from three-spine stickleback was investigated. The vector *p5E-Pel2.5kb* that contained the original sequence was provided by Emily Kate Don (Macquarie University, Sydney). On the basis of this, the plasmid *pTol2\_Pel2.5kb:mClover\_α-crystallin:mRFP* (Fig. 25) was constructed and co-injected with *Tol2* mRNA (40 ng/μl each) in the one-cell stage of zebrafish eggs (*Casper* strain). This finally led to the identification of two F0 founder fish (♂10 and ♂12), whose F1 offsprings stably expressed the *mRFP* marker gene in the eye lenses (Borrero Malo, 2018; Nardini, 2018; Ng, 2019; Stacker, 2018). Despite this strong expression of the lens marker, in neither of the two lines any mClover fluorescence could be detected in the pelvic fin region of F1 larvae at an age of approximately 3 - 4 weeks (data not shown). This was unexpected due to the fact that the enhancer has previously been shown to be able to drive *eGFP* expression in transgenic zebrafish (Chan et al., 2010; Don, 2013). Possibly, the mClover fluorescence was quite weak and got superimposed by background fluorescence originating from the intestines. Repressing interactions would also be conceivable, either from within the construct, for

example caused by the  $\alpha$ -*crystallin*-promoter, or due to integration in the genome at an unfavourable position, where neighbouring regulators influence the expression.

Previously to this doctoral thesis, the question about similar regulatory elements for *Pitx1* in the zebrafish genome was addressed (Merkel, 2016). In the course of this project, the 2.5 kb stickleback enhancer fragment was compared to the 45 kb zebrafish genome region upstream of the first *Pitx1* exon. The alignment revealed two 700 bp long, non-coding regions that are conserved without containing sections of highly repetitive sequences (Fig. S16). These interesting sequences were henceforth referred to as putative *Pitx1* enhancer 1 (PPE1) and 2 (PPE2) and further examined for enhancer activity (Merkel, 2016). In this study, this project was continued, starting with the assembly of *pTol2\_mClover* reporter plasmids that contained either PPE1 or PPE2 in combination with an additional  $\alpha$ -*crystallin:mRFP* marker gene (Table 3). Upon injection of *pTol2\_PPE1:mClover\_α-crystallin:mRFP* together with *Tol2* mRNA in fertilized zebrafish eggs, F0 fish show intense mClover fluorescence at the age of 3 - 4 wpf in several parts of the body, including the somites, eye lenses, heart, pelvic and pectoral fins (Fig. 26) (Merkel, 2016; Nardini, 2018). It should be noted that this could partly be nonspecific expression due to integration of the *PPE1:mClover* construct in a genomic region where it is influenced by another enhancer or promoter and must not necessarily be a result of PPE1 activity.

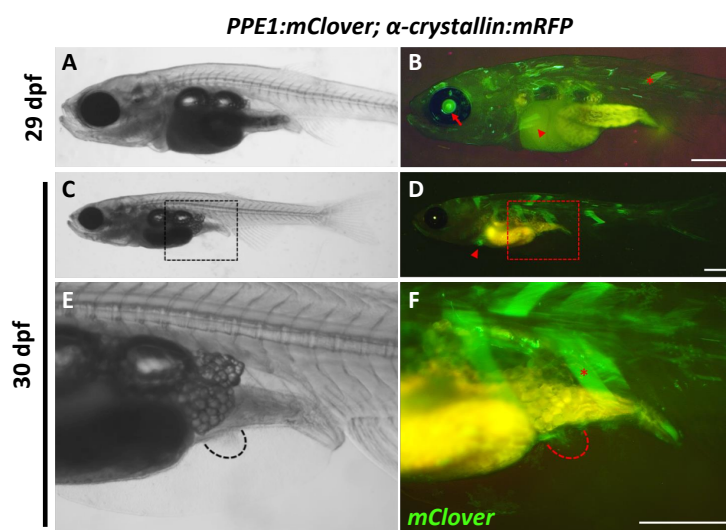


**Fig. 26** Transgene expression in the F0 generation of the *PPE1:mClover\_α-crystallin:mRFP* reporter line. Two examples of 29 dpf (A/B) and 30 dpf (C-F) juveniles are shown. **B:** mClover fluorescence is visible in various body parts, like the somites (asterisks), eye lens (arrow) and in the fin rays of the pectoral fin (arrowhead). **D/F:** mClover expression is detected in the heart (arrowhead), somites (asterisks) and in the pelvic fin (indicated with dashed line). **F** shows a higher magnification of the framed area in **D**. Scale bars: 500  $\mu$ m. Pictures by Niels Nardini; taken and modified from Nardini, 2018.

After reaching sexual maturity, *PPE1:mClover\_α-crystallin:mRFP* F0 fish were mated with wild type fish of the *Casper* strain and the examination of the F1 progeny resulted in the identification of two founder fish (♂6 and ♂12). However, in contrast to the widespread mClover fluorescence observed in F0 fish, F1 larvae from founder fish ♂6 exhibited mClover fluorescence only in very distinct parts of the brain at 3 - 4 wpf (data not shown). Moreover, in F1 progeny from founder ♂12 no mClover fluorescence was detected at this age in any part of the larvae. This indicates, that despite the strong transgene expression in F0 mosaic fish, the sequence PPE1 seems to have low activity in non-mosaic F1 fish or even is completely inactive.

In contrast to that, *PPE2:mClover\_α-crystallin:mRFP* F0 larvae showed no *mClover* expression at 3 - 4 wpf (data not shown) (Merkel, 2016; Nardini, 2018). Outcrossing of adult F0 fish with fish of the *Casper* strain and subsequent examination of the F1 generation did not reveal any founder fish, which is most probably due to an imprecise injection process. A repetition of the injections was not performed yet.

### 2.3.2.3 *Prrx1* enhancers

The third fin specific enhancers that were examined were those from the orthologous zebrafish genes *Prrx1a* and *Prrx1b*. Three enhancers sequences, *Prrx1a*, *Prrx1b1* and *Prrx1b2*, were identified previously and confirmed for driving transgene expression in zebrafish embryos (Hernández-Vega & Minguillón, 2011). For this study, the sequences *Prrx1a* and *Prrx1b1* were chosen to create *pTol2\_mClover* reporter constructs. Since *Prrx1a* and *Prrx1b* are already expressed very early in zebrafish embryonic development, beginning during the segmentation stages and continuing as the pectoral fins develop (Thisse et al., 2001), an additional *α-crystallin:mRFP* marker gene was dispensed with. Based on the published sequence information (Hernández-Vega & Minguillón, 2011), both enhancers (266 bp *Prrx1a* and 286 bp *Prrx1b1*) were PCR-amplified from zebrafish genomic DNA and assembled with the linearized *pTol2\_mClover* vector by means of traditional cloning. Following Sanger sequencing to verify the sequence, co-injections of *pTol2\_Prrx1a:mClover* or *pTol2\_Prrx1b1:mClover* with *Tol2* mRNA in the one-cell stage of zebrafish eggs (*Casper* strain) were conducted. Thereupon, one F0 founder pair could be identified for *Prrx1a:mClover* (♂11 / ♀11) and three founder (pairs) for *Prrx1b1:mClover* (♂6 / ♀6; ♂9 / ♀9; ♂22), which were further bred to stable transgenic lines.

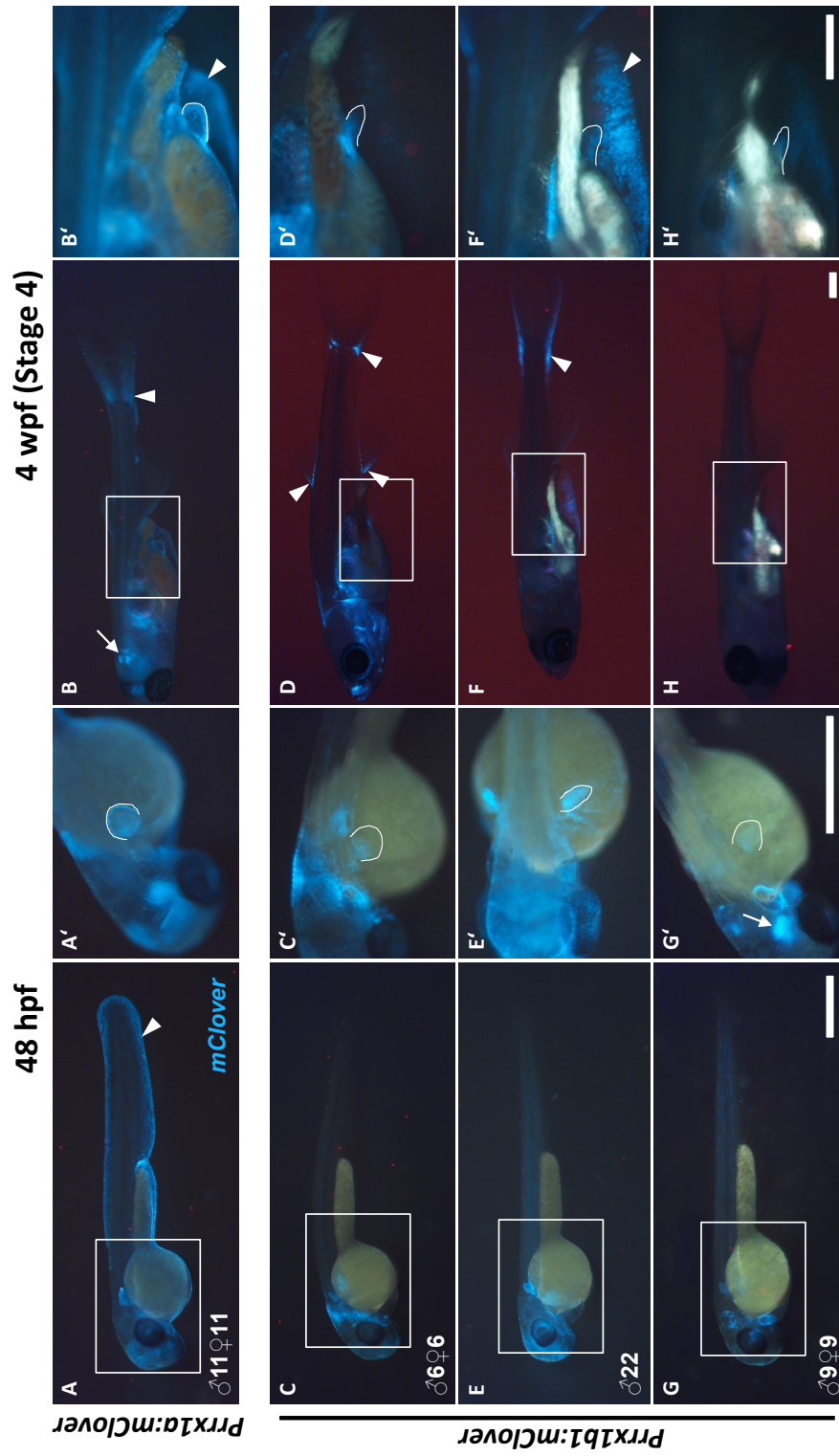


**Fig. 27 Transgene expression in the F3 generation of *Prrx1a:mClover* (A-B) and *Prrx1b1:mClover* (C-H) reporter lines from different founder fish.** Specific mClover fluorescence is visible in pectoral and pelvic fins at 48 hpf (**A,C,E,G**) or 4 wpf (Stage 4) (**B,D,F,H**), respectively. Images **A'-H'** show a higher magnification of framed areas in A-H. In the *Prrx1a:mClover* line, the fluorescence intensity is highest in the distal part of the fin bud. In the *Prrx1b1:mClover* lines, transgene expression is observed more proximally, but the exact localization varies between the three lines originating from different founder fish. White lines highlight the outline of pectoral or pelvic fins. Throughout all four lines, mClover fluorescence is frequently observed in the fin edges, the fin rays or at the bases of dorsal, anal or caudal fin (arrowheads) as well as in the brain (arrows). Embryos and larvae are shown in lateral or dorsolateral view with anterior to the left. Scale bars: 500  $\mu$ m.

Both, *Prrx1a:mClover* and *Prrx1b1:mClover* reporter lines, showed specific *mClover* expression in the pectoral and pelvic fins at 48 hpf and 4 wpf, respectively (Fig. 27 and Fig. S17 - S20). In the *Prrx1a:mClover* line (Fig. 27A,B and Fig. S17) transgene expression was detected especially in the distal part of the pectoral and pelvic fin buds, mainly concentrated in the fin edges. Furthermore, fluorescence was observed throughout the minor and major lobe. At 3 - 4 wpf mClover was present in the fin rays of the dorsal, anal and caudal fin. Apart from the fins, transgene activity localized in the branchial arches and in distinct parts of the telen- and diencephalon.

In all three *Prrx1b1:mClover* zebrafish lines, mClover fluorescence was found more proximally in both, pectoral and pelvic fin buds. However, the exact localization varies among the three individual lines. In the transgenic line founded by  $\sigma$ 6 and  $\varphi$ 6 (Fig. 27C,D and Fig. S18), mClover fluorescence was specifically located in the pectoral girdle, whereas the transgene expression level in the exoskeletal part of the pectoral fin was comparably low. A similar pattern was found in case of the pelvic fins as well. Among the other labelled fin structures were the bases of the dorsal, anal and caudal fin. Moreover, striking fluorescence was found in the branchial arches and the swim bladder.

The *Prrx1b1:mClover* line originating from  $\sigma$ 22 exhibits a similar expression pattern (Fig. 27E,F and Fig. S19). However, differing from the line founded by  $\sigma$ 6 and  $\varphi$ 6 is the strong transgene expression in the minor and major lobe, similar to the observations that were made in the *Prrx1a:mClover* line.

The third *Prrx1b1:mClover* line was founded by  $\sigma$ 9 and  $\varphi$ 9 and generally showed comparably weak transgene expression (Fig. 27G,H and Fig. S20). Its special characteristics were the intense mClover fluorescence in the ventricle of the heart and in a distinct part of the diencephalon up to 96 hpf, which, however, weakened in later larval states.

### 2.3.3 Establishment of ERT2-Gal4 driver lines

Following the preliminary studies on the functionality of the pelvic enhancers in the zebrafish, the establishment of the Gal4 driver lines was started. The same vector backbone as for the mClover reporter plasmids was used to generate the *pTol2\_ERT2-Gal4-VP16-GI* driver plasmids. To assemble the first series of driver plasmids, the marker gene *mClover* was excised by restriction digest and replaced by a gene encoding the ERT2-Gal4-VP16x2 fusion protein in combination with a downstream-located  *$\beta$ -globin* intron sequence (GI) (Fig. 28). The ERT2 part enables the timing of Gal4 activity via the induction with 4-hydroxy-tamoxifen (4-OHT) (Akerberg et al., 2014; Gerety et al., 2013). Its functionality has been confirmed in preliminary test series using 4-OHT concentrations between 1 - 5  $\mu$ M (Fig. S13). The  *$\beta$ -globin* intron sequence is useful since it was reported to have an enhancing effect on the transgene expression (Annweiler et al., 1991; Falcone & Andrews, 1991; Pourzadegan et al., 2016). In addition each driver construct was equipped with the  *$\alpha$ -crystallin:mRFP* lens marker, since otherwise the identification of transgenic fish would have been very difficult. Again, successfully assembled *pTol2\_ERT2-Gal4-VP16-GI* driver plasmids were confirmed by Sanger sequencing and subsequently co-injected with *Tol2* mRNA (40 ng/ $\mu$ l each) in the one-cell stage of zebrafish eggs of the *Casper* strain. In Table 4 all created driver constructs are listed with further information about the status of the established zebrafish lines.

**Table 4. Driver constructs for specific expression of ERT2-Gal4-VP16-GI in zebrafish paired fins.** Summary of cloned *pTol2\_ERT2-Gal4-VP16-GI* driver plasmids. Stable transgenic lines were established for Pel2.5kb and both Prrx1 enhancer constructs.

Driver plasmid	Stable transgenic zebrafish line
<i>pTol2_HLEA:ERT2-Gal4_<math>\alpha</math>-crystallin:mRFP</i>	-
<i>pTol2_2xHLEB:ERT2-Gal4_<math>\alpha</math>-crystallin:mRFP</i>	-
<i>pTol2_Pel2.5kb:ERT2-Gal4_<math>\alpha</math>-crystallin:mRFP</i>	2 lines in F2 generation
<i>pTol2_Prrx1a:ERT2-Gal4_<math>\alpha</math>-crystallin:mRFP</i>	3 lines in F3 generation
<i>pTol2_Prrx1b1:ERT2-Gal4_<math>\alpha</math>-crystallin:mRFP</i>	2 lines in F3 generation
<i>pTol2_Prrx1ax4:ERT2-Gal4_<math>\alpha</math>-crystallin:mRFP</i>	-
<i>pTol2_Prrx1b1x4:ERT2-Gal4_<math>\alpha</math>-crystallin:mRFP</i>	-

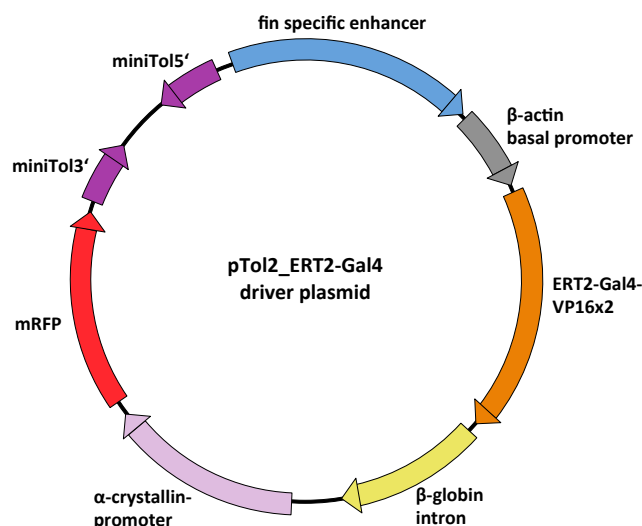


**Fig. 28 Schematic representation of the *pTol2\_ERT2-Gal4-VP16-GI* driver plasmid. A:** In the driver constructs, the fin specific enhancers are located upstream of a  $\beta$ -actin basal promoter, driving the expression of the reporter gene *ERT2-Gal4-VP16x2* with a downstream-located  $\beta$ -globin intron sequence. An  $\alpha$ -crystallin-promoter connected to *mRFP* was added additionally, driving *mRFP* expression in the eye lenses from 4 dpf onwards facilitating identification of transgenic zebrafish larvae. Minimal Tol2 *cis* sequences (MiniTol) flank the whole cassette. They enable the integration of the transgenes into the zebrafish genome by Tol2 transposase activity. Tol2 is injected as mRNA into zebrafish zygotes.

### 2.3.3.1 *Pel2.5kb:ERT2-Gal4*

In the first created *ERT2-Gal4-VP16-GI* zebrafish lines, the *Pitx1* enhancer *Pel2.5kb* drove transgene expression. Two individual lines, founded by the F0 pairs  $\sigma 1/\eta 1$  and  $\sigma 6/\eta 4$ , were successfully established (Table 4). The transgene activity was confirmed via detection of *ERT2-Gal4-VP16* transcripts by means of whole-mount *in situ* hybridisation (WISH). For this, a RNA antisense probe was designed that specifically hybridizes with the sequence encoding the Gal4 DNA binding domain (DBD) (Table 15). In order to examine *ERT2-Gal4-VP16* expression during early pelvic fin development, zebrafish larvae were fixed in pelvic fin developmental stages between S2 and S5. Since these lines contain no *fli:eGFP* marker, the staging process was carried out only regarding the size of the pelvic fin bud in relation to the edge of the minor lobe (see Fig. 10 and Fig. S1). An exact assignment to S1 was therefore not possible.

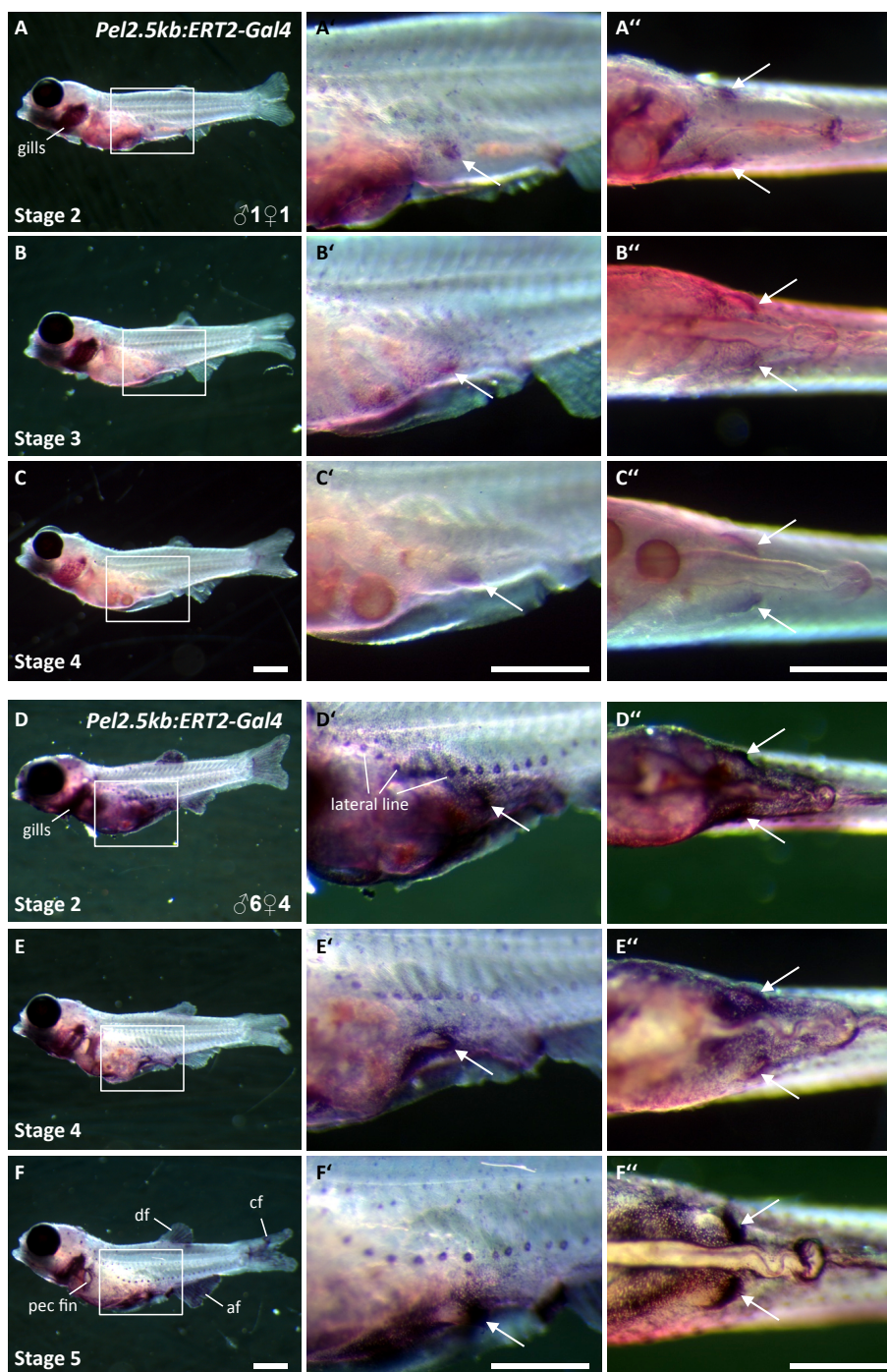


**Fig. 29 Expression of *ERT2-Gal4-VP16* in *Pel2.5kb:ERT2-Gal4-VP16-GI* F2 larvae from two different founder pairs at pelvic fin developmental stages between 2 - 5 (approximately 28 dpf) determined by whole-mount *in situ* hybridization against *Gal4 DBD*. **A-C**: founder pair ♂1/♀1 **D-F**: founder pair ♂6/♀4. Framed areas are shown in higher magnification in the middle column of the panel (**A'-F'**). Specific WISH staining is visible in the pelvic fin buds of both driver lines in all stages (highlighted by white arrows). Additionally, *ERT2-Gal4-VP16* expression was detected in the gills, in the dorsal, anal and caudal fin and in the lateral line. Larvae are shown with anterior to the left in lateral or ventral view (**A''-F''**). pec fin: pectoral fin; df: dorsal fin; cf: caudal fin; af: anal fin. Scale bars: 500  $\mu$ m.**

Larvae of the F2 generation of both individual *Pel2.5kb:ERT2-Gal4-VP16-GI* lines, exhibited specific *ERT2-Gal4-VP16* expression in the pelvic fin buds in all examined developmental stages (Fig. 29). The WISH staining was always detected in the fin bud mesenchyme, with an increasing shift to the proximal domain in later stages, which is in conformity with the previous observations from the *Pitx1* expression analysis (Fig. 13) (Breu, 2017; Weber, 2020). Apart from the pelvic fin buds, other surface exposed structures were labelled. Among these were the gills, the lateral line as well as the pectoral fins, and the dorsal, anal and caudal fin. Moreover, it was noted that the *Pel2.5kb:ERT2-Gal4-VP16-GI* driver line founded by ♂6 and ♀4 showed much stronger transgene expression, but also augmented background staining, in comparison to the line by ♂1 and ♀1 (compare Fig. 29D-F to 29A-C).

The variations in expression strength can be attributed to different integration sites in the genome experiencing different influences from neighbouring regulatory sequences. Furthermore varying numbers of *ERT2-Gal4-VP16-GI* gene copies could have been integrated in the individual founder fish. Altogether, the results clearly demonstrate that the *Pel2.5kb:ERT2-Gal4-VP16-GI* driver construct is able to drive specific transgene expression in the pelvic fin region of zebrafish larvae. Crossing this driver line with the previously established *5xUAS:dnRara2a-IRES-eGFP* effector line and subsequent treatment of the larvae with 4-OHT should therefore result in spatially restricted *dnRara2a* and *eGFP* expression in double transgenic individuals.

### **2.3.3.2 *Prrx1:ERT2-Gal4***

The second zebrafish driver lines contained *ERT2-Gal4-VP16-GI* controlled by the regulatory sequences *Prrx1a* and *Prrx1b1*. In case of *Prrx1a*, three founder fish (♂6, ♂8 and ♂9) and in case of *Prrx1b1* two founder fish (♂6 and ♀7) were identified. Based on these founders, F2 and F3 generations were bred by crossing them with wild type fish of the *Casper* strain. This way, five individual *Prrx1a:* and *Prrx1b1:ERT2-Gal4-VP16-GI* driver lines could have been established (Table 4).

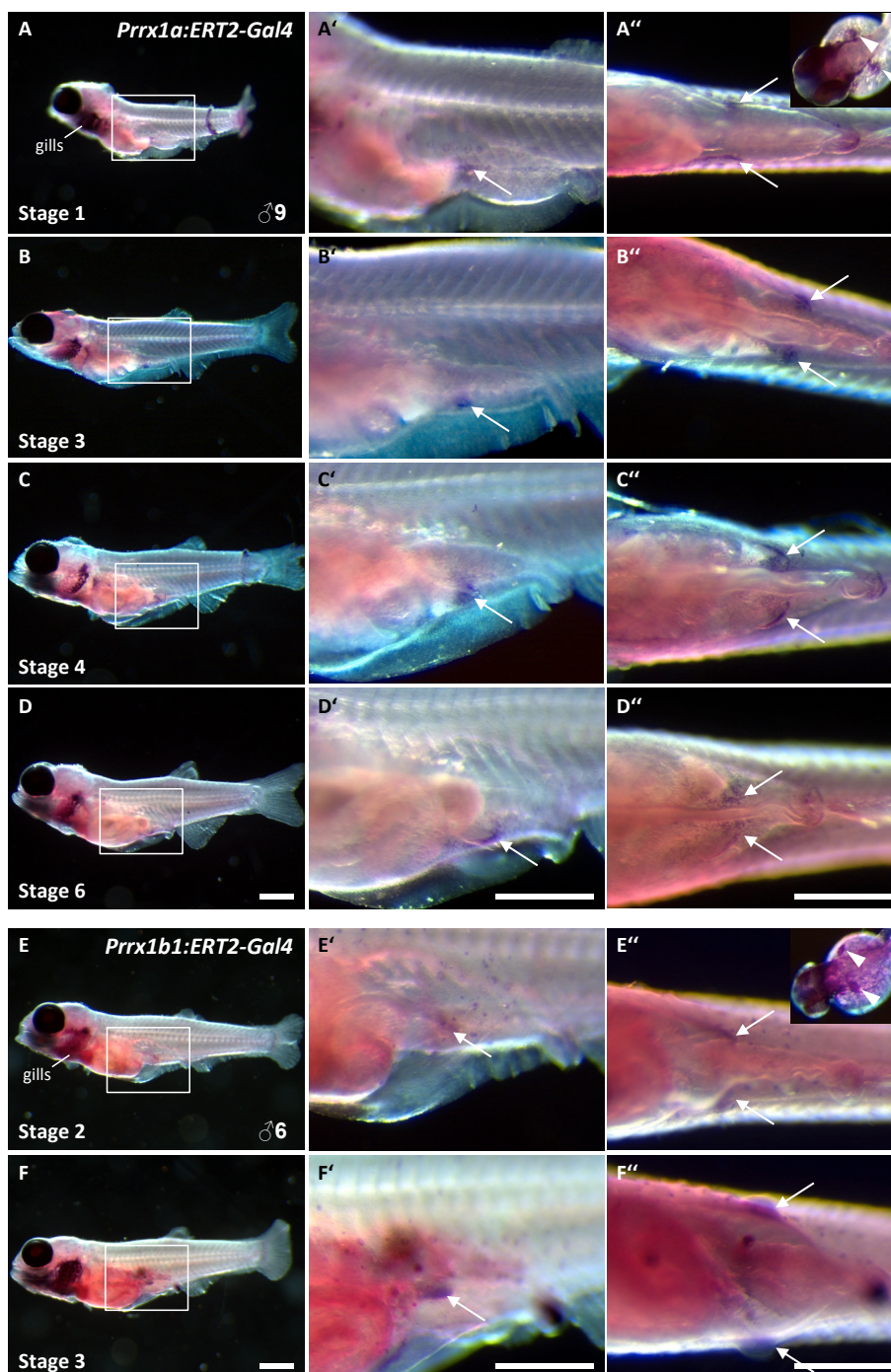


**Fig. 30** Expression of *ERT2-Gal4-VP16* in *Prrx1a:ERT2-Gal4-VP16-GI* F2 larvae (from founder ♂9) (A-D) and *Prrx1b1:ERT2-Gal4-VP16-GI* F3 larvae (from founder ♂6) (E-F) at pelvic fin developmental stages between 1 - 6 (approximately 28 dpf) determined by whole-mount *in situ* hybridisation against *Gal4 DBD*. Framed areas are shown in higher magnification in the middle column of the panel (A'-F'). Specific WISH staining is visible in the pelvic fin buds in all examined stages (highlighted by white arrows). Additionally, *ERT2-Gal4-VP16* expression was detected in the gills. Larvae are shown with anterior to the left in lateral or ventral view (A''-F''). Insets in A'' and E'' show an embryo at 48 hpf in dorsal view demonstrating *ERT2-Gal4-VP16* expression in the pectoral fin bud (arrowheads). Scale bars: 500  $\mu$ m.

In order to investigate the transgene expression in the F2 or F3 generation, WISH against *Gal4 DBD* was conducted at an age of 3 - 4 wpf as it was done with the corresponding Pel2.5kb driver lines. This time, developmental stages between S1 - S6 were taken into account, whereby assignment to S1 is based on an estimate and should therefore be treated with caution. Due to the missing *fli:eGFP* marker in this line, the identification of Stage 1 is actually not possible. In addition, WISH was performed on 48 hpf embryos to examine the *Prrx1a/1b1* mediated transgene expression in the developing pectoral fins as well.

An intense and specific WISH staining was detected in the pectoral fin in each individual line at 48 hpf. A similar picture emerged later at 3 - 4 wpf, where transgene expression was observed in the pelvic fin buds in all examined developmental stages (Fig. 30 and Fig. S21). The expression was localized throughout the entire mesenchyme of the pectoral and pelvic fin buds, respectively, as it was expected from previously performed gene expression studies (Fig. 13) (Eberlein, 2018a; Hernández-Vega & Minguillón, 2011). In these WISH experiments, the best results were obtained for the *Prrx1a:ERT2-Gal4-VP16-GI* line founded by ♂9, in which *ERT2-Gal4-VP16* transcripts could be detected from Stage 1 onwards (Fig. 30A-D). Apart from the expression in the paired fins, WISH staining was documented in the gills and partly in the lateral line (Fig. S21A,B). The transgene expression pattern in the *Prrx1b1:ERT2-Gal4-VP16-GI* line founded by ♀7 has not been determined.

#### **2.3.4 Functionality tests of driver plasmids containing Gal4 derivates**

In the further course of the Gal4-UAS project, several modifications concerning the inducible Gal4 driver lines were made and evaluated in terms of functionality and effectiveness. The following experimental series revolved around the practical application of the two Gal4 derivates KalTA4 and GAVPO (Distel et al., 2009; Wang et al., 2012). As explained in the introduction, KalTA4 is a version of Gal4, which has been adapted to the special properties of the zebrafish model system, characterized by an additional Kozak sequence, an optimized codon usage and a lower toxicity. Its advantage should be an enhanced transgene expression and lesser side effects in the organism (Distel et al., 2009). In contrast to that, GAVPO has been modified in terms of inducibility, which was changed to activation by blue light irradiation. This would avoid the use of toxic substances like 4-OHT, while retaining all

other advantages of the system, such as rapid reversibility and low background activity (Wang et al., 2012).

As another approach to optimize the driver lines, the fin specific enhancers were modified. Consecutive enhancer repeats are used regularly during *in vitro* or *in vivo* assays in order to achieve increased expression, which can be used to address diverse scientific questions (Cohen & Carmichael, 1986; Infante et al., 2013; Menke et al., 2008; Ondek et al., 1987). Interestingly it seems that such mechanisms even evolved in nature as an ingenious way to acquire resistance (Hamamoto et al., 2000). Here, constructs were created that contain four tandem repeats of the Prrx1a or Prrx1b1 limb enhancer sequences. They are henceforth referred to as Prrx1ax4 and Prrx1b1x4, respectively (ordered from eurofins.com and ProteoGenix). These were used in the same way as their single-copy counterparts. First, the fragments were excised from the vectors supplied by the manufacturer and then cloned into the previously established pTol2 driver plasmids in combination with the mentioned Gal4 variants ERT2-Gal4-VP16-GI, KalTA4-ERT2-GI and GAVPO (Table 4, 5, 6).

#### 2.3.4.1 KalTA4

Concerning KalTA4, two different variants were used. On the one hand was the basic *KalTA4-GI* consisting of the *KalTA4* gene sequence in combination with a downstream-located  $\beta$ -globin intron sequence (Distel et al., 2009). On the other hand was the 4-OHT-inducible variant *KalTA4-ERT2-GI*, which is likewise equipped with a  $\beta$ -globin intron sequence (Kajita et al., 2014; vector provided by Masazumi Tada, University College London).

**Table 5. Driver constructs for specific expression of *KalTA4-GI* or *KalTA4-ERT2-GI* in zebrafish paired fins.** Summary of cloned *KalTA4-GI* and *KalTA4-ERT2-GI* driver constructs using diverse fin specific enhancers. So far, no stable transgenic zebrafish lines have been established yet.

Driver plasmid	Stable transgenic zebrafish line
<i>pTol2_Hsp70l:KalTA4-GI_α-crystallin:mRFP</i>	-
<i>pTol2_Pel2.5kb:KalTA4-GI_α-crystallin:mRFP</i>	-
<i>pTol2_Prrx1b1: KalTA4-GI_α-crystallin:mRFP</i>	-
<i>pTol2_Pel2.5kb:KalTA4-ERT2-GI_α-crystallin:mRFP</i>	-
<i>pTol2_Prrx1a: KalTA4-ERT2-GI_α-crystallin:mRFP</i>	-
<i>pTol2_Prrx1b1: KalTA4-ERT2-GI_α-crystallin:mRFP</i>	-
<i>pTol2_Prrx1ax4: KalTA4-ERT2-GI_α-crystallin:mRFP</i>	-
<i>pTol2_Prrx1b1x4: KalTA4-ERT2-GI_α-crystallin:mRFP</i>	-

First of all, the general functionality of KalTA4 in combination with the available 5xUAS effector lines has been tested. The *KalTA4-GI* containing plasmid p300 (Distel et al., 2009) was linearized and used for *in vitro* transcription of *KalTA4-GI* mRNA, which was subsequently injected in zebrafish eggs (one-cell stage) that were obtained from an outcross of the *5xUAS:Cyp26a1-eGFP* strain (see 2.3.1.1; and Eberlein, 2018a, 2018b) with *Casper*. Tessellated eGFP fluorescence was observed at 24 hpf (Fig. 31D), which was similar to the observations following injections of *ERT2-Gal4-VP16* mRNA (Fig. 20D), indicating that KalTA4 is able to activate 5xUAS equally effective as the corresponding Gal4 variant (Mück, 2019).

Afterwards, a universally applicable driver plasmid containing *KalTA4-GI* was created. For this, the *KalTA4-GI* gene sequence was placed downstream of the heat-shock promoter Hsp70I, which was taken from the *Hsp70I:Cyp26a1* vector (p22B, Nicola Blum). Both fragments were PCR-amplified, with recognition sites for DNA endonucleases added at the 5' and 3' ends of the PCR product at the same time. The *pTol2\_enhancer:ERT2-Gal4-VP16-GI* driver plasmids (Fig. 28) were used as backbone. During the cloning procedure, the entire *enhancer:ERT2-Gal4-VP16-GI* cassette was excised while leaving the *α-crystallin:mRFP* marker gene in place. In the end, this resulted in the assembly of the *pTol2\_Hsp70I:KalTA4-GI* driver plasmid, schematically presented in Fig. 31A (Ng, 2019). To test the functionality of this construct, the plasmid was injected in the one-cell stage of zebrafish eggs obtained either from an incross of *UAS:GFP* fish or from an outcross of the *5xUAS:Cyp26a1-eGFP* strain with *Casper*. At 50 % epiboly, a single heat-shock treatment was performed at 40 °C for 2 h. This resulted in intense GFP/eGFP fluorescence at 24 hpf in both, *UAS:GFP* and *5xUAS:Cyp26a1-eGFP* embryos (Fig. 31I,J). In case of *5xUAS:Cyp26a1-eGFP* embryos the distribution of the fluorescence was in a mosaic pattern, whereas *UAS:GFP* embryos exhibited a more even patterning. To exclude intrinsic GFP fluorescence, a control group was heat-shocked without previous plasmid injection (Fig. 31H) (Ng, 2019). Injections of p22B served as a positive control, however, heat-shock-induced *Cyp26a1* overexpression had fatal effects on the embryos (data not shown) (Ng, 2019). These experiments demonstrated that the heat-shock treatment was able to induce *KalTA4* expression. KalTA4 in turn bound to UAS and effectively activated *GFP/eGFP* expression in transgenic zebrafish effector lines, suggesting that the construct is working (Ng, 2019).

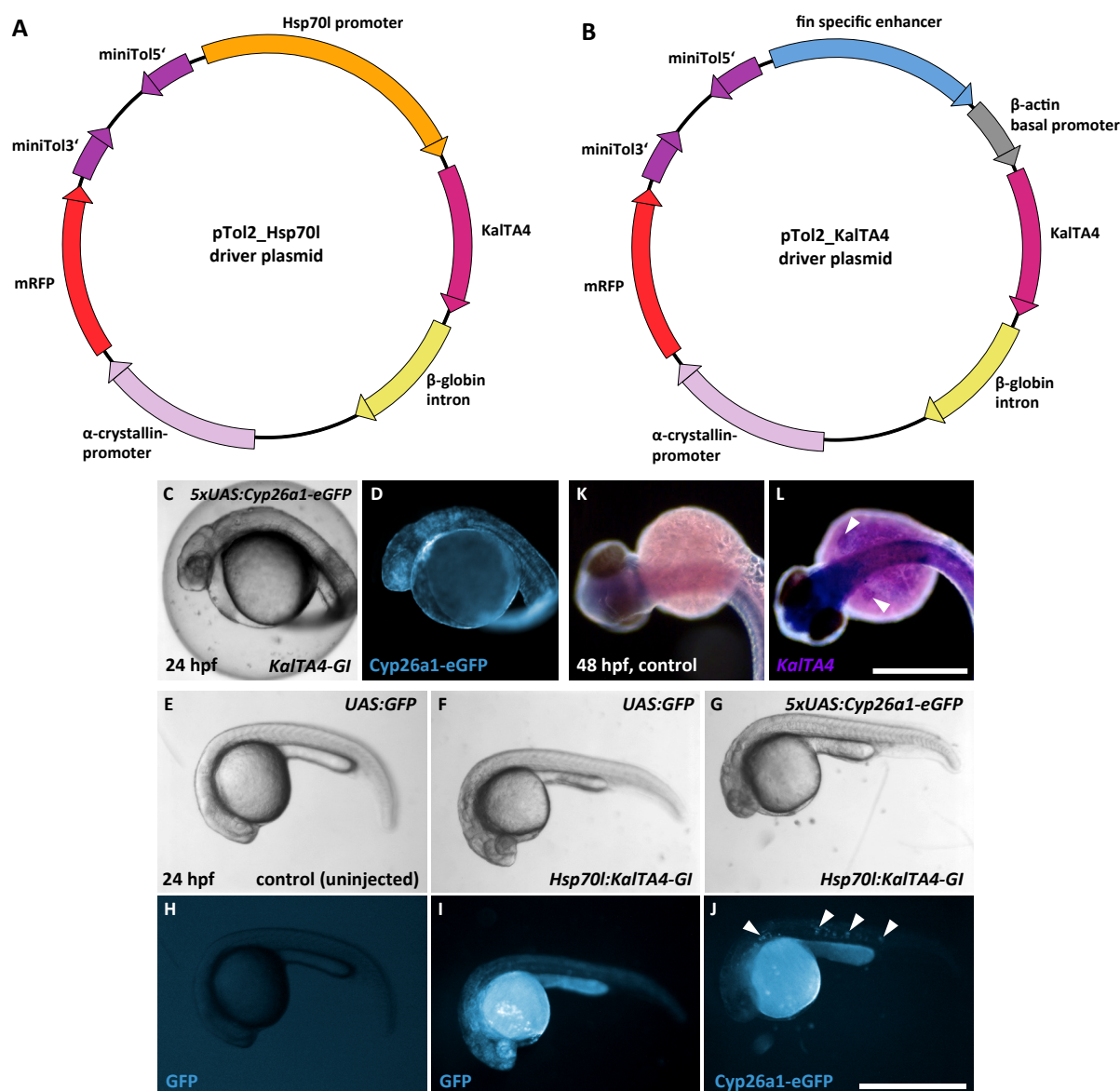


**Fig. 31** *KalTA4* induces transgene expression in UAS effector lines. **A/B**: Schematic representations of driver plasmids containing either *KalTA4* with a downstream located  $\beta$ -globin intron sequence (*KalTA4-GI*) under the control of the Hsp70I promoter (**A**) or under the control of different fin specific enhancers (**B**). The marker gene  $\alpha$ -crystallin:*mRFP* facilitates the identification of transgenic zebrafish by driving the expression of red fluorescent protein in the eye lenses. **C/D**: *KalTa4-GI* mRNA (30 ng/ $\mu$ l) was injected in zebrafish eggs of the *5xUAS:Cyp26a1-eGFP* strain at the one-cell stage. At 24 hpf eGFP fluorescence is visible throughout the entire body. **E-J**: Zebrafish eggs of the strains *UAS:GFP* or *5xUAS:Cyp26a1-eGFP* were injected with *pTol2\_Hsp70I:KalTA4-GI* (40 ng/ $\mu$ l) at the one-cell stage. The heat-shock was performed at 40 °C for 2 h at 50 % epiboly. Uninjected embryos were used as control to exclude intrinsic fluorescence of the *UAS:GFP* strain. At 24 hpf, intense GFP fluorescence was observed in *UAS:GFP* embryos (**I**), while *5xUAS:Cyp26a1-eGFP* embryos showed a more tessellated eGFP fluorescence (**J**, arrowheads). Scale bar: 500  $\mu$ m. **K/L**: *KalTA4* is expressed under the control of fin specific enhancers. The driver plasmid *pTol2\_Prrx1b1:KalTA4-GI\_α-crystallin:mRFP* (**B**) was injected (40 ng/ $\mu$ l) together with *Tol2* mRNA (30 ng/ $\mu$ l) in zebrafish eggs of the *Casper* strain at the one-cell stage. WISH against *KalTA4* mRNA demonstrates *KalTA4* expression in pectoral fin buds at 48 hpf (**L**, arrowheads), while uninjected control embryos show no staining (**K**). Scale bar = 300  $\mu$ m. Pictures C,D,K,L by Amelie Mück; taken and modified from Mück, 2019. Pictures E-J by Xuen J. Ng; taken and modified from Ng, 2019.

Furthermore, it was continued with the cloning of selected *pTol2\_enhancer:KalTA4-GI* driver plasmids (Fig. 31B, Table 5). The already existing *pTol2\_enhancer:ERT2-Gal4-VP16-GI* driver constructs were used as backbone and the *ERT2-Gal4-VP16-GI* fragment replaced with *KalTA4-GI* (Mück, 2019). In order to test whether the fin specific enhancers spatially restrict *KalTA4* expression, the driver plasmid containing the *Prrx1b1* enhancer was exemplary co-injected with *Tol2* mRNA in zebrafish eggs of the *Casper* strain (one-cell stage). The detection of *KalTA4* transcripts was carried out via whole-mount *in situ* hybridisation (WISH) using a specific *KalTA4* antisense probe (Table 15). This revealed a local concentration of WISH staining in the pectoral fin buds at 48 hpf, while uninjected embryos were completely colourless, confirming the tissue specificity of the enhancer mediated *KalTA4* expression (Fig. 31K,L) (Mück, 2019).

Next, the tamoxifen-inducible version of *KalTA4* was tested. First, *in vitro* transcribed *KalTA4-ERT2-GI* mRNA was produced from the vector p431 (Kajita et al., 2014). Subsequently it was injected in zebrafish eggs at the one-cell stage, that were obtained from an incross of the *5xUAS:dnRara2a-IRES-eGFP* strain (from founder fish ♂10 and ♂13; see 2.3.1.2 and Schmidt, 2017). At 50 % epiboly, *KalTA4-ERT2* activity was induced by treating the larvae with 5 µM 4-OHT. Control groups were supplied with equivalent amounts of pure EtOH. At 24 hpf, only induced embryos exhibited intense eGFP fluorescence that was predominantly distributed in the head and trunk as well as in the yolk (Fig. 32E-G). Moreover, larvae showed a bulge in the 'neck' (Fig. 32C,D), which is a typical characteristic of the *Aldh1a2* mutant *neckless* and indicates RA deficiency (Begemann et al., 2001), which is in this case mediated by *dnRara2a* activity. In addition, WISH against *Epha4a* and *MyoD* revealed a shortening of the anteriorposterior axis, resulting in an approaching of the rhombomere 5 to the first somite. In some individuals, even a partly disappearance of rhombomere 5 was documented (Fig. 32H-J), pointing to an effective suppression of the RA signalling pathway (Ng, 2019).

Since these experiments confirmed the functionality of *KalTA4-ERT2-GI* with regard to its inducibility with 4-OHT and also its compatibility with the established 5xUAS effector lines, new driver plasmids were cloned that contained this particular gene construct. For this purpose, the existing driver plasmids (Fig. 28) were again modified by removing the *ERT2-Gal4-VP16-GI* part and replacing it with *KalTA4-ERT2-GI*. This was conducted for all available

fin specific enhancers, including the recently obtained *Prrx1ax4* and *Prrx1b1x4* tandem copy variants (Fig. 32A; Table 5) (Ng, 2019; Lina Stacker).

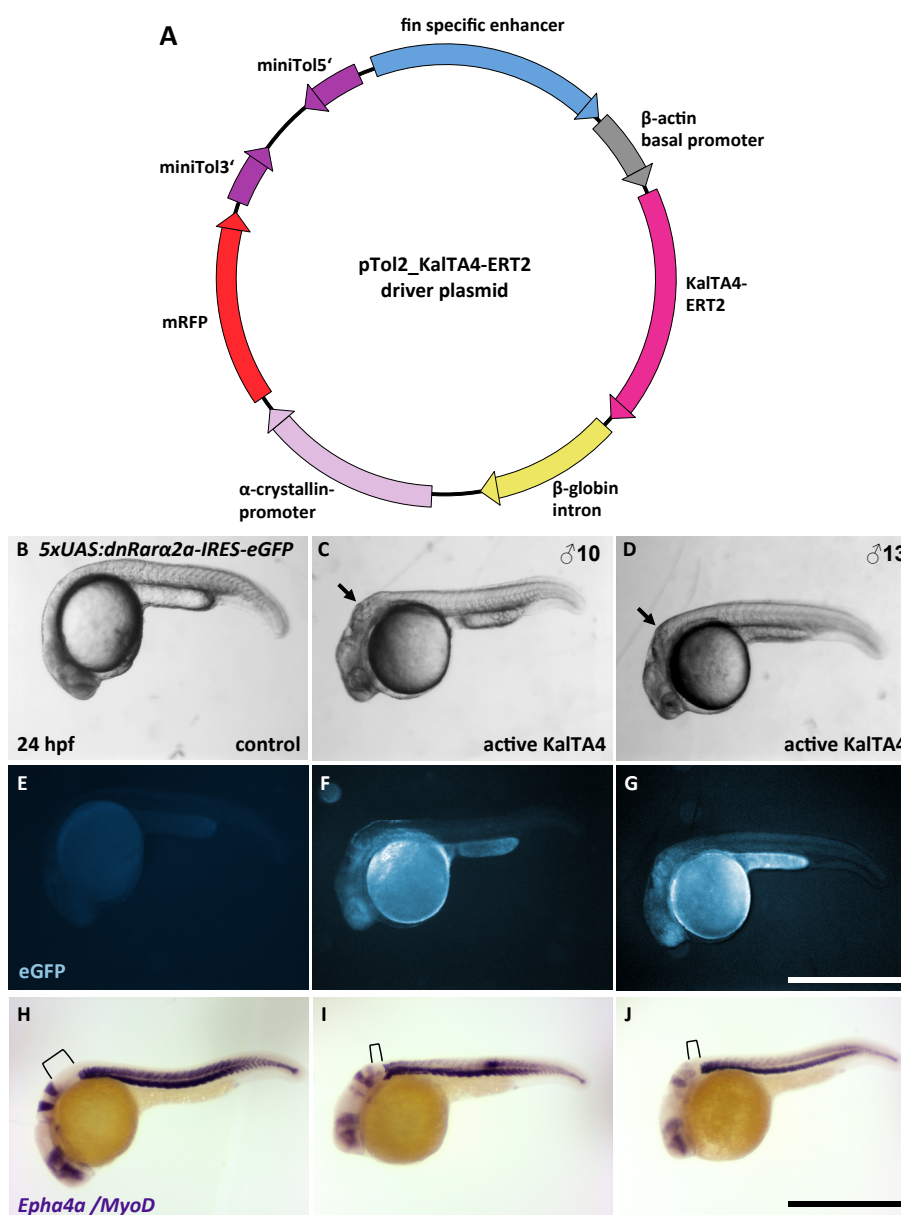


**Fig. 32** *KalTA4-ERT2* induces transgene expression in UAS effector lines. **A**: Driver plasmid containing *KalTA4-ERT2-GI*, a fusion construct of the *Gal4*-derived gene *KalTA4* and an estrogen ligand-binding domain requiring 4-hydroxy-tamoxifen for activity, driven by different fin specific enhancers that are present either in a single copy (*Prrx1a/Prrx1b1/Pel2.5kb*) or in four tandem repeats (*Prrx1ax4/Prrx1b1x4*). **B-G**: *KalTA4-ERT2* induces transgene expression in *5xUAS* effector lines. *KalTA4-ERT2-GI* mRNA (40 ng/ $\mu$ l) was injected in *5xUAS:dnRara2a-IRES-eGFP* F3 zygotes of founder fish  $\delta$  10 and  $\delta$  13 and subsequently treated with 5  $\mu$ M 4-OHT or EtOH (control) at 50% epiboly. At 24 hpf only induced embryos show the characteristic bulge in the 'neck' of the RA-deficiency phenotype (highlighted with arrows) (**C/D**). eGFP fluorescence is visible in these embryos throughout the whole body (**F/G**). Whole-mount *in situ* hybridisation (WISH) against *Epha4a* and *MyoD* shows a truncation of the anteroposterior axis anterior to the somites. The distance between rhombomere 5 and somite 1 is indicated with brackets (**H-J**). Scale bars: 500  $\mu$ m. Pictures B-J by Xuen J. Ng; taken and modified from Ng, 2019.

### 2.3.4.2 GAVPO

In the next project, the light-inducible Gal4 derivative GAVPO was investigated (Fig. 33A). Again, an universal driver plasmid was cloned first, which contained GAVPO under the control of the ubiquitously expressed ubiquitin promoter (*ubi*) (Mosimann et al., 2011). As backbone, one of the 'zero background' Tol2 plasmids designed by David Richter (University of Bayreuth) was used, the one possessing the  $\alpha$ -*crystallin:Citrine* marker gene (Fig. S15A). In addition to the toxic *ccdB* gene (Couturier et al., 1998), the 4xnrUAS sequences were removed as well in this case. The two fragments to be inserted - the *ubi* promoter and GAVPO - were PCR-amplified from the vectors pENTR5'\_*ubi* (p334; Mosimann et al., 2011) and pGAVPO (p427; Wang et al., 2012), respectively, and ligated with the linearized pTol2 backbone by means of Gibson Assembly to obtain *pTol2\_ubi:GAVPO* (Fig. 33B).

In order to test whether GAVPO is working in combination with the 4xnrUAS effector constructs, the driver plasmid *pTol2\_ubi:GAVPO* was co-injected with the effector plasmid *pTol2\_4xnrUAS:dnRara2a-IRES-eGFP* (Schmidt, 2017) (each 12,5 ng/ $\mu$ l) in zebrafish eggs of the *Casper* strain at the one-cell stage. At 50 % epiboly, the embryos were illuminated with blue LED light until 24 hpf under the exclusion of further external light exposure (Mayer, 2020). This treatment resulted in *eGFP* expression in 16 % of the embryos that were kept under blue-light (21/126), while only 1 % of the control embryos that were kept in the dark during the whole time showed a weak fluorescence signal (2/149) (Fig. 33G-I) (Mayer, 2020). This indicates, that GAVPO is in fact able to bind to the 4xnrUAS and activate downstream gene expression. It also demonstrates the blue-light inducibility and the low background activity of GAVPO, since the control groups that were kept in the dark barely showed any transgene expression. In most *eGFP* expressing embryos, the fluorescence was found in the yolk (Fig. 33H), however, some also exhibited expression in distinct body cells (Fig. 33I) (Mayer, 2020). Apart from *eGFP* fluorescence, many embryos showed several malformations like a shortened tail or reduced eyes, but did not represent the RA deficiency phenotype known from the *nls* mutant (Begemann et al., 2001). This is in conformity with the expectations, since plasmid injections always results only in mosaic expression of the transgene, which means that no holistic effect can be achieved in the entire embryo. However, the observed side effects indicate that GAVPO seems to be quite toxic to the embryos. This probably could be improved by lowering the injected plasmid concentration or maybe by the application of *GAVPO* mRNA instead of the plasmid.

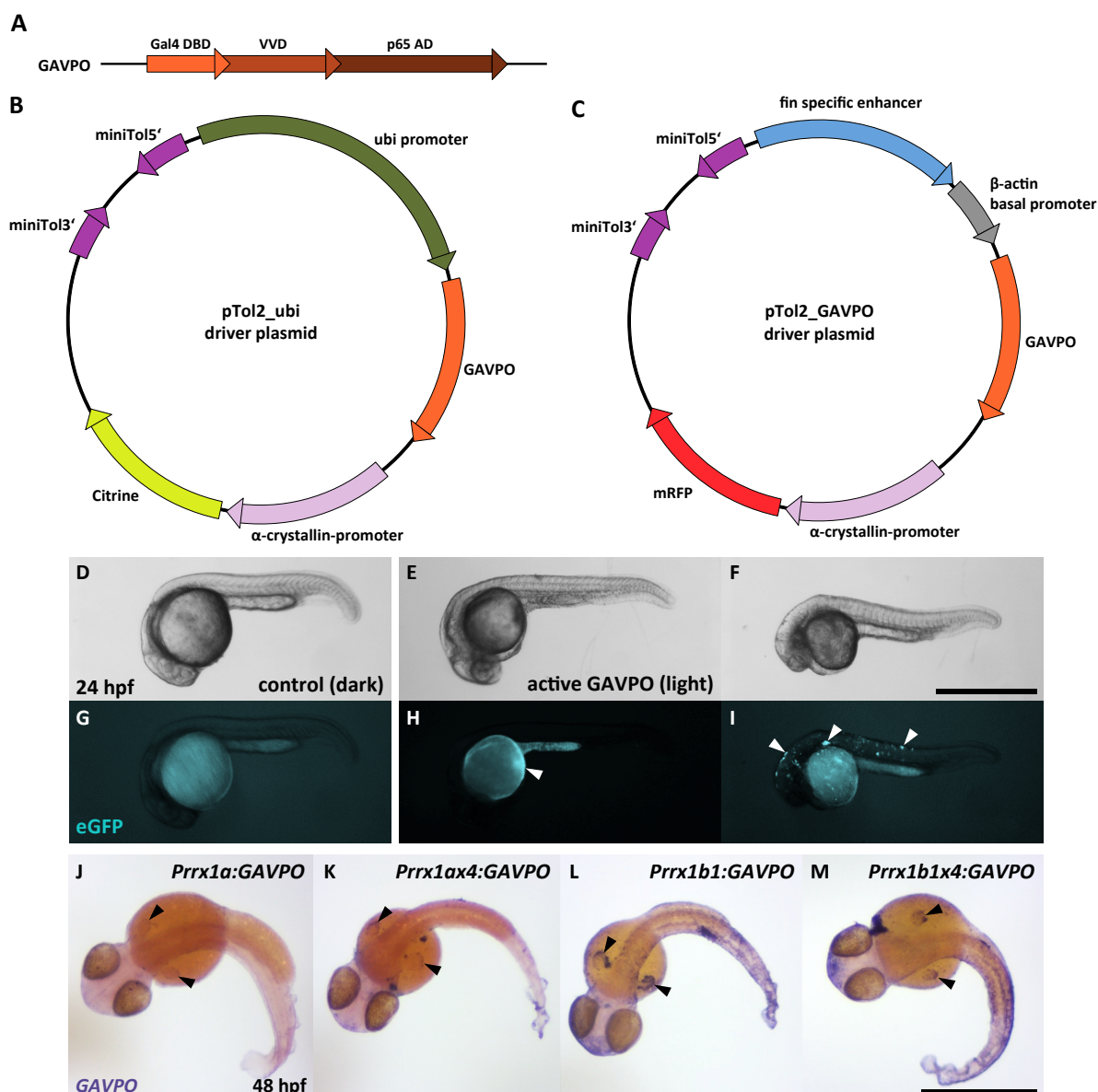


**Fig. 33 Schematic representations of GAVPO driver plasmids. A:** Gene architecture of the light-inducible, *Gal4*-derived construct *GAVPO*, consisting of the Gal4 DNA binding domain (DBD), the smallest light-oxygen-voltage (LOV) domain Vivid (VVD) and the p65 transactivation domain (AD). **B:** Driver plasmid containing *GAVPO* under the control of the ubi promoter. **C:** Driver plasmid containing *GAVPO* driven by different fin specific enhancers, either present in a single copy (*Prrx1a/Prrx1b1/Pel2.5kb*) or in four tandem repeats (*Prrx1ax4/Prrx1b1x4*). The marker genes *α-crystallin:Citrine* or *α-crystallin:mRFP* facilitate the identification of transgenic zebrafish. **D-I:** *GAVPO* is able to bind to *4xnrUAS* and initiate gene expression upon blue-light activation. Zebrafish eggs of the *Casper* strain were co-injected with *pTol2\_ubi:GAVPO* and *pTol2\_4xnrUAS:dnRara2a-IRES-eGFP* (12,5 ng/μl each) at the one-cell stage and illuminated with blue LED light from 50 % epiboly onwards. eGFP fluorescence was observed almost exclusively in embryos that were exposed to blue-light, mostly located in the yolk (**H**), but also in distinct body cells (**I**) (arrowheads). Embryos are shown in lateral view with anterior to the left. **J-M:** *GAVPO* is expressed under the control of fin specific enhancers. Driver plasmids containing *GAVPO* and either *Prrx1a*, *Prrx1ax4*, *Prrx1b1*, or *Prrx1b1x4* enhancer (**C**) were co-injected with *Tol2* mRNA (40 ng/μl each) in zebrafish eggs of the *Casper* strain at the one-cell stage. WISH against *GAVPO* mRNA demonstrates its expression in pectoral fin buds at 48 hpf (arrowheads). Embryos are shown in dorsal view with anterior to the left. Scale bars = 500 μm. Pictures D-M by Anna-Maria Mayer; taken and modified from Mayer, 2020.

**Table 6. Driver constructs for specific expression of *GAVPO* in zebrafish paired fins.** Summary of cloned *GAVPO* driver constructs using diverse fin specific enhancers. So far, no stable transgenic zebrafish lines have been established yet.

Driver plasmid	Stable transgenic zebrafish line
<i>pTol2_ubi:GAVPO_α-crystallin:Citrine</i>	-
<i>pTol2_Pel2.5kb:GAVPO_α-crystallin:mRFP</i>	-
<i>pTol2_Prrx1a:GAVPO_α-crystallin:mRFP</i>	-
<i>pTol2_Prrx1b1:GAVPO_α-crystallin:mRFP</i>	-
<i>pTol2_Prrx1ax4:GAVPO_α-crystallin:mRFP</i>	-
<i>pTol2_Prrx1b1x4:GAVPO_α-crystallin:mRFP</i>	-

Based on these results, driver plasmids that contain *GAVPO* under the control of the five available fin specific enhancers - *Pel2.5kb*, *Prrx1a*, *Prrx1b1*, *Prrx1ax4* and *Prrx1b1x4* - were cloned and tested for activity and tissue specific expression (Table 6; Fig. 33J-M). The cloning process was started on the basis of the *pTol2\_enhancer:KalTA4-ERT2-GI* driver plasmids (Table 5; Fig. 32A), from which the *KalTA4-ERT2-GI* fragment was excised and replaced with *GAVPO*. DNA assembly was carried out by means of Gibson Assembly (Mayer, 2020).

Then, the fin specific expression of *GAVPO* under the control of the respective enhancers was assayed. In parallel, an evaluation of the effectiveness of the four tandem repeats of *Prrx1a* and *Prrx1b1* took place. For this, each of the driver plasmids with the enhancers *Prrx1a* and *Prrx1ax4* as well as *Prrx1b1* and *Prrx1b1x4* was co-injected with *Tol2* mRNA (40 ng/μl each) in the one-cell stage of zebrafish eggs of the *Casper* strain. The detection of *GAVPO* transcripts took place via whole-mount *in situ* hybridisation (WISH) using a *GAVPO* specific RNA antisense probe (Table 15) (Mayer, 2020). It was found that all four driver constructs mediated pectoral fin specific *GAVPO* expression at 48 hpf (Fig. 33J-M). The intensity of WISH staining was significantly stronger following injections of *Prrx1b1* and *Prrx1b1x4* driver plasmids compared to *Prrx1a* and *Prrx1ax4*. This was not observed in earlier expression studies in which *ERT2-Gal4-VP16* transcripts have been detected (Fig. 30, insets in A'' and E''). Also the expression level of *Prrx1a* and *Prrx1b* itself was found to be approximately the same previously (Fig. 13) (Eberlein, 2018a). Therefore the observed variations are most likely attributable to different qualities of the injection process. Furthermore, no significant differences between the transgene expression mediated by the tandem-copy enhancers compared to their single-copy counterparts were observed (Mayer, 2020).

It is conceivable that this experimental setup is not suitable to detect differences in enhancer activity due to the mosaic distribution of the injected nucleic acids and that stable transgenic lines are needed to carry out more detailed investigations.

### 2.3.5 Crossing driver and effector lines to manipulate retinoic acid signalling

The next and essential step in establishing the Gal4-UAS system is the crossing of driver and effector lines and the subsequent induction of UAS-mediated transgene expression to achieve spatially restricted manipulation of RA signalling. Several crossings were conducted with different combinations of driver and effector lines, which were available as F2 generation at this time (Table 7).

**Table 7. Zebrafish driver and effector lines available in F2 generation.** Summary of *ERT2-Gal4-VP16-GI* driver lines and 5xUAS effector lines that were established in the course of this study and are now available at least in F2 generation. The line *UAS:GFP* was already present in the zebrafish facility and is listed for the sake of completeness.

Zebrafish driver lines	Zebrafish effector lines
<i>PeI2.5kb:ERT2-Gal4-VP16-GI_α-crystallin:mRFP</i>	<i>UAS:GFP</i>
<i>Prrx1a:ERT2-Gal4-VP16-GI_α-crystallin:mRFP</i>	<i>5xUAS:Cyp26a1-eGFP_α-crystallin:mRFP</i>
<i>Prrx1b1:ERT2-Gal4-VP16-GI_α-crystallin:mRFP</i>	<i>5xUAS:dnRara2a-IRES-eGFP_α-crystallin:mRFP</i>

Embryos obtained from crossings of the *Prrx1a* or *Prrx1b1* driver lines with any UAS effector line were grown to 24 hpf and then treated with 5  $\mu$ M 4-OHT. As these enhancers are already active during pectoral fin development, expression of eGFP and evaluation of the RA-deficiency phenotype mediated by activity of *dnRara2a* took place at 48 hpf first. Here it should be noted that the *Cyp26a1-eGFP* fusion construct, since it seems to be non-functional (see 2.3.1.1 and Eberlein, 2018a, 2018b), was used only for reporting purposes rather than manipulation of RA signalling. As soon as these experiments work satisfactorily, the study of pelvic fin development should be started. However, none of the tested combinations led to a visible transgene expression at 48 hpf, based on the presence of eGFP fluorescence (data not shown).

The only exception were the embryos obtained from the crossing of the driver line *Prrx1a:ERT2-Gal4-VP16-GI* (from founder ♂9) with the effector lines *UAS:GFP* or *5xUAS:Cyp26a1-eGFP* (founder pair ♂8/♀8). In the progeny, pronounced GFP/eGFP signal was detected at 48 hpf, following 24 h of treatment with 5  $\mu$ M 4-OHT (Fig. 34A-D).

However, contrary to the expectation, the fluorescence was not located in the pectoral fin buds, but was detected in the trunk and tail in a stripe pattern. A GFP signal in the pectoral fins could be observed at 5 dpf in *UAS:GFP* embryos concentrating in few defined stripes (Fig. 34C, arrowhead). Since the observed fluorescence never occurred in EtOH-treated control embryos, an intrinsic GFP signal can be excluded, which shows that the induction is dependent on 4-OHT (data not shown).

Concerning the crossing of *Prrx1a:ERT2-Gal4-VP16-GI* (from founder ♂9) with *5xUAS:Cyp26a1-eGFP* (founder pair ♂8/♀8), this streak-like eGFP fluorescence pattern was observed in about 20 % of the induced offspring (Fig. 34D). This fits well with the statistical percentage (25 %) of double transgenic individuals who carry both components of the Gal4-UAS system. The embryos of this clutch were subsequently sorted by fluorescence and subjected to a WISH using the RNA antisense probe detecting the *Gal4 DBD* sequence (Table 15) in order to check the location of *ERT2-Gal4-VP16* transcripts. Specific WISH staining was found in the pectoral fin buds of embryos from both groups, the GFP-positive (GFP+) and GFP-negative (GFP-) ones (Fig. 34E,F).

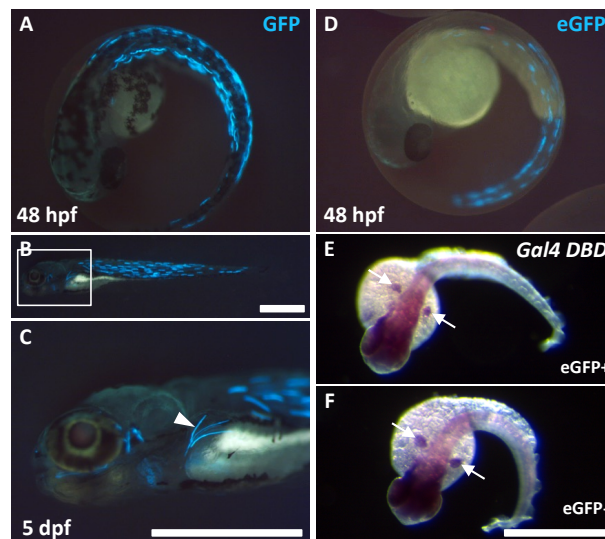


**Fig. 34 Crossings of driver and effector lines.** The induction of transgene expression took place with 5  $\mu$ M 4-OHT from 24 hpf onwards. **A-C:** Offspring of a crossing of *Prrx1a:ERT2-Gal4-VP16-GI* F2 (♂9) with *UAS:GFP*. 4-OHT-treatment results in *GFP* expression in the trunk and tail in a stripe pattern at 48 hpf and 5 dpf. Transgene expression in the pelvic fins was detected in defined stripes at 5 dpf (arrowhead). **D-F:** Offspring of a crossing of *Prrx1a:ERT2-Gal4-VP16-GI* F2 (♂9) with *5xUAS:Cyp26a1-eGFP* F1 (♂8♀8). After 4-OHT-induction, eGFP fluorescence was detected in a stripe pattern in the trunk and tail at 48 hpf in about 20 % of the embryos (**D**). Embryos were sorted in eGFP-positive ones (eGFP+) and eGFP-negative ones (eGFP-). Whole-mount *in situ* hybridisation against *Gal4 DBD* shows specific expression of *ERT2-Gal4-VP16* in the pelvic fins (marked with arrows) in eGFP+ and eGFP- embryos (**E,F**). Scale bars = 500  $\mu$ m.

These results raised the question why the location of *ERT2-Gal4-VP16* expression deviates from the location of eGFP fluorescence originating from the Cyp26a1-eGFP fusion protein. It is certain that the *Prrx1a* driver line expresses *ERT2-Gal4-VP16* in the expected tissue (Fig. 30; Fig. 34E,F), which is the mesenchyme of the pectoral fin bud. It is also certain that the presence of GFP/eGFP fluorescence is dependent on the treatment with 4-OHT. In order to clarify a potential translocation of the ERT2-Gal4-VP16 protein after its translation, fluorescence immunostaining was performed with a primary antibody that binds to the Gal4 DBD. However the method used did not work as expected, probably due to technical problems, so that the location of ERT2-Gal4-VP16 protein remains elusive (data not shown) (Ng, 2019). Another question that was raised was, why transgene expression is only achieved upon crossing these particular driver and effector lines, while in all other combinations the 4-OHT inductions remained unsuccessful.

In case the Pel2.5kb driver line was used, larvae were treated with a concentrations of 2, 3 or 5  $\mu$ M 4-OHT at an age of 3 - 4 wpf, at the point when pelvic fins begin to develop. However, concentrations of 5 and 3  $\mu$ M caused severe side effects in larvae of this age, although they were well tolerated in embryos and larvae up to 5 dpf. The side effects included rapid breathing and degeneration of fins and gills (data not shown). The experiments were therefore henceforth performed with 2  $\mu$ M 4-OHT, which did not seem to be toxic to the animals. However, also in the offspring from crossing the Pel2.5kb driver line with one of the effector lines, no UAS-mediated transgene expression could be initiated (data not shown).

Altogether, this brings about the hypothesis that there is any basic methodical problem in the Gal4-UAS system as it was established here. However, more testing is needed to uncover the cause for the failure of the method. Probably further modifications and optimisations are required to resolve the problem in order to establish a stable, functioning genetic tool.

## 2.4 Creation and testing of *dnRara2a*/ERT2 fusion constructs

As the establishment of the Gal4-UAS system turned out to be problematic, one further idea was to circumvent the binary system and combine driver and effector in one single construct. Accordingly, new fusion constructs have been designed, in which *dnRara2a* and *ERT2* were directly linked to each other. In two different variants, *ERT2* was positioned either at the 3' or 5' end of *dnRara2a* (Fig. 35A,B), since both positions proved to be functional, for example in *ERT2-Gal4* or *KalTA4-ERT2* constructs (Akerberg et al., 2014; Distel et al., 2009; Gerety et al., 2013; Kajita et al., 2014).

The pTol2 vector (p365) was used as backbone again. Its minimal Tol2 *cis* sequences flank the insert and enable the integration of the transgene into the zebrafish genome by Tol2 transposase activity. In the first design, *dnRara2a*/ERT2 fusion constructs were put under the control of the *Prrx1ax4* enhancer consisting of four consecutive repeats. Additionally, they were linked to *mRFP* via an IRES sequence. Based on this arrangement, the expression of *mRFP* should take place completely independently of induction with 4-OHT, thus avoiding the necessity of an additional marker gene in the plasmid to facilitate identification of transgenic individuals.

In order to test the functionality of the fusion constructs, the plasmids were co-injected with *Tol2* mRNA in zebrafish zygotes of the *Casper* strain, which were subsequently treated with 5  $\mu$ M 4-OHT or EtOH as control. At 48 hpf, induced embryos injected with the *dnRara2a-ERT2* construct showed a mild growth retardation indicated by reduced body length and eye pigmentation. Additionally a reduction of the pectoral fin size could be observed (Fig. 35C,D). This phenotype became more evident at 72 hpf (Fig. 35E,F). In contrast to that, induced embryos injected with the *ERT2-dnRara2a* plasmid showed severe malformations at 48 hpf. Pectoral fins were partially or completely reduced and some embryos exhibited a bulge in the neck, resembling the RA-deficiency phenotype observed in the *nls* mutant (Begemann et al., 2001) (Fig. 35H). However, also control embryos were affected, though not as severe (Fig. 35G). Neither control nor 4-OHT-treated embryos survived until 72 hpf, indicating that the *ERT2-dnRara2a* construct is quite toxic to the embryos and has a significant background activity.

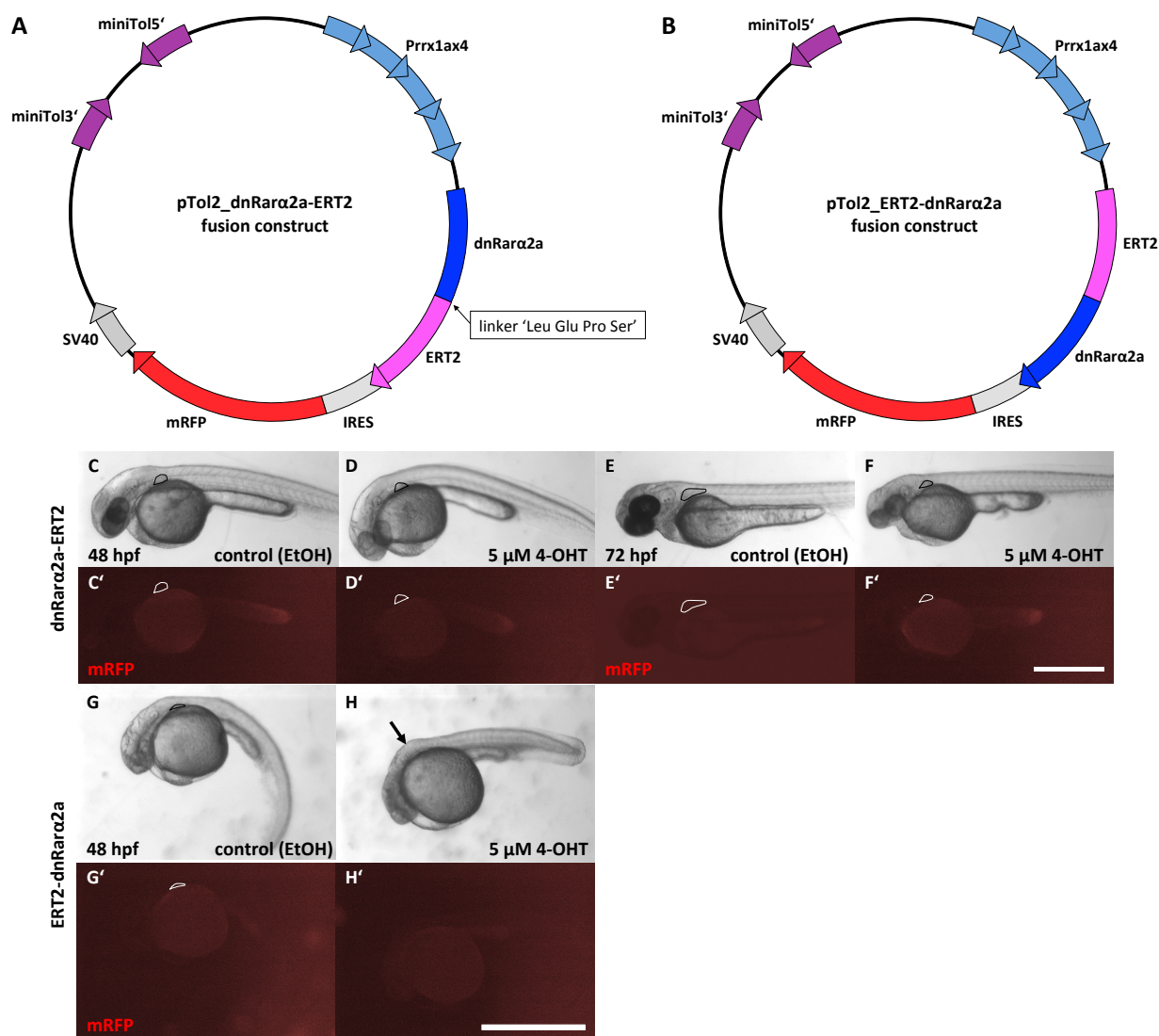


**Fig. 35 Local expression of fusion constructs of *dnRara2a* and *ERT2* result in developmental defects of zebrafish embryos.** **A,B:** Schematic representations of two constructs of *ERT2* linked to *dnRara2a* either at the 3' (**A**) or the 5' end (**B**). In *dnRara2a-ERT2*, a sequence encoding a linker peptide consisting of four amino acids is located between both genes to separate the individual components of the fusion protein. The red fluorescent marker gene *mRFP* is connected to each construct via an IRES sequence, creating two separate reading frames. These cassettes are each under the control of the zebrafish *Prrx1ax4* enhancer, driving transgene expression in both, pectoral and pelvic fins. **C-H:** The plasmids *pTol2\_Prrx1ax4:dnRara2a-ERT2-IRES-mRFP* (**C-F**) or *pTol2\_Prrx1ax4:ERT2-dnRara2a-IRES-mRFP* (**G-H**) were co-injected with *Tol2* mRNA (40 ng/μl each) in fertilized zebrafish zygotes and subsequently treated with 5 μM 4-OHT or EtOH (control) at 50 % epiboly. The observation took place at 48 and 72 hpf. The *dnRara2a-ERT2* fusion construct resulted in growth retardation of the embryo and in a reduction of the pectoral fin size (marked by black or white outline). The control embryos seemed to develop normally (**C-F**). Embryos injected with the *ERT2-dnRara2a* fusion construct showed more severe phenotypes. Some had a bulge in the 'neck' indicating a RA-deficiency phenotype (arrow) (**H**) and also the control embryos were affected with growth retardation - observations that both are suggesting a background activity of *ERT2-dnRara2a* (**G**). Neither control nor 4-OHT-treated embryos injected with this construct survived until 72 hpf. A red fluorescence originating from *mRFP* was visible with neither construct (**C'-H'**). Embryos are shown in lateral view with anterior to the left. Scale bar = 500 μm.

Such pronounced developmental defects were not expected from injecting a *dnRara2a* construct controlled by the fin specific *Prrx1a* enhancer. One possible explanation would be that the *Prrx1ax4* construct does not work as expected or its tissue specificity is lost, however, the conducted expression studies in the course of the GAVPO test series refute this theory (see Fig. 33J,K). Moreover, no mRFP fluorescence was observed in the pectoral fins of the injected embryos, which should in principle occur independently of the 4-OHT-induction (Fig. 35C'-H'). Most likely the mRFP fluorescence was too weak to be detected. This is due to the mosaic expression as a result of the injection process and to the comparably low intensity of mRFP fluorescence (Wan et al., 2002).

Based on these results, mRNAs of the *dnRara2a-ERT2* and *ERT2-dnRara2a* constructs were synthesized *in vitro*. The objective was to analyse the phenotype of the fusion constructs independently of the spatial restrictions originating from the *Prrx1ax4* enhancer activity. The mRNA was injected in fertilized zebrafish eggs of the *Casper* strain with subsequent 4-OHT treatments (partially performed by Lina Stacker). Maximal mRNA concentrations of 200 ng/ $\mu$ l (for *dnRAara2a-ERT2*) and 586 ng/ $\mu$ l (for *ERT2-dnRara2a*) were used. However, this did not result in any phenotype at 24 or 48 hpf (data not shown). Probably the mRNAs were inactive or even higher concentrations would be required to achieve an effect.

Further experiments therefore focused on the creation of a plasmid containing the *dnRara2a-ERT2* construct under the control of the ubiquitously expressed *ubi* promoter (Fig. 36A). This should achieve an evenly distribution of the transgene expression in injected embryos. Because of its significant background activity, the *ERT2-dnRara2a* construct was not used any further. This new pTol2\_ubi vector, whose backbone was based on the 'zero-background' Tol2 vectors by David Richter (Fig. S15B), was assembled from five single fragments by means of Gibson Assembly. In this course, recognition sites for DNA endonucleases were added between every component to simplify future cloning strategies. Injections of this plasmid (20 ng/ $\mu$ l) were performed in fertilized zebrafish eggs of the *Casper* strain at the one-cell stage. Subsequent treatment with 5  $\mu$ M 4-OHT or an equivalent amount of EtOH (control) resulted in pronounced malformation of the embryos at 24 and 48 hpf (Fig. 36B-M). The percentage of malformed embryos was always higher in 4-OHT treated groups compared to control groups, indicating an inducibility of the fusion protein by 4-OHT. The malformations particularly affected the eyes and the body length, but included also pericardial edema (Fig. 36J,L,M).

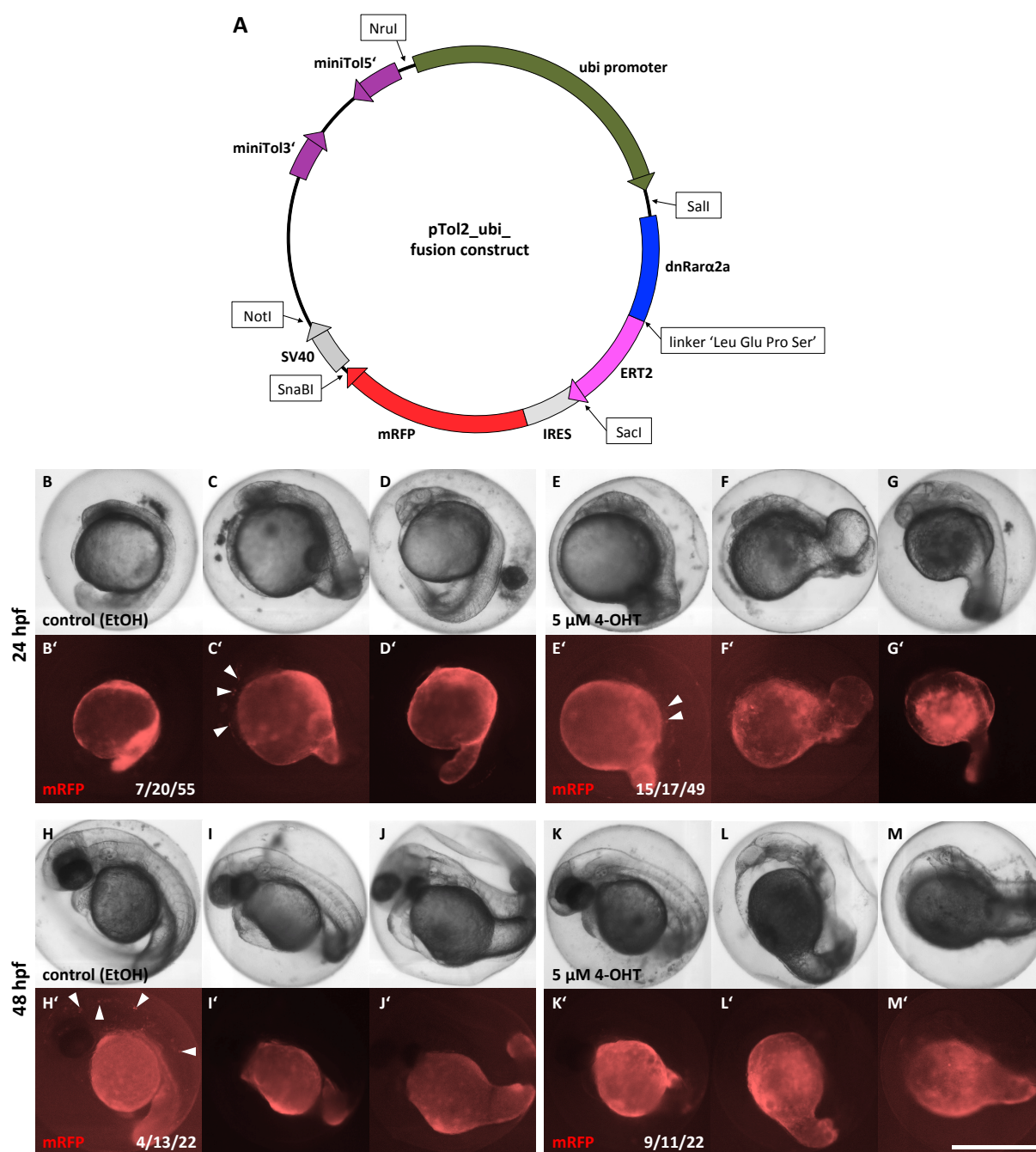


**Fig. 36 Ubiquitous expression of a *dnRara2a*-ERT2 fusion construct results in developmental defects of zebrafish embryos.** **A:** Schematic representations of a construct of *dnRara2a* linked to *ERT2* at the 5' end. A sequence encoding a 4-amino acid linker peptide is located between both genes to separate the components of the fusion protein. The red fluorescent marker *mRFP* is connected to this construct via an IRES sequence, creating two reading frames. This cassette is under the control of the ubi promoter. Specific recognition sites for DNA endonucleases simplify further cloning strategies. **B-M:** The plasmid *pTol2\_ubi:dnRara2a-ERT2-IRES-mRFP* (20 ng/ $\mu$ l) was injected in zebrafish eggs and those treated with 5  $\mu$ M 4-OHT or EtOH (control) at 30 % epiboly. The observation took place at 24 (**B-G**) or 48 hpf (**H-M**), respectively. Meaning of the numbers: malformed embryos / mRFP+ embryos / total number of embryos. In EtOH control, about one third of the mRFP+ embryos showed malformations at 24 and 48 hpf (7/20 and 4/13, respectively). In 4-OHT groups more than 80 % of mRFP+ embryos were malformed (15/17 and 9/11, respectively). Red fluorescence was visible independently of 4-OHT treatments. It was located almost exclusively in the yolk (**B'-M'**), but also in a few individual body cells (arrowheads) (**C',E',H'**). Embryos are shown in lateral view with anterior to the left. Scale bar: 500  $\mu$ m.

These phenotypes have often been observed after DNA or RNA injections (see Fig. 23; Fig. S12). However, since they occurred in some cases independently of *dnRara2a*, they might represent a toxic effect rather than a specific phenotype connected with the manipulation of the RA pathway. Concerning the eye defects, several different phenotypes have been observed with varying frequencies: the reduction of one or both eyes, the complete absence of one eye, the merging of both eyes and the Cyclops phenotype (Fig. S22) (Bule, 2019; Eberlein, 2018b; Mück, 2019; Schmidt, 2017).

In a separate project, the characterisation of these eye deformations was attempted (Bule, 2019). For this, *dnRara2a* mRNA (250 - 350 ng/ $\mu$ l) was injected in zebrafish eggs in the one-cell stage. Control embryos were injected only with water and fixed at the same stages to exclude that the injection process caused the defects. The embryos were subsequently fixed at various developmental stages during early embryonic development, before and after the onset of eye formation (Bule, 2019). The stages 50 % epiboly, bud, 75 % epiboly, 6-somite, 14-somite and prim-6 were chosen for analysis (Kimmel et al., 1995). Afterwards, WISH was performed, detecting transcripts of the genes *Pax6a*, *Pax2a*, *Six3* and *Shh* due to their central role in zebrafish eye development (Ando et al., 2005; Glass & Dahm, 2004; Macdonald & Wilson, 1997; Moosajee et al., 2008; Samuel et al., 2016; Sinn & Wittbrodt, 2013; Stenkamp, 2015), as well as *Cyp26a1* as part of the RA pathway (Niederreither & Dollé, 2008; Rhinn & Dollé, 2012). For each of the investigated genes, WISH staining revealed frequently occurring shifts in the location of the gene expression domain or the appearance of an asymmetrical expression pattern compared to the control. This was observable throughout all developmental stages (Bule, 2019) (data not shown). A precise connection between *dnRara2a* activity, the observed changes in the respective gene expression pattern and the resulting eye malformations could, however, not be derived from this.

Altogether, based on the performed experiments, the functionality of the *dnRara2a*/ERT2 fusion constructs is not clarified yet. More detailed investigations are necessary for a final evaluation of their potential to manipulate RA signalling. In this context, assaying the effect of different linkers between both genes might be an option for future strategies.

## 2.5 Establishment of a *Pitx1* Knock-out line using the CRISPR/Cas9 system

A further major project focused on the establishment of a zebrafish *Pitx1* knockout mutant using the CRISPR/Cas9 system. A functional *Pitx1* knockout has so far only been generated in mice leading to severe impairments of the mouse embryos that are mostly affecting the hindlimbs, jaw and pituitary gland, which ultimately led to the lethality of the newborns (Lanctôt et al., 1999; Szeto et al., 1999). It was therefore of great interest to generate a comparable mutation in zebrafish for the subsequent investigation of its corresponding phenotype in this model organism.

### 2.5.1 Design of sgRNAs

Regarding sgRNA design, there are precise guidelines for achieving efficiency and selectivity (Doench et al., 2016, 2014; Moreno-Mateos et al., 2015; Xu et al., 2015). To synthesize sgRNAs a cloning-free method was used in this case for practical and time-saving reasons (Gagnon et al., 2014; Varshney et al., 2016). In this process an sgRNA template with a length of 117 basepairs (bp) was assembled and directly used for *in vitro* transcription. It was composed of a 17-nucleotide (nt) T7 promoter, a 20-nt target sequence and a 80-nt sgRNA scaffold (Table 16), whereby the target sequence mediates the gene specificity while the universal scaffold sequence is necessary for Cas9 recruitment. The CHOPCHOP webtool was used for searching appropriate targets (Labun et al., 2016). The initial settings of this program were set in a way to find targets with a protospacer adjacent motif (PAM) being 3' NGG (Fig. 37A). Moreover, in terms of efficiency score and self-complementarity, the guidelines of Moreno-Mateos et al., 2015 and Thyme et al., 2016 were followed. To enable *in vitro* transcription of sgRNAs using T7 polymerase, the two bases at the 5' end of the target sequence were adjusted to GG if necessary. The online tool Cas-OFFinder was consulted to elucidate potential off targets (Bae et al., 2014).

Established protocols for CRISPR/Cas9 genome editing suggest selecting target sequences that target either early exons or particularly conserved genomic regions that encode important protein domains. Moreover, it is recommended to select a target region that locates in some distance to intron-exon boundaries in order to avoid difficulties caused by alternative splicing (Holmborn et al., 2018 - unpublished protocol; Varshney et al., 2016).

Since previous studies documented an efficient genetically manipulation of the germline for about 85 % of the targets, it is advised to choose at least two different target sites (Gagnon et al., 2014; Varshney et al., 2015, 2016).

Therefore, in order to achieve a knockout in zebrafish *Pitx1*, the gene locus was studied first under consultation of the database *Ensembl* (<https://www.ensembl.org>). *Pitx1* is located on chromosome 21 and contains four exons. Based on this, three mRNA splice variants are generated, which are translated into three *Pitx1* protein variants (201, 202, 203) (Fig. 37B,C). Of the four exons, the 3' part of exon 2, the complete exon 3 and the 5' part of exon 4 are protein coding. The exon 1 is only a part of the *Pitx1* mRNA 202, but is not translated into protein sequence. Though the mRNAs 202 and 203 are quite different in their composition they eventually result in the same protein consisting of 285 amino acids (aa). The *Pitx1* variant 201 is translated beginning from an alternative start codon and is therefore 4 aa shorter. Exon 3 and 4 contain the conserved homeobox domain, which is essential for the function of *Pitx1* as a transcription factor.

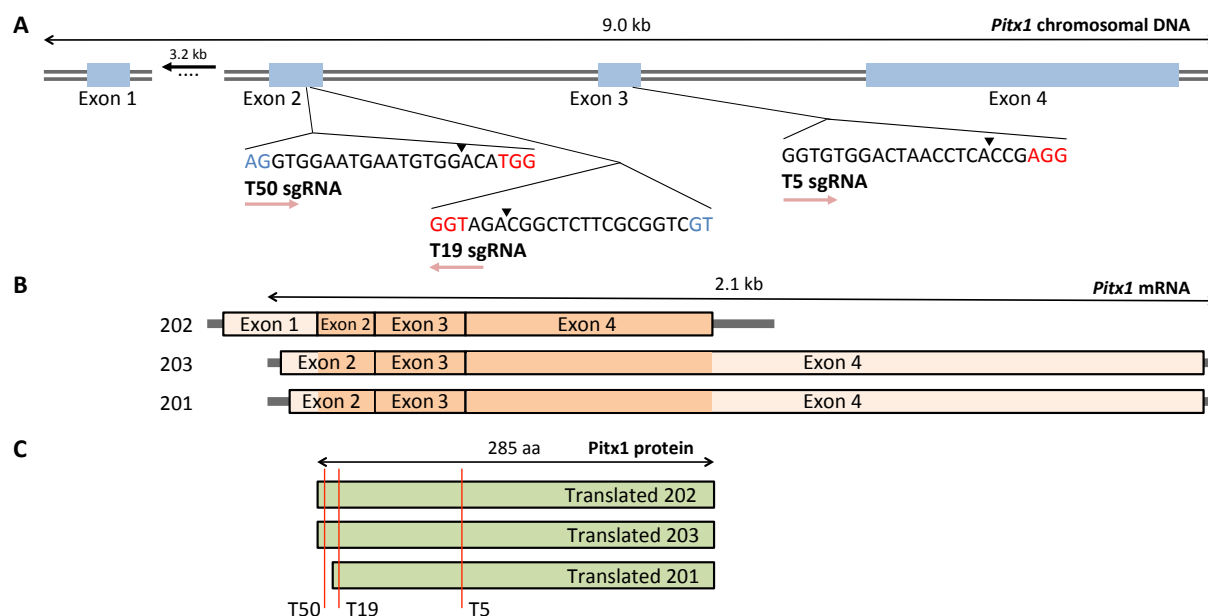


**Fig. 37 *Pitx1* gene topology and sgRNA design for a *Pitx1* knockout.** *Pitx1* contains four exons (A) that produce three *Pitx1* splice variants (201, 202, 203) (B,C). Two sgRNAs (T19, T50) target the exon 2 just past the transcriptional start site. The third sgRNA (T5) targets exon 3 including the conserved homeobox domain. A: 3' NGG PAM sequences are highlighted in red. Arrowheads mark the Cas9 restriction sites. Blue-labelled nucleotides at the 5' end were exchanged to GG to fit the requirements of the T7 polymerase used for *in vitro* transcription of sgRNAs. B: Dark orange shading represents protein coding exon parts. C: red lines mark mutation sites mediated by the different *Pitx1* targets. Scheme designed by José A. Borrero Malo; taken and modified from Borrero Malo, 2018.

Following the above-mentioned recommendations, three sgRNAs were selected (Borrero Malo, 2018; Stacker, 2018). Of these, two sgRNAs (T19, T50) target the exon 2 shortly after the transcriptional start site. At this site, CRISPR/Cas9-induced indel mutations potentially cause a frameshift that will affect almost the entire protein sequence. The third selected sgRNA (T5) targets the 3' part of exon 3 including the conserved homeobox domain. This sgRNA as part of the CRISPR/Cas9 machinery will therefore mediate the disruption of the functional core of Pitx1, leading to an ineffective transcription factor (Fig. 37). According to CHOPCHOP and Cas-OFFinder, Pitx1 T5 and T19 had the highest predicted efficiency and no off-targets. In contrast to that, T50 had three off-targets (with precondition of three permitted mismatches). In case of T19 and T50, the first two bases from the 5' end of the target sequence were changed to GG to meet the requirements of the T7 polymerase (Fig. 37). Thus, a mismatch was produced in the 5' region, which might lower the calculated efficiency for these two targets. DNA cleavage by Cas9 takes place three bases upstream of the PAM. Therefore T50 only affects the splice variants 202 and 203. Because Pitx1 variant 201 uses an alternative start codon, 12 bases further downstream, it does not fall within the scope of T50 (Fig. 37) (Borrero Malo, 2018; Stacker, 2018).

### 2.5.2 Functionality tests of sgRNAs

For this project, a Cas9 was chosen that was optimized for the use in the zebrafish model organism (zCas9). The codon usage of the synthetic zCas9 gene was adapted to meet the requirements in zebrafish. Moreover it was modified with a Kozak sequence and with nuclear localisation signals (NLS) at both, the 5' and the 3' end (Jao et al., 2013).

To test the functionality of the CRISPR/Cas9 system, a gene knockout of *Tyrosinase* (*Tyr*) was conducted. Tyrosinase is involved in the establishment of zebrafish pigmentation by transforming tyrosine into the pigment melanin (Camp & Lardelli, 2001). Its functional disruption therefore leads to a pigmentation defect that is easily visible at 48 hpf. The target sequence of *Tyr* T1 has been taken from Varshney et al., 2016. According to this protocol, the *in vitro* transcribed *Tyr* T1 sgRNA (50 pg) and *Cas9* mRNA (300 pg) were co-injected to zebrafish eggs of the wild type *Bayreuth* (*BT*) strain at the one-cell stage (Borrero Malo, 2018; Stacker, 2018). At 2 dpf, the embryos exhibited a significant reduction of pigmentation. This was observed to different extends, from almost wild type appearance to nearly unpigmented (Fig. 38B-E). This effect was particularly evident in the eye of the

embryos (Fig. 38B'-E'). It persisted up to an age of 5 dpf, indicating that it is indeed due to a CRISPR/Cas9 mediated *Tyr* gene disruption and not a consequence of a minimally variable speed of larval development (Fig. 38F-J). This proved the function of the CRISPR/Cas9 system used here and confirmed *Tyr* as a suitable gene for a positive control (Borrero Malo, 2018; Stacker, 2018).

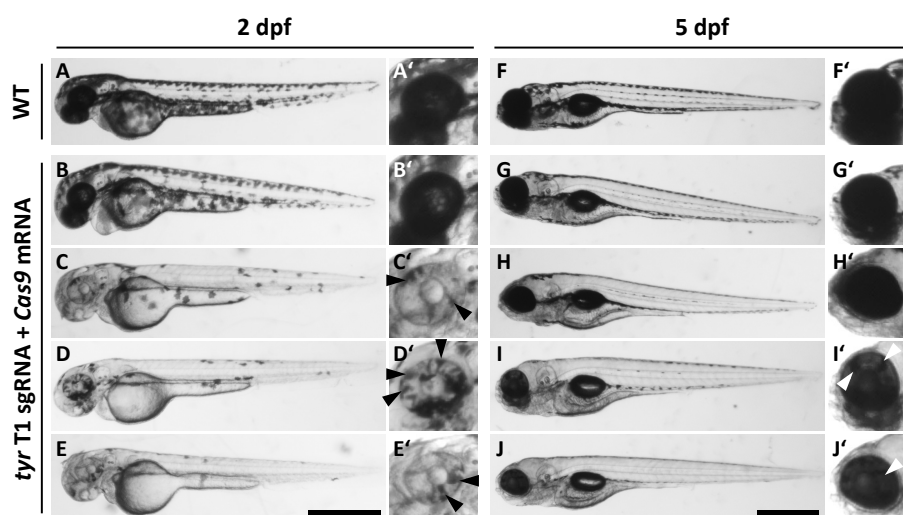


**Fig. 38 Knock-out of *Tyr* as a proof-of-principle for the CRISPR/Cas9 system.** *Tyr* T1 sgRNA was co-injected with *Cas9* mRNA in the one-cell stage of zebrafish embryos of the wild type *BT* strain. At 2 dpf reduced pigmentation was observed in injected embryos (B-E) compared to the uninjected control (A). The phenotype varied from wild type-like appearance (B) to almost unpigmented (E). The pigmentation defects are still observable at 5 dpf (F-J). Pictures A'-J' show magnification of the eye, where pigmentation defects are particularly striking (arrowheads). Scale bars: 500  $\mu$ m. Pictures by Lina Stacker and José A. Borrero Malo; taken and modified from Borrero Malo, 2018 and Stacker, 2018.

Since predicted and real efficiency of sgRNAs can significantly differ, especially in case of zebrafish, the activity of the *Pitx1* sgRNAs T5, T19 and T50 was evaluated in preliminary experiments. For this, three methods were utilized: CRISPR Somatic Tissue Activity Test (CRISPR-STAT) (Carrington et al., 2015), Tracking of Indels by DEcomposition (TIDE) (Brinkman et al., 2014) and T7 Endonuclease 1 (T7E1) assay (Tsuji & Niida, 2008). In each case, the sgRNA *Tyr* T1 was used as a control.

### 2.5.2.1 CRISPR Somatic Tissue Activity Test (CRISPR-STAT)

The technique CRISPR-STAT enables the analysis of somatic activity of sgRNAs by comparing the target locus of zebrafish embryos that were co-injected with sgRNA and *Cas9* mRNA to uninjected siblings. This is based on fluorescence PCR with subsequent analysis by means of

capillary electrophoresis. In the resulting peak profiles, wild type alleles exhibit one single, pronounced peak representing the size of the PCR product. In contrast to that, mutant alleles result in a lower primary peak and several secondary peaks, representing fragments carrying different small indel mutations with few additional or missing bases. On this basis, the fold-change can be calculated to obtain a measure for sgRNA activity (Carrington et al., 2015).

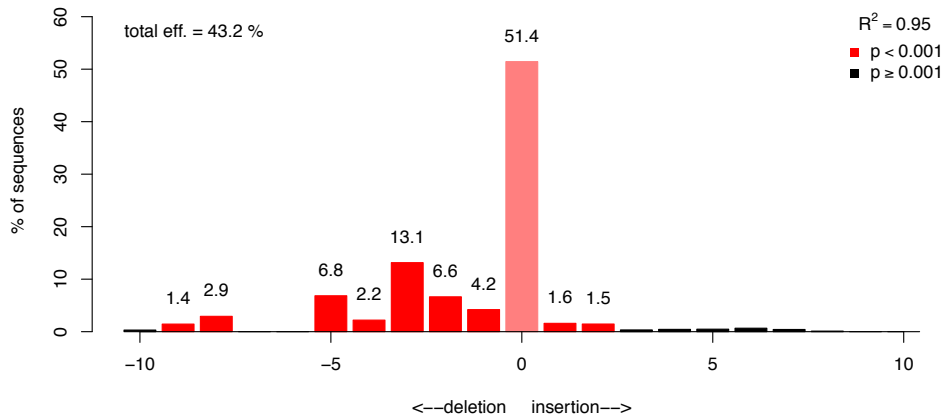
The method was basically performed according to the protocol by Varshney et al., 2016, however, some essential instructions have been changed to adapt the protocol to the existing laboratory equipment. First, zebrafish eggs of the *Casper* or *BT* strains were co-injected at the one cell-stage with sgRNA (*Pitx1* T5, T19, T50 or *Tyr* T1) and *Cas9* mRNA using an amount of 50 pg and 300 pg, respectively. Control embryos were left uninjected. At 48 hpf, for each sgRNA eight injected and eight uninjected embryos were taken for isolation of genomic DNA. Based on this, the *Pitx1* and *Tyr* locus were subsequently amplified by means of PCR (Borrero Malo, 2018; Stacker, 2018). The primers were designed to amplify a region of approximately 275 bp with the predicted cutting site being located roughly in the middle. A M13 sequence was added to the 5' end of the forward primer and a pigtail sequence to the 5' end of the reverse primer to facilitate later genotyping and sequencing (Brownstein et al., 1996; Sood et al., 2013). The recommended fluorescent PCR using a third M13-FAM/5'6-FAM (Fluorescein amidite) primer (Carrington et al., 2015; Varshney et al., 2016) was not carried out as the technology for its evaluation was not available. Instead, the PCR products were handed over to the laboratory of Alfons Weig (University of Bayreuth) for analysis with the Fragment Analyser (Advanced Analytical). However, the peak profiles obtained by this capillary electrophoresis did not show any aberrations between the control and the injected embryos, neither in case of any of the three *Pitx1* sgRNAs nor for *Tyr* T1 sgRNA (data not shown) (Borrero Malo, 2018; Stacker, 2018). At least for *Tyr* T1 a significantly different peak profile, with a lowered primary peak and several secondary peaks, was expected as its activity has already been demonstrated previously in a visual way (Fig. 38). This suggests that the analysis using the Fragment Analyser might not be sensitive enough to detect size differences in PCR fragments of just a few bases. Fluorescence PCR is probably absolutely necessary to detect such small deviations (Borrero Malo, 2018; Stacker, 2018). Therefore the focus was laid on other methods to evaluate the efficacy of the *Pitx1* sgRNAs.

### 2.5.2.2 Tracking of Indels by DEcomposition (TIDE)

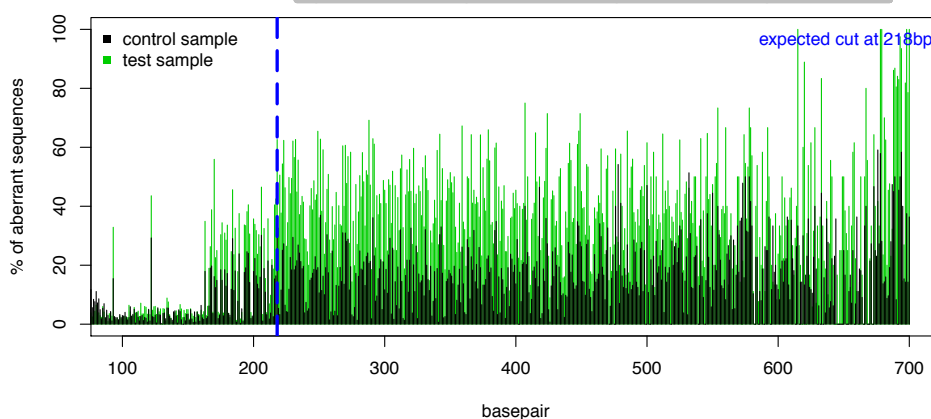
Another method that enables the detection and quantification of CRISPR/Cas9 induced indel mutation in a simple, quick and inexpensive way is Tracking of Indels by DEcomposition (TIDE). This method requires two PCR reactions based on samples treated with sgRNA and Cas9 and untreated controls. The PCR products are then sequenced and analysed using an algorithm that provides precise information about the introduced mutations. It aligns the sequences of control and mutant samples in order to detect aberrant signals, which are then visually presented. At the same time, the composite sequence trace is decomposed by TIDE to reveal its individual components. This information is used for the estimation of type and frequency of introduced indel mutations (Brinkman et al., 2014). The suitability of this method for the model organism zebrafish was examined and confirmed in a separate study (Etard et al., 2017).

To start off, PCR primers were designed that amplify the *Pitx1* and *Tyr* target loci generating products of approximately 750 bp length with the cutting sites locating ca. 250 bp from the 5' ends. These requirements are essential prerequisites for the later application of the TIDE algorithm. Then, zebrafish eggs of the *Casper* or *BT* strains were again co-injected at the one-cell stage with an amount of 50 pg sgRNA (*Pitx1* T5, T19, T50 or *Tyr* T1) and 300 pg *Cas9* mRNA (Borrero Malo, 2018). At 24 hpf, 15 embryos were taken from each group, pooled and used for extraction of genomic DNA. Following PCR, the sequences of the amplified products were determined by traditional Sanger sequencing. The sequencing data obtained from control and mutated samples were uploaded to the TIDE webtool under specification of the respective target sequence (<http://shinyapps.datacurators.nl/tide-batch/>) (Borrero Malo, 2018). Based on the decomposition of the sequence trace, TIDE estimated a total mutagenesis efficiency of 43.2 % for thy *Tyr* T1 sgRNA, which served again as a positive control (Fig. 39A). This means that more than 40 % of the co-injected embryos were predicted to carry an indel mutation. The high effectiveness matched the expectations from the visual analysis of the mutants (Fig. 38) and suggested that TIDE is actually able to provide an evaluation of sgRNA activity. The predicted indel mutations ranged between deletions of 9 base pairs (-9) to insertions of two base pairs (+2), whereby for deletions of 3, 5 and 2 base pairs the highest frequencies were calculated (Borrero Malo, 2018). In this regard, it should be kept in mind that indels of three or a multiple of three base pairs will not produce a frameshift mutation.

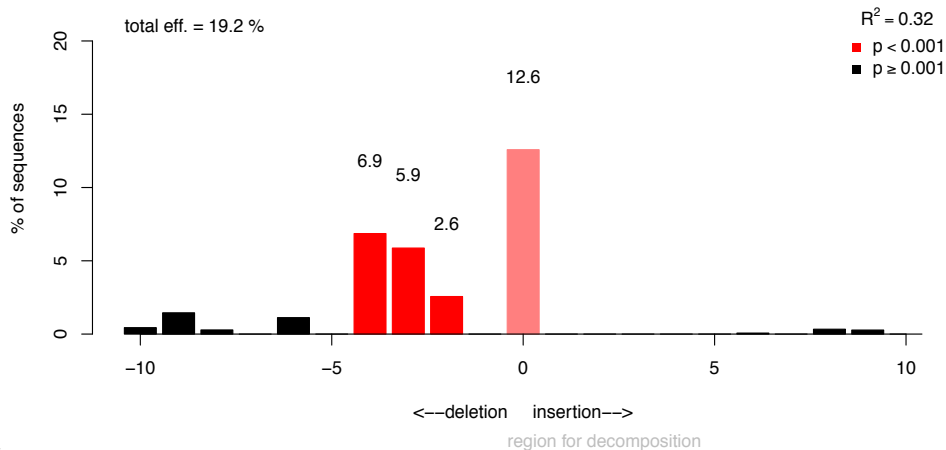
**A Tyr T1 sgRNA**



**A'**



**B Pitx1 T19 sgRNA**



**B'**

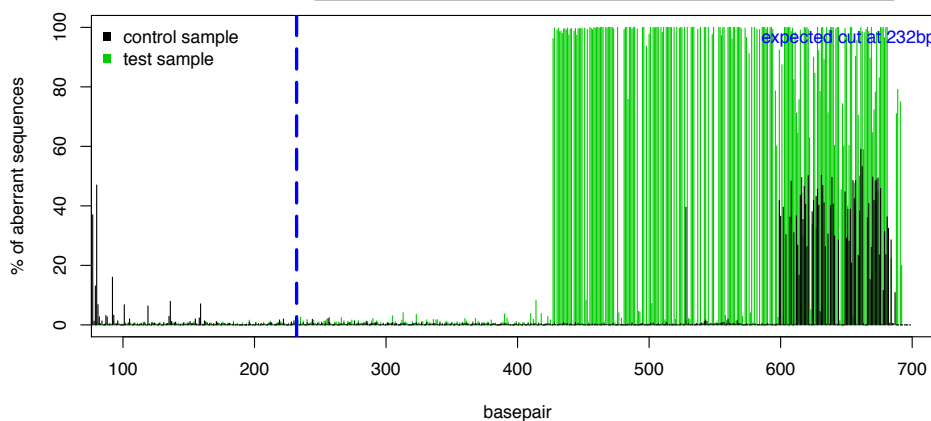


**Fig. 39 TIDE to estimate spectrum and frequency of CRISPR/Cas9 mediated indel mutations.** *Tyr* T1 or *Pitx1* T19 sgRNA (50 pg) were co-injected with *Cas9* mRNA (300 pg) in zebrafish eggs of the *BT* or *Casper* strain, respectively, at the one-cell stage. Genomic DNA was isolated of a pool of 15 injected (test sample) or uninjected embryos (control sample) at 24 hpf. The targeted region was amplified via PCR and sequenced using Sanger sequencing. The aberrant signals of control and test samples are visualized for *Tyr* and *Pitx1* in **A'** and **B'**, respectively. For *Tyr* T1 sgRNA a total efficiency of 43.2 % is predicted with a wide spectrum of induced indel mutations ranging from -9 to +2 base pairs (**A**). *Pitx1* T19 sgRNA is rated with an efficiency of 19.2 % with predicted most frequent indel mutations of -2, -3 and -4 base pairs (**B**). Graphs created with TIDE webtool (Brinkman et al., 2014). Taken and modified from Borrero Malo, 2018.

The *Pitx1* sgRNAs were rated with efficacies of 4.5 % for T5, 19.2 % for T19 and 24.2 % for T50 (Fig. 39B and Fig. S23A,B) (Borrero Malo, 2018). Surprisingly, the lowest effectiveness was calculated for T5. This contradicts the predictions of CHOPCHOP, which rated T5 as the most active target. Since T19 and T50 locate right next to each other, in this case the same PCR fragment was used as control. For both targets T19 and T50 the effectiveness was roughly on the same level at around 20 %. Deletions of 4, 3 and 2 base pairs are predicted with statistical significance for *Pitx1* T19. Therefore, of the approximately 19.2 % of injected embryos that are probably mutant, 5.9 % are predicted to carry a deletion of 3 base pairs that does not cause a frameshift mutation (Fig. 39B). The calculated indel mutations for T50 are widely distributed, but also contain frequent deletions of three or a multiple of three base pairs (Fig. S23B) (Borrero Malo, 2018). From these results it was concluded that *Pitx1* sgRNA T5 is most likely unsuitable to effectively induce mutations in zebrafish embryos, whereas the *Pitx1* sgRNAs T19 and T50 seem about equally potent. However, due to the fact that T19, unlike T50, affects all three *Pitx1* splice variants (Fig. 37), this sgRNA was the first choice for the establishment of the *Pitx1* knockout mutant. Nevertheless, since the  $R^2$  value, which represents a measure of the goodness of fit, was comparably low between the *Tyr* T1 and the three *Pitx1* targets (Fig. 39 and Fig. S23), the results can only serve as rough guide and not as a direct representation of the given situation (Borrero Malo, 2018).

### 2.5.2.3 T7 Endonuclease 1 Assay

To get a comprehensive picture of sgRNA performance, the results obtained from the TIDE analysis were additionally verified via a third method, which was the T7 Endonuclease I (T7E1) assay (Tsuji & Niida, 2008). The enzyme T7E1 detects and cleaves mismatched DNA double strands. These are obtained by denaturation and re-annealing of PCR products, amplified from the genomic DNA of mutated samples. In this case, the mutated and control

samples were prepared just like it was done previously for the TIDE experiment. Again, the PCR products were about 750 bp in length with the mutation site about 250 bp from the 5' end. T7E1 cleavage should therefore result in smaller fragments of about 250 bp and 500 bp in length, which would confirm successful mutagenesis (Fig. 40A) (Borrero Malo, 2018).

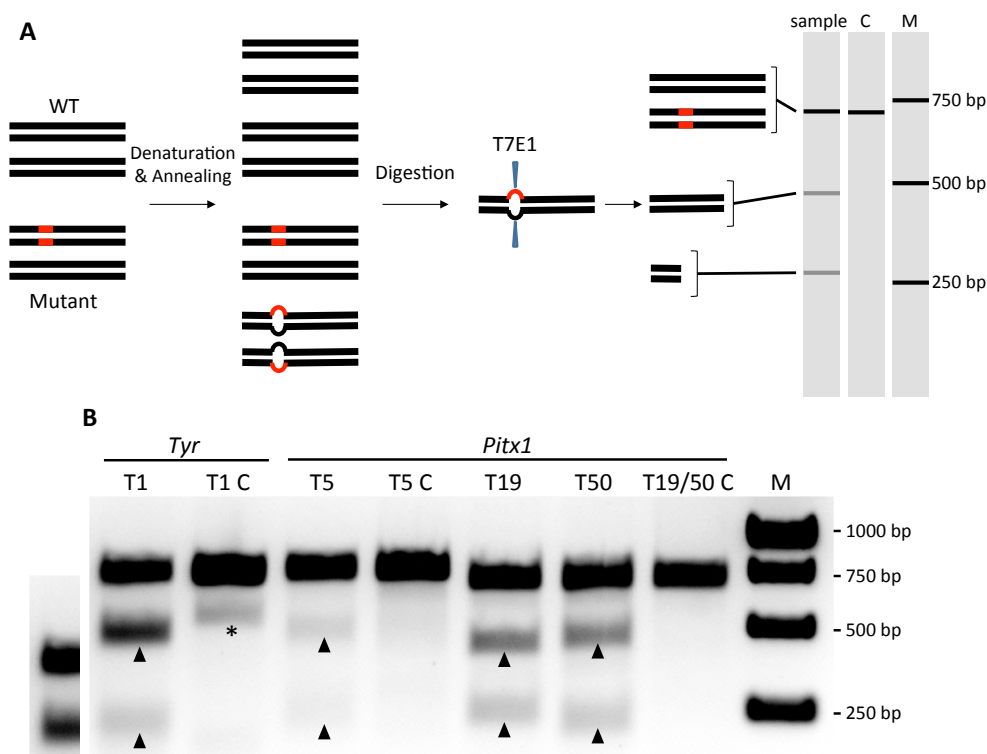


**Fig. 40 T7E1 Assay to analyse genome-targeting efficiency of sgRNAs. A:** Schematic representation of the T7E1 Assay. The targeted region is amplified from genomic DNA of treated or untreated zebrafish embryos via PCR. A denaturation and re-annealing step produces perfectly matched and mismatched PCR fragments. T7E1 detects those mismatches and cuts the DNA resulting in smaller fragments that can be visualized by agarose gel electrophoresis. **B:** Agarose gel for the detection of T7E1-mediated mismatch cleavage. The PCR products were amplified from genomic DNA isolated from a pool of 15 embryos (24 hpf) that were either co-injected with *Tyr* T1 sgRNA or *Pitx1* sgRNA (T5, T19, T50) and *Cas9* mRNA at the one-cell stage or left uninjected serving as control embryos (C). Arrowheads point to 250 bp and 500 bp fragments caused by T7E1 cleavage. Asterisks mark false positive bands observed in *Tyr* control sample. M = 1 kb DNA ladder. Scheme and gel picture by José A. Borrero Malo, taken and modified from Borrero Malo, 2018.

These smaller bands were discovered in all samples, *Tyr* T1 and *Pitx1* T5, T19 and T50, while in control samples no cleavage products were present. The only exception is the control sample for the *Tyr* T1 sgRNA. However, since the bands observed here are not of the expected size, they were considered false positives. The highest amounts of cleaved products were observed in case of *Tyr* T1 as well as *Pitx1* T19 and T50 (Fig. 40B) indicating that these sgRNAs have the highest potential for the generation of indel mutations (Borrero

Malo, 2018). The results of the T7E1 assay are thus conform to the TIDE calculations. This shows that these two analytical methods are suitable for providing assessments regarding the effectiveness of sgRNAs. For the reasons mentioned above, the sgRNA *Pitx1* T19 was rated the best and thus selected for the further experimental procedure (Borrero Malo, 2018).

### 2.5.3 Identification of F0 founder fish

Several co-injections of *Pitx1* T19 sgRNA (50 pg) and *Cas9* mRNA (300 pg) in fertilized zebrafish eggs of the *Casper* line were conducted to induce mutations in the *Pitx1* gene (Borrero Malo, 2018). About 80 of these co-injected fish were raised to fertility. The adult fish (F0 generation) were then crossed with wild type *Casper* fish. At 24 hpf the embryos (F1 generation) were used to extract genomic DNA and subsequently to amplify the *Pitx1* locus via PCR (Stacker, 2020). For each F0 fish at least 100 offspring were analysed. These were divided in groups of a maximum of 15 individuals, which were then pooled to perform the extraction of genomic DNA. The PCR was performed with different sets of primer pairs in order to optimize the yield of the reaction. Afterwards the PCR products were purified and used for T7E1 assay. In this way, it was possible to identify those F0 fish that inherit the *Pitx1* indel mutation to their offspring (Stacker, 2020).

So far, approximately 40 % of the F0 fish were examined via this method. In case of six different F0 individuals a cleavage of PCR products following T7E1 digest could be detected in the offspring sample. These associated F0 fish, namely ♀4, ♂4, ♂6, ♂7, ♂8 and ♂15, were therefore identified as founder fish (Fig. S24) (Stacker, 2020). Each founder was then again crossed with fish of the *Casper* strain, but this time the progeny (F1 generation) was raised to adulthood for further examination and identification of heterozygous individuals (Stacker, 2020).

### 2.5.4 Identification of heterozygous F1 fish

To identify the F1 fish that are heterozygotes for the mutated *Pitx1* allele, genomic DNA was isolated from fin tissue of each adult and used for PCR and T7E1 assay. In this way, several heterozygous F1 fish could be identified for all six founder fish (Fig. 41) (Stacker, 2020).

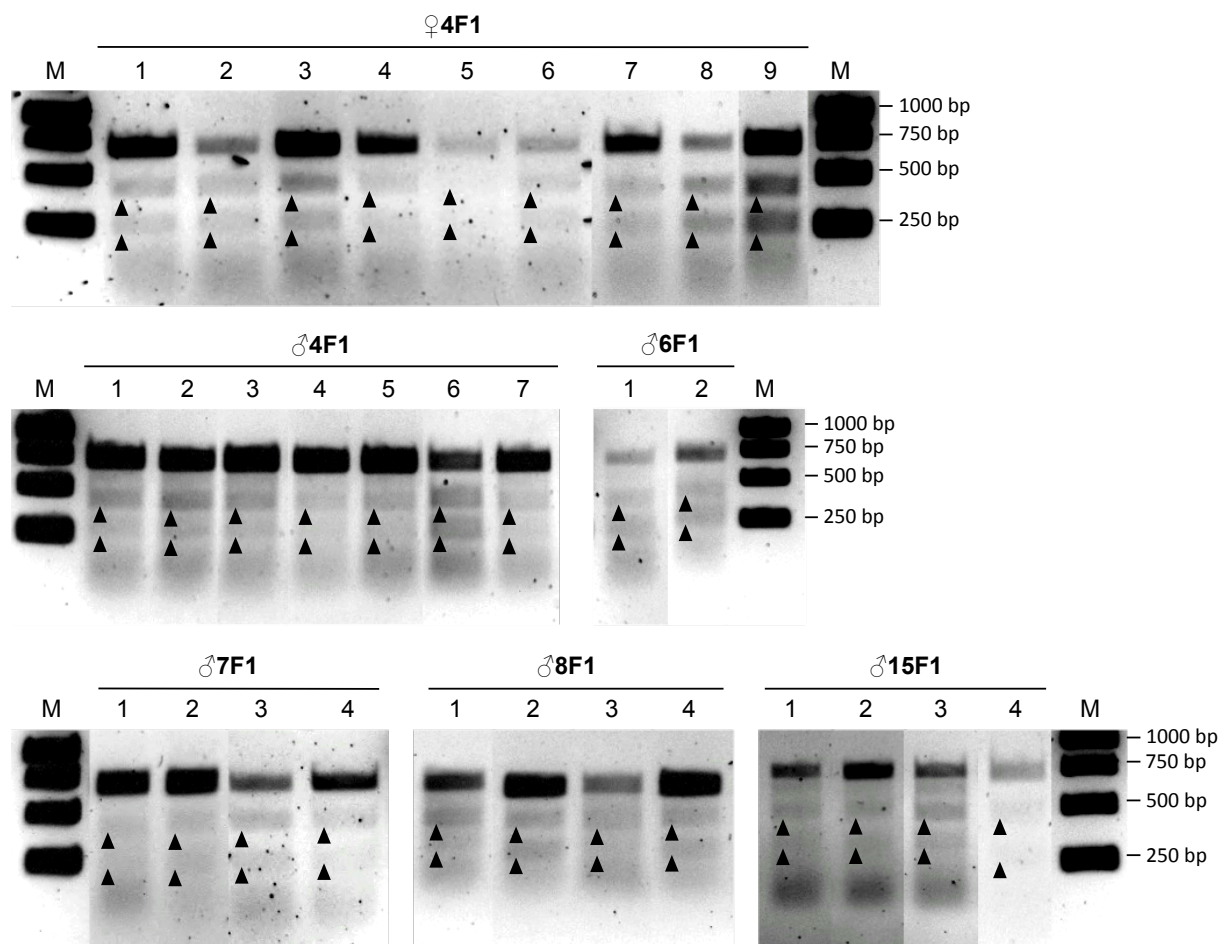


**Fig. 41 T7E1 Assay to identify indel mutations in the *Pitx1* locus.** Agarose gel for the detection of T7E1-mediated mismatch cleavage. The PCR products were amplified from genomic DNA isolated from fin tissue of adult F1 fish derived from the F0 founder fish ♀4, ♂4, ♂6, ♂7, ♂8 and ♂15. The picture shows a compilation of the T7E1 assays for all F1 fish for which an indel mutation was detected (represented by numbers). Arrowheads point to 250 bp and 500 bp fragments caused by T7E1 cleavage. M = 1 kb DNA ladder.

In addition, for each founder the PCR products of one F1 fish that was identified as heterozygous were subjected to Sanger sequencing in order to analyse them with the TIDE algorithm. This revealed indel mutations with a calculated frequency of over 45.2 % for ♂7 and 48.5 % for ♂8, which is close to the theoretical value of 50 % expected for a heterozygous individual (Fig. 42). The predicted mutation for the line founded by ♂7 was a deletion of 8 base pairs, indicating that this deletion may result in a frameshift mutation and thus probably lead to a non-functional or truncated *Pitx1* protein in case that a premature Stop codon is created. In case of the F1 fish derived from ♂8, a deletion of 6 base pairs was predicted. Since this is a multiple of three it will most likely not cause a frameshift mutation but result in the deletion of a few base pairs. This in turn would ultimately mean the replacement or the lack of some amino acids at the N-terminus of *Pitx1*.

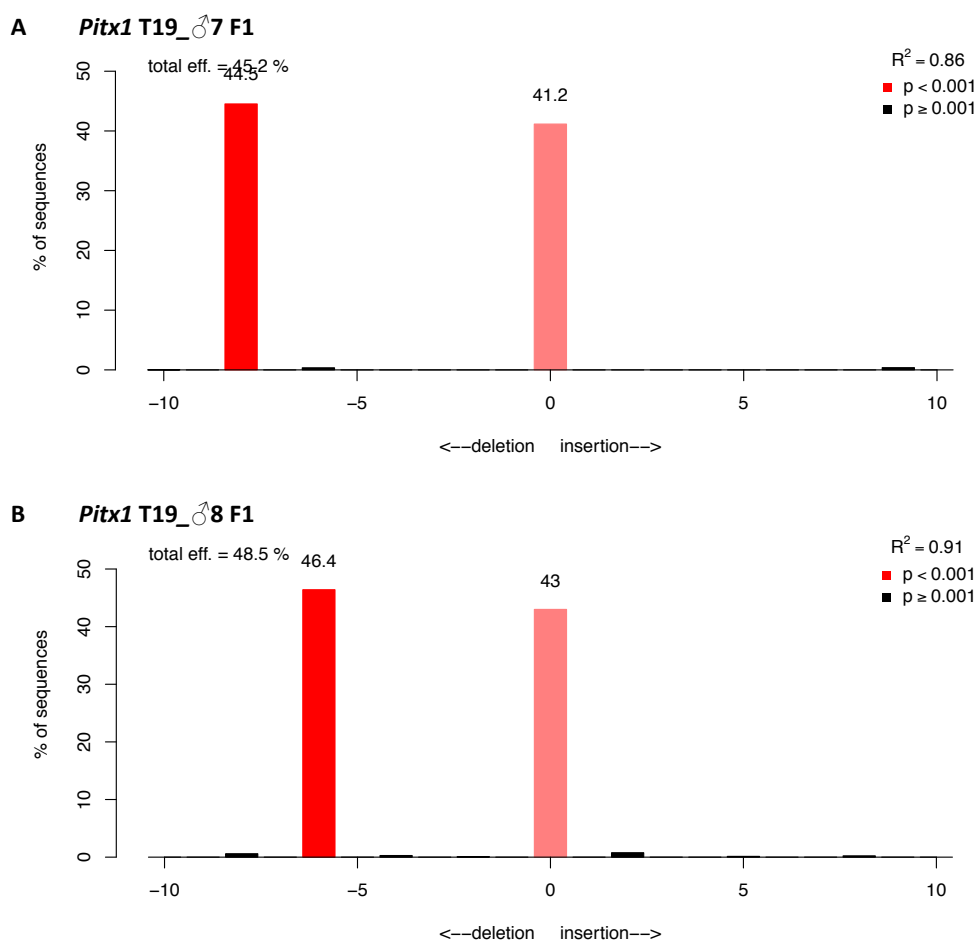


**Fig. 42 TIDE to predict the nature of CRISPR/Cas9 mediated indel mutation in heterozygous F1 fish.** *Pitx1* T19 sgRNA was co-injected with *Cas9* mRNA in zebrafish embryos at the one-cell stage (F0). F0 fish were outcrossed to wild type fish of the *Casper* strain. The offspring (F1) were raised to adulthood. Genomic DNA was isolated from fin tissue of adult F1 fish. The targeted region was amplified via PCR and sequenced using Sanger sequencing. For heterozygous individuals derived from ♂7 (**A**) and ♂8 (**B**) mutational frequencies of 45.2 % and 48.5 % are calculated with predicted deletions of 8 and 6 base pairs, respectively. Graphs created with TIDE webtool (Brinkman et al., 2014).

For the F1 fish derived from founder ♂4, ♂6 or ♂15, the mutational frequency ranged between 11.2 and 17 % (Fig. S25). These low values could be attributed to several reasons. In case of ♂15 F1 the quality of sequencing was quite poor, leading to inaccurate calculations of TIDE. In contrast to that, the sequencing results for ♂4 and ♂6 F1 were of good quality, so the TIDE result may indicate that the associated founders are probably false positives. However, in order to be able to make a precise statement about this, the F2 generation was examined. In case of ♀4 no preliminary TIDE assay was performed and the investigation of the F2 generation was proceeded directly.

### 2.5.5 Identification of homozygous F2 fish

For the generation of F2 individuals, the identified F1 fish were incrossed in order to obtain a statistical percentage of 25 % offspring that are homozygous for the mutant *Pitx1* allele. At least eight F2 larvae were taken for each of the six lines in order to extract genomic DNA from them and subsequently carry out the PCR to amplify the *Pitx1* locus. The PCR products were then subjected to Sanger sequencing in order to determine the respective mutant *Pitx1* sequences.

**Table 8. *Pitx1* T19 F0 founder fishes and the indel mutations they inherit.** Summary of all identified *Pitx1* T19 founder fish. Sanger sequencing and alignment with the wild type *Pitx1* sequence revealed the precise indel mutation in homozygous F2 larvae. On this basis, the resulting changes in the amino acid sequence were determined.

Founder	Mutation	Resulting changes in <i>Pitx1</i> amino acid sequence
♀4	3 bp deletion	Pro(12), Arg(13) are replaced with Phe
♂4	no mutation	-
♂6	no mutation	-
♂7	8 bp deletion	Frameshift after Ser(8) and premature Stop codon after 48 aa
♂8	6 bp deletion	Phe(9) and His(10) are missing
♂15	9 bp deletion	Ser(8), Phe(9), His(10), Leu(11), Pro(12) are replaced with Met and Cys

In case of ♂4 and ♂6 F2 larvae only wild type *Pitx1* sequences were obtained by the sequencing reaction. The sequencing profiles were consistently of good quality and, in addition, did not show obvious peak overlays indicating that there were no heterozygous larvae among them either (data not shown). This strongly supports the hypothesis derived from the TIDE assay that the founders ♂4 and ♂6 are actually false positives, even if the results of the T7E1 assay looked very promising.

In contrast to that, for all other lines founded by F0 fish ♀4, ♂7, ♂8 and ♂15, homozygous F2 larvae carrying a mutated *Pitx1* allele were found. The mutations were all determined as deletions of a few base pairs (bp): 3 bp for ♀4, 8 bp for ♂7, 6 bp for ♂8 and 9 bp for ♂15 (Table 8). Thus the results are in conformity with the predictions obtained by TIDE (Fig. 42). In case of the lines founded by ♀4, ♂7 and ♂15 the deletions were identified as three or multiples of three base pairs. A detailed examination of the mutant *Pitx1* sequence revealed that, as expected, none of these lines contained a frameshift mutation, which would lead to a totally different amino acid sequence or even a premature Stop codon. Instead it was found that some amino acids were missing or have been replaced. The individual sequence

results for the *Pitx1* locus in these three lines and the resulting amino acid sequences are visually presented in Fig. S26 and summarized in Table 8. Whether these changes in the *Pitx1* protein sequence cause a phenotype in the larvae cannot be said with certainty yet. No obvious phenotype was found in F2 larvae from founder ♀4, ♂7 and ♂15 up to an age of 7 dpf. The exception were the F2 descendants of founder ♀4. Here, approximately 25 % of the F2 embryos exhibited a striking phenotype with enlarged and misshaped head and a pronounced pericardial edema at 48 hpf (Fig. S27). However, Sanger sequencing revealed that this phenotype is not connected to the mutation in the *Pitx1* locus and thus might probably represent an off-target mutation in this line.

#### *Pitx1* T19\_ ♂7 F2

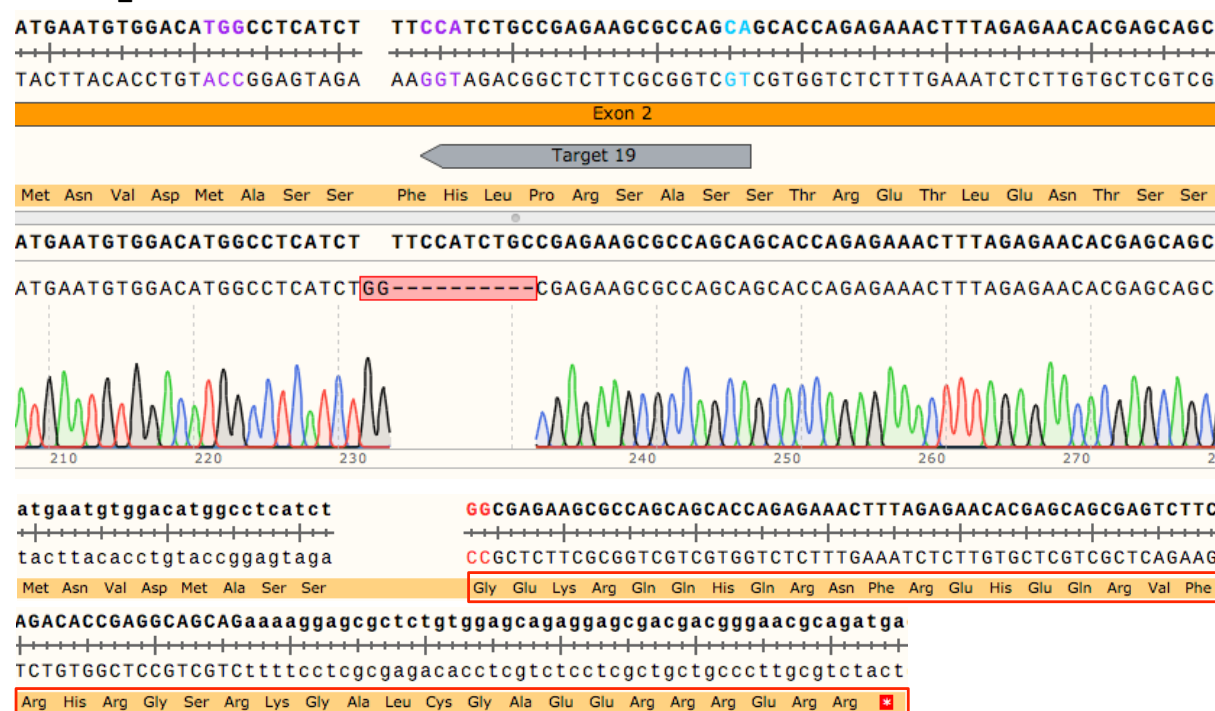


**Fig. 43 Sequence information of homozygous *Pitx1* T19 F2 fish.** Genomic DNA was isolated from F2 larvae derived by founder fish ♂7. Sanger sequencing revealed the genotype of homozygous fish carrying the indel mutation of -8 base pairs. A total of ten base pairs were deleted and two new ones added, resulting in the overall deletion of eight base pairs. The consequence was a shift in the reading frame affecting the complete amino acid (aa) sequence after Ser(8) (framed in red). In addition a premature stop codon (\*) was created after 48 aa. In combination this led to a truncated nonsense protein. Sanger sequencing carried out by eurofins.com. Alignment performed with SnapGene.

The most promising indel mutation was found in the *Pitx1* locus of homozygous F2 descendants from ♂7. The introduced deletion of eight bases causes a shift in the reading frame that results in a completely different amino acid sequence after Ser(8). Moreover, a premature Stop codon is created after 48 amino acids consequently resulting in a truncated protein (Fig. 43). Therefore the expectation was that this mutation causes a pronounced phenotype, which might even result in embryonic lethality. However, contrary to this hypothesis, larvae survived at least up to an age of 7 dpf with normal appearance and behaviour. WISH detecting *Pitx1* transcripts revealed a normally developed pituitary gland at the 14-somite stage; examined in a complete clutch of the F2 generation (>50 embryos) (Fig. S28). Consequently, several F2 fish from founder ♂7 were raised to juveniles and adults in order to investigate a potentially reduction, malformation or lack of the pelvic fin. Each of 31 examined adult fish exhibited a normal sized pelvic fin (data not shown). Tail fin biopsy with subsequent genotyping revealed that 18 heterozygous (58 %) and 13 homozygous wild type fish (42 %) were among the 31 F2 individuals. The homozygous mutant *Pitx1* allele was not detected in any adult F2 individual, although, statistically speaking, a number of 7-8 individuals would have been expected in 31 fish. This indicated, although the larva does not appear to have a phenotype, that the fish homozygously carrying the deletion of 8 bp in *Pitx1* do not reach adulthood. The fitness of the larvae might be attributed to a partial compensation of the *Pitx1* function by its close homologues *Pitx2* and *Pitx3*, which are both expressed simultaneously with *Pitx1* in the pituitary gland during early somitogenesis (Angotzi et al., 2008). Another prominent expression site of *Pitx1* is the mandibular arch during early larval jaw development (Askary et al., 2017). A detailed examination of the correct organisation of the jawbones might therefore reveal a dysfunction of the mutated *Pitx1* gene in the ♂7 F2 generation in future studies. Repeated examinations at regularly intervals between 7 dpf and 90 dpf should be performed to figure out the exact time frame and the cause at which the homozygous carriers die.

## 3 Discussion

### 3.1 Signalling pathways in the early zebrafish pelvic fin bud

#### 3.1.1 General overview

The results of the performed gene expression analysis during the early stages of pelvic fin development (Fig. 13 - 15) mostly fit the expectations and are in conformity with previous observations in zebrafish or other model organisms.

The analysis of *Pitx1* and *Tbx4* expression domains complement and support previous published studies, describing a strong abundance of these genes in the outgrowing pelvic fin bud mesenchyme (Don et al., 2016; Ruvinsky et al., 2000). The observed expression patterns of *Prrx1a* and *Prrx1b* in the mesenchyme were also as expected and match those described for pectoral fins and mice fore- and hindlimbs (Chesterman & Kern, 2002; Hernández-Vega & Minguillón, 2011).

In this study, several genes of the RA signalling pathway were shown to be active during early pelvic fin formation, which are *Rdh10a*, *Aldh1a2*, *Cyp26b1* and *Cyp26c1*, strongly indicating a participation of RA in this process. In the case of *Aldh1a2* expression, however, the patterning differs considerably from that in the pectoral fins (Gibert et al., 2006) pointing to a different regulatory mechanism and possibly also a different function.

*Shh* expression in the ZPA and later in the forming fin rays could be reproduced as described previously (Harris et al., 2008; Laforest et al., 1998). The expression domains of the two *Fgf* genes examined in this study, *Fgf8a* and *Fgf10a*, were found to localize in the mesenchyme of the pelvic fin bud, which was surprising as *Fgf8a* was so far generally seen as a marker for the AER (Fernandez-Teran & Ros, 2008). In addition it was observed that *Fgf10a* and *Shh* expression arise in advance to *Fgf8a*, which is differing from findings obtained in chicken studies in which *Shh* was shown to be a downstream target of *Fgf8* (Crossley et al., 1996; Ohuchi et al., 1997).

A more detailed assessment of the newly achieved data regarding Fgf and RA signalling follows in the sections below.

### 3.1.2 Fgf signalling

The finding that the expression of *Fgf8a* was restricted to the fin mesenchyme during early pelvic fin developmental stages (Fig. 15) was surprising and is contradicting the knowledge gathered from studies on chicken, mouse or *Xenopus* limbs in which *Fgf8* was consistently classified as a marker of the AER in both, fore- and hindlimbs (Boulet et al., 2004; Crossley & Martin, 1995; Fernandez-Teran & Ros, 2008; Lewandoski et al., 2000; Mariani et al., 2008; Ohuchi et al., 1997; Xu et al., 1998) (Fig. 44A-D). Even in species that do not form an morphological AER, among others certain frog or marsupial species, the expression of *Fgf8* is nevertheless localized in the ectodermal tissue (Doroba & Sears, 2010; Gross et al., 2011) (Fig. 44E-H).

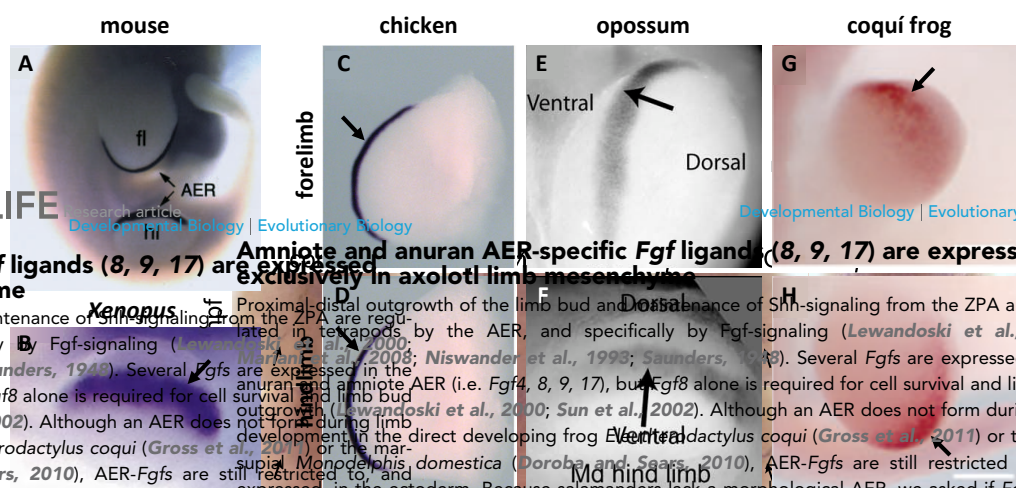


**Fig. 44 *Fgf8* expression in ectodermal limb structures of diverse vertebrates.** In limb development of diverse vertebrate species *Fgf8* is generally known as marker for the AER (e.g in mouse, chicken or *Xenopus*, A-D) or, in case that no morphological AER is present, for the most proximal ectodermal tissue (e.g in opossum or coquí frog, E-H). The *Fgf8* expression sites were detected by WISH and are marked with arrows. Pictures taken and modified from: A: Crossley & Martin, 1995; B: Christen & Slack, 1998; C/D: Fernandez-Teran & Ros, 2008; E/F: Doroba & Sears, 2010; G/H: Gross et al., 2011.

During mouse limb development, several *Fgf* genes, namely *Fgf4*, *Fgf8*, *Fgf9* and *Fgf17*, were demonstrated to be specifically expressed in the AER in slightly differing time spans (Casci, 2008; Mariani et al., 2008; Sun et al., 2000). In this context it was shown that the contribution of *Fgf8* to the AER signal is the most important to drive limb development forward. In a situation of simultaneous depletion of *Fgf4*, *Fgf9* and *Fgf17*, the presence of functional *Fgf8* is sufficient to develop normal limbs in mouse embryos (Mariani et al., 2008). Nevertheless, partial compensation of *Fgf8* takes place upon functional loss of this gene so

that limbs are formed, but smaller in size and with impairments of the skeletal patterning (Lewandoski et al., 2000; Mariani et al., 2008; Moon & Capecchi, 2000; Sun et al., 2000). This is roughly in accordance with the molecular processes taking place during zebrafish pectoral fin development. In zebrafish pectoral fins four different *Fgf* genes were shown to be expressed in the AER, which are *Fgf4*, *Fgf8a*, *Fgf16* and *Fgf24* (Fischer et al., 2003; Muto et al., 2014; Nomura et al., 2006) (Fig. 45). The first gene to be activated is *Fgf24*, with its expression domain initially being located in the LPM (18 - 24 hpf) and later shifting towards the AER (32 hpf). Its activity is essential for the formation of pectoral fins with regard to the fact that the zebrafish *Fgf24* mutant *ika* does not develop any pectoral fin structures (Fischer et al., 2003). A knockdown of *Fgf16* also impaired pectoral fin outgrowth leading to a significant reduction of their size (Laurell et al., 2014; Nomura et al., 2006). In contrast to that, loss of *Fgf8* does not cause a reduction of pectoral fins. This is seen in the zebrafish mutant *ace* in which expression pattern of important patterning genes (*Shh*, *Eng1*) as well as pectoral fin size and shape are unaffected (Reifers et al., 1998).



**Fig. 45 Expression of *Fgf* genes in the AER of zebrafish pectoral fins.** Four *Fgf* genes, *Fgf4*, *Fgf8a*, *Fgf16* and *Fgf14*, are specifically expressed in the AER during pectoral fin formation in slightly different time spans. The expression was determined by WISH and the respective patterns were documented at 36 hpf (C,D), 40 hpf (A,B) and 48 hpf (E-H). Embryos are shown in dorsal view with anterior to the top. Expression domains are marked with arrows. Pictures taken and modified from Muto et al., 2014.

A completely different picture emerges if the limb development in axolotls is considered (Purushothaman et al., 2019). In this salamander species, *Fgf8* expression was detected exclusively in the mesenchyme throughout limb development. First visible in stage 44, the expression domain located in the most distal part of the limb bud, just beneath the ectodermal layer. Later in stage 47, the area is segregated, now forming two distinct domains on the dorsal and ventral side (Fig. 46A). In addition to *Fgf8*, other components of the *Fgf* signalling pathway were investigated for their expression in the axolotl limb bud. For *Fgf9*, *Fgf10*, *Fgf17* a specific WISH staining was observed, which was in each case also

restricted to the limb mesenchyme, mostly concentrating in the distal part (Fig. 46B). Meanwhile the genes encoding the Fgf receptors, *Fgfr1* and *Fgfr2*, are active in the proximal part of the limb mesenchyme, spatially separated from the area of the *Fgf* expression (Fig. 46B) (Purushothaman et al., 2019).

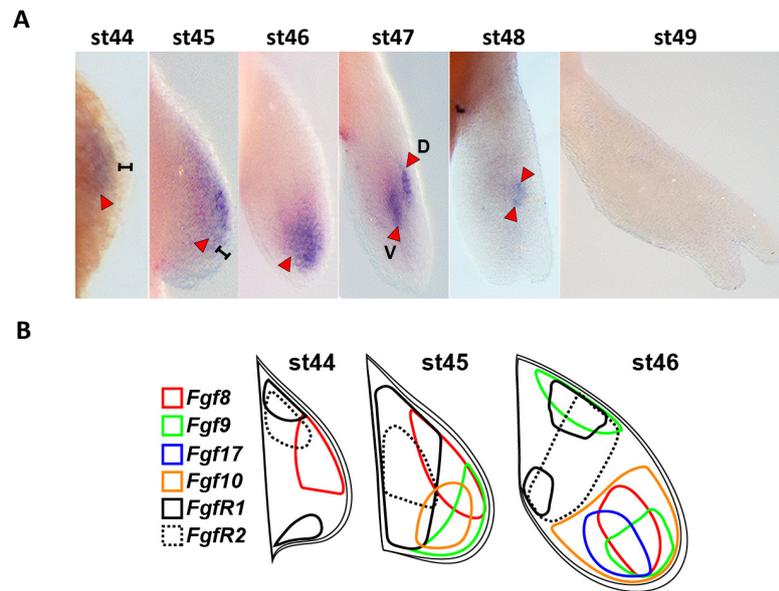


**Fig. 46 Expression of *Fgf8* and other parts of the Fgf signalling pathway during axolotl limb formation.** **A:** WISH against *Fgf8* mRNA in the developing axolotl limb throughout diverse developmental stages. Transcripts were detected exclusively in the mesenchyme of the outgrowing limb (red arrowheads). Brackets mark ectodermal layer. D: dorsal; V: ventral. **B:** Schematic representation visualizing the expression domains of those components of the Fgf signalling pathway for which expression in the developing axolotl limb was found. The expression area of each gene is restricted to the limb mesenchyme. Moreover, expression sites of *Fgf* and *Fgfr* genes are spatially separated. Picture and drawing taken and modified from Purushothaman et al., 2019.

It was already known that urodeles do not form a morphological AER (Sturdee & Connock, 1975; Tank et al., 1977) and this recent axolotl study indicates that they do not form a molecular AER neither (Purushothaman et al., 2019). From this it can be concluded that limb development in different vertebrate species does not take place in the same way (Christen & Slack, 1998; Purushothaman et al., 2019). In zebrafish, the AER morphology is also differing from those of land vertebrate species like mice or chickens. Therefore it is possible that the processes take place differently here as well. In zebrafish an apical thickening forms transiently and is immediately transformed to the apical fold, which is often taken as an equivalent to the AER. In case of pectoral fins this takes place within a few hours. The apical thickening appears at approximately 31 hpf and already at 36 hpf the apical fold is present (Grandel et al., 2000; Grandel & Schulte-Merker, 1998; Masselink et al., 2016; Yano et al.,

2012). In case of pelvic fins, the temporal processes are much slower. This is due to the fact that the pelvic fin bud appears earliest at 3 wpf. The onset of pelvic fin development therefore strongly depends on the overall growth speed of the fish, which is in turn dependent of type and frequency of feeding as well as other external influences (under laboratory conditions this could be for example the size of the group or the water temperature). Once the fin bud has formed, the progression from one pelvic fin developmental stage to the next takes place within approximately 2 days.

In this study, the expression domains of the two examined *Fgf* genes, *Fgf8a* and *Fgf10a*, was found to localize in the mesenchyme of the pelvic fin bud. In a previous thesis, conducted 2013 by Emily Don, *Fgf* gene expression was also investigated during pelvic fin development (Don, 2013). Contrary to the results presented here, Don reported *Fgf8a* expression in the most distal area of the pelvic fin bud at 21 and 28 dpf, respectively, thus locating in the apical thickening and apical fold, respectively. However she rated the expression as 'difficult to detect' and on closer inspection of the images one could suspect that *Fgf8a* expression may also be seen in the mesenchyme of the fin buds (Fig. 47) (Don, 2013), which is why these two different interpretations are not necessarily mutually exclusive.

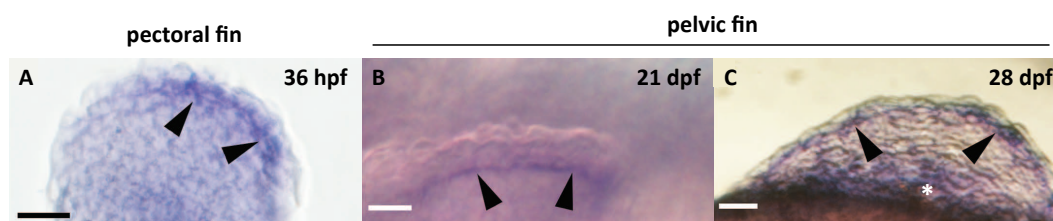


**Fig. 47 Expression of *Fgf8a* in zebrafish paired fins.** *Fgf8a* transcripts were detected by WISH in the pectoral and pelvic fin buds of zebrafish embryos and larvae at 36 hpf and 3 - 4 wpf, respectively. Arrowheads point to the expression domains in the most distal part of the fin bud. The white asterisk marks potential *Fgf8a* expression in the pelvic fin bud at 28 dpf. Pictures taken and modified from Don, 2013.

Overall, these results suggests a differing *Fgf* signalling network acting during the development of pectoral and pelvic fins in zebrafish. This has already been established before, considering the zebrafish *Fgf24* mutant *ika*, lacking the entire pectoral fin while at the same time the pelvic fin remains completely unaffected (Fischer et al., 2003). Possibly this might also be attributed to a differing evolutionary origin of both types of paired fins since pectoral fins most likely arose earlier than pelvic fins (Coates, 1993; Coates & Cohn, 1998; Don et al., 2013). How this process works in detail and in what way it could be

comparable to the development of pectoral fins on the one hand, and on the other hand be similar to the processes taking place in axolotl limb formation remains to be determined. It is therefore necessary to perform further, more detailed investigations concerning the expression of *Fgf* genes in the pelvic fin to make a definite conclusion. In future studies, the gene expression study should be expanded, aiming for the identification of all *Fgf* genes participating in pelvic fin development and their respective expression domains. To start of with, genes that are known to have a role in pectoral fin development would be recommended, which are *Fgf4*, *Fgf16* and *Fgf24* (Fischer et al., 2003; Muto et al., 2014; Nomura et al., 2006). Such investigations could also help to understand the interaction of *Fgf8a* with *Fgf10a* and *Shh* and the entire hierarchy of the *Fgf* genes and their interaction partners in this complex network.

### 3.1.3 RA signalling

Four components of the RA signalling pathway were found to be active during early pelvic fin development, which are *Rdh10a*, *Aldh1a2*, *Cyp26b1* and *Cyp26c1* (Fig. 14 and Fig. 48).

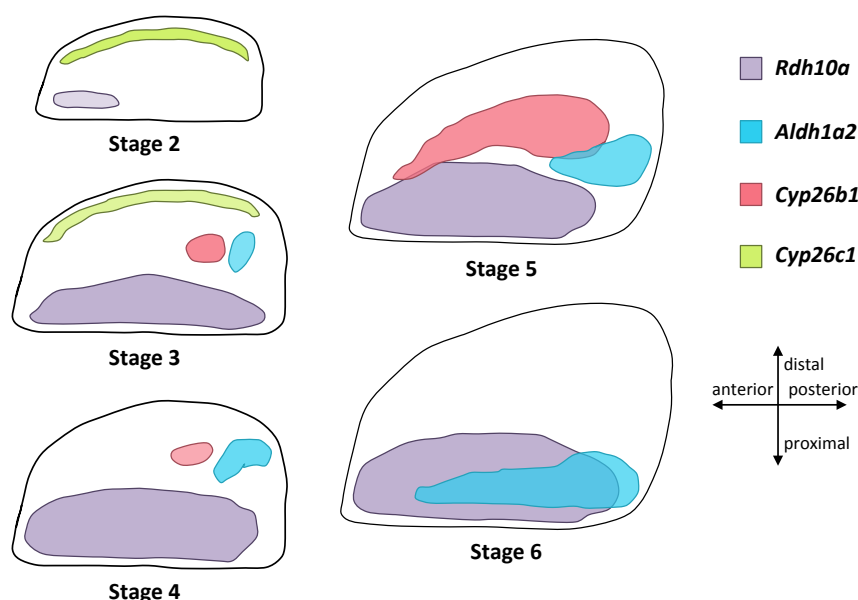


**Fig. 48 Expression domains of RA signalling genes during pelvic fin development.** Schematic representation of pelvic fin buds illustrating expression patterns of *Rdh10a*, *Aldh1a2*, *Cyp26b1* and *Cyp26c1* during S2 - S6 of pelvic fin development as determined by WISH staining (see Fig. 14). Lighter and darker shading represent different expression intensities. *Rdh10a* is weakly expressed in S2 and from S3 onwards strongly throughout the proximal half of the fin bud. Expressions of *Aldh1a2* and *Cyp26b1* arise in S3, locating adjacent to each other, first limited to the posterior half of the fin bud, later (in S5 and S6) shifting anteriorly. *Cyp26b1* was not longer detected in S6. Activity of *Cyp26c1* is restricted to the most distal margin of the fin mesenchyme in S2 and S3. The cross shows orientation of the fin buds.

The first genes to be expressed are *Rdh10a* and *Cyp26c1*. The appearance of *Rdh10a* activity in advance of *Aldh1a2* is comprehensible since it synthesizes retinaldehyde, the precursor of RA. Its expression persists in the proximal half of the fin bud until S6, from where on it overlaps with the *Aldh1a2* expression domain (Fig. 48).

*Cyp26c1* expression was restricted to the most distal part of the fin bud. A comparison to the situation in pectoral fins reveals that it seems to occur in a similar pattern there (Gu et al., 2005). A recent study reported that a knockdown of *Cyp26c1* causes a significant reduction of pectoral fin size accompanied by a decrease of *Col2a1* and *Shox* expression, genes that are both involved in formation of skeletal elements (Montalbano et al., 2016; Sawada et al., 2015).

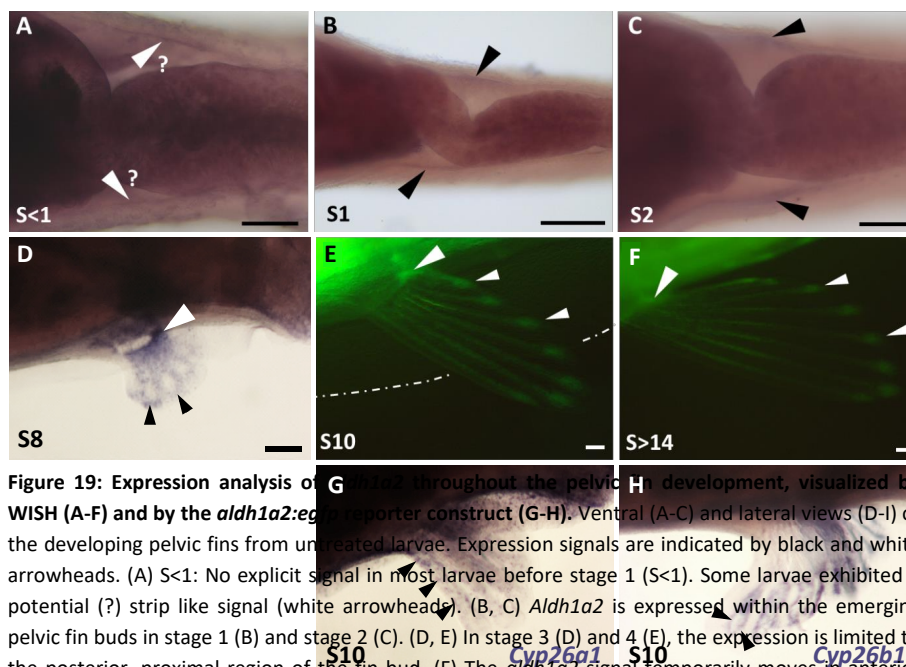


**Fig. 49 Expression of *Aldh1a2* during early and late stages of pelvic fin development.** Determination either by WISH (A-D) or via *Aldh1a2:eGFP* reporter line (E,F). **A-C:** Ventral view of zebrafish larvae in S<1, S1 and S2. *Aldh1a2* expression is visible in a strip like pattern of anteroposterior orientation along the pelvic fin field (arrowheads). In S<1 the signal is not clearly detectable (?). **D-H:** Lateral view of zebrafish juvenile in S8, S10 and S>14. **D:** In S8, *Aldh1a2* expression is edging the developing fin rays (small arrowheads). Further strong signal is observed in the proximal part of the pelvic fin (arrowhead). **E-F:** *Aldh1a2:eGFP* signal in the fin rays, especially at the tips (small arrowheads) as well as at the fin base in the proximal, posterior area (arrowhead). **G/H:** Expression of *Cyp26a1* and *Cyp26b1* in S10, both locating in different patterns at the lateral borders of the fin rays (arrowheads). Scale bars: 100  $\mu$ m. Pictures A-C and E-F taken from Breu, 2017. Pictures D,G,H by Amelie Mück, taken and modified from Mück, 2018.

In the gene expression study *Aldh1a2* expression was found to arise in S3 (Fig. 14). However, in the project where the effects of *Cyp26a1* overexpression on the *Aldh1a2* expression pattern were investigated, it was also detected in S1 and S2, in a strip like pattern in the presumptive area of pelvic fin bud formation (Fig. S10) (Weber, 2020). This is in conformity with previous observations (Fig. 49A-C) (Breu, 2017). The reason for this discrepancy remains elusive. It seems that a clear detection of the early *Aldh1a2* expression is difficult, probably due to methodical reasons. In this study, no treatment with Proteinase K was performed to avoid damage of the pelvic fin structure in order to facilitate its dissection. However Proteinase K treatment might be helpful to reach areas further beneath the skin (Vauti et al., 2020).

Nevertheless, three independently performed studies agree in the expression pattern of *Aldh1a2* in Stages 3 to 5 of pelvic fin development (Fig. 48) (Breu, 2017; Welte, 2011; this study). The restriction of *Aldh1a2* to this distinct area in the posterior fin bud mesenchyme completely differs from the expression pattern observed in pectoral fin formation (Fig. 50) (Gibert et al., 2006). Here *Aldh1a2* expression is visible from 28 hpf just after the onset of the formation of the pectoral fin bud. Shortly thereafter (32 hpf), *Aldh1a2* expression extends over the entire fin bud mesenchyme, while the most distal ectodermal layer is excluded. This pattern persists up to 2 dpf. From 3 dpf *Aldh1a2* activity is limited to a distinct mesenchymal stripe on the anterior side of the fin extending along the edge to the fin fold (Fig. 50) (Gibert et al., 2006). Further functional studies revealed an early requirement of RA for pectoral fin induction and a later participation of RA in the formation of the cartilaginous endoskeleton elements. The RA needed for the initial induction process is generated in the neighbouring somites and reaches the fin field by diffusion (Gibert et al., 2006).

Further investigations are recommended to reproduce the *Aldh1a2* expression in the early stages of pelvic fin development, observed by Breu, 2017, and Weber, 2020, in order to examine its exact localisation, for example by preparing cross-sections of the tissue. By means of these experiments it might be revealed whether RA is indeed present before the onset of pelvic fin formation or only thereafter, which is important to elucidate its potential function in pelvic fin initiation. As already mentioned, in case of pectoral fin induction, RA diffuses from the somites to its site of action. It would be interesting to see whether there is also a source of RA spatially separated from the developing pelvic fin. This should also be revealed through further WISH experiments.

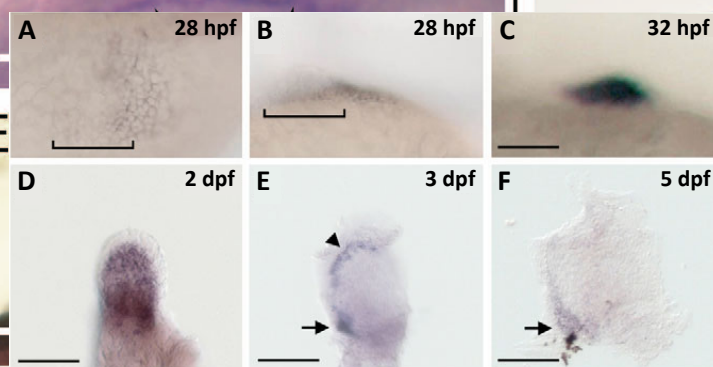


**Fig. 50 Expression of *Aldh1a2* in zebrafish pectoral fins.** Determination by WISH. **A/B:** 28 dpf. Expression of *Aldh1a2* in the posterior part of the pectoral fin bud (bracket) and especially the adjacent lateral plate mesoderm. **C/D:** 32 hpf and 2 dpf. Expression in the entire fin bud mesenchyme. The distal, ectodermal layer is unstained. **E:** 3 dpf. Restriction to a defined proximodistally orientated stripe along the anterior border of the fin mesenchyme. Arrowhead marks distal margin, arrow points to most proximal expression domain. **F:** 5 dpf. Expression in the proximal, anterior part of the fin mesenchyme (arrow). Anterior is to the left. Scale bar: 100  $\mu$ m. Pictures taken and modified from Gibert et al., 2006.

Contrary to the situation in pectoral fins, the conspicuous expression pattern of *Aldh1a2* in pelvic fins from S3 to S5 in a way reminds of the expression pattern of *Shh*, which characterizes the ZPA in the posterior margin of the fin bud (Fig 15K-M). Beginning from S5, an anterior shift of the *Aldh1a2* expression domain takes place. At the same time it is counteracted by *Cyp26b1*, which is expressed in immediate vicinity to *Aldh1a2* from S3 - S5, most likely establishing an anterioposterior gradient of RA concentration (Fig. 48). Even later *Aldh1a2* gene activity is detected surrounding the forming lepidotrichs (Fig. 49D). This is also roughly comparable to the shift in *Shh* expression that occurs in between S4 and S5 whereafter it is found right at the site of the arising lepidotrichs (Fig. 15N). In S10 and later, using the *Aldh1a2:eGFP* zebrafish line, *Aldh1a2* activity has been detected in the fin rays with enhanced signal in the distal tips (Breu, 2017). There, RA synthesis is counteracted by simultaneous expression of *Cyp26a1* and *Cyp26b1* along the lateral limits of the fin rays, in a punctiform pattern or in a continuous strip, respectively (Fig. 49G,H).

Altogether, this raises the hypothesis that RA might be involved in the early anteroposterior patterning of the pelvic fin bud and later in the coordination of the correct positioning and formation of the fin rays. This might take place in interaction with *Shh* signalling, however, based on the data obtained here an precise statement about this is not possible, which is why more detailed investigations in future studies are advisable.

### 3.2 The role of RA in zebrafish pelvic fin development

Via overexpression of *Cyp26a1* using a transgenic *Hsp70l:Cyp26a1* zebrafish line (Mayer, 2020; this study) or via inhibition of Aldhs by DEAB treatment (Breu, 2017) an reduction of RA level could be achieved in zebrafish larvae over a period of 4 - 6 weeks. Both approaches led to similar results, which are the complete or partial inhibition of pelvic fin formation in case the treatment was started from fin developmental stages S<1, S1 or to a lesser extend S2. This indicates that RA signalling is particularly important during the early stages of pelvic fin development. As soon as the first signs of the pelvic fin bud appear (S2) its influence seems to shrink. Overall, a complete inhibition of pelvic fin formation (SM5, FM3) was observed in 24 % (4/17) of *Hsp70l:Cyp26a1*<sup>+/-</sup> individuals treated from S<1 and 7 % (1/14) treated from S1 (Fig. 17). All other larvae developed at least minimal pelvic fin structures, considering both, the endoskeletal pelvic girdle and the exoskeletal fin part.

In contrast to that, Breu, 2017, achieved a complete reduction of all pelvic fin structures in comparably higher percentages of treated animals, precisely 50 % (7/14) of S<1 larvae, 44 % (14/32) of S1 and 6 % (2/31) of S2 larvae (Fig. 12) (Breu, 2017). This different distribution is probably due to the different approaches of the experiments. The heat-shock treatment does not affect every individual at the same intensity. This is also reflected in the various severity of the eye lens destruction observed in several *Hsp70l:Cyp26a1*<sup>+/-</sup> larvae (Fig. S5). Some fish show only minor impairments and some exhibiting a totally destroyed eye structure. This could be due to differing copy numbers of the transgene present in the larvae. The transgenic line was created using the I-SceI meganuclease system (Blum & Begemann, 2012; Kikuchi et al., 2011). Similar to the Tol2 transposon system, this technique mediates the insertion of transgenes in the genome, however the number of insertion events and the length of the concatemers are variable (Rembold et al., 2006; Thermes et al., 2002). A larva with a higher number of transgene copies will therefore experience enhanced *Cyp26a1* overexpression. Moreover, the heat-shocks in this study were performed in 100 ml Petri dishes in a 38.5 °C tempered incubator. Naturally, the water in the dish does not warm up completely evenly and therefore some individuals are affected more than others, depending on their occupied positions. This is why it is necessary to use a larger number of larvae in order to get a comprehensive picture.

It is also interesting, that a low percentage of *Hsp70l:Cyp26a1*<sup>-/-</sup> larvae, lacking the heat-shock promoter transgene, exhibited severe to medium malformations (SM4 - SM2) of the endo- and exoskeletal parts of their pelvic fins. This indicates that there is a background effect on pelvic fin development potentially caused by the stress arising with the heat-shock treatment. During the procedure, the fish are regularly caught, undergo the heat-shock treatment and are put back in the cooler facility water afterwards. Control fish that were left completely untreated showed a significantly higher growth rate within the four weeks of treatment period (data not shown).

Nevertheless, the differences in pelvic fin appearance between *Hsp70l:Cyp26a1*<sup>+/-</sup> and *Hsp70l:Cyp26a1*<sup>-/-</sup> larvae are striking. The vast majority of *Hsp70l:Cyp26a1*<sup>+/-</sup> fish treated from S<1 and S1 developed at least minimal pelvic structures or exhibited severe to medium pelvic reductions (categorized in SM4 - SM2). The most frequent reductions were observed for the posterior process and the radials (Fig. 16E,F). These structures serve as anchors of the lepidotrichs, which is why incorrectly attached fins were often associated with it (Fig. 16E,E'). The structure, which was mostly little affected, was the anterior process. Even in fish assigned SM4, a basic anterior process structure was present, albeit shortened (Fig. 16C). Those fish in which this skeletal element was nearly lost (Fig. 16D) were the exception. The anterior process is the structure that is formed first in pelvic girdle development (see Fig. 3) and only afterwards the posterior processes and the fin base appear. This indicates that the formation of the early skeletal elements of the pelvic girdle might follow a set program, less prone to tampering, and that the formation and growth of the late structures are more variable.

In previous studies on fish of the Konstanz wild type (KN WT) line, a cleavage of the fin base was found after DEAB treatment (Fig. 9G) (Welte, 2011). This phenotype has not been documented in the long-term DEAB experiments conducted by Breu, 2017. However, in this study, it was observed again following heat-shock treatment in few *Hsp70l:Cyp26a1*<sup>+/-</sup> individuals (Fig. 16E, arrowhead). Since it appears in another genetic context than KN WT, this suggests that it might actually be due to reduced RA signalling. The further observation made by Welte, 2011, concerning the mirror image duplication of the posterior process (Fig. 9F) could neither be reproduced by Breu, 2017, nor in this study. It is believed that this phenotype is due to effects of inbreeding that arose over several generations in the KN WT strain (Gerrit Begemann, personal communication).

Furthermore it was observed that RA deficiency had the most impact on the length and internal organization of the pelvic girdle (Fig. 18E-G). In contrast to that, the total width generally was little affected (Fig. 18E). The reduced length might be attributed to an impaired chondrogenesis. Several studies described and reviewed the participation of RA in chondrogenesis and bone formation (Adams et al., 2007; Draut et al., 2019; Jiang et al., 1995; Laue et al., 2008; Wang et al., 2014). Studies on facial and axial bones demonstrated *Cyp26b1* expression in chondrocytes, osteoblasts as well as their associated precursor cells. Increased RA concentration, either in the *Cyp26b1* mutant *dolphin (dol)* or after *Cyp26b1* knockdown led to defects of the facial cartilage with missing and fused structures, particularly affecting the midline elements (Laue et al., 2008). This was attributed to a mediolateral RA gradient with lower RA concentrations towards the midline (Laue et al., 2008). An *in vitro* study on isolated rat hindlimb bud mesenchymal cells postulated a dose-dependent inhibition of *Pitx1* expression upon exposure to excess RA. The modulation of *Pitx1* signalling caused downregulation of *Sox9* and *Col2a1* and therefore impaired chondrogenesis (Wang et al., 2014). Another *in vitro* study, based on cultured mouse limb bud mesenchymal cells is in conformity with this. It focused on manipulation of RA signalling by downregulation of *Rar* genes, in particular *Rarβ2*, which had an enhancing effect on chondrogenesis (Jiang et al., 1995). From this it can be concluded that well regulated RA signalling is needed to ensure correct skeletal development. Thus in this study, disrupted RA signalling might indeed be responsible for the defective pelvic girdle structures. Therefore, revealing the effects of RA deficiency on the proliferation of chondrocytes of the developing pelvic girdle was a project worth investigating in. However, the establishment of an EdU assay for detection and quantification of cell proliferation failed for zebrafish larvae of an age of 3 - 4 wpf (Jean Eberlein, data not shown), leaving this question unanswered. It would be worthwhile to resume this project, possibly using a commercial EdU kit. Alternatively, a BrdU assay, which is based on a similar functional principle, could be established.

Regarding the exoskeletal part of the fin, it was generally developed in the majority of treated *Hsp70l:Cyp26a1<sup>+/-</sup>* individuals (Fig. 17B). However, significant reductions of the fin (bud) length and the number of the fin rays suggest that growth was nevertheless impaired. This effect was still measurable even in treatment group S2 (Fig. 18C,D). This is comprehensible considering that the expression of *Aldh1a2* was detectable earliest in S3 and increased with growing pelvic fin bud (Fig. 14, Fig. 48). In later stages, WISH experiments and

*Aldh1a2:eGFP* reporter constructs indicated the participation of RA signalling in lepidotrich formation and growth (Fig. 49) (Breu, 2017; Mück, 2018). This need for RA signalling during later stages of pelvic fin outgrowth most likely explains the reduction of size and number of fin rays following *Cyp26a1* overexpression.

In this context, it would additionally be interesting to see what effect *Cyp26a1* overexpression has on the appearance of the pectoral fins. Their metamorphosis from the larval to the adult form takes place during approximately the same time span and likewise involves RA signalling as revealed in the course of a side project of this thesis (Fig. S29) (Mück, 2018).

Overall, the combined results from this study, and from Breu, 2017, and Welte, 2011, are consistent and indicate the participation of RA during pelvic fin induction and patterning of the skeletal elements of the pelvic girdle. Nonetheless, the question remains of whether the observed effects on pelvic fin development are actually specific or just a combined result of overall growth retardation, stress and other side effects caused by heat-shock treatment and *Cyp26a1* overexpression or DEAB treatment in case of the previous studies (Breu, 2017; Welte, 2011). The growth retardation caused by the long-term RA deficiency situations was clearly significant (Fig. 18B) (Breu, 2017; this study). Moreover, side effects like the destruction of the eye lenses resulted in lower food intake and impaired the general condition of the *Hsp70l:Cyp26a1<sup>+/-</sup>* larvae. Besides, since irregularities in pelvic girdle formation also occur frequently in wild type fish (Fig. 3) (Draut, 2020; Marzi, 2015), not all significant variations concerning the distances within the pelvic girdle (Fig. 18F,G) can in fact be attributed to reduced RA signalling. A comparison of the phenotypes shown in Fig. 16 with the pelvic girdles in Fig. 3 dissected from WT fish suggests that some appearances represent a younger developmental stage rather than a malformation due to manipulated RA signalling.

In this context, it also has to be mentioned that no changes in the expression pattern of the investigated pelvic fin specific genes, *Pitx1*, *Tbx4*, *Fgf10a*, *Fgf8a*, could be detected in the course of the performed gene expression studies (Fig. S6 - S11) (Weber, 2020). This is in line with the observations of Breu, 2017. Following short-time DEAB treatments, no changes in the expression of *Pitx1* or *Tbx4* were detectable as well. Therefore, a direct or indirect regulation of key factors of pelvic fin development by RA was not proven. However, even the

expression level of *Aldh1a2* was unchanged following *Cyp26a1* overexpression (Fig. S10), possibly indicating that the experimental setup of the expression studies was not suitable.

In several studies, a feedback mechanism between RA production and degradation has been described, agreeing that excess RA leads to upregulation of *Cyp26a1* in combination with simultaneous downregulation of *Aldh1a2* expression (Begemann et al., 2001; Dobbs-McAuliffe et al., 2004; Emoto et al., 2005; Kudoh et al., 2002). The other way round, in zebrafish *nls* mutants, which are bearing a point mutation in the *Aldh1a2* gene that leads to an inactive protein, an upregulation of *Aldh1a2* gene expression was documented (Begemann et al., 2001). Thus, following *Cyp26a1* overexpression an upregulation of *Aldh1a2* would be conceivable. More detailed investigation using a higher number of zebrafish larvae might be useful here. An upregulation of *Aldh1a2* may actually occur, but it is only noticeable after dissection of the pelvic fin bud followed by a more close analysis of the intensity of the WISH staining.

It remains therefore open for future investigations to clarify whether the observed defects in pelvic girdle skeleton are actually due to RA deficiency and to elucidate the exact mechanism how they are caused. Surely, one of the most elegant ways to approach this question is to accomplish a local disruption of RA signalling, affecting only the pelvic region and not the entire organism. For this purpose, extensive work was carried out in this study to establish the Gal4-UAS system (see chapter 2.3 and 3.3). In principle, a local heat-shock treatment of *Hsp70l:Cyp26a1<sup>+/-</sup>* larvae would also be possible (Shoji & Sato-Maeda, 2008), however, in practice this is probably a major challenge for fish of an age of 3 - 4 wpf when pelvic fin development begins.

### 3.3 Prospects and limitations of the Gal4-UAS system

The main task of this work was to establish the Gal4-UAS system, with the aim of developing a system that enables the spatially and temporally controlled manipulation of RA signalling, in this case specifically for the area of pelvic fin development. Different approaches for driver and effector lines were tested in order to ultimately develop a system that meets all the desired criteria: a simplified screening process, the visualisation of transgene activity, the use of the pelvic fin staging system (Marzi, 2015), a simple and practical application and an optimization for the zebrafish model organism (Fig. 51).

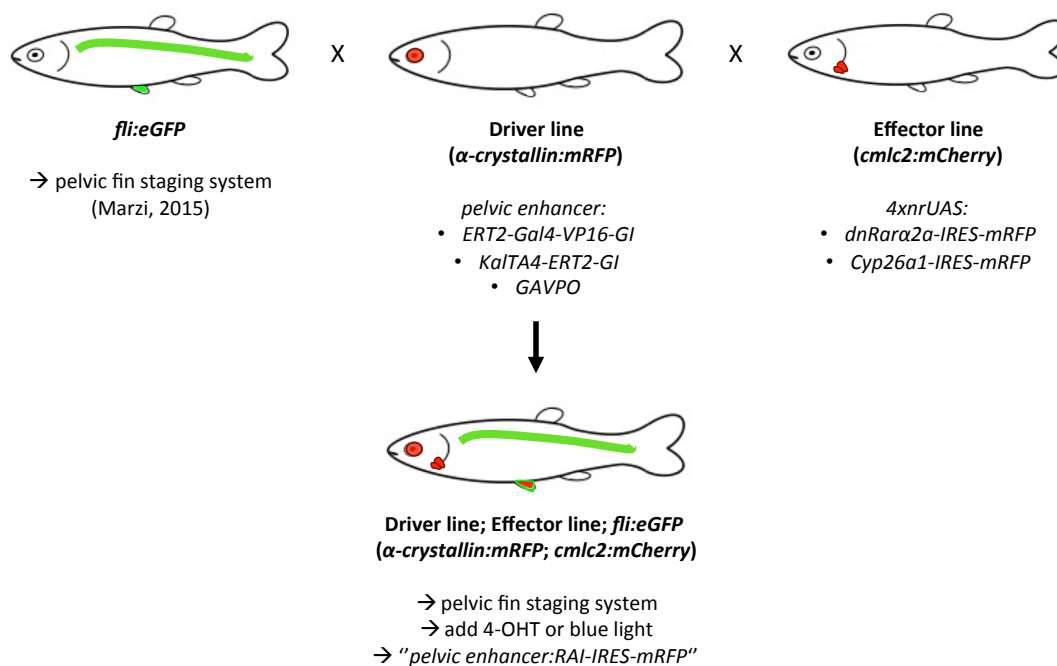


**Fig. 51 The Gal4-UAS system to manipulate RA signalling in zebrafish pelvic fins.** Schematic representation of the Gal4-UAS system as could be created on the basis of the findings from this work. The driver lines express an inducible Gal4 variant under the control of pelvic fin specific enhancers. On the other hand, in the effector lines, genes inhibiting RA signalling (RAI) are under the control of 4xnrUAS. Both lines are equipped with different marker genes (*α-crystallin:mRFP* or *cmlc2:mCherry*) that facilitate identification of transgenic fish. Upon backcrossing of fish from driver or effector lines with the *fli:eGFP* line, application of the pelvic fin staging system (Marzi, 2015) is possible. Triple transgenic fish possessing the *fli:eGFP* transgene as well as the driver and effector element can be identified by red fluorescence in the eye lenses and the heart. Following the staging procedure, the induction of the respective Gal4 variants either by 4-OHT treatment (ERT2 constructs) or blue light irradiation (GAVPO) mediates the expression of *RAI* and *mRFP* specifically in the pelvic region.

### 3.3.1 Prospects

Summarizing this project, all tested components of the Gal4-UAS system have proven to be functional on their own. In case of the effector lines, the 5xUAS used at the beginning of this project and the later evaluated 4xnrUAS were shown to be equivalent in terms of their potential to activate downstream located target genes. For this reason, the 4xnrUAS would be the perfect choice for establishing transgenic zebrafish for long-term breeding due to their lower susceptibility to silencing (Akitake et al., 2011; Goll et al., 2009). The dominant-negative version of the zebrafish *Rara2a* gene (*dnRara2a*) turned out to be suitable in order to effectively block RA signal transduction (Fig. 21, Fig. 24; Fig. 32). The created effector plasmids and zebrafish lines containing this gene can therefore be used for further studies. In case of *dnRara2a* all tested versions - fusion or IRES construct; in combination with eGFP or mRFP - have proven to be effective. Thus it is less important which of the construct is

used in future. However, for the simultaneous application of the pelvic fin staging system as it is visualized in Fig. 51, the constructs using mRFP as a reporter gene would be recommended as otherwise the eGFP signal would be superimposed by the strong signal of the *fli:eGFP* marker and undistinguishable from it.

In case of *Cyp26a1* the situation is different. *Cyp26a1* was inactive as a fusion protein, regardless of its combination with eGFP at the N- or C-terminus or with mRFP (Fig. 20, Fig. 24, Fig. 31). Most likely the used linker peptide consisting of three Glycine residues (3xGly) was too short and/or too flexible. Glycine (Gly) linkers are frequently used to provide flexibility between the single components of fusion proteins based on the small size of the amino acid. In this context, linkers of six or eight consecutive Gly were reported to be functional (Chen et al., 2013; de Bold et al., 2012; Sabourin et al., 2007). Also the usage of Gly and Ser residues was proven to function in linkers due to the combination of small and polar amino acids (Chen et al., 2013). However, in this particular case a more rigid linker could be useful instead. It ensures the spatial distance between the individual components and can thus facilitate correct folding. *Cyp26a1* needs to preserve its ability to bind RA as well as its catalytic activity to transform the bound RA to more polar metabolites. In this process, several amino acid residues of *Cyp26a1* are involved, which is why a correct protein structure is absolutely essential (Awadalla et al., 2016). The use of *Cyp26a1* in an IRES construct, however, has proven to be functional (Fig. 24) and can therefore be applied for further experiments and for establishing a stable transgenic line.

The pelvic enhancers selected for establishment of the *mClover* reporter and the driver lines have in most cases proven to be good choices. Working with the two *Tbx4* enhancers HLEA and HLEB turned out to be difficult. This was actually unexpected since they work extremely well in the mouse model and at least HLEB is strongly conserved in teleosts as well (Infante et al., 2013; Menke et al., 2008). Apart from this, the other tested enhancers mediated specific transgene expression in pelvic fins and pectoral fins in the case of *Prrx1a* and *Prrx1b1*. The tandem constructs containing four consecutive repeats of *Prrx1a* or *Prrx1b1* enhancer, however, have neither shown to be more active nor less, but to function approximately on the same level (Fig. 33). In contrast to that, a significantly increased expression is often reported in the literature when multiple enhancer or gene copies are present (Infante et al., 2013; Loehlin & Carroll, 2016; Menke et al., 2008; Ondek et al., 1987).

For all three evaluated Gal4 variants - ERT2-Gal4-VP16, KalTA4-ERT2 and GAVPO - the functionality in the zebrafish model as well as their compatibility either with 5xUAS or 4xnrUAS was demonstrated. Based on the results of the experiments, their triggered activation of UAS-controlled target genes is estimated to be equivalent. No significant background activity was observed for any of the ERT2-fused Gal4 variants. The low background activity resulting from GAVPO is most likely due to the fact that the injection process was performed under normal room lighting. By optimizing this setup, by further reducing the light exposure, for example through the usage of coloured Petri dishes, any remaining non-specific GAVPO activation is likely to be avoided.

Consequently, all tested Gal4 versions are recommended for further application in zebrafish experiments, however, regarding the tolerance in zebrafish, KalTA4-ERT2 would actually be the first choice since with this construct the fewest side effects were observed. In this context and in order to complement the 'zero-background' vector cloning system (Richter et al., 2019), another Tol2 vector was constructed in cooperation with David Richter (University of Bayreuth) (Fig. S15C). This new, universal driver plasmid is equipped with the *GAVPO* gene sequence downstream of a  $\beta$ -actin basal promoter and the *CmR-ccdB* cassette, containing the Chloramphenicol resistance gene and the toxic gene *ccdB*. Upon restriction digest with *XhoI*, the entire *CmR-ccdB* cassette can be removed, enabling the quick and simple insertion of any enhancer sequence of interest. Altogether, this *Tol2\_ccdB-GAVPO* vector (Fig. S15C), together with the two previously mentioned *Tol2\_4xnrUAS-ccdB* vectors (Fig. S15A,B), provide the basis for the application of the optimized Gal4-UAS system to any specific tissue or structure in the zebrafish (conducted in cooperation with David Richter).

### 3.3.2 Limitations

In each of the reporter and driver lines established here, gene expression was detected in various other structures in addition to the paired fins. The detection of *ERT2-Gal4-VP16* transcripts using WISH usually led to the identification of expression sites in surface-exposed structures such as the gills, the lateral line or other fins. This can either be gene expression that is actually controlled by the respective enhancer, or it can be a non-specific staining. Another possibility would be an expression that results from the integration of the transgene at a position in the genome, at which neighbouring regulators influence it. One possibility to avoid such effects would be the usage of insulator sequences that shield the inserted

transgene from its surrounding (Chung et al., 1993; Hernández-Vega & Minguillón, 2011; Hnisz et al., 2016; Minguillon et al., 2005; Sekkali et al., 2008; Wendt et al., 2008).

The latter point could also be a way to solve the further problem, namely that the Gal4-UAS system is not able to activate UAS-controlled transgene expression when combining driver and effector lines. This contradicts earlier studies, since the functionality of the elements used here has already been proven and established in several previous studies (Akerberg et al., 2014; Distel et al., 2009; Gerety et al., 2013; Kajita et al., 2014; Wang et al., 2012). Therefore the mistake must originate in the present experimental setup.

Several different promoter and enhancer combinations were used in the driver and effector plasmids constructed here. Most plasmids contained two different functional units: the driver or effector part and an additional marker construct, which is used to simplify the identification of transgenic fish. One way to possibly improve the stability of the system could be to insert insulator sequences between these individual components. This could suppress mutual negative influences. Using tandem repeats can also be problematic for long-term stability. Repeat-induced silencing has already been well studied in mammals and plants (Assaad et al., 1993; Garrick et al., 1998; Matzke et al., 1989; Ye & Signer, 1996) and is also known from multiple copies of UAS, which led, as mentioned before, to the creation of variations like the 4xnrUAS (Akitake et al., 2011; Goll et al., 2009). The combination of two genes that are very similar to each other in a single genetic construct, as it was done with *mRFP* and *mCherry* in some of the effector plasmids, might also cause problems in transgenic zebrafish lines and probably lead to comparable silencing effects (Usdin, 2008).

Overall, although the foundation for the use of the Gal4-UAS system has been established in the course of this work, there is still a need for optimisation. Further modifications must be incorporated in order to enable a practical application of the system in the context of the question posed, to elucidate the role of RA in the development of pelvic fins.

Of course there is also the possibility of switching from the Gal4-UAS system to a completely different method that enables tissue-specific gene expression. In this context the Cre/loxP system should be mentioned. Apart from tissue-specificity, this method provides also the option of a temporal control due to the compatibility of the Cre recombinase with the hormone-binding domain of ERT2 (Branda & Dymecki, 2004; Jungke et al., 2015; Mosimann et al., 2011; Pan et al., 2005). Therefore it should be equally suitable to address the initial question.

Another possibility would be to further develop the CRISPR/Cas9 system with the aim to use it for other applications in addition to the knock-out, as it was carried out for *Pitx1*. Meanwhile, the CRISPR/Cas9 technology offers numerous options, including tissue-specific gene disruption (Ablain et al., 2015). Applying this method to disrupt essential genes of the RA signalling pathway, spatially limited on the pelvic area, could be a very promising approach. Moreover, there is also the option of performing a specific knock-in via homology-independent DNA repair (Auer et al., 2014; Hisano et al., 2015). A few years ago, an attempt was already made in our working group to specifically knock-in *ERT2-Gal4-VP16-GI* in-frame with *Tbx4* to mediate tissue specific transgene expression (Bayer, 2015; Ivanovski, 2016), however, the project was put aside and the focus was laid on other approaches. Now, the current study has contributed to gain some experience with the CRISPR/Cas9 system and the knock-out procedure has been successfully established. Therefore a renewed attempt to the knock-in project might be worthwhile.

Another project investigated in this study was the direct combination of *dnRara2a* and *ERT2* in one single construct. The results obtained from the functionality tests of these fusion constructs, however, were not completely convincing, which is why their potential is rated rather mediocre. Nevertheless, the *dnRara2a-ERT2* construct seemed to be inducible by 4-OHT, whereas the *ERT2-dnRara2a* variant exhibited a high activity that was completely independent of the presence of 4-OHT (Fig. 35). Looking at the structure of the Rar/Rxr heterodimer, the reason for this might become clearer (Fig. 52). The interaction of Rar and Rxr takes place via the helices 10 (H10), while H1 and H2 are the major elements responsible for detection of RAREs and DNA binding (Rastinejad et al., 2000; Sato et al., 2010). As mentioned in the introduction, the truncated *dnRara2a* protein is missing the essential helix 12, which is needed for transcriptional activation of target genes (Stafford et al., 2006). In the *dnRara2a-ERT2* fusion protein, the place of H12 is thus taken by ERT2. It is therefore conceivable that ERT2 now occupies an exposed position, like H12 would normally do, and in this way is spatially separated from *dnRara2a*. As a result, its hormone-binding properties could be retained, while in the *ERT2-dnRara2a* fusion protein they may be disturbed due to the spatial proximity to H1 and its interaction with the DNA.

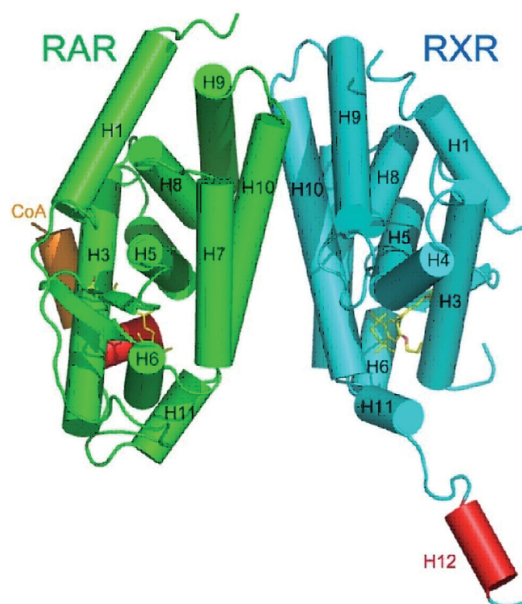


**Fig. 52 Structure of the human RAR $\alpha$ -RA/RXR $\alpha$ -ligand heterodimer.** Rar is coloured green, Rxr is shown in blue. Helices are represented as cylindrical shapes and numbered from 1 - 12. Helices 12 are coloured in red. Ligands are drawn in yellow and shown in stick representation. Picture taken from Sato et al., 2010.

### 3.4 Establishment of a zebrafish *Pitx1* knockout mutant

The basic aim of this project, the establishment of the protocol for the CRISPR/Cas9-mediated knock-out, was successful. Four individual zebrafish strains carrying different mutated *Pitx1* alleles were established. Three of them possess deletions that lead to the replacement of few amino acids in the N-terminal region of the *Pitx1* protein. The fourth one contains a deletion of eight base pairs leading to a shift in the *Pitx1* reading frame whereby a truncated nonsense protein is created.

The induced mutations were all deletions of a few bases and thus confirm the statements in the literature, which describe that small indels occur most frequently (Canver et al., 2014). In the preliminary TIDE calculation for *Pitx1* sgRNA T19, deletions of 4, 3 and 2 base pairs were predicted with an estimated frequency of 6.9, 5.9 and 2.6 %, respectively (Fig. 39B). In fact, however, deletions of 9, 8, 6 and 3 base pairs were found in the four established *Pitx1* knock-out lines. The effectiveness of the *Pitx1* sgRNA T19 was stated by TIDE with 19.2 %. In practice, four founders, who were ultimately confirmed as such, were found out of approximately 32 F0 fish investigated. This gives an actual germline mutation efficiency of approximately 12.5 % and is thus below the estimated value. The TIDE calculations based on samples obtained from the F0 generation can therefore only serve as rough estimates, but do not necessarily represent the actual situation. Is TIDE however used based on sequences

obtained from heterozygous F1 individuals, it reliably calculates the underlying indel mutation, under the prerequisite that the sequencing data are of sufficiently high quality (compare Fig. 42 to Fig. 43 and Fig. S26B).

The accuracy of the mutagenesis detection using T7E1 assay is generally rated very good (Sentmanat et al., 2018). However, of six potential founders, two turned out to be false positives. A possibly explanation for this could be sequence polymorphisms present in the selected target locus (Germini et al., 2017; Kim et al., 2014), although no indication of this was found in the course of repeatedly performed sequencing processes of this particular *Pitx1* area.

With regard to the phenotypic effects of the four different mutations, no conclusive observations could be made. The three different deletions present in the zebrafish lines derived from the founders ♀4, ♂8 and ♂15, only affect few amino acids directly at the N-terminus of Pitx1. For the molecular activity of homeodomain transcription factors primarily the homeodomain is responsible, which has therefore also the highest degree of conservation (Poulin et al., 2000; Rezsóhazy et al., 2015). The three-dimensional structure of the homeodomain is composed of three helices that are connected via two loops and the N-terminal arm. The N-terminal arm and the helix 3 contact the DNA at the minor and major groove, respectively, and are thus decisive for DNA binding (Rezsóhazy et al., 2015). Since the introduced mutations are located in a non-conserved range in his case (Angotzi et al., 2008), next to the fact that the larvae do not exhibit any obvious phenotype, their effect on Pitx1 functionality is estimated to be rather minor.

In contrast to that, the phenotypic effects resulting from the frameshift mutation in *Pitx1* present in the zebrafish line derived from ♂7 were expected to be more drastic since all subsequent amino acids after Ser(8) are affected (Fig. 43; Table 8), including the conserved homeodomain. The corresponding mouse *Pitx1*<sup>-/-</sup> null mutants was generated either by deletion of the homeodomain-encoding exon or by replacing the homeodomain by a *lacZ* construct (Lanctôt et al., 1999; Szeto et al., 1999). As explained in the introduction, the mice embryos die upon birth and exhibit severe defects of the hindlimbs and jawbones and the pituitary gland. In zebrafish embryos of the F2 generation from founder ♂7, the pituitary gland seemed normally developed at the 14-somite stage (Fig. S28). This might be attributed to partial compensation by *Pitx2* or *Pitx3* activity, which are active simultaneously with *Pitx1* in the same organ (Angotzi et al., 2008). The phenomenon of genetic compensation was

recently found to correlate with a decay of mutant mRNA (El-Brolosy et al., 2019; El-Brolosy & Stainier, 2017; Rossi et al., 2015). In this context, the level of *Pitx1* expression seemed at first glance to be at the same level in *Pitx1*<sup>+/+</sup>, *Pitx1*<sup>+/-</sup> and *Pitx1*<sup>-/-</sup> zebrafish embryos (Fig. S28). Detailed investigations on the *Pitx1* expression levels using qPCR analysis were, however, not conducted yet. Combined with a simultaneously study of possible changes in the expression levels of the homologous genes *Pitx2* and *Pitx3*, this would be an interesting project for future research.

Since it seems that the homozygous offsprings from ♂7 do not reach the juvenile or adult state, an assessment of the effects of the mutation on pelvic fin development is not possible. Now it remains to be clarified when exactly and for what cause the homozygous carriers of the frameshift mutation die. A close examination of the jawbones would therefore be advisable. The *Pitx1*<sup>-/-</sup> mouse model exhibits deformations, reductions or loss of jaw structures derived from the first branchial arch. This is affecting for example the Meckel's cartilage or the tympanic bone. Furthermore, a cleft palate was documented (Lanctôt et al., 1999; Szeto et al., 1999). In zebrafish embryos, *Pitx1* is expressed in the ventral mandibular arch at 36 hpf (Askary et al., 2017), which is why further investigation should focus on this area.

Another possibility to investigate missing *Pitx1* activity would be to analyse the expression of its downstream targets. Various studies that have carried out extensive investigations into *Pitx1* target genes may prove helpful in this regard (Infante et al., 2013; Nemeč et al., 2017; Taher et al., 2011; Wang et al., 2018).

## **4 Material and Methods**

### **4.1 Material**

#### **4.1.1 Hard- and Software**

To write this thesis, Microsoft Word for Mac 2011, version 14.7.3 was used. Images were taken using the following microscopes and cameras: Fluo II stereomicroscope (Leica) in combination with AxioCam MRc (Zeiss) color camera or AxioCam ICm (Zeiss); Axio Imager.M2 (Zeiss) in combination with AxioCam MRc (Zeiss) color camera and AxioCam MRm (Zeiss); Stemi 2000-C (Zeiss) in combination with AxioCam ERc5s (Zeiss) color camera. For image editing and figure creation, gimp2.8.18 and Microsoft PowerPoint 2011, version 14.7.3 were utilized.

DNA samples in agarose gels were documented using UVSolo TS imaging system (Biometra). The visualization of plasmid maps as well as simulation of cloning processes was done with SnapGene 4.3.4 (GSL Biotech LLC).

Microsoft Excel 2011, version 14.7.3, was used for data analysis and creation of graphics. For literature and gene research, the databases NCBI (National Centre for Biotechnology Information; <https://ncbi.nlm.nih.gov>), zfin (<https://zfin.org>) and Ensembl (<https://www.ensembl.org>) were utilized. The TIDE algorithm (<http://shinyapps.datacurators.nl/tide-batch/>) was used for the quantification of CRISPR/Cas9 mediated mutagenesis.

#### **4.1.2 Chemicals and reagents**

If not otherwise stated, chemicals and reagents were purchased from the following manufacturers: Carl-Roth (Karlsruhe, Germany), Sigma-Aldrich (St. Louis, Missouri, USA), Fluka (Buchs, Switzerland), Merck (Darmstadt, Germany) and Roche (Basel, Switzerland). Enzymes were obtained from NEB (Ipswich, Massachusetts, USA) or Thermo Fisher Scientific (Waltham, Massachusetts, USA). Kits manufactured by QIAGEN (Hilden, Germany), Zymo Research (Irvine, California, USA), Jena Bioscience (Jena, Germany) and Sigma-Aldrich (St. Louis, Missouri, USA) were used for extraction, clean-up or synthesis of DNA and RNA samples.

### 4.1.3 Buffers and solutions

**Table 9. List of buffers, solutions and their ingredients.**

Buffer/Solution	Ingredients
Alcian Blue stock solution	0.2 % (w/v) Alcian Blue 70 % (v/v) EtOH 200 mM MgCl <sub>2</sub> in H <sub>2</sub> O
Alizarin Red S stock solution	0.5 % (w/v) Alizarin Red S in H <sub>2</sub> O
BCL buffer	0.1 M Tris HCl pH 9.5 50 mM MgCl <sub>2</sub> 0.1 M NaCl in H <sub>2</sub> O
Blocking solution	0.05 % (v/v) Blocking reagent (Roche) in PBTw
DEPC-H <sub>2</sub> O	0.1 % (v/v) DEPC in H <sub>2</sub> O
Double skeletal staining solution	0.02 % (w/v) Alcian Blue 0.005 % (w/v) Alizarin Red S 50 mM MgCl <sub>2</sub> 70 % (v/v) EtOH in H <sub>2</sub> O
E3 medium	0.33 mM CaCl <sub>2</sub> 0.17 mM KCl 5 mM NaCl 0.33 mM MgSO <sub>4</sub> 0.0005 % (w/v) methylene blue in de-ionized water
Formamide solution	9 mM citric acid 50 % (v/v) formamide (deionized) 5x SSC 0.1 % (v/v) Tween 20 in DEPC-H <sub>2</sub> O
Hybridization solution	9 mM citric acid 50 % (v/v) formamide (deionized) 5x SSC 0.1 % (v/v) Tween 20 1 mg/ml tRNA in DEPC-H <sub>2</sub> O
LB agar (plates)	1.5 % (w/v) agar 2.5 % /w/v) LB in H <sub>2</sub> O
LB medium	2.5 % (w/v) LB in H <sub>2</sub> O

PFA	4 % (w/v) paraformaldehyde in H <sub>2</sub> O
PBS	2.7 mM KCl 1.8 mM KH <sub>2</sub> PO <sub>4</sub> 137 mM NaCl 10 mM Na <sub>2</sub> HPO <sub>4</sub> in H <sub>2</sub> O
PBTw	0.1 % (v/v) Tween 20 in 1x PBS
PBTx	1 % (v/v) Triton X-100 in 1x PBS
SOC medium	0.5 % (w/v) yeast extract 2 % (w/v) tryptone 10 mM NaCl 2.5 mM KCl 20 mM MgSO <sub>4</sub> 20 mM glucose in H <sub>2</sub> O
SSC 20x	3 M NaCl 300 mM trisodium citrate in H <sub>2</sub> O
TAE buffer	20 mM acetic acid 40 mM Tris pH 8 1 mM EDTA in H <sub>2</sub> O
TE buffer	10 mM Tris 1 mM EDTA in H <sub>2</sub> O

#### 4.1.4 Plasmids

**Table 10. Plasmid list 1.** Summary of plasmids used as templates or backbones for diverse cloning strategies in the course of this project.

No.	Name	Additional information	Source	Reference
22B	<i>I-SceI-pBSII-SK_Hsp70I:Cyp26a1</i>	Heat-shock promoter, <i>Cyp26a1</i> gene sequence	Nicola Blum	(Blum & Begemann, 2012)
147	<i>pSP64T-XB</i>	SP6 promoter	Masazumi Tada	(Cunliffe & Smith, 1992)
191	<i>pCS2_dnRara2a</i>	<i>dnRara2a</i> gene sequence	Victoria Prince	(Stafford et al., 2006)
259	<i>p5E_UAS</i>	10xUAS sequence	Carl Neumann	TOL2 Kit (5' entry clone)
274	<i>p3E_IRES-EGFPpA</i>	IRES sequence	Carl Neumann	TOL2 Kit (3' entry clone)

300	<i>pCS_KalTA4-GI</i>	<i>KalTA4-GI</i> gene sequence	Martin Distel, Reinhard Köster	(Distel et al., 2009)
334	<i>pENTR5'_ubi</i>	Ubiquitin promoter	Leonard Zon, Addgene #27320	(Mosimann et al., 2011)
347	'SELF' <i>p1081-self-T2_UAS-E1B-MCS-AC</i>	5xUAS, <i>α-crystallin:mRFP</i> cassette, Flanking Tol2 sites	Sebastian Gerety	(Gerety et al., 2013)
356	<i>pEbeEGV 4.1.2</i>	<i>ERT2-Gal4-GI</i> gene sequence, <i>α-crystallin:mRFP</i> cassette	Nemanja Ivanovski	(Gerety et al., 2013)
357	<i>p501bp SALR</i>	Stickleback 501bp Pitx1 enhancer x2	Yingguang Frank Chan	(Chan et al., 2010)
365	<i>pTol2_d43:mClover</i>	Flanking Tol2 sites, β-actin basal promoter, <i>mClover</i> marker gene	Reinhard Köster	
368	<i>pDBM7</i>	Mouse HLEA	Douglas Menke	(Menke et al., 2008)
369	<i>pDBM20</i>	Stickleback HLEB x4	Douglas Menke	(Menke et al., 2008)
384	<i>p5E_Pel2.5kb</i>	Stickleback 2.5kb Pitx1 enhancer (Pel2.5kb; PelA), with Gata2 minimal promoter	Emily Don	(Chan et al., 2010; Don, 2013; Thompson et al., 2018)
403	<i>pTol2_4xnrUAS_ccdB;</i> <i>α-crystallin:Citrine</i>	4xnrUAS, <i>α-crystallin:Citrine</i> cassette, Flanking Tol2 sites	David Richter	(Akitake et al., 2011; Richter et al.2019)
404	<i>pTol2_4xnrUAS_ccdB;</i> <i>cmlc2:mCherry</i>	4xnrUAS, <i>cmlc2:mCherry</i> cassette, Flanking Tol2 sites	David Richter	(Akitake et al., 2011; Richter et al., 2019)
427	<i>pGAVPO</i>	<i>GAVPO</i> gene sequence	Xue Wang	(Wang et al., 2012)
431	<i>pCS2_KalTA4-ERT2-GI</i>	<i>KalTA4-ERT2-GI</i> gene sequence	Masazumi Tada	(Distel et al., 2009; Kajita et al., 2014)
432	<i>pEX-A128_zfPrrx1ax4</i>	Zebrafish Prrx1a enhancer x4	Heidrun Draut, eurofins.com	(Hernández-Vega & Minguillón, 2011)
433	<i>pBluescript II</i> <i>SK(+)_zfPrrx1b1x4</i>	Zebrafish Prrx1b1 enhancer x4	Heidrun Draut, ProteoGenix	(Hernández-Vega & Minguillón, 2011)

**Table 11. Plasmid list 2.** Summary of plasmids that were cloned in the course of this whole project.

No.	Name	Origin Backbone and Insert	Cloned by	Reference
371	<i>pTol2_HLEA:mClover</i>	p365, p368	Fabian Merkel	(Menke et al., 2008; Merkel, 2016)
372	<i>pTol2_HLEBx2:mClover</i>	p365, p369	Fabian Merkel	(Menke et al., 2008; Merkel, 2016)
373	<i>pTol2_PPE1:mClover</i>	p365	Fabian Merkel	(Merkel, 2016)
374	<i>pTol2_PPE2:mClover</i>	p365	Fabian Merkel	(Merkel, 2016)
376	<i>pTol2_5xUAS:eGFP-Cyp26a1_α-crystallin:mRFP</i>	p90, p347	Fabian Merkel	(Merkel, 2016)
380	<i>pSP64T-XB_ERT2-Gal4-VP16</i>	p147, p356	Heidrun Draut	(Gerety et al., 2013)
381	<i>pTol2_Prx1a:mClover</i>	p365	Heidrun Draut	(Hernández-Vega & Minguillón, 2011)
382	<i>pTol2_Prx1b1:mClover</i>	p365	Heidrun Draut	(Hernández-Vega & Minguillón, 2011)
383	<i>pTol2_Pel2.5kb:mClover</i>	p365, p384	Heidrun Draut	(Chan et al., 2010)
388	<i>pSP64T-XB_dnRara2a</i>	p147, p390	Marlene Schmidt	(Schmidt, 2017; Stafford et al., 2006)
389	<i>pSP64T-XB_dnRara2a-IRES-eGFP</i>	p147, p390	Marlene Schmidt	(Schmidt, 2017; Stafford et al., 2006)
390	<i>pTol2_5xUAS:dnRara2a-IRES-eGFP_α-crystallin:mRFP</i>	p191, p274, p347	Marlene Schmidt	(Schmidt, 2017; Stafford et al., 2006)
393	<i>pTol2_Prx1a:ERT2-Gal4-VP16-Gl_α-crystallin:mRFP</i>	p356, p365, p381	Heidrun Draut	(Gerety et al., 2013; Hernández-Vega & Minguillón, 2011)
394	<i>pTol2_Prx1b1:ERT2-Gal4-VP16-Gl_α-crystallin:mRFP</i>	p356, p365, p382	Heidrun Draut	(Gerety et al., 2013; Hernández-Vega & Minguillón, 2011)
395	<i>pTol2_Pel2.5kb:ERT2-Gal4-VP16-Gl_α-crystallin:mRFP</i>	p356, p365, p384	Heidrun Draut	(Chan et al., 2010; Gerety et al., 2013)
396	<i>pTol2_HLEBx2:ERT2-Gal4-VP16-Gl_α-crystallin:mRFP</i>	p356, p365, p372	Heidrun Draut	(Gerety et al., 2013; Menke et al., 2008)
397	<i>pTol2_5xUAS:Cyp26a1-eGFP_α-crystallin:mRFP</i>	p347, p376	Jean Eberlein, Heidrun Draut	(Eberlein, 2018a, 2018b)
398	<i>pSP64T-XB_Cyp26a1</i>	p147, p376	Jean Eberlein, Heidrun Draut	(Eberlein, 2018b)
399	<i>pSP64T-XB_Cyp26a1-eGFP</i>	p147, p376	Jean Eberlein, Heidrun Draut	(Eberlein, 2018b)
402	<i>pTol2_HLEA:ERT2-Gal4-VP16-Gl_α-crystallin:mRFP</i>	p356, p365, p371	Heidrun Draut	(Gerety et al., 2013; Menke et al., 2008)
405	<i>pTol2_4xnrUAS:dnRara2a-IRES-eGFP_α-crystallin:Citrine</i>	p403, p390	Heidrun Draut	(Mück, 2019; Stafford et al., 2006)
406	<i>pTol2_4xnrUAS:dnRara2a-mRFP_α-crystallin:Citrine</i>	p403, p390	Amelie Mück	(Mück, 2019; Stafford et al., 2006)

407	<i>pTol2_4xnrUAS:Cyp26a1-mRFP_α-crystallin:Citrine</i>	p403, p397	Amelie Mück	(Mück, 2019)
408	<i>pTol2_4xnrUAS:dnRara2a-mRFP_cmlc2:mCherry</i>	p404, p390	Amelie Mück	(Mück, 2019; Stafford et al., 2006)
409	<i>pTol2_4xnrUAS:Cyp26a1-mRFP_cmlc2:mCherry</i>	p404, p397	Amelie Mück	(Mück, 2019)
410	<i>pTol2_4xnrUAS:dnRara2a-IRES-mRFP_cmlc2:mCherry</i>	p404, p390	Amelie Mück	(Mück, 2019; Stafford et al., 2006)
411	<i>pTol2_4xnrUAS:Cyp26a1-IRES-mRFP_cmlc2:mCherry</i>	p404, p397	Amelie Mück	(Mück, 2019)
412	<i>pTol2_Prrx1a:KalTA4-ERT2-Gl_α-crystallin:mRFP</i>	p365, p431, p381	Heidrun Draut	(Distel et al., 2009; Hernández-Vega & Minguillón, 2011)
413	<i>pTol2_Prrx1b1:KalTA4-ERT2-Gl_α-crystallin:mRFP</i>	p365, p431, p382	Lina Stacker, Heidrun Draut	(Distel et al., 2009; Hernández-Vega & Minguillón, 2011)
414	<i>pTol2_Pel2.5kb:KalTA4-ERT2-Gl_α-crystallin:mRFP</i>	p365, p384, p431	Xuen J. Ng, Heidrun Draut	(Chan et al., 2010; Distel et al., 2009; Ng, 2019)
415	<i>pTol2_Prrx1ax4:KalTA4-ERT2-Gl_α-crystallin:mRFP</i>	p365, p431, p432	Heidrun Draut	(Distel et al., 2009; Hernández-Vega & Minguillón, 2011)
416	<i>pTol2_Prrx1b1x4:KalTA4-ERT2-Gl_α-crystallin:mRFP</i>	p365, p431, p433	Lina Stacker, Heidrun Draut	(Distel et al., 2009; Hernández-Vega & Minguillón, 2011)
417	<i>pTol2_Prrx1a:GAVPO_α-crystallin:mRFP</i>	p365, p381, p427	Anna-Maria Mayer, Heidrun Draut	(Hernández-Vega & Minguillón, 2011; Mayer, 2020; Wang et al., 2012)
418	<i>pTol2_Prrx1b1:GAVPO_α-crystallin:mRFP</i>	p365, p382, p427	Anna-Maria Mayer, Heidrun Draut	(Hernández-Vega & Minguillón, 2011; Mayer, 2020; Wang et al., 2012)
419	<i>pTol2_Pel2.5kb:GAVPO_α-crystallin:mRFP</i>	p365, p384, p427	Anna-Maria Mayer, Heidrun Draut	(Chan et al., 2010; Mayer, 2020; Wang et al., 2012)
420	<i>pTol2_Prrx1ax4:GAVPO_α-crystallin:mRFP</i>	p365, p427, p432	Anna-Maria Mayer, Heidrun Draut	(Hernández-Vega & Minguillón, 2011; Mayer, 2020; Wang et al., 2012)
421	<i>pTol2_Prrx1b1x4:GAVPO_α-crystallin:mRFP</i>	p365, p427, p433	Anna-Maria Mayer, Heidrun Draut	(Hernández-Vega & Minguillón, 2011; Mayer, 2020; Wang et al., 2012)

422	<i>pTol2_Hsp70l:KalTA4-GI</i>	p22B, p300	Xuen J. Ng, Heidrun Draut	(Distel et al., 2009; Ng, 2019)
423	<i>pTol2_ubi:dnRara2a-ERT2-IRES-mRFP</i>	p334, p403, p410, p431	Heidrun Draut	(Gerety et al., 2013; Stafford et al., 2006)
424	<i>pTol2_Prx1ax4:dnRara2a-ERT2-IRES-mRFP</i>	p356, p365, p410, p431, p432	Heidrun Draut	(Gerety et al., 2013; Hernández-Vega & Minguillón, 2011; Stafford et al., 2006)
425	<i>pTol2_Prx1ax4:ERT2-dnRara2a-IRES-mRFP</i>	p356, p365, p410, p431, p432	Heidrun Draut	(Gerety et al., 2013; Hernández-Vega & Minguillón, 2011; Stafford et al., 2006)
426	<i>pTol2_ubi:GAVPO_α-crystallin:Citrine</i>	p334, p403, p427	Heidrun Draut	(Wang et al., 2012)
428	<i>pSP64T-XB_GAVPO</i>	p147, p427	Lina Stacker, Heidrun Draut	(Wang et al., 2012)
429	<i>pTol2_Prx1ax4:ERT2-Gal4-VP16-GI_α-crystallin:mRFP</i>	p356, p365, p432	Heidrun Draut	(Hernández-Vega & Minguillón, 2011)
430	<i>pTol2_Prx1b1x4:ERT2-Gal4-VP16-GI_α-crystallin:mRFP</i>	p356, p365, p433	Heidrun Draut	(Hernández-Vega & Minguillón, 2011)
434	<i>p5E-10xUAS-eGFP</i>	p259, p397	Heidrun Draut	TOL2 Kit (5'entry clone)
435	<i>pTol2_PPE1:mClover_α-crystallin:mRFP</i>	p372, p390	Niels Nardini, Heidrun Draut	(Merkel, 2016; Nardini, 2018)
436	<i>pTol2_PPE2:mClover_α-crystallin:mRFP</i>	p374, p390	Niels Nardini, Heidrun Draut	(Merkel, 2016; Nardini, 2018)
437	<i>pTol2_pel2.5kb:mClover_α-crystallin:mRFP</i>	p383, p390	Niels Nardini, Heidrun Draut	(Chan et al., 2010; Nardini, 2018)
438	<i>pTol2_Prx1b1:KalTA4-GI_α-crystallin:mRFP</i>	p300, p365, p382	Amelie Mück	(Chan et al., 2010; Mück, 2019)
439	<i>pTol2_Pel2.5kb:KalTA4-GI_α-crystallin:mRFP</i>	p300, p365, p384	Amelie Mück	(Hernández-Vega & Minguillón, 2011; Mück, 2019)
440	<i>pTol2_HLEA:mClover_α-crystallin:mRFP</i>	p365, p368	Heidrun Draut	(Menke et al., 2008; Merkel, 2016)
441	<i>pSP64T-XB_ERT2-Gal4-VP16-GI</i>	p147, p356	Heidrun Draut	(Gerety et al., 2013)
442	<i>pSP64T-XB_dnRara2a-ERT2</i>	p147, p356, p390	Heidrun Draut	(Gerety et al., 2013; Stafford et al., 2006)
443	<i>pSP64T-XB_ERT2-dnRara2a</i>	p147, p356, p390	Heidrun Draut	(Gerety et al., 2013; Stafford et al., 2006)
444	<i>pTol2_XhoI-ccdB-XhoI_GAVPO_α-crystallin:mRFP</i>	p403, p427, p419	Heidrun Draut, David Richter	(Richter et al., 2019; Wang et al., 2012)

**Table 12. Plasmid list 3.** Summary of plasmids used as templates for *in vitro* transcription of DIG-labelled antisense probes. The named restriction enzymes and RNA polymerases were used for linearization of the plasmid and synthesis of antisense RNA probes, respectively.

No.	Gene name	Backbone	Restriction enzyme/ RNA Polymerase	Source
17	<i>MyoD</i>	unknown	XbaI, T7	-
20	<i>Pax6a (Pax-a)</i>	unknown	SmaI, T7	Stefan Krauss
21	<i>Pax2a (Pax-b)</i>	pGEM-3Zf+	BamHI, T7	Stefan Krauss
22	<i>Epha4a (Rtk1)</i>	unknown	BamHI, T7	Lindsey Durbin
25	<i>Six3</i>	pBSK	EcoRI, T7	Gerrit Begemann
41B	<i>Rdh10a</i>	pCMV-SPORT6.1	SmaI, T7	Nicola Blum
90	<i>Cyp26a1</i>	pBKS (+)	Sall, T7	Stephen Wilson
101	<i>Fgf8a</i>	pCRII	EcoRV, SP6	Didier Stainier
124	<i>Shh</i>	unknown	HindIII, T7	Sudipto Roy
128	<i>Cyp26c1 (Cyp26d1)</i>	pGEM-T	BamHI, T7	Qingshun Zhao
135	<i>Fgf10a</i>	unknown	HindIII, T7	Carl Neumann
137	<i>Fgf24</i>	unknown	XbaI, T7	Carl Neumann
163	<i>Aldh1a2</i>	pCR4-Topo	NotI, T3	Heiner Grandel
167	<i>Tbx4</i>	pGEM-T	SacII, SP6	Robert Ho
178	<i>Cyp26b1</i>	pSPORT1	BglII, SP6	Cecilia Moens
392	<i>Pitx1</i>	pBS-KS	BamHI, T3	Mike Breu

**Table 13. Plasmid list 4.** Summary of plasmids used as template for mRNA synthesis. The named restriction enzymes and RNA polymerases were used for linearization of the plasmid and synthesis of mRNA probes, respectively:

No.	Gene name	Backbone	Restriction enzyme/ RNA Polymerase	Source
300	<i>KalTA4-GI</i>	pCS	NotI, SP6	Martin Distel, Reinhard Köster
348	<i>Tol2</i>	pCS2 TP p1208	NotI, SP6	Sebastian Gerety
377	<i>Gal4-VP16</i>	pSP64T-XB	BamHI, SP6	Masazumi Tada
380	<i>ERT2-Gal4-VP16</i>	pSP64T-XB	BamHI, SP6	Heidrun Draut
388	<i>dnRara2a</i>	pSP64T-XB	SacI, SP6	Marlene Schmidt
389	<i>dnRara2a-IRES-eGFP</i>	pSP64T-XB	XhoI, SP6	Marlene Schmidt
398	<i>Cyp26a1</i>	pSP64T-XB	XbaI, SP6	Heidrun Draut, Jean Eberlein
399	<i>Cyp26a1-eGFP</i>	pSP64T-XB	XbaI, SP6	Heidrun Draut, Jean Eberlein
401	<i>Cas9</i>	PT3TS	XbaI, T3	Addgene #46757
428	<i>GAVPO</i>	pSP64T-XB	NotI, SP6	Heidrun Draut, Lina Stacker
431	<i>KalTA4-ERT2-GI</i>	pCS2	NotI, SP6	Masazumi Tada
441	<i>ERT2-Gal4-VP16-GI</i>	pSP64T-XB	BamHI, SP6	Heidrun Draut
442	<i>dnRara2a-ERT2</i>	pSP64T-XB	EcoRI, SP6	Heidrun Draut
443	<i>ERT2-dnRara2a</i>	pSP64T-XB	EcoRI, SP6	Heidrun Draut

#### 4.1.5 DNA oligonucleotides

DNA oligonucleotides were purchased lyophilized and salt-free from eurofins.com or biomers.net, resolved in TE buffer to a concentration of 100  $\mu$ M and stored at -20 °C. The only exception is oligonucleotide Nr. 284, which was stored at -80 °C.

**Table 14. List of oligonucleotides with sequence information.**

No.	Name	Sequence	Application
46	T7-Primer	TAATACGACTCACTATAGGG	Sequencing
91	M13fw	GTAAAACGACGGCCAG	Sequencing, Genotyping of <i>Hsp70l:Cyp26a1</i>
92	hsp:cyp26a1-fw2	GAGCAAAGGTCTGGAGGA	Genotyping of <i>Hsp70l:Cyp26a1</i>
183	ERT2-Gal4-EcoRV	ACGTAGATATCGAATGGCCGGTGAC ATGAG	Cloning of p380
184	ERT2-Gal4-NotI	ATAGCGGCCGCTTAGTTACCCGGGA GCATATCG	Cloning of p380
185	zfprrx1a_f_Sall	ATTGTGACAAAGTCTCGCGCTGGCA CCAGGCAGC	Cloning of p381
186	zfprrx1a_r_BamHI	ATCGGATCCATCGAGCTCCGCATGT GTCGCAATG	Cloning of p381
187	zfprrx1b1_f_Sall	ACTGTGACTGAGAGAAGTCGCTTG TAGAGAAGC	Cloning of p382
188	zfprrx1b1_r_BamH	ATCGGATCCACTTGCTGAGTTATAAG CGGTGGC	Cloning of p382
189	pel2,5kb_fw_Sall	GAGGTCGACGGTACAAGGCCTATCG	Cloning of p383
190	pel2,5kb_rv_AgeI	CAGACCGTTCTAGAACTAGTGGAT CC	Cloning of p383
191	Sall sHLEB 4x	AAAGTCGACTCACTATAGGGCGAAT TG	Cloning of <i>pTol2_4xHLEB:mClover</i>
192	AgeI sHLEB 4x	AACCGGTGATGTTCTGGAGCTCGG TAC	Cloning of <i>pTol2_4xHLEB:mClover</i>
193	pTol_Seq1	CCTCACTTTGAGCTCCTCCACACG	Sequencing
194	pTol_Seq2	GCTGGGCGCGCTCTTTTATATG	Sequencing
195	pTol_Seq3	CTCAAGTAAGATTCTAGCCAG	Sequencing
196	pTol_Seq4	TCGAGCCGGGCCAAGTG	Sequencing
197	pel2,5kb Seq1	CCTTTATTTTCACCTTTTCACCCCTC	Sequencing of Pel2.5kb
198	pel2,5kb Seq2	GAGCTTCCACGGATTGTTGTGG	Sequencing of Pel2.5kb
199	pel2,5kb Seq3	GCCGCTAATGCTACCTGTTAGCGG	Sequencing of Pel2.5kb
200	pel2,5kb Seq4	GGGGCAGAGCAGCTTATCTCGGC	Sequencing of Pel2.5kb
201	pTol-ERT2-Gal4 f	CGAATTCGCCGCCACATGGCCGGTG ACATGAGAG	Cloning of p396
202	pTol-ERT2-Gal4 r	GTAATCCGCGGTGGCAACTGTTTAT TGCAGCTTATAATGGTTACAAA	Cloning of p396

203	pTol-ERT2Gal4 r2	GTATCTTATCATGTCTGGATCTACTT AGGCGCCGGTGGAGTGG	Cloning of p396
204	pTol-ERT2Gal4 r3	CAAAGAATTTCCCCCTGAACCTGAA ACATAAAATGAATGCAATTGTTG	Cloning of p396
205	pTol-crys-RFP fw	TCAGGGGGAAATTCTTTTGAATAAC AGTTCAGTAAGTATGGCAAACAA	Cloning of p396
206	pTol-crys-RFP rv	GTATCTTATCATGTCTGGATCTACGT ATTAGGCGCCGGT	Cloning of p396
207	crys-RFP fwd2	TGGGAGGTTTTTTAATTCGCCCGCTC TAGATGGCCAGATCG	Cloning of p396
208	crys-RFP rev2	TAACAGGGTAATCCGCGGTGGCGCG CTGATGCCAGTTTAAT	Cloning of p396
209	crys-RFP fw NotI	AAAGCGGCCGCTCTAGATGGCCAGA TCG	Cloning of p396
210	crys-RFP rv NotI	TTTGCGGCCGGAATTGCGCTGATG CCCAG	Cloning of p396
211	zfprx1a fwd	AACTGAAGCGGGCAGCTGGG	<i>Prrx1a</i> WISH probe
212	zfprx1a rev T7	ACGTAATACGACTCACTATAGGTTCA TCACTTACATACATGGCC	<i>Prrx1a</i> WISH probe
213	zfprx1b fwd	AACTAAGCCTGAAAAGAGGGAC	<i>Prrx1b</i> WISH probe
214	zfprx1b rev T7	ACGTAATACGACTCACTATAGGCAG ATACATATGTCACCATGGG	<i>Prrx1b</i> WISH probe
215	prrx1a_rv_SpeI	ATCACTAGTATCGAGCTCCGCATGTG TCGCAATG	Cloning of p393
216	prrx1b1_rv_SpeI	ATCACTAGTACTTGCTGAGTTATAAG CGGTGGC	Cloning of p393
239	T3 Primer	AATTAACCCTCACTAAAGGG	Sequencing
240	cyp26a1 fwd EcoRV	ACGGAGATATCATGGGGCTGTACAC CCTTAT	Cloning of p398
241	cyp26a1 rev NotI	AAAGCGGCCGCGCTAATTTCTGACA TAACTAGTG	Cloning of p398
242	Gibson eGFP fwd	TGTCAGAAATGGCGGTGGAATGGTG AGCAAGGGCGAG	Cloning of p397
243	Gibson eGFP rev	GTTCTAGAGGCTCGAAGTTTCTACTT GTACAGCTCGTCCATGC	Cloning of p397
244	Gibson cyp26a1 fwd	GAGCTCCTCCACACGAATTCGATATG GGGCTGTACACCCTTATG	Cloning of p397
245	Gibson cyp26a1 rev	CACCATTCCACCGCCATTTCTGACAT AACTAGTGAATTTGGTAG	Cloning of p397
246	UAS Seq1	CCGAGCGGAGACTCTAGAGG	Sequencing
247	cyp26a1 Seq1	ACCTTCTCCTGAACCTCCTC	Sequencing
248	eGFP rev NotI	AAAGCGGCCGCTACTTGTACAGCT CGTCC	Cloning of p399
249	Seq3 dnRAR	GGGGAAGGTCTCTTGGTGGG	Sequencing
250	Seq4 dnRAR	CCCACCAAGAGACCTTCCCC	Sequencing

253	4xnrUAS_dnRAR fw	CTCGAAGACGCGTGGATCCAATGTA TGAGAGTGTGGATG	Cloning of p405
254	4xnrUAS_dnRAR rev	GGCCATCCACCGCCAATCTCCATCT TCAGGGTG	Cloning of p406
255	4xnrUAS_dnRAR- eGFP rev	GGCCATCTAGAGCGGCCGAGCGAA TTAAAAAACCTCC	Cloning of p405
256	4xnrUAS_mRFP fwd	GATGGAGATTGGCGGTGGAATGGC CTCCTCCGAGGAC	Cloning of p406
257	4xnrUAS_mRFP rev	GGCCATCTAGAGCGGCCGCACGAAT TAAAAAACCTCCCACACCTC	Cloning of p406
258	ERT2-Gal4 Seq1	GCATGAAGTGCAAGAACGTGG	Sequencing
259	ERT2-Gal4 Seq2	CCACGTTCTTGCACTTCATGC	Sequencing
260	crys-RFP fw BglII	CCCAGATCTAGATGGCCAGATCGAT C	Cloning of p440
261	crys-RFP rv BglII	CCCAGATCTGAATTGCGCTGATGCCC A	Cloning of p440
262	ERT2-Gal4 Seq3	CAGGATCTCTAGCCAGGCAC	Sequencing
263	ERT2-Gal4-Globin- NotI	AAAGCGGCCGCGTTGCCAGGAGC TGTAGG	Cloning of p441
264	Gal4 DBD fw	ATGAAGCTACTGTCTTCTATCGAAC	<i>Gal4</i> DBD WISH probe
265	Gal4 DBD rev T7	ACGTAATACGACTCACTATAGGGCG ATACAGTCAACTGTCTTTG	<i>Gal4</i> DBD WISH probe
266	4xnrUAS_cyp26a1_ fw	CTCGAAGACGCGTGGATCCAATGGG GCTGTACACCT	Cloning of p407
267	4xnrUAS_cyp26a1_ rv	AGGAGGCCATTCCACCGCCATTTCTG AC	Cloning of p407
268	4xnrUAS_cyp26a1- mRFP_fw	TGGCGGTGGAATGGCCTCCTCCGAG GAC	Cloning of p407
269	4xnrUAS_cyp26a1- mRFP_rv	GGCCATCTAGAGCGGCCGCAATTAA AAAACCTCCCACACCTCC	Cloning of p407
270	eGFP fw SpeI	CCCCTAGTATGGTGAGCAAGGGCG AGGA	Cloning of p434
271	eGFP rev SacII	AAACCGCGGCTATAGGGCTGCAGAA TCTAGAGG	Cloning of p434
272	cyp26a1-3xGly rv	GGCCATCCACCGCCATTTCTGACAT AACTAGTGAATTTGGTAG	Cloning of p407
273	3xGly-mRFP fw	TGTCAGAAATGGCGGTGGAATGGCC TCCTCCGAGGAC	Cloning of p407
274	mRFP-bh rv	GAAGCACTAGTGCGGCCGAACTT GTTTATTGCAGCTTATAATGG	Cloning of p409
275	mRFP-eye rv	GGCCATCTAGAGCGGCCGAACTT GTTTATTGCAGCTTATAATGG	Cloning of p407
280	Seq_ccdB	CGGGGAAGAAGTGGCTGATC	Sequencing
281	Pitx1 Target 5	TAATACGACTCACTATAGGTGTGGA CTAACCTCACCGGTTTTAGAGCTAGA AATAGC	sgRNA synthesis with T7 polymerase

282	Pitx1 Target 19	TAATACGACTCACTATAGGCTGGCG CTTCTCGGCAGAGTTTTAGAGCTAGA AATAGC	sgRNA synthesis with T7 polymerase
283	Pitx1 Target 50	TAATACGACTCACTATAGGGTGGAA TGAATGTGGACAGTTTTAGAGCTAG AATAGC	sgRNA synthesis with T7 polymerase
284	universal bottom- strand	GTTTTAGAGCTAGAAATAGCAAGTT AAAATAAGGCTAGTCCGTTATCAACT TGAAAAAGTGGCACCGAGTCGGTGC TTTT	sgRNA synthesis
285	Tyr Target 1	TAATACGACTCACTATAGGACTGGA GGACTTCTGGGGTTTTAGAGCTAG AATAGC	sgRNA synthesis with T7 polymerase
286	Tyr T1 fw M13	TGTA AACGACGGCCAGTAGCTCTT CAGCTCGT CTCTC	Genotyping of <i>Tyr</i> KO
287	Tyr T1 rv PIG	GTGTCTTTGAGTGAGGATACTGC GG	Genotyping of <i>Tyr</i> KO
288	Pitx1 T5 fw M13	TGTA AACGACGGCCAGTCCCGAAG AAGAAGAAGCAGCGGCGG	Genotyping of <i>Pitx1</i> KO
289	Pitx1 T5 rv PIG	GTGTCTTCGTGTA CTCTG CAGAGCTC CTCCTG	Genotyping of <i>Pitx1</i> KO
290	Pitx1 T19 fw M13	TGTA AACGACGGCCAGTGCATTA GATGTGGCAAAGCAGACA	Genotyping of <i>Pitx1</i> KO
291	Pitx1 T19 rv PIG	GTGTCTTGTCGCTTGCTTGCATGTT C	Genotyping of <i>Pitx1</i> KO
292	Pitx1 T50 fw M13	TGTA AACGACGGCCAGTCCGCTGC TTCACGCGTTATTC	Genotyping of <i>Pitx1</i> KO
293	Pitx1 T50 rv PIG	GTGTCTTACAGTGAATGCGTGTATT CCAGTGC	Genotyping of <i>Pitx1</i> KO
294	Seq_cmlc2	GGGGACGAACAGAAACTGCAGAC CC	Sequencing
295	ERT2-Gal4 Seq4	GGGAGAGGAGTTTGTGTGCC	Sequencing
296	Tyr T1 fw M13 (2)	TGTA AACGACGGCCAGTTGCGTAA AGGGGGCTCTCCAGC	Genotyping of <i>Tyr</i> KO
297	Tyr T1 rv (2)	GAGCAGAGCGTCCCGGGACAC	Genotyping of <i>Tyr</i> KO
298	Pitx1 T5 fw M13 (2)	TGTA AACGACGGCCAGTCCAAAAA TAGCGAGTAACAGCA	Genotyping of <i>Pitx1</i> KO
299	Pitx1 T5 rv (2)	TTAATTTTCATGCCGAGAACAAG	Genotyping of <i>Pitx1</i> KO
300	Pitx1 T19 T50 fw M13 (2)	TGTA AACGACGGCCAGTGGGTGG GTCTCTGCGGCTCGC	Genotyping of <i>Pitx1</i> KO
301	Pitx1 T19 T50 rv (2)	GCGAACACAGCGCAAAAGCTGGC	Genotyping of <i>Pitx1</i> KO
302	cyp26a1 Seq2	CCAGGTTTAACTACATCCCC	Sequencing
303	4xnrUAS Seq	GGTGGCTTCTAATCCGTGAGTC	Sequencing
304	Seq5 dnRAR	GAGACGGGACTGCTCAGTGCTATAT GTC	Sequencing
305	Seq $\beta$ -globin	AAGAACAATCAAGGGTCCCC	Sequencing
306	KalTA4 fw + SacI	TTTGAGCTCCTCCACACGATGTACAA GCTACTTGTTTC	PCR <i>KalTA4</i> , Restriction cloning
307	KalTA4 rv + XbaI	CCATCTAGAACTTGTATTGCAGC	PCR <i>KalTA4</i> , Restriction cloning
308	IRES-mRFP rv	AGGAGGCCATGGTTGTGGCCATATT ATCATCG	Cloning of p410, p411

309	IRES-mRFP fw	GGCCACAACCATGGCCTCTCCGAG G	Cloning of p410, p411
310	cyp26a1-IRES rv	GGGAGAGGGGATTTCTGACATAACT AGTGAATTTGGTAGGGAG	Cloning of p411
311	cyp26a1-IRES fw	TGTCAGAAATCCCCTCTCCCTCCCC CC	Cloning of p411
312	cyp26a1-IRES fw 2	TGTCAGAAATTGACCCCTCTCCCTCC CCCC	Cloning of p411
313	cyp26a1-IRES rv 2	GGGAGAGGGGTCAATTTCTGACATA ACTAGTGAATTTGGTAGGGAG	Cloning of p411
314	zfHsp70l fw_BglII	CCCAGATCTGATCCTTCAGGGGTGTC GCTTGG	Cloning of 422
315	zfHsp70l rv_SacI	CCCGAGCTCCCAATAAGAGCCAAGC CTGCAGG	Cloning of 422
316	zfHsp70l fw_Sall	AAAGTCGACGATCCTTCAGGGGTGT CG	Cloning of p422
317	zfHsp70l rv_SacI	CCCGAGCTCCCTGCAGGAAAAAAAA ACAATTAGAATTAATTTTATATTTA	Cloning of p422
318	Seq IRES 2	GGCTCTCTCAAGCGTATTC	Sequencing
319	KalTA4 fw	GCTACTTGTCTTTTTGCAGGATCCC ATCGATTCTGAATTCGCCGCC	<i>KalTA4</i> WISH probe
320	KalTA4 rv T7	ACGTAATACGACTCACTATAGGGTTA GTTACCCGGGAGGATGT	<i>KalTA4</i> WISH probe
321	Gibson KalTA4- ERT2-GI fw	ACTTTGAGCTCCTCCACACGGAATTC GCCGCCACCATGA	Cloning of p412-p416
322	Gibson KalTA4- ERT2-GI rv	TAAATAGATCGATCTGGCCATGGTA CCGGGCCCAATGC	Cloning of p412-p416
323	KalTA4 Seq1	CCAGTCTCTCTAGCCTGCTC	Sequencing
324	Seq2 $\beta$ -globin	CCAAACCGGGCCCCTCTGCT	Sequencing
325	ERT2-Gal4 Seq 5	CTCGAGCCATCTGCTGGAGACA	Sequencing
326	pTol_Seq5	CACCGGTTGGCTAGAGCCGGC	Sequencing
327	pEX-A128 Seq1	GGCTTAACTATGCGGCATCAGAGC	Sequencing
328	lac primer	CACTTTATGCTTCCGGCTCGTATG	Sequencing
329	ERT2-Gal4 Seq6	GTGTCTGTGATCTTGTCAGG	Sequencing
330	ERT2-Gal4 Seq7	GAGGCACACAACTCCTCTCCC	Sequencing
335	Gibson pTol-dnRAR fw	CTTTGAGCTCCTCCACACGGCGCGTG GATCCAATGTATGAGAGTGTGG	Cloning of p424
336	Gibson ERT2- dnRAR rw	ATGGCTCGAGAATCTCCATCTCAGG GTGATCACACGCTCCG	Cloning of p424
337	Gibson dnRAR- ERT2 fw	GGAGAGGGGCTTAGAGCTCTGAGA CTGTGGCAGGGAAAC	Cloning of p424
338	Gibson IRES-ERT2 rw	GGAGAGGGGCTTAGAGCTCTGAGA CTGTGGCAGGGAAAC	Cloning of p424
339	Gibson ERT2-IRES fw	AGAGCTCTAAGCCCCTCTCCCTCCCC CCC	Cloning of p424
340	Gibson pTol- mCherry rw	GTATCTTATCATGTCTGGATCTACGC GGCCGCTTACTTGTACAGCTCG	Cloning of p424
341	Gibson2 pTol-ERT2 fw	TTGAGCTCCTCCACACGGATGCTCGA GCCATCTGCTGGAGACATGAGAGC	Cloning of p425

342	Gibson2 dnRAR-ERT2 rw	TCTCATACATGAGCTCTGAGACTGTG GCAGGGAAACC	Cloning of p425
343	Gibson2 ERT2-dnRAR fw	CTCAGAGCTCATGTATGAGAGTGTG GATGTGAACCCCTTCCT	Cloning of p425
344	Gibson pTol-mcherry_2	AACAGGGTAATCCGCGGTGGCTCCT GCAGTGCTGAAAAGCCTCTCACAGG	Cloning of p424, p425
345	Gibson mRFP-IRES rw	TAACAGGGTAATCCGCGGTGGCGCG GCCGCAAACCTGTTTATTGCAGCT	Cloning of p424, p425
346	Pitx1 T19 T50 fw M13 (3)	TGTA AACGACGGCCAGGACTGACA CGGGTTGGAGAGGA	Genotyping of <i>Pitx1</i> KO
347	Pitx1 T19 T50 rv (3)	TAGCGAACACAGCGCAAAAGCTG	Genotyping of <i>Pitx1</i> KO
348	dnRAR fw SpeI	CCCACTAGTATGTATGAGAGTGTGG ATGTGAACCC	Cloning of p442
349	ERT2 rw NotI	AAAGCGGCCGCTTAGAGCTCTGAGA CTGTGGCAG	Cloning of p442
350	ERT2 fw SpeI	CCCACTAGTATGCTCGAGCCATCTGC TGGAGAC	Cloning of p443
351	dnRAR rw NotI	ACAGCGGCCGCTCAAATCTCCATCTT CAGGGTGATCACACGC	Cloning of p443
352	pTol_Seq6	TAGATCTAATCTCGACGCGCG	Sequencing
353	Pitx1 T19 T50 fw (4)	GGACTGACACGGGTTGGAGAGGA	Genotyping of <i>Pitx1</i> KO
354	Pitx1 T19 T50 rv (3)	TAGCGAACACAGCGCAAAAGCTG	Genotyping of <i>Pitx1</i> KO
355	ubi fw Sall	CATGTGACGCCCTTAAACTCGAG ACCAGC	Cloning of p423
356	ubi rw XcmI	CCAACCACTATCTGGCGCCCTTTTGG GATCCCTGTAAAC	Cloning of p423
357	Gibson ubi fw	AACAGGGTAATGGGCCCCCTCGA GACCAGCAAAGTTCTAGAATTTG	Cloning of p423
358	Gibson ubi rw	CATGTCTCCAGCAGATGGCTCGAGC ATGTCGAATTCGCCCTTTTGGATC	Cloning of p423
359	GAVPO fw XhoI	ACGTCTCGAGGATCCGCTAGCGCTA TGAAGC	Cloning of p428
360	GAVPO rw NotI	AAAGCGGCCGCCCTCTACAAATGTG GTATGGCTG	Cloning of p428
361	GAVPO fw XhoI 2	CCGGCTCGAGATGAAGCTACTGTCTT CTATCG	Cloning of p428
362	ubi.FOR	CTGTCTCCCGCGGGCCCCCGCCC TTAAACTCGAGACCAGC	Cloning of p423
363	ubi.REV	TCTCATACATGTCGACTCGCCCTTTT GGATCCCTGTAAAC	Cloning of p423
364	dnRAR.FOR	AAAAAGGGCGAGTCGACATGTATGA GAGTGTGGATGTGAACC	Cloning of p423
365	dnRAR.REV	ATGGCTCGAGAATCTCCATCTCAGG GTGATCACACG	Cloning of p423
366	ERT2.FOR	GATGGAGATTCTCGAGCCATCTGCT GGAG	Cloning of p423
367	ERT2.REV	GAGAGGGGCTCTTAGAGCTCTGAGA CTGTGGCAG	Cloning of p423
368	IRES-mRFP.FOR	GAGCTCTAAGAGCCCCTCTCCCTCCC	Cloning of p423

369	IRES-mRFP.REV	CTGAAAAGCCTCTCACAGGAGCGGC CGCAAACCTTGT	Cloning of p423
370	Gibson ubi prom fw	CGACGGTATCGATAAGCTTGATCGC CCTTAAACTCGAGACCAGC	Cloning of p426
371	Gibson ubi prom rv	CTAGCGGATCCGCCCTTTTTGGATCC CTGTAAAC	Cloning of p426
372	Gibson GAVPO fw	AAAAAGGGCGGATCCGCTAGCGCTA TGAAGC	Cloning of p426
373	Gibson GAVPO rv	GGCCATCTAGAGCGGCCGCACGCCT TAAGATACATTGATGAGTTTGG	Cloning of p426
374	Pitx1_T19_Calc_Lo ng_1_for	GGGGTTTAGATGGAAAGCTCTGCTT G	Genotyping of <i>Pitx1</i> KO
375	Pitx1_T19_Calc_Lo ng_1_rev	GCCTAGCTCATTGTTTACAGCACGC	Genotyping of <i>Pitx1</i> KO
376	Gibson GAVPO fw	ACTTTGAGCTCCTCCACACGAATTCA TGAAGCTACTGTCTTCTATCGAAC	Cloning of p417-p421
377	Gibson GAVPO rv	TAAATAGATCGATCTGGCCATCTAGA TACGCCTTAAGATACATTGATGAG	Cloning of p417-p421
378	GAVPO Sonde fw	ATGAAGCTACTGTCTTCTATCGAACA AGCATGCG	GAVPO WISH probe
379	GAVPO Sonde rv T7	ACGTAATACGACTCACTATAGGGTTC CGTTTCGCACTGGAAACCC	GAVPO WISH probe
382	ccdB Gibson fw	AACAGGGTAATGGGCCCCCTCGA GGGATCCGTCGAGATTTTCAGGAGC	Cloning of p444
383	ccdB Gibson rv	CTAGCCAACCGGTGGATCCACTCGA GCCGCACCGTCAATTTATATTTCC	Cloning of p444
390	Primer SP6 seq	CGCCAAGCTATTTAGGTGACACTATA G	Sequencing

#### 4.1.6 RNA antisense probes

**Table 15. Sequences of template DNA for *in vitro* transcription of RNA antisense WISH probes using T7 polymerase.**

Target	Sequence 5' -> 3'
<i>Prrx1a</i>	ACGTAATACGACTCACTATAGGTTCACTTACATACATGGCCAGAGTTCTGTATATGCCAAAA TGAACCAATACCCCTTGCATGTTTTTTAAACAGACAACAGTGAAGAGTGATTTTAGAGTCCGGT AACAGGAAAGCCAAATTTCACTCTGTTCCCAAATAACCAAATATCCAAATCCCAATTTGTGGCC TCAGTGCGCATTACGAGTTCCAATGAGAAATCGAGGGGAAATCCTAAAACTCCCAGATGTC CGCAAGATTGTAGTATATGGATTCCGAGAGGTCATCAAATCCCTGTGGTCGGCAGGAGTCTCA AGAAAGAAATCTATAGTAAGCCACGATCCAAAAGGGTTGACCACGCTTACGCTGCCACAGTG AGTGTGAACAGTGAAAACTTTCCATTTTGTGCTGTCCAAAACCAATTTTCCCACATGTCATTTCC CCACATACCAGGAACATGACGGTTCAATGTAAATCATTGGTTTTAGAAAAGCTTGGTACCTTGGGA GCTGTTCTCGTTTCTTCTGTTCTTTGATGGATAAGAGTAAAACACATAGAGGAGGACAGAAAA CGTTGTTTATGTCAATAGATTTGGGGCTGGGACATTGGGATTGTTCTGAGAGTCTTTGACAGCCC AGCTGCCCGCTTCAGTT

<i>Prrx1b</i>	ACGTAATACGACTCACTATAGGCAGATACATATGTCACCATGGGGAACCGTATTAACCTTAAAG AGTGGTGAATATTCAGACCTAAAAATATGTAATCCGGCCCTAATGCTTCCGTTAGCACTGACAG TTGTAACATCTCATATACTGATTATAGTCCACAAATGTGTCTTTATTTTACCAAAGGCAGACGTG GAGACATTTTAAGCCACTTTGTTGCCAAATCTCCACATTAATAATTCTGGTGAATTTAAACCATT AGTGGTGAATGGCGCAAACAGTCTCCATTGTGTTCTTGAAAGTTTCTTTACTTTCCATCCGG ATGACCCAAAATAAAGCCAAAAGAACATGGAAAGAACAGCATAACAGCATCCAGGCACTTCGTC TGCCACTTCTTTGTGATTTAGCGGAGCCCTTCTCGTTGATTTGATCTCCAAAAGCAGAACATGT GCTGTCTTTACAATCTTCATATCAGTACAAAATGAGATTGAGTTTCTCAAAAACGTACCTTAATCT ATGATGAAGAAAAAGCCAATTGAGAGGGACAACAACGCAATTTCAATTGTTAAGGAGGGGGC CAAAAGTCATATCCACTCTGCTTTAACTGCGAAAAGCCAGAAAATCACTGTTACCGCTAAAC CAGTCCAGCTCTTCTGAGATCTTCTTCTCAGTGTGTCTTCTTTTTTACGTCCCCTCATTCCGTCC CTCTTTTCAGGCTTAGTT
<i>Gal4 DBD</i>	ACGTAATACGACTCACTATAGGGCGATACAGTCAACTGTCTTTGACCTTTGTTACTACTCTCTTCC GATGATGATGTGCACTTATTCTATGCTGTCTCAATGTTAGAGGCATATCAGTCTCCACTGAAGC CAATCTATCTGTGACGGCATCTTTATTCATTATCTTGACAAAATAATCTGTTAACAATGCTTTT ATATCCTGTAAAGAATCCATTTTCAAATCATGTCAAGGTCTTCTCGAGGAAAAATCAGTAGAAA TAGCTGTTCCAGTCTTTCTAGCCTTGATTCCACTTCTGTGAGATGTGCCCTAGTCAGCGGAGACCT TTTGGTTTTGGGAGAGTAGCGACACTCCAGTTGTTCTTCAGACACTTGGCGCACTTCGGTTTTTC TTTGGAGCACTTGAGCTTTTTAAGTCGGCAAATATCGCATGCTTGTTTCGATAGAAGACAGTAGCT TCAT
<i>KalTA4</i>	ACGTAATACGACTCACTATAGGGTTAGTTACCCGGGAGGATGTCCAGGTCGTAGTCGTCCAGGG CGTCGGCCGGGAGCATATCCAGATCGAAATCATCGAGAGCATCAGCAGGCAGCATGTCCAGGT CGCCGTCGTCCAGGGCGTCGGCCGGGACGGGGTCGACCTGCTCGAAACAGTCAGCTGTCTCT GTCCCTTGTTAGAAGACTCTTCGCTTGAGGAAGTAGCGCTGATTCTGTGCTGTCTCAGTGTCAGA GGCATATCGGTCTCGACACTTGCCAATCGGTCTGTACAGCGTCTTTGTTACATTGTCCTGGAC GAATAAGCCAGTCAAAGGGCTTTAATATCCTGGAGAGAATCCATCTTGAGGATCATGTCAAGG TCCTCTAGGGAAAGATGAGCAAAAAGAGTTGTTCCAGTCTCTAGCCTGCTCTCCACTTCGGT CAGATGAGCCCTGTGAGTGGACTTCGCTTGGTTTTGGGAGAGTAACGACATTCCAATTGTTCT TCAGGCATTTGGCACATTTGGGCTTTTCTTGGAGCATTTAGCTTCTTAAGCCGACAAATGTGCG AGGCTTGCTCGATGGATGAGAGCAGTTTCATGGTGGCGGCGAATTCGAATCGATGGGATCCTG CAAAAAGAACAAGTAGC
<i>GAVPO</i>	ACGTAATACGACTCACTATAGGGTTCCGTTTCGCACTGGAAACCCATGCTGTACCGGTATTCCC TGTTTCATCTCGCACCGGAATCATCGTCAAGAAGTTGACAAACCGTTGGCCGTTCTTCTTAAAT GACCACCTCAACCTGCACCTCGGCGTTCTATCAATCGCTTTCCTCATCGTATTGATCGTGTGG GTCGACGTAATCCTTGTGATTTGCGCTTGACCATTCGTCGGGTGACTGAAGAAAACGGCAGT TTCTCCCAAGACCTCCGATTGCTGTATCCTGTATATAGAGAAAAGCTTCCGAGGCGTACACA ATTGGCGTGTCTTTTCTTTCAGGTGCGACAGAATCAGAGCAACTGACGTGTCAACAGGTCCCA GTTCTACTTGGGGGTTTGGCCTTTCATAATCTGAATCAGATAGCCATAATGTCATAACCGCCG GGAGCGTAGAGCGTATGAGATCTGGTGGCGATGGATCTTCCAGTCTTCTAGCCTTGATTCCAC TTCTGTCAGATGTGCCCTAGTCAGCGGAGACCTTTTGGTTTTGGGAGAGTAGCGACACTCCAGT TGTTCTTCAGACACTTGGCGCACTTCGGTTTTTCTTGGAGCACTTGAGCTTTTTAAGTCGGCAA TATCGCATGCTTGTTTCGATAGAAGACAGTAGCTTCAT

### 4.1.7 Single-guided RNAs (sgRNAs)

**Table 16. Sequences of template DNA for *in vitro* transcription of sgRNAs using T7 polymerase.**

Target	Sequence 5' -> 3'
<i>Pitx1</i> T5	TAATACGACTCACTATAGGTGTGGACTAACCTCACCGGTTTTAGAGCTAGAAATAGCAAGTTAAA ATAAGGCTAGTCCGTTATCAACTTGAAAAAGTGGCACCGAGTCGGTGCTTTT
<i>Pitx1</i> T19	TAATACGACTCACTATAGGCTGGCGCTTCTCGGCAGAGTTTTAGAGCTAGAAATAGCAAGTTAA AATAAGGCTAGTCCGTTATCAACTTGAAAAAGTGGCACCGAGTCGGTGCTTTT
<i>Pitx1</i> T50	TAATACGACTCACTATAGGGTGAATGAATGTGGACAGTTTTAGAGCTAGAAATAGCAAGTTAA AATAAGGCTAGTCCGTTATCAACTTGAAAAAGTGGCACCGAGTCGGTGCTTTT
<i>Tyr</i> T1	TAATACGACTCACTATAGGACTGGAGGACTTCTGGGGGTTTTAGAGCTAGAAATAGCAAGTTAA AATAAGGCTAGTCCGTTATCAACTTGAAAAAGTGGCACCGAGTCGGTGCTTTT

## 4.2 Molecular biological methods

### 4.2.1 Polymerase chain reaction (PCR)

PCR was performed to amplify DNA sequences either from plasmid or genomic DNA as a template. For all applications, Q5 High-Fidelity DNA polymerase from NEB was utilized. The dNTP mix was either purchased as a finished mixture or mixed from the single components dATP, dTTP, dCTP and dGTP (each 10 mM final concentration in H<sub>2</sub>O). Primers were designed using SnapGene and the NEB online tools ([www.neb.com](http://www.neb.com)). Primer stocks were diluted 1:20 in TE buffer to reach a concentration of 5  $\mu$ M. Of major importance, the PCR reaction was assembled on ice and the thermocycler (BioRad C1000 Touch Thermal Cycler) was pre-heated to 98 °C. Filter tips were used during the whole procedure. After PCR, quality and quantity of the amplified product were checked by agarose gel electrophoresis.

Sequences from plasmid DNA were amplified according to the following protocol:

Amount	Component (Concentration)	Repeats	Temperature	Time
32.5 $\mu$ l	H <sub>2</sub> O	1x	98 °C	2 min
10 $\mu$ l	Q5 Buffer (5x)	30-35x	98 °C	10 sec
2.5 $\mu$ l	Primer forward (5 $\mu$ M)		61-72 °C	30 sec
2.5 $\mu$ l	Primer reverse (5 $\mu$ M)		72 °C	20-30 sec/kb
1 $\mu$ l	dNTP mix (10 mM)	1x	72 °C	2 min
1 $\mu$ l	Plasmid DNA (200-800 ng/ $\mu$ l)	1x	8 °C	$\infty$
0.5 $\mu$ l	Q5 Polymerase (2000 U/ml)			
50 $\mu$ l				

Sequences from genomic DNA were amplified according to the following protocol:

Amount	Component (Concentration)	Repeats	Temperature	Time
13.25 $\mu$ l	H <sub>2</sub> O	1x	98 °C	2 min
5 $\mu$ l	Q5 Buffer (5x)		98 °C	10 sec
1.5 $\mu$ l	Primer forward (5 $\mu$ M)	30x	61-72 °C	30 sec
1.5 $\mu$ l	Primer reverse (5 $\mu$ M)		72 °C	20-30 sec/kb
0.5 $\mu$ l	dNTP mix (10 mM)	1x	72 °C	2 min
3 $\mu$ l	Genomic DNA (1:10)	1x	8 °C	$\infty$
0.25 $\mu$ l	Q5 Polymerase (2000 U/ml)			
25 $\mu$ l				

#### 4.2.2 PCR purification

PCR products were purified utilizing different methods. For cloning or sequencing, the DNA was purified by agarose gel extraction. For this, after agarose gel electrophoresis (4.2.8), the desired DNA band was cut out of the agarose gel with the help of a scalpel and extracted using the Zymoclean Gel DNA Recovery Kit (Zymo Research) according to the manufacturer's instructions.

In case the PCR product was used for T7 Endonuclease 1 Assay, it was purified with QIAquick PCR purification Kit (QIAGEN) according to the manufacturer's instructions.

#### 4.2.3 Restriction digest

Enzymatic restriction digest was used to cut DNA for cloning, to confirm successful cloning or in order to use the linearized DNA as a template for *in vitro* transcription. Restriction enzymes from NEB or Thermo Fisher Scientific were used in combination with the respective buffer recommended by the manufacturer. Reactions were assembled according to the following basic protocol and incubated at 37 °C for 1 h:

<b>Amount</b>	<b>Component (Concentration)</b>
8 $\mu$ l	H <sub>2</sub> O
1 $\mu$ l	Buffer (10x)
0.5 $\mu$ l	DNA solution (200-1000 ng/ $\mu$ l)
0.5 $\mu$ l	Restriction enzyme (20.000 U/ml)
<hr/>	
10 $\mu$ l	

If necessary, the reaction was up-scaled and in case a higher amount of digested DNA was required, the amount of added water was adjusted. Afterwards, the success of the reaction was checked by agarose gel electrophoresis and for further usage, the DNA was purified using Oligo Clean and Concentrator Kit (Zymo Research) according to the manufacturer's instructions.

#### 4.2.4 Dephosphorylation

Dephosphorylation of linearized DNA was performed in order to prevent a re-ligation of the backbone DNA during cloning processes. Plasmid DNA was linearized and purified as described in 4.2.3 (elution in 15  $\mu$ l H<sub>2</sub>O). The dephosphorylation reaction took place at 37 °C for 30 min using Antarctic phosphatase (NEB) according to the following protocol:

<b>Amount</b>	<b>Component (Concentration)</b>
19 $\mu$ l	H <sub>2</sub> O
15 $\mu$ l	Linearized plasmid DNA
4 $\mu$ l	Antarctic Phosphatase Buffer (10x)
2 $\mu$ l	Antarctic phosphatase (5.000 U/ml)
<hr/>	
40 $\mu$ l	

Subsequently, the DNA was purified using Oligo Clean and Concentrator Kit (Zymo Research) according to the manufacturer's instructions.

#### 4.2.5 Ligation

Ligation was used to join DNA fragments with blunt or sticky ends. 50 ng of linearized and dephosphorylated vector DNA was combined with insert DNA (from PCR or restriction digest) in a molar ratio of 2:1 to 5:1, depending on the size of the insert. The reaction was catalysed by T4 DNA ligase (Thermo Fisher Scientific) and took place at room temperature for 1 h. Importantly, for blunt end joining, the amount of ligase was increased and additionally 50 % PEG 4000 solution was added to the mixture to increase the ligation efficiency. Subsequently, 2 - 5  $\mu$ l of the ligated product were directly used for transformation of competent *E. coli* cells (50  $\mu$ l).

Reaction mixture for sticky-end ligation:

Amount	Component (Concentration)
50 ng	Linearized, dephosphorylated vector DNA
x ng	Insert DNA
(2:1 to 5:1 molar ratio over vector)	
2 $\mu$ l	T4 ligase Buffer (10x)
0.5 $\mu$ l	T4 ligase (5 U/ $\mu$ l)
to 20 $\mu$ l	H <sub>2</sub> O
<hr/>	
20 $\mu$ l	

Reaction mixture for blunt-end ligation:

Amount	Component (Concentration)
50 ng	Linearized, dephosphorylated vector DNA
x ng	Insert DNA
(2:1 to 5:1 molar ratio over vector)	
2 $\mu$ l	T4 ligase Buffer (10x)
1 $\mu$ l	T4 ligase (5 U/ $\mu$ l)
2 $\mu$ l	PEG 4000 50 % (w/v)
to 20 $\mu$ l	H <sub>2</sub> O
<hr/>	
20 $\mu$ l	

#### 4.2.6 Gibson Assembly

In order to assemble 2 - 5 DNA fragments in one reaction, Gibson Assembly was performed. The design of primers, which possess the appropriate overhangs for fragment annealing, was carried out with SnapGene. 75 ng vector DNA was combined with fragment DNA in a molar ratio of 2:1 (for 2 - 3 fragments) or 1:1 (for 4 - 5 fragments). The reaction was mediated by NEBuilder HiFi DNA Assembly Master Mix and took place at 50 °C for 30 - 60 min. Afterwards, 2 µl of the assembled product were directly used for transformation of competent *E. coli* cells (50 µl).

Reaction mixture for Gibson Assembly:

Amount	Component (Concentration)
75 ng	Vector DNA
x ng	Insert DNA
(2:1 or 1:1 molar ratio over vector)	
10 µl	NEBuilder HiFi DNA Assembly Master Mix (2x)
to 20 µl	H <sub>2</sub> O
<hr/> 20 µl	

#### 4.2.7 Aqua Cloning

Aqua cloning was used as an alternative method to Gibson Assembly, in order to assemble 2 or 3 fragments in one reaction (Beyer et al., 2015). The design of primers, which possess the appropriate overhangs for fragment annealing, was carried out with SnapGene. To assemble the reaction, 200 ng vector DNA were mixed with insert DNA in a molar ratio of 5:1 (over vector). No additional water was added. The mixture was incubated for 1 h at room temperature. Afterwards, 5 µl of the assembled product were used to transform competent *E. coli* cells (50 µl).

#### **4.2.8 Agarose gel electrophoresis**

Agarose gel electrophoresis was performed for qualitative and quantitative analysis of DNA and RNA samples. To prepare the gels, 1x TAE buffer containing 1 - 2.5 % (w/v) agarose was heated in the microwave until the agarose was completely dissolved. Subsequently, Ethidium bromide was added to a final concentration of 0.5 µg/ml and the solution was put into the gel chamber. Previous to gel loading, 6x loading dye was added to DNA/RNA samples to reach a final concentration of 1x. The separation of fragments took place at 120 - 140 V for 30 - 40 min. Afterwards, DNA/RNA was visualized using UVSolo TS imaging system (Biometra).

#### **4.2.9 Capillary electrophoresis**

To detect mutations via the CRISPR/STAT method, PCR products were analysed by capillary electrophoresis. After PCR, the unpurified PCR samples were given to the laboratory of Alfons Weig (University of Bayreuth), where the electrophoresis was performed using a Fragment Analyser (Advanced Analytical) according to the recommended protocol of the manufacturer.

#### **4.2.10 Isolation of plasmid DNA from *E. coli***

First, the *E. coli* cells of a 2 ml over-night culture were pelleted by centrifugation (5 min, 8000 rpm, eppendorf Centrifuge 5430R). Subsequently, the plasmid DNA was isolated using commercial Mini-Prep Kits according to the manufacturer's instructions: Fast-n-Easy Plasmid Mini-Prep Kit (Jena Bioscience), QIAprep Spin Miniprep Kit (QIAGEN). Plasmid-DNA solutions were then stored at -20 °C.

#### **4.2.11 Measurement of DNA/RNA concentration**

DNA and RNA concentration as well as the purity of the nucleic acid solutions were determined by measuring the absorption at a wavelength of 260 nm using the BioPhotometer plus (eppendorf) in combination with a µCuvette G1.0 (eppendorf).

#### 4.2.12 Extraction of genomic DNA

Preparation of genomic DNA from fin tissue, zebrafish larvae or embryos was performed with a modified Extract-N-Amp extraction protocol (Sigma-Aldrich) (Varshney et al., 2016). In case a pool of embryos was used, the sample was first frozen and thawed to crack the chorions and enable the extraction solutions to reach the tissue. To extract DNA from zebrafish embryos or larvae, a mixture of 25  $\mu$ l Extraction Solution and 7  $\mu$ l Tissue Preparation Solution was prepared for each sample. These 32  $\mu$ l of Extraction/Tissue Preparation Solution were added to the sample either in a 200  $\mu$ l reaction tube or in one well of a 96-well PCR plate. After assuring that the embryo(s)/larva is completely submerged in solution, the tube/plate was put, without further mixing, in the thermocycler (BioRad C1000 Touch Thermal Cycler), running the following program:

Repeats	Temperature	Time
1x	22 °C	10 min
1x	95 °C	5 min
1x	22 °C	$\infty$

Afterwards, 25  $\mu$ l of Neutralization Solution B were added to the semi-dissolved embryo, the tube/well was sealed and the extract well mixed by vortexing. Of major importance, for extraction of genomic DNA from fin tissue, the double amount of each of the three Extract-N-Amp solutions was used. To use this DNA extract for PCR, the remaining tissue fragments were first pelleted and then, the clear extract was diluted 1:10 in DEPC-H<sub>2</sub>O.

#### 4.2.13 T7 Endonuclease 1 Assay

T7 Endonuclease 1 (T7E1) Assay was used to determine the targeting efficiency of sgRNAs previous to CRISPR/Cas9 mediated gene editing and later to identify F1 zebrafish carrying a heterozygous indel mutation mediated by CRISPR/Cas9 gene editing. The T7 Endonuclease 1 by NEB was used according to the recommended protocol of the manufacturer.

First, a PCR was run to amplify the desired target locus and the PCR product was purified as described in 4.2.1 and 4.2.2. Then, for each sample, the following reaction was assembled in a 200  $\mu$ l reaction tube or in one well of a 96-well PCR plate:

**Amount      Component (Concentration)**

8 $\mu$ l	Purified PCR product
2 $\mu$ l	NEBuffer 2 (10x)
9 $\mu$ l	H <sub>2</sub> O
<hr/>	
19 $\mu$ l	

To denaturate and re-anneal the DNA fragments, the tube/plate was put in a thermocycler (BioRad C1000 Touch Thermal Cycler) and the following program was run:

**Repeats      Temperature      Time/Ramp rate**

1x	95 °C	5 min
1x	95-85 °C	-2 °C/sec
1x	85-25 °C	-0.1 °C/sec
1x	4 °C	$\infty$

Afterwards, 1  $\mu$ l T7 Endonuclease 1 (10.000 U/ml) was added to each sample to reach a volume of 20  $\mu$ l. The reaction then was performed at 37 °C for 15 min in the termocycler. Subsequently, the reaction was stopped by adding 2  $\mu$ l of 0.25 M EDTA. The fragmentation of the PCR products was documented by agarose gel electrophoresis (4.2.8).

**4.2.14 Sequencing**

Sequencing of purified plasmid DNA and PCR products was conducted using the LIGHTRUN Sanger sequencing service of eurofins Genomics. The samples were prepared and submitted according the requirements of the company.

**4.2.15 Synthesis of sgRNA**

For the synthesis of sgRNAs, a cloning-free method was applied according to the protocol by Varshney et al., 2016. First, top strand DNA oligos, which contain the sequence of the desired target site, were designed. For detailed target gene and sequence information, the Ensembl database was utilized. Then, target regions were chosen with the help of two online tools, CHOPCHOP and Cas-OFFinder. To the target sequences, the T7 promoter sequence was added at the 5' end and a 20-nt overlapping sequence, matching an universal-bottom-strand oligo, at the 3' end. The universal bottom-strand is composed of the crRNA-tracrRNA

sequences, which are recognized by Cas9. All DNA oligonucleotides were ordered by eurofins Genomics, resolved in TE buffer to reach a stock concentration of 100  $\mu\text{M}$  and then diluted 1:10 to obtain a working concentration of 10  $\mu\text{M}$ . Importantly, the diluted universal bottom-strand was aliquoted and stored at  $-80\text{ }^{\circ}\text{C}$ .

To obtain the DNA oligo that can be used as a template for sgRNA transcription, the top- and bottom-strand oligos were annealed and extended. The reaction was assembled and carried out in a thermocycler (BioRad C1000 Touch Thermal Cycler) using the following reaction mixture and program:

Amount	Component (Concentration)	Repeats	Temperature	Time
36.5 $\mu\text{l}$	DEPC-H <sub>2</sub> O	1x	98 $^{\circ}\text{C}$	2 min
10 $\mu\text{l}$	Q5 Buffer (5x)	1x	50 $^{\circ}\text{C}$	10 min
1 $\mu\text{l}$	dNTP mix (10 mM)	1x	72 $^{\circ}\text{C}$	10 min
1 $\mu\text{l}$	Top-strand oligo (10 $\mu\text{M}$ )	1x	4 $^{\circ}\text{C}$	$\infty$
1 $\mu\text{l}$	Bottom-strand oligo (10 $\mu\text{M}$ )			
0.5 $\mu\text{l}$	Q5 Polymerase (NEB, 2.000 U/ml)			
50 $\mu\text{l}$				

Afterwards, successful assembly was verified by agarose gel electrophoresis.

The synthesis of sgRNA was then conducted with MAXIScript T7 Kit from Thermo Fisher Scientific according to the recommendations of the manufacturer. The detailed reaction mixture is following, whereby the assembled oligo was used without further purification:

Amount	Component (Concentration)
4 $\mu\text{l}$	DEPC-H <sub>2</sub> O
1 $\mu\text{l}$	Transcription Buffer (10x)
2 $\mu\text{l}$	Assembled oligo
0.5 $\mu\text{l}$	ATP (10 mM)
0.5 $\mu\text{l}$	CTP (10 mM)
0.5 $\mu\text{l}$	GTP (10 mM)
0.5 $\mu\text{l}$	UTP (10 mM)
1 $\mu\text{l}$	T7 Enzyme Mix
10 $\mu\text{l}$	

After incubation at 37 °C for 4 h in the thermocycler, 1 µl TURBO DNase was added and the mixture was incubated for another 20 min at 37 °C. The sgRNA was purified using RNA Clean & Concentrator KIT (Zymo Research). The elution of the RNA from the column was done with DEPC-H<sub>2</sub>O. The RNA quality was checked by agarose gel electrophoresis. Storage took place at -80 °C.

#### 4.2.16 *In vitro* transcription of mRNA

To generate the template DNA needed for *in vitro* transcription, approximately 1.5 µg plasmid DNA was linearized in a total volume of 60 µl for about 2 h as described in 4.2.3. Importantly, DEPC-H<sub>2</sub>O was used for the reaction mixture. After this time, 4.8 µl Proteinase K (Thermo Fisher Scientific, >600 U/ml) were added directly to the reaction mixture and incubated for 20 min at 56 °C. Afterwards, successful linearization was verified by agarose gel electrophoresis and the linear template DNA was purified with Oligo Clean & Concentrator Kit (Zymo Research).

For the *in vitro* transcription itself, mMessage mMachine SP6 and T3 Kits, manufactured by Thermo Fisher Scientific, were utilized according to the provided synthesis recommendations. The following reaction mixture was incubated for 2 h at 37 °C:

Amount	Component (Concentration)
to 20 µl	DEPC-H <sub>2</sub> O
10 µl	NTP/CAP (2x)
2 µl	Reaction Buffer (10x)
0.1 - 1 µg	Linear template DNA
2 µl	T3 or SP6 Enzyme Mix
<hr/>	
20 µl	

Then 1 µl TURBO DNase was added to remove the template DNA (Incubation at 37 °C for 15 min). To purify the mRNA, Oligo Clean & Concentrator Kit (Zymo Research) was used according to the manufacturer's instructions. The elution of the RNA from the column was done with DEPC-H<sub>2</sub>O. The mRNA quality was checked by agarose gel electrophoresis. Storage took place at -80 °C.

#### 4.2.17 Synthesis of cDNA

To synthesize cDNA, total RNA was extracted from dechorionated, 24 hpf zebrafish larvae using Quick-RNA Mini-Prep Kit (Zymo Research) according to the manufacturer's instructions. Then, 1 µg total RNA was treated with DNase I (Thermo Fisher Scientific) at 37 °C for 30 min using the following reaction mixture:

Amount	Component (Concentration)
1 µg	Total RNA from zebrafish larvae (24 hpf)
1 µl	Reaction Buffer + MgCl <sub>2</sub> (10x)
1 µl	DNase I (1 U/µl)
to 10 µl	DEPC-H <sub>2</sub> O
10 µl	

The reaction was stopped by addition of 1 µl 50 mM EDTA (Thermo Fisher Scientific) and subsequent incubation at 65 °C for 10 min.

Afterwards, purification of DNase treated RNA was performed with Oligo Clean & Concentrator Kit (Zymo Research) using an elution volume of 11.5 µl. The purified RNA was then directly used for reverse transcription. For this, 1 µl Oligo dT Primer (0.5 µg) was added to the 11.5 µl total RNA and incubated for 5 min at 65 °C to destroy secondary structures. After cooling down the mixture on ice for 5 min, the following components (Thermo Fisher Scientific) were added and the reverse transcription reaction was incubated for 60 min at 42 °C:

Amount	Component (Concentration)
4 µl	Reaction Buffer for RT (5x)
0.5 µl	RiboLock RNase inhibitor (40 U/µl)
2 µl	dNTP mix (10 mM)
1 µl	RevertAid Reverse transcriptase (200 U/µl)
20 µl	

To inactivate all enzymes after the reaction, the mixture was incubated for 10 min at 70 °C. The cDNA was stored at -20 °C. For 50 µl PCR, 2 µl of the cDNA were applied.

#### 4.2.18 *In vitro* transcription of DIG-labelled RNA antisense probes

The template DNA containing the probe sequence and either a T3, T7 or SP6 promoter was generated by plasmid linearization (4.2.3) or PCR (4.2.1) and purified by ethanol precipitation. For that, to 30  $\mu$ l DNA solution, 3  $\mu$ l sodium acetate (3 M) and 60  $\mu$ l ethanol absolute were added, well mixed by vortexing and kept over night at -20 °C. Then, the precipitated DNA solution was pelleted (14.000 rpm, 10 min, eppendorf Centrifuge 5430R), washed once with ice-cold 70 % ethanol (in DEPC-H<sub>2</sub>O) and air-dried for 5 min.

The precipitated DNA was re-solved in 6  $\mu$ l DEPC-H<sub>2</sub>O. Importantly, 0.5  $\mu$ l of the DNA solution was used for gel analysis, the remaining 5.5  $\mu$ l for assembling the following transcription reaction (reagents by Thermo Fisher Scientific and Roche), which was performed at 37 °C for 2 h:

Amount	Component (Concentration)
5.5 $\mu$ l	Template DNA
2 $\mu$ l	Transcription Buffer (5x)
0.5 $\mu$ l	RiboLock RNase inhibitor (40 U/ $\mu$ l)
1 $\mu$ l	DIG RNA labelling mix (10x)
1 $\mu$ l	T7/T3/SP6 RNA polymerase (20 U/ $\mu$ l)
10 $\mu$ l	

Afterwards, 1  $\mu$ l DNase I (1 U/ $\mu$ l, Thermo Fisher Scientific) was added and incubated for 15 min at 37 °C to remove the template DNA. Then, 0.5  $\mu$ l were taken for gel analysis, before adding 0.5 volumes (5.2  $\mu$ l) of 7.5 M ammonium acetate and 3 volumes (31.5  $\mu$ l) of ethanol (absolute) to precipitate RNA. After vortexing, precipitation took place for 30 min at room temperature. The RNA precipitate was pelleted (14.000 rpm, 15 min, eppendorf Centrifuge 5430R), washed once with ice-cold 70 % ethanol (in DEPC-H<sub>2</sub>O), air-dried for 5 min and re-solved in 100  $\mu$ l Hybridisation solution. The antisense RNA probes were stored at -80 °C.

#### 4.2.19 Whole-mount *in situ* Hybridisation (WISH)

First, chemically fixed zebrafish embryos and larvae (see 4.4.5) were transferred to methanol. For this, PBTw was removed and zebrafish were washed twice in 100 % methanol, first for 5 min, then for 10 min. Subsequently, methanol was changed again and zebrafish were kept at -20 °C for at least one night.

Then, zebrafish were rehydrated. For that, methanol was removed up to 0.6 ml and diluted with 0.6 ml DEPC-PBTw, followed by two washing steps in DEPC-PBTw, each for 5 min with shaking. A post-fixation followed, which was performed in 4 % PFA at room temperature for 20 min with shaking. Afterwards, zebrafish were rinsed and washed three times in DEPC-PBTw, twice for 5 min and once for 10 min with shaking.

For pre-hybridization, zebrafish were washed twice in formamide solutions, for 5 min each with shaking. The first step was performed with diluted formamide solution (250 µl formamide solution + 250 µl DEPC-PBTw), the second step with 250 µl pure formamide solution. This was then replaced with 250 µl hybridization solution and incubated for 4 h at 68 °C in a water bath.

Shortly before the end of the 4 h incubation time, the antisense RNA probe was thawed and diluted by adding 3 µl probe to 30 µl hybridisation solution. Just as much solution was removed from the zebrafish, so that they were still completely submerged. Then, 33 µl of the diluted probe was added to the zebrafish and the sample was kept over night at 68 °C in the water bath.

The next day, the diluted RNA probe was removed and kept at -80 °C for usage in the next experiment. The zebrafish were washed twice with 500 µl pre-warmed formamide solution at 68 °C in the water bath. Then, the samples were transferred to room temperature and 500 µl PBTw were added. The mixture was removed and zebrafish were rinsed and washed twice in PBTw for 15 min each with shaking.

Afterwards, zebrafish were incubated for 30 min in PBTw containing 0.5 % Blocking reagent. This solution was replaced with 0.5 ml of antibody solution: Anti-Digoxigenin-AP Fab fragments from sheep (Roche), 1:2000 in 0.5 % Blocking reagent in PBTw. Antibody incubation was performed at room temperature for 4 h or at 4 °C over night with gently shaking.

Subsequently, the antibody solution was removed and stored at 4 °C to be used in the next experiment. The zebrafish samples were washed at least 4x 20 min or over night in PBTw. It is important to change the solution as often as possible. The washes were performed at room temperature with shaking.

To prepare digoxigenin detection, the samples were first equilibrated in freshly prepared BCL buffer by washing 3x 5 min at room temperature with shaking. Then BCL buffer was removed and 0.5 ml (for embryos) or 1 ml (for larvae of ca. 3 - 4 wpf) of staining solution was added, containing 2.25 µl 4-Nitro blue tetrazolium chloride (NBT) and 1.75 µl BCIP 4-toluidine salt per 1 ml BCL buffer (both reagents by Roche). The colour reaction was performed in 12-well plates and protected from light. The duration varied from 20 min to 24 h depending on the probe to be detected.

Subsequently, the colour reaction was stopped by washing 2x 2 min with PBTw. Then, a post-fixation was performed in 4 % PFA for 1 h at room temperature or over night at 4 °C. The fixative was removed by rinsing and washing in PBTw (2x 5 min, room temperature, shaking). To store the zebrafish samples, they were sequentially transferred in 70 % glycerol (30 %/50 %/70 % glycerol for 15 min each) and kept at 4 °C.

#### **4.2.20 Fluorescent immunostaining**

To detect Gal4 protein in zebrafish larvae, a fluorescent immunostaining was performed using a modified protocol by Inoue & Wittbrodt, 2011. For that, larvae at an age of 48 hpf were decorionated, chemically fixed (see 4.4.5) and then transferred in PBTx. PBTx was removed and larvae were rinsed and washed once for 5 min with 150 mM Tris-HCl (pH 9) under shaking.

Afterwards, a heat-shock was performed in 150 mM Tris-HCl (pH 9) at 70 °C for 15 min. This was done in a block heater using 2 ml reaction tubes. Then, the larvae were washed twice in 1 % PBTx for five minutes each.

Subsequently, the blocking step was performed by incubation of the larvae in 150 µl 5 % goat serum in 1 % PBTx (in the following referred as blocking solution) for at least 30 min at room temperature. The blocking solution was replaced by 150 µl of a 1:500 dilution of Gal4 DBD antibody (Gal4 DBD, sc-577, Lot#/1914, rabbit polyclonal IgG, 200 µg/µl, Santa Cruz Biotechnology) in blocking solution. Antibody incubation was performed for 48 h at room temperature with gently shaking. Then, antibody solution was removed and larvae were

washed three times with 250  $\mu$ l blocking solution for 1 h each and two times with 1 ml 1 % PBTx for 10 min each. All washing steps were performed at room temperature with shaking. Another blocking step was performed by incubation in 250  $\mu$ l blocking solution, first for 1 h at room temperature, then over night at 4 °C. The next step was the incubation with 150  $\mu$ l of a 1:500 dilution of the secondary antibody (Anti-rabbit IgG Fab2, Alexa Fluor (R) 555, Molecular Probes, 2 mg/ml, Cell signalling technologies) in blocking solution. This step was performed for three days at 4 °C.

Finally, the secondary antibody was removed and larvae were transferred stepwise into 70 % glycerol (30 %/50 %/70 % glycerol for 15 min each) for microscopy.

### 4.3 Microbiological methods

#### 4.3.1 *E. coli* strains

For all transformations, chemically competent *E. coli* cells of the strain DH5 $\alpha$  were used. The competent bacteria were either generated in the lab (see 4.3.4) or purchased from Thermo Fisher Scientific (Invitrogen Subcloning Efficiency DH5 $\alpha$  Competet Cells). For propagation of ccdB containing plasmids, the *E. coli* strain DB3.1 was used.

**Table 17. List of *E. coli* strains used during this thesis.**

<i>E. coli</i> strain	Genotype
DH5 $\alpha$	F <sup>-</sup> <i>endA1 glnV44 thi-1 recA1 relA1 gyrA96 deoR nupG purB20</i> $\phi$ 80d <i>lacZ</i> $\Delta$ M15 $\Delta$ ( <i>lacZYA-argF</i> )U169, <i>hsdR17</i> ( <i>r<sub>K</sub><sup>-</sup>m<sub>K</sub><sup>+</sup></i> ), $\lambda$ <sup>-</sup>
DB3.1	F- <i>gyrA462 endA1 glnV44</i> $\Delta$ ( <i>sr1-recA</i> ) <i>mcrB mrr hsdS20</i> ( <i>r<sub>B</sub><sup>-</sup>,m<sub>B</sub><sup>-</sup></i> ) <i>ara14 galK2 lacY1 proA2 rpsL20</i> (Sm <sup>r</sup> ) <i>xyl5</i> $\Delta$ <i>leu mtl1</i>

#### 4.3.2 Cultivation and storage of *E. coli*

To get single colonies, bacteria were spread on selective LB plates containing Ampicillin (100  $\mu$ g/ml), Kanamycin (50  $\mu$ g/ml) or Chloramphenicol (5  $\mu$ g/ml) and incubated at 37 °C. Chloramphenicol was used in a concentration five times lower than recommended as it was used in combination with Ampicillin.

Liquid bacteria cultures were incubated at 37 °C with shaking in selective LB media containing the same concentration of antibiotics.

To store the bacteria, 500 µl of an over night culture were mixed with 500 µl glycerol (50 % in 1x PBS) and transferred to a 2 ml tube with screw cap, which was kept at -80 °C.

#### **4.3.3 Transformation of *E. coli***

To transform chemically competent *E. coli*, generated in the lab (4.3.4), 50 µl cell suspension was thawed on ice. Then, 1 - 5 µl plasmid DNA were added, gently mixed and the mixture was incubated on ice for 30 min. The subsequent heat-shock was performed for 1 min at 37 °C on a block heater. The cells were then immediately put on ice again for another two minutes, before 950 µl pure LB medium were added. After incubation for 1 h at 37 °C with gently shaking, cells were pelleted and 900 µl of the LB medium was removed. The pellet was re-suspended in the remaining 100 µl LB medium and spread on selective LB plates containing the respective antibiotic.

For DB3.1 cells, the same protocol was used, except for the changes: the heat-shock was shortened to 30 sec, the second incubation on ice was performed for 5 min instead of 2 min and before the 1 h-shaking period, the cell suspension was incubated for 5 min at 37 °C without shaking.

Purchased chemically competent *E. coli* cells were transformed according to the manufacturer's instructions.

#### **4.3.4 Preparation of chemical competent cells**

Chemically competent cells were basically prepared according to the protocol by Inoue et al., 1990. However, different from the protocol, cells were grown at 18 °C over three generation. This was performed in SOC media, which was additionally supplemented with 20 mM MgSO<sub>4</sub>. Everything else was done as described (Inoue et al., 1990). The bacteria suspension was aliquoted à 50 µl in the cold (4 °C) and stored at -80 °C.

## 4.4 Zebrafish techniques

### 4.4.1 Maintenance

The zebrafish were kept under standard conditions (Westerfield, 2000) at a temperature ranging from 27 - 28 °C under a day/night cycle of 14 h light and 10 h darkness. For fish maintenance an aquatic research system installed by Aqua Schwarz was used. Adult zebrafish were kept in 10 litre-glass tanks or 3 litre-boxes (AquaBoxes 3), depending on the size of the group. Embryos and larvae were raised in 30 ml-Petri dishes containing E3 medium in an incubator (Liebherr) at 28 °C until an age of 5 - 7 days. Then, they were transferred in 3 litre-boxes and raised in the system to adulthood. Zebrafish were fed two to three times a day with paramecia (for larvae), NovoTom Artemia Powder (JBL, for larvae and juveniles), TetraMin Flakes (Tetra, for juveniles and adults) and Great Salt Lake Artemia (Sanders, for juveniles and adults).

### 4.4.2 Zebrafish strains

For generating new transgenic lines and for most other experiments, fish of the *Casper* strain ( $roy^{-/-};nacre^{-/-}$ ) were used (White et al., 2008). The major advantage of this strain is, that the fish lack iridophores and melanocytes, which make them appear completely transparent even in the adult state. Most used transgenic lines were also in *Casper* background. For the Heat-shock treatments, double transgenic  $Tg(fli:EGFP)^{y1}; Tg(col2a1BAC:mCherry)^{hu5900}$  fish (Hammond & Moro, 2012; Lawson & Weinstein, 2002) were crossed to  $Tg(hsp70l:Cyp26a1)^{kn1}$  fish (Blum & Begemann, 2012), identified for both fluorescent markers and raised to an age of about 21 days to be suitable for the experiment. To test the Gal4-UAS system,  $Tg(UAS:GFP)$  zebrafish in wild type *Bayreuth* (BT) background were used.

#### **4.4.3 Mating fish and collection of eggs**

To mate zebrafish, one fish pair was put in 1 litre-box or up to five fish pairs in a 3 litre-box containing a spawn insert with sieve bottom (SpawningBoxes 1 and 3 by Aqua Schwarz). This was done in the afternoon after 4 pm. Mating is triggered the next morning upon light exposure. The sieve prevents the parents from eating the spawn, so that the eggs could be harvested with the help of a sieve. The parents were put back in the aquatic system. The eggs were transferred into Petri dishes containing 30 ml E3 medium and kept in an incubator (Liebherr) at 28 °C.

For microinjections the one-cell stage is needed, so the fish were kept separated in the boxes until the next morning - one fish below the spawn insert and one fish above - and put together only then. The freshly laid spawn was then harvested as described above.

#### **4.4.4 Microinjection of zebrafish eggs**

Microinjections were performed with zebrafish eggs in one-cell stage. The eggs were laid and harvested just before the injection (see 4.4.3) and then lined up along a glass coverslip. For precise injection, glass needles were prepared from thin capillaries (1 mm diameter, GB100TF-8P, Science products) using a vertical micropipette puller (David Kopf Instruments, Model 700C). The injections were performed with the Pneumatic PicoPump PV820 from WPI. Nucleic acid solutions were injected preferably directly in the cell or in the yolk just below the cell. They were prepared in DEPC-H<sub>2</sub>O containing DNA, RNA or a mixture of both with concentrations ranging between 12.5 - 40 ng/μl for DNA and 20 - 600 ng/μl for RNA. For a better visualization, each injection mixture additionally contained 20 % of a phenol red solution. After the injection, the eggs were transferred in E3 medium and kept at 28 °C in an incubator (Liebherr). Unfertilized and dead eggs were removed and medium changed about 4 h and 24 h after the injection.

#### 4.4.5 Chemical fixation of zebrafish

Before fixation, zebrafish embryos, larvae and juveniles were anesthetized (see 4.4.9) and put on ice for about 10 min. Then, the water was removed and zebrafish were fixed in 4 % Paraformaldehyde (PFA) either over night at 4 °C or for 4 h at room temperature, gently shaking during the whole time. Afterwards, PFA was removed. Fixed zebrafish were rinsed once in PBTw and then washed twice for 5 min (in PBTw) while shaking gently. Storage took place in PBTw at 4 °C.

#### 4.4.6 Sorting of zebrafish based on their pelvic fin developmental stage

To manipulate retinoic acid signalling during early pelvic fin development, a reproducible experimental setup is needed. For this, a staging system designed 2015 by Lisa Marzi as part of her master thesis was used (Marzi, 2015). This staging system is based on the fluorescence marker *fli:eGFP*, which labels, among others, chondrocytes and chondrocyte precursor cells and allows the determination of reproducible starting points for the pharmacological and heat-shock treatments. It was mainly focused on the Stages 1 - 6, of which the definition is shown in Fig. 10. For the whole classification see Fig. S1. Those fish that, at the time of staging, had no ventral eGFP fluorescence in the prospective area of pelvic fin development, yet, but were approximately the same size as Stage 1 fish, were defined as Stage <1.

#### 4.4.7 Heat-shock treatment of zebrafish

The transgenic *fli:eGFP<sup>+/-</sup>;col2a1:mCherry<sup>+/-</sup>;Hsp70l:Cyp26a1<sup>+/-</sup>* and *fli:eGFP<sup>+/-</sup>;col2a1:mCherry<sup>+/-</sup>;Hsp70l:Cyp26a1<sup>-/-</sup>* were first sorted at an age of 3 - 4 wpf based on their pelvic fin developmental stage (see 4.4.6). To activate gene expression controlled by Heat-shock promoters (Hsp70l), transgenic zebrafish were transferred in their staging groups into Petri dishes containing 100 ml fish water. The heat-shock treatment was performed in an incubator (VWR Incu-Line) at 38.5 °C for 1.5 h. Subsequently, the zebrafish were put back in in the aquatic system and maintained separated in the staging groups in 3 litre-boxes. This was repeated first every day and from day eight onwards every second day for about four

weeks. The phenotypes of the pelvic fins and of the pelvic girdle skeleton were then documented by fluorescence microscopy (4.4.12).

During the microscopy process, the tips of the caudal fins were removed with a scalpel for a later extraction of genomic DNA (4.4.10 and 4.2.12) for genotyping the *Hsp70l:Cyp26a1*<sup>+/−</sup> and *Hsp70l:Cyp26a1*<sup>−/−</sup> fish by PCR (4.2.1).

#### 4.4.8 Pharmacological treatment of zebrafish

Pharmacological treatments of zebrafish embryos or larvae were performed in Petri dishes. The treatment of embryos was done in Petri dishes containing 30 ml E3 medium, larvae (3 - 4 wpf) were treated either in dishes containing 30 ml or 100 ml E3 medium, depending on the size of the group. Per larvae, at least 10 ml water was calculated. Pharmacological substances were added from 10 mM stock solutions to reach the desired end concentration. Incubation took place at 28 °C in an incubator (Liebherr). During longer treatments, fish were fed twice a day with NovoTom Artemia Powder (JBL) and the water was changed daily with subsequent addition of new substance. Control treatments were conducted with an identical volume of the respective solvent. Table 18 summarizes the substances, concentration and conditions that were used.

**Table 18. List of pharmacological agents and details of their use.**

Substance	Solvent	Final Concentration	Condition
(Z)-4-Hydroxy-tamoxifen (4-OHT, Sigma-Aldrich)	EtOH abs.	1 - 5 µM	Protect from light
4-Diethylaminobenzaldehyde (DEAB, Fluka)	DMSO	10 µM	-

#### 4.4.9 Anesthetization of zebrafish

For anesthetizing zebrafish, a 0,4 % (w/v) solution of Ethyl 3-aminobenzoate methanesulfonate (MS-222, Tricaine) in H<sub>2</sub>O was used. Zebrafish embryos, larvae or juveniles were transferred to Petri dishes and Tricaine solution was added dropwise using a plastic Pasteur pipette, whereby 8 - 10 drops were applied to a 30 ml Petri dish. This corresponds to a final concentration of about 0,02 % Tricaine. Adult fish were anesthetized in a beaker containing 0,02 % Tricaine diluted in fish water.

#### **4.4.10 Fin clips of adult zebrafish**

Anesthetized zebrafish (see 4.4.9) were transferred one by one from the beaker into a 30 ml-Petri dish filled with Tricaine solution (0,02 % in fish water). The fish were gently fixed between the fingers and the tip of the caudal fin was clipped with a scalpel. The treated fish was then immediately transferred back into a 3 litre-box filled with fresh fish water. The fin tissue was put in the wells of a 96-well plate for extraction of genomic DNA (4.2.12) and further PCR analysis. Until the analysis was completed, the fish were kept separately.

#### **4.4.11 Skeletal staining**

Skeletal staining was performed according to the protocols by Dewit et al., 2011 and Walker & Kimmel, 2007. Zebrafish larvae and juveniles were first chemically fixed in 4 % PFA at 4 °C over night. Subsequently, the fixed fish were rinsed with water and then dehydrated in 50 % ethanol for 10 min with shaking. Afterwards, double skeletal staining solution was applied and incubated over night at room temperature with shaking. The double staining solution was prepared from Alcian Blue and Alizarin Red S stock solution, as listed in 4.1.3. The next day, the samples were rinsed with 70 % ethanol and then gradually rehydrated in 70 %/50 %/30 % ethanol and water for 7 min each. This happened at room temperature and with shaking. To clear the tissue, fish were treated with bleaching solutions, first with 20 % glycerol + 0.25 % KOH for 30 min, then with 50 % glycerol + 0.25 % KOH until the tissue turns transparent (this takes at least 2 h up to several days). During this time samples were kept at room temperature with shaking. To store the samples, they were transferred in 50 % glycerol + 0.1 % KOH and put at 4 °C.

#### **4.4.12 Microscopy of zebrafish**

To prepare chemically fixed zebrafish for microscopy, they were gradually transferred in 70 % glycerol (in 1x PBS). Living juvenile zebrafish were anesthetized and put in 1.5 % methylcellulose. To mount zebrafish samples, several cover glasses (22 x 22 mm) were stacked and glued together with a drop of nail polish. The amount of cover glasses depended on the size of the zebrafish to be mounted (up to 15 cover glasses were needed for juvenile zebrafish). Two of these towers of cover glasses were glued on the left and right side of a glass slide (25 x 75 mm). The zebrafish sample was put in the middle and covered with a rectangular cover glass. Microscopy and imaging was performed with an Axio Imager.M2 (Zeiss) in combination with with an HXP 120 C fluorescence lamp (Leica) and the color cameras AxioCam MRc and MRm (Zeiss).

For observation and imaging of zebrafish with a lower magnification, a Fluo II stereomicroscope (Leica) in combination with an HXP 120 C fluorescence lamp (Leica) and the AxioCam MRc (Zeiss) color camera or AxioCam ICm (Zeiss) was used. In this case, the zebrafish were photographed directly in Petri dishes or plates without further mounting.

For the documentation of some WISH samples, the Stemi 2000-C Binocular (Zeiss) together with the ERc5s colour camera was utilized. An additional cold-light source served for optimal illumination of the sample.

## 5 Literature

- Ablain, J., Durand, E. M., Yang, S., Zhou, Y., & Zon, L. I. (2015). A CRISPR/Cas9 vector system for tissue-specific gene disruption in zebrafish. *Developmental Cell*, 32(6), 756–764. <https://doi.org/10.1016/j.devcel.2015.01.032>
- Adachi, N., Robinson, M., Goolsbee, A., & Shubin, N. H. (2016). Regulatory evolution of Tbx5 and the origin of paired appendages. *Proceedings of the National Academy of Sciences of the United States of America*, 113(36), 10115–10120. <https://doi.org/10.1073/pnas.1609997113>
- Adams, S. L., Cohen, A. J., & Lassová, L. (2007). Integration of signaling pathways regulating chondrocyte differentiation during endochondral bone formation. *Journal of Cellular Physiology*, 213(3), 635–641. <https://doi.org/10.1002/jcp.21262>
- Agarwal, P. (2003). Tbx5 is essential for forelimb bud initiation following patterning of the limb field in the mouse embryo. *Development*, 130(3), 623–633. <https://doi.org/10.1242/dev.00191>
- Akerberg, A. A., Stewart, S., & Stankunas, K. (2014). Spatial and temporal control of transgene expression in zebrafish. *PLoS ONE*, 9(3). <https://doi.org/10.1371/journal.pone.0092217>
- Akitake, C. M., Macurak, M., Halpern, M. E., & Goll, M. G. (2011). Transgenerational analysis of transcriptional silencing in zebrafish. *Developmental Biology*, 352(2), 191–201. <https://doi.org/10.1016/j.ydbio.2011.01.002>
- Ando, H., Kobayashi, M., Tsubokawa, T., Uyemura, K., Furuta, T., & Okamoto, H. (2005). Lhx2 mediates the activity of Six3 in zebrafish forebrain growth. *Developmental Biology*, 287(2), 456–468. <https://doi.org/10.1016/j.ydbio.2005.09.023>
- Angotzi, A. R., Ersland, K. M., Mungpakdee, S., Stefansson, S., & Chourrout, D. (2008). Independent and dynamic reallocation of pitx gene expression during vertebrate evolution, with emphasis on fish pituitary development. *Gene*, 417(1–2), 19–26. <https://doi.org/10.1016/j.gene.2008.03.013>
- Annweiler, A., Hipskind, R. A., & Wirth, T. (1991). A strategy for efficient in vitro translation of cDNAs using the rabbit  $\beta$ -globin leader sequence. *Nucleic Acids Research*, 19(13), 3750. <https://doi.org/10.1093/nar/19.13.3750>
- Arens, J. F., & van Dorp, D. A. (1946a). Activity of “Vitamin A-Acid” in the Rat. *Nature*, 158, 622–623.
- Arens, J. F., & van Dorp, D. A. (1946b). Biological Activity of Vitamin A Acid. *Nature*, 158, 60. <https://doi.org/10.1038/158060b0>
- Arens, J. F., & van Dorp, D. A. (1946c). Synthesis of some Compounds Possessing Vitamin A Activity. *Nature*, 157, 190–191.
- Asakawa, K., & Kawakami, K. (2008). Targeted gene expression by the Gal4-UAS system in zebrafish. *Development Growth and Differentiation*, 50(6), 391–399. <https://doi.org/10.1111/j.1440-169X.2008.01044.x>
- Askary, A., Xu, P., Barske, L., Bay, M., Bump, P., Balczerski, B., ... Crump, J. G. (2017). Genome-wide analysis of facial skeletal regionalization in zebrafish. *Development*, 144(16), 2994–3005. <https://doi.org/10.1242/dev.151712>
- Assaad, F. F., Tucker, K. L., & Signer, E. R. (1993). Epigenetic repeat-induced gene silencing (RIGS) in Arabidopsis. *Plant Molecular Biology*, 22(6), 1067–1085. <https://doi.org/10.1007/BF00028978>
- Asson-Batres, M. A., & Rochette-Egly, C. (2016). *The Biochemistry of Retinoid Signaling II : The Physiology of Vitamin A - Uptake, Transport, Metabolism and Signaling*. Springer Science+Business Media (Vol. 81). Dordrecht: Springer Science+Business Media. [https://doi.org/10.1007/978-94-024-0945-1\\_9](https://doi.org/10.1007/978-94-024-0945-1_9)
- Auer, T. O., Duroure, K., De Cian, A., Concordet, J. P., & Del Bene, F. (2014). Highly efficient CRISPR/Cas9-mediated knock-in in zebrafish by homology-independent DNA repair. *Genome Research*, 24(1), 142–153. <https://doi.org/10.1101/gr.161638.113>
- Awadalla, M. K. A., Alshammari, T. M., Eriksson, L. A., & Saenz-Méndez, P. (2016). Improved homology model of the human all-trans retinoic acid metabolizing enzyme CYP26A1. *Molecules*, 21(3), 1–13. <https://doi.org/10.3390/molecules21030351>
- Bae, S., Park, J., & Kim, J. S. (2014). Cas-OFFinder: A fast and versatile algorithm that searches for

- potential off-target sites of Cas9 RNA-guided endonucleases. *Bioinformatics*, 30(10), 1473–1475. <https://doi.org/10.1093/bioinformatics/btu048>
- Barrow, J. R., Thomas, K. R., Boussadia-Zahui, O., Moore, R., Kemler, R., Capecchi, M. R., & McMahon, A. P. (2003). Ectodermal Wnt3/beta-catenin signaling is required for the establishment and maintenance of the apical ectodermal ridge. *Molecular and Cellular Biology*, 394–409. <https://doi.org/10.1101/gad.1044903>
- Bayer, K. (2015). *A CRISPR PROJECT: CRISPR/Cas9 mediated knock-out and the construction of a CRISPR knock-in vector, Research module*. Universität Bayreuth.
- Begemann, G., Schilling, T. F., Rauch, G. J., Geisler, R., & Ingham, P. W. (2001). The zebrafish neckless mutation reveals a requirement for raldh2 in mesodermal signals that pattern the hindbrain. *Development*, 128(16), 3081–3094.
- Bellovino, D., Aprea, M., Gragnoli, S., Massimi, M., & Gaetani, S. (2003). Vitamin A transport: In vitro models for the study of RBP secretion. *Molecular Aspects of Medicine*, 24(6), 411–420. [https://doi.org/10.1016/S0098-2997\(03\)00037-2](https://doi.org/10.1016/S0098-2997(03)00037-2)
- Beyer, H. M., Gonschorek, P., Samodelov, S. L., Meier, M., Weber, W., & Zurbriggen, M. D. (2015). AQUA cloning: A versatile and simple enzyme-free cloning approach. *PLoS ONE*, 10(9), 1–20. <https://doi.org/10.1371/journal.pone.0137652>
- Blum, N., & Begemann, G. (2012). Retinoic acid signaling controls the formation, proliferation and survival of the blastema during adult zebrafish fin regeneration. *Development*, 139(1), 107–116. <https://doi.org/10.1242/dev.065391>
- Blumberg, B. (1997). An essential role for retinoid signaling in anteroposterior neural patterning. *Development*, 124(2), 373–379. <https://doi.org/10.1006/scdb.1997.0165>
- Borrero Malo, J. (2018). *CRISPR / Cas9-mediated mutagenesis of zebrafish pitx1 and quantitative assessment of genome editing, Bachelor thesis*. Universität Bayreuth.
- Boulet, A. M., Moon, A. M., Arenkiel, B. R., & Capecchi, M. R. (2004). The roles of Fgf4 and Fgf8 in limb bud initiation and outgrowth. *Developmental Biology*, 273(2), 361–372. <https://doi.org/10.1016/j.ydbio.2004.06.012>
- Bourguet, W., Germain, P., & Gronemeyer, H. (2000). Nuclear receptor ligand-binding domains: Three-dimensional structures, molecular interactions and pharmacological implications. *Trends in Pharmacological Sciences*, 21(10), 381–388. [https://doi.org/10.1016/S0165-6147\(00\)01548-0](https://doi.org/10.1016/S0165-6147(00)01548-0)
- Brand, A. H., & Perrimon, N. (1993). Targeted gene expression as a means of altering cell fates and generating dominant phenotypes. *Development*, 118(2), 401–415.
- Branda, C. S., & Dymecki, S. M. (2004). Talking about a revolution: The Impact of Site-Specific Recombinases on Genetic Analyses in Mice. *Developmental Cell*, 6, 7–28. [https://doi.org/10.1016/S1754-4548\(08\)70123-2](https://doi.org/10.1016/S1754-4548(08)70123-2)
- Breu, M. (2017). *Development of zebrafish pelvic fins and dependency on retinoic acid signaling, Master thesis*. Universität Bayreuth.
- Brinkman, E. K., Chen, T., Amendola, M., & Van Steensel, B. (2014). Easy quantitative assessment of genome editing by sequence trace decomposition. *Nucleic Acids Research*, 42(22), 1–8. <https://doi.org/10.1093/nar/gku936>
- Brownstein, M. J., Carpten, J. D., & Smith, J. R. (1996). Modulation of Non-Templated Nucleotide Addition by Taq DNA Polymerase: Primer Modifications that Facilitate Genotyping. *BioTechniques*, 20(6), 1004–1010.
- Bule, A. (2019). *Molekulare Charakterisierung von Augenfehlbildungen bei Danio rerio nach Manipulation des Retinsäure-Signalweges in der frühen Embryogenese, Bachelorarbeit*. Universität Bayreuth.
- Burke, A. C., Nelson, C. E., Morgan, B. A., & Tabin, C. (1995). Hox genes and the evolution of vertebrate axial morphology. *Development*, 121(2), 333–346.
- Camp, E., & Lardelli, M. (2001). Tyrosinase gene expression in zebrafish embryos. *Development Genes and Evolution*, 211(3), 150–153. <https://doi.org/10.1007/s004270000125>
- Canver, M. C., Bauer, D. E., Dass, A., Yien, Y. Y., Chung, J., Masuda, T., ... Orkin, S. H. (2014). Characterization of genomic deletion efficiency mediated by clustered regularly interspaced palindromic repeats (CRISPR)/cas9 nuclease system in mammalian cells. *Journal of Biological*

- Chemistry*, 289(31), 21312–21324. <https://doi.org/10.1074/jbc.M114.564625>
- Carrington, B., Varshney, G. K., Burgess, S. M., & Sood, R. (2015). CRISPR-STAT: An easy and reliable PCR-based method to evaluate target-specific sgRNA activity. *Nucleic Acids Research*, 43(22), 1–8. <https://doi.org/10.1093/nar/gkv802>
- Casci, T. (2008). Development: Extending the role of FGFs in the limb. *Nature Reviews Genetics*, 9(6), 6876. <https://doi.org/10.1038/nrg2385>
- Chambon, P. (1996). A decade of molecular biology of retinoic acid receptors. *The FASEB Journal*, 10(9), 940–954. <https://doi.org/10.1096/fasebj.10.9.8801176>
- Chan, Y. F., Marks, M. E., Jones, F. C., Jr., G. V., Shapiro, M. D., Brady, S. D., ... Kingsley, D. M. (2010). Adaptive Evolution of Pelvic Reduction. *Science*, 302(2010), 302–305. <https://doi.org/10.1126/science.1182213>
- Chen, X., Zaro, J., & Shen, W.-C. (2013). Fusion Protein Linkers: Property, Design and Functionality. *Advanced Drug Delivery Reviews*, 65(10), 1357–1369.
- Chesterman, E. S., & Kern, M. J. (2002). Comparative analysis of Prx1 and Prx2 expression in mice provides evidence for incomplete compensation. *Anatomical Record*, 266(1), 1–4. <https://doi.org/10.1002/ar.10028>
- Chithalen, J. V., Luu, L., Petkovich, M., & Jones, G. (2002). HPLC-MS/MS analysis of the products generated from all-trans-retinoic acid using recombinant human CYP26A. *Journal of Lipid Research*, 43(7), 1133–1142. <https://doi.org/10.1194/jlr.M100343-JLR200>
- Christen, B., & Slack, J. M. W. (1998). All limbs are not the same. *Nature*, 395(6699), 230–231. <https://doi.org/10.1038/26133>
- Chung, J. H., Whiteley, M., & Felsenfeld, G. (1993). A 5' element of the chicken  $\beta$ -globin domain serves as an insulator in human erythroid cells and protects against position effect in *Drosophila*. *Cell*, 74(3), 505–514. [https://doi.org/10.1016/0092-8674\(93\)80052-G](https://doi.org/10.1016/0092-8674(93)80052-G)
- Coates, M. (1993). Hox genes, fin folds and symmetry. *Nature*, 364(6434), 195–196. <https://doi.org/10.1038/364195a0>
- Coates, M. I., & Cohn, M. J. (1998). Fins, limbs, and tails: Outgrowths and axial patterning in vertebrate evolution. *BioEssays*, 20(5), 371–381. [https://doi.org/10.1002/\(SICI\)1521-1878\(199805\)20:5<371::AID-BIES4>3.0.CO;2-R](https://doi.org/10.1002/(SICI)1521-1878(199805)20:5<371::AID-BIES4>3.0.CO;2-R)
- Cohen, B., & Carmichael, G. G. (1986). A Method for Constructing Multiple Tandem Repeats of Specific DNA Fragments. *DNA*, 5(4), 339–343. <https://doi.org/10.1089/dna.1986.5.339>
- Cohn, M. J., Patel, K., Krumlauf, R., Wilkinson, D. G., Clarke, J. D. W., & Tickle, C. (1997). Hox9 genes and vertebrate limb specification. *Nature*, 387(6628), 97–100. <https://doi.org/10.1038/387097a0>
- Cong, L., Ran, F. A., Cox, D., Lin, S., Barretto, R., Habib, N., ... Zhang, F. (2013). Multiplex Genome Engineering Using CRISPR/Cas Systems. *Science*, 819–824.
- Couturier, M., Bahassi, E. M., & Van Melderen, L. (1998). Bacterial death by DNA gyrase poisoning. *Trends in Microbiology*, 6(7), 269–275. [https://doi.org/10.1016/S0966-842X\(98\)01311-0](https://doi.org/10.1016/S0966-842X(98)01311-0)
- Creative-biolabs. (2020). Tol2 Transposon System. Retrieved September 1, 2020, from <https://www.creative-biolabs.com/drug-discovery/therapeutics/tol2-transposon-system.htm>
- Cretekos, C. J., Wang, Y., Green, E. D., Martin, J. F., Rasweiler IV, J. J., & Behringer, R. R. (2008). Regulatory divergence modifies limb length between mammals. *Genes and Development*, 22(2), 141–151. <https://doi.org/10.1101/gad.1620408>
- Crossley, P. H., & Martin, G. R. (1995). The mouse Fgf8 gene encodes a family of polypeptides and is expressed in regions that direct outgrowth and patterning in the developing embryo. *Development*, 121(2), 439–451.
- Crossley, P. H., Minowada, G., MacArthur, C. A., & Martin, G. R. (1996). Roles for FGF8 in the induction, initiation, and maintenance of chick limb development. *Cell*, 84(1), 127–136. [https://doi.org/10.1016/S0092-8674\(00\)80999-X](https://doi.org/10.1016/S0092-8674(00)80999-X)
- Cserjesi, P., Lilly, B., Bryson, L., Wang, Y., Sassoon, D. A., & Olson, E. N. (1992). MHox: A mesodermally restricted homeodomain protein that binds an essential site in the muscle creatine kinase enhancer. *Development*, 115(4), 1087–1101.
- Cunliffe, V., & Smith, J. C. (1992). Ectopic mesoderm formation in *Xenopus* embryos caused by

- widespread expression of a Brachyury homologue. *Nature*, 358(6385), 427–430.  
<https://doi.org/10.1038/358427a0>
- Cunningham, T. J., & Duester, G. (2015). Mechanisms of retinoic acid signalling and its roles in organ and limb development. *Nature Reviews Molecular Cell Biology*, 16(2), 110–123.  
<https://doi.org/10.1038/nrm3932>
- Cunningham, T. J., Lancman, J. J., Berenguer, M., Dong, P. D. S., & Duester, G. (2018). Genomic Knockout of Two Presumed Forelimb Tbx5 Enhancers Reveals They Are Nonessential for Limb Development. *Cell Reports*, 23(11), 3146–3151. <https://doi.org/10.1016/j.celrep.2018.05.052>
- Cunningham, T. J., Zhao, X., Sandell, L. L., Evans, S. M., Trainor, P. A., & Duester, G. (2013). Antagonism between Retinoic Acid and Fibroblast Growth Factor Signaling during Limb Development. *Cell Reports*, 3(5), 1503–1511. <https://doi.org/10.1016/j.celrep.2013.03.036>
- da Silva, S., & Cepko, C. L. (2017). Fgf8 Expression and Degradation of Retinoic Acid Are Required for Patterning a High-Acuity Area in the Retina. *Developmental Cell*, 42(1), 68–81.e6.  
<https://doi.org/10.1016/j.devcel.2017.05.024>
- Damm, K., Heyman, R. A., Umesono, K., & Evans, R. M. (1993). Functional inhibition of retinoic acid response by dominant negative retinoic acid receptor mutants. *Proceedings of the National Academy of Sciences of the United States of America*, 90(7), 2989–2993.  
<https://doi.org/10.1073/pnas.90.7.2989>
- de Bold, M. K., Sheffield, W. P., Martinuk, A., Bhakta, V., Eltringham-Smith, L., & de Bold, A. J. (2012). Characterization of a long-acting recombinant human serum albumin-atrial natriuretic factor (ANF) expressed in *Pichia pastoris*. *Regulatory Peptides*, 175(1–3), 7–10.
- DeLaurier, A., Schweitzer, R., & Logan, M. (2006). Pitx1 determines the morphology of muscle, tendon, and bones of the hindlimb. *Developmental Biology*, 299(1), 22–34.  
<https://doi.org/10.1016/j.ydbio.2006.06.055>
- Dewit, J., Witten, P. E., & Huyseune, A. (2011). The mechanism of cartilage subdivision in the reorganization of the zebrafish pectoral fin endoskeleton. *Journal of Experimental Zoology Part B: Molecular and Developmental Evolution*, 316 B(8), 584–597.  
<https://doi.org/10.1002/jez.b.21433>
- Diez del Corral, R., Olivera-Martinez, I., Goriely, A., Gale, E., Maden, M., & Storey, K. (2003). Opposing FGF and Retinoid Pathways Control Ventral Neural Pattern, Neuronal Differentiation, and Segmentation during Body Axis Extension. *Neuron*, 40, 65–79.
- Distel, M., Wullmann, M. F., & Köster, R. W. (2009). Optimized Gal4 genetics for permanent gene expression mapping in zebrafish. *Proceedings of the National Academy of Sciences*, 106(32), 13365–13370. <https://doi.org/10.1073/pnas.0903060106>
- Dobbs-McAuliffe, B., Zhao, Q., & Linney, E. (2004). Feedback mechanisms regulate retinoic acid production and degradation in the zebrafish embryo. *Mechanisms of Development*, 121(4), 339–350. <https://doi.org/10.1016/j.mod.2004.02.008>
- Doench, J. G., Fusi, N., Sullender, M., Hegde, M., Vaimberg, E. W., Donovan, K. F., ... Root, D. E. (2016). Optimized sgRNA design to maximize activity and minimize off-target effects of CRISPR-Cas9. *Nature Biotechnology*, 34(2), 184–191. <https://doi.org/10.1038/nbt.3437>
- Doench, J. G., Hartenian, E., Graham, D. B., Tothova, Z., Hegde, M., Smith, I., ... Root, D. E. (2014). Rational design of highly active sgRNAs for CRISPR-Cas9-mediated gene inactivation. *Nature Biotechnology*, 32(12), 1262–1267. <https://doi.org/10.1038/nbt.3026>
- Dollé, P. (2009). Developmental expression of retinoic acid receptors (RARs). *Nuclear Receptor Signaling*, 7. <https://doi.org/10.1621/nrs.07006>
- Don, E. K. (2013). *The Morphological and Genetic Characterisation of Pelvic Finless Zebrafish*, Doctoral thesis. University of Sydney.
- Don, E. K., Currie, P. D., & Cole, N. J. (2013). The evolutionary history of the development of the pelvic fin/hindlimb. *Journal of Anatomy*, 222(1), 114–133. <https://doi.org/10.1111/j.1469-7580.2012.01557.x>
- Don, E. K., De Jong-Curtain, T. A., Doggett, K., Hall, T. E., Heng, B., Badrock, A. P., ... Cole, N. J. (2016). Genetic basis of hindlimb loss in a naturally occurring vertebrate model. *Biology Open*, 5(3), 359–366. <https://doi.org/10.1242/bio.016295>

- Doroba, C. K., & Sears, K. E. (2010). The divergent development of the apical ectodermal ridge in the marsupial *Monodelphis domestica*. *Anatomical Record*, *293*(8), 1325–1332. <https://doi.org/10.1002/ar.21183>
- Doyon, Y., McCammon, J. M., Miller, J. C., Faraji, F., Ngo, C., Katibah, G. E., ... Amacher, S. L. (2008). Heritable targeted gene disruption in zebrafish using designed zinc-finger nucleases. *Nature Biotechnology*, *26*(6), 702–708. <https://doi.org/10.1038/nbt1409>
- Draut, H. (2020). *The role of retinoic acid in the development of zebrafish pelvic fins*, *Progress report 2019*. Universität Bayreuth.
- Draut, H., Liebenstein, T., & Begemann, G. (2019). New Insights into the Control of Cell Fate Choices and Differentiation by Retinoic Acid in Cranial, Axial and Caudal Structures. *Biomolecules*, *9*(12). <https://doi.org/10.3390/biom9120860>
- Driever, W., Solnica-Krezel, L., Schier, A. F., Neuhauss, S. C. F., Malicki, J., Stemple, D. L., ... Boggs, C. (1996). A genetic screen for mutations affecting embryogenesis in zebrafish. *Development*, *123*, 37–46. <https://doi.org/10.5167/uzh-215>
- Dubey, A., Rose, R. E., Jones, D. R., & Saint-Jeannet, J. P. (2018). Generating retinoic acid gradients by local degradation during craniofacial development: One cell's cue is another cell's poison. *Genesis*, *56*(2), 1–20. <https://doi.org/10.1002/dvg.23091>
- Duboc, V., & Logan, M. P. O. (2011). Pitx1 is necessary for normal initiation of hindlimb outgrowth through regulation of Tbx4 expression and shapes hindlimb morphologies via targeted growth control. *Development*, *138*(24), 5301–5309. <https://doi.org/10.1242/dev.074153>
- Duester, G. (2008). Retinoic Acid Synthesis and Signaling during Early Organogenesis. *Cell*, *134*(6), 921–931. <https://doi.org/10.1016/j.cell.2008.09.002>
- Duester, G. (2017). Retinoic acid's reproducible future. *Science*, *358*(6369), 1395.
- Eberlein, J. (2018a). *Die Rolle des Retinsäure-Signalweges während der Bauchflossenentwicklung von Danio rerio*, *Masterarbeit*. Universität Bayreuth.
- Eberlein, J. (2018b). *Entwicklung einer transgenen UAS::cyp26a1-eGFP Zebrafischlinie und Tests auf deren Funktionalität*, *Forschungsmodul*. Universität Bayreuth.
- Egea, P. F., Rochel, N., Birck, C., Vachette, P., Timmins, P. A., & Moras, D. (2001). Effects of ligand binding on the association properties and conformation in solution of retinoic acid receptors RXR and RAR. *Journal of Molecular Biology*, *307*(2), 557–576. <https://doi.org/10.1006/jmbi.2000.4409>
- El-Brolosy, M. A., Kontarakis, Z., Rossi, A., Kuenne, C., Günther, S., Fukuda, N., ... Stainier, D. Y. R. (2019). Genetic compensation triggered by mutant mRNA degradation. *Nature*, *568*(7751), 193–197. <https://doi.org/10.1038/s41586-019-1064-z>
- El-Brolosy, M. A., & Stainier, D. Y. R. (2017). Genetic compensation: A phenomenon in search of mechanisms. *PLoS Genetics*, *13*(7), 1–17. <https://doi.org/10.1371/journal.pgen.1006780>
- Emoto, Y., Wada, H., Okamoto, H., Kudo, A., & Imai, Y. (2005). Retinoic acid-metabolizing enzyme Cyp26a1 is essential for determining territories of hindbrain and spinal cord in zebrafish. *Developmental Biology*, *278*(2), 415–427. <https://doi.org/10.1016/j.ydbio.2004.11.023>
- Engeszer, R. E., Patterson, L. B., Rao, A. A., & Parichy, D. M. (2007). Zebrafish in the wild: A review of natural history and new notes from the field. *Zebrafish*, *4*(1), 21–40. <https://doi.org/10.1089/zeb.2006.9997>
- Ersgenomics. (2020). Crispr-Cas9-technology. Retrieved September 1, 2020, from <http://www.ersgenomics.com/images/crispr-cas9-technology.png>
- Etard, C., Joshi, S., Stegmaier, J., Mikut, R., & Strähle, U. (2017). Tracking of Indels by DEcomposition is a simple and effective method to assess efficiency of guide RNAs in zebrafish. *Zebrafish*, *14*(6), 586–588. <https://doi.org/10.1089/zeb.2017.1454>
- Fahrenkrug, S. C., Clark, K. J., Dahlquist, M. O., & Hackett, P. B. (1999). Dicistronic Gene Expression in Developing Zebrafish. *Marine Biotechnology*, *1*, 552–561.
- Falcone, D., & Andrews, D. W. (1991). Both the 5' untranslated region and the sequences surrounding the start site contribute to efficient initiation of translation in vitro. *Molecular and Cellular Biology*, *11*(5), 2656–2664. <https://doi.org/10.1128/mcb.11.5.2656>
- Farboud, B., & Privalsky, M. L. (2004). Retinoic acid receptor- $\alpha$  is stabilized in a repressive state by its

- C-terminal, isotype-specific F domain. *Molecular Endocrinology*, *18*(12), 2839–2853. <https://doi.org/10.1210/me.2004-0236>
- Feneck, E., & Logan, M. (2020). The role of retinoic acid in establishing the early limb bud. *Biomolecules*, *10*(2). <https://doi.org/10.3390/biom10020312>
- Fernandez-Teran, M., & Ros, M. A. (2008). The Apical Ectodermal Ridge: Morphological aspects and signaling pathways. *International Journal of Developmental Biology*, *52*(7), 857–871. <https://doi.org/10.1387/ijdb.072416mf>
- Fischer, S., Draper, B. W., & Neumann, C. J. (2003). The zebrafish *fgf24* mutant identifies an additional level of Fgf signaling involved in vertebrate forelimb initiation. *Development*, *130*(15), 3515–3524. <https://doi.org/10.1242/dev.00537>
- Gagnon, J. A., Valen, E., Thyme, S. B., Huang, P., Ahkmetova, L., Pauli, A., ... Schier, A. F. (2014). Efficient mutagenesis by Cas9 protein-mediated oligonucleotide insertion and large-scale assessment of single-guide RNAs. *PLoS ONE*, *9*(5), 5–12. <https://doi.org/10.1371/journal.pone.0098186>
- Garrick, D., Fiering, S., Martin, D. I. K., & Whitelaw, E. (1998). Repeat-induced gene silencing in mammals. *Nature Genetics*, *18*(1), 56–59. <https://doi.org/10.1038/ng0198-56>
- Gerety, S. S., Breau, M. A., Sasai, N., Xu, Q., Briscoe, J., & Wilkinson, D. G. (2013). An inducible transgene expression system for zebrafish and chick. *Development*, *140*(10), 2235–2243. <https://doi.org/10.1242/dev.091520>
- Germini, D., Saada, Y. B., Tsfasman, T., Osina, K., Robin, C., Lomov, N., ... Vassetzky, Y. (2017). A One-Step PCR-Based Assay to Evaluate the Efficiency and Precision of Genomic DNA-Editing Tools. *Molecular Therapy - Methods and Clinical Development*, *5*(June), 43–50. <https://doi.org/10.1016/j.omtm.2017.03.001>
- Gibert, Y., Gajewski, A., Meyer, A., & Begemann, G. (2006). Induction and prepatterning of the zebrafish pectoral fin bud requires axial retinoic acid signaling. *Development*, *133*(14), 2649–2659. <https://doi.org/10.1242/dev.02438>
- Gibson-Brown, J. J., Agulnik, S. I., Chapman, D. L., Alexiou, M., Garvey, N., Silver, L. M., & Papaioannou, V. E. (1996). Evidence of a role for T-box genes in the evolution of limb morphogenesis and the specification of forelimb / hindlimb identity and the specification of forelimb / hindlimb identity. *Mechanisms of Development*, *56*, 93–101. [https://doi.org/10.1016/0925-4773\(96\)00514-X](https://doi.org/10.1016/0925-4773(96)00514-X)
- Gill, G., & Ptashne, M. (1988). Negative effect of the transcriptional activator GAL4. *Nature*, *334*(6184), 721–724. <https://doi.org/10.1038/334721a0>
- Giniger, E., Varnum, S. M., & Ptashne, M. (1985). Specific DNA binding of GAL4, a positive regulatory protein of yeast. *Cell*, *40*(4), 767–774. [https://doi.org/10.1016/0092-8674\(85\)90336-8](https://doi.org/10.1016/0092-8674(85)90336-8)
- Glass, A. S., & Dahm, R. (2004). The zebrafish as a model organism for eye development. *Ophthalmic Research*, *36*(1), 4–24. <https://doi.org/10.1159/000076105>
- Goll, M. G., Anderson, R., Stainier, D. Y. R., Spradling, A. C., & Halpern, M. E. (2009). Transcriptional silencing and reactivation in transgenic zebrafish. *Genetics*, *182*(3), 747–755. <https://doi.org/10.1534/genetics.109.102079>
- Gonzales, A. P. W., & Yeh, J.-R. J. (2014). *Cas9-Based Genome Editing in Zebrafish*. *Methods in Enzymology* (1st ed., Vol. Volume 546). Elsevier Inc. <https://doi.org/10.1016/B978-0-12-801185-0.00018-0>
- Grandel, H., & Brand, M. (2011). Zebrafish limb development is triggered by a retinoic acid signal during gastrulation. *Developmental Dynamics*, *240*(5), 1116–1126. <https://doi.org/10.1002/dvdy.22461>
- Grandel, H., Draper, B. W., & Schulte-Merker, S. (2000). Dackel acts in the ectoderm of the zebrafish pectoral fin bud to maintain AER signaling. *Development*, *127*(19), 4169–4178.
- Grandel, H., Lun, K., Rauch, G. J., Rhinn, M., Piotrowski, T., Houart, C., ... Brand, M. (2002). Retinoic acid signalling in the zebrafish embryo is necessary during presegmentation stages to pattern the anterior-posterior axis of the CNS and to induce a pectoral fin bud. *Development*, *129*(12), 2851–2865.
- Grandel, H., & Schulte-Merker, S. (1998). The development of the paired fins in the Zebrafish (*Danio*

- erio). *Mechanisms of Development*, 79, 99–120.
- Green, M. H., Ho, R. K., & Hale, M. E. (2011). Movement and function of the pectoral fins of the larval zebrafish (*Danio rerio*) during slow swimming. *Journal of Experimental Biology*, 214(18), 3111–3123. <https://doi.org/10.1242/jeb.057497>
- Gross, J. B., Kerney, R., Hanken, J., & Tabin, C. J. (2011). Molecular anatomy of the developing limb in the coquí frog, *Eleutherodactylus coqui*. *Evolution and Development*, 13(5), 415–426. <https://doi.org/10.1111/j.1525-142X.2011.00500.x>
- Gu, X., Xu, F., Wang, X., Gao, X., & Zhao, Q. (2005). Molecular cloning and expression of a novel CYP26 gene (*cyp26d1*) during zebrafish early development. *Gene Expression Patterns*, 5(6), 733–739.
- Haffter, P., Granato, M., Brand, M., Mullins, M. C., Hammerschmidt, M., Kane, D. A., ... Nüsslein-Volhard, C. (1996). The identification of genes with unique and essential functions in the development of the zebrafish, *Danio rerio*. *Development*, 123, 1–36.
- Hamamoto, H., Hasegawa, K., Nakaune, R., Lee, Y. J., Makizumi, Y., Akutsu, K., & Hibi, T. (2000). Tandem repeat of a transcriptional enhancer upstream of the sterol 14 $\alpha$ -demethylase gene (CYP51) in *Penicillium digitatum*. *Applied and Environmental Microbiology*, 66(8), 3421–3426. <https://doi.org/10.1128/AEM.66.8.3421-3426.2000>
- Hamilton, F. (1822). *An Account of the Fishes of the Ganges*. Edinburgh: Archibald Constable and Company.
- Hammond, C. L., & Moro, E. (2012). Using transgenic reporters to visualize bone and cartilage signaling during development in vivo. *Frontiers in Endocrinology*, 3(JUL), 1–8. <https://doi.org/10.3389/fendo.2012.00091>
- Harfe, B. D., Scherz, P. J., Nissim, S., Tian, H., McMahon, A. P., & Tabin, C. J. (2004). Evidence for an Expansion-Based Temporal Shh Gradient in Specifying Vertebrate Digit Identities. *Cell*, 118(4), 517–528. <https://doi.org/doi:10.1016/j.cell.2004.07.024>.
- Harris, J. E. (1938). The Role Of The Fins In The Equilibrium Of The Swimming Fish: II. The Role Of The Pelvic Fins. *Journal of Experimental Biology*, 15(1), 32–47.
- Harris, M. P., Rohner, N., Schwarz, H., Perathoner, S., Konstantinidis, P., & Nüsslein-Volhard, C. (2008). Zebrafish *eda* and *edar* mutants reveal conserved and ancestral roles of ectodysplasin signaling in vertebrates. *PLoS Genetics*, 4(10). <https://doi.org/10.1371/journal.pgen.1000206>
- Hauksdottir, H., Farboud, B., & Privalsky, M. L. (2003). Retinoic acid receptors  $\beta$  and  $\gamma$  do not repress, but instead activate target gene transcription in both the absence and presence of hormone ligand. *Molecular Endocrinology*, 17(3), 373–385. <https://doi.org/10.1210/me.2002-0340>
- Hernández-Vega, A., & Minguillón, C. (2011). The *Prx1* limb enhancers: Targeted gene expression in developing zebrafish pectoral fins. *Developmental Dynamics*, 240(8), 1977–1988. <https://doi.org/10.1002/dvdy.22678>
- Hisano, Y., Sakuma, T., Nakade, S., Ohga, R., Ota, S., Okamoto, H., ... Kawahara, A. (2015). Precise in-frame integration of exogenous DNA mediated by CRISPR/Cas9 system in zebrafish. *Scientific Reports*, 5, 1–7. <https://doi.org/10.1038/srep08841>
- Hnisz, D., Day, D. S., & Young, R. A. (2016). Insulated Neighborhoods: Structural and Functional Units of Mammalian Gene Control. *Cell*, 167(5), 1188–1200. <https://doi.org/10.1016/j.cell.2016.10.024>
- Holmborn, K., Ledin, J., Varshney, G. K., Klingström, T., & Filipek-Gorniok, B. (2018). *Large scale CRISPR/Cas9 mutagenesis in zebrafish*. University of Uppsala.
- Howe, K., Clark, M. D., Torroja, C. F., Torrance, J., Berthelot, C., Muffato, M., ... Stemple, D. L. (2013). The zebrafish reference genome sequence and its relationship to the human genome. *Nature*, 496(7446), 498–503. <https://doi.org/10.1038/nature12111>
- Huang, C. J., Tu, C. T., Hsiao, C. Der, Hsieh, F. J., & Tsai, H. J. (2003). Germ-line transmission of a myocardium-specific GFP transgene reveals critical regulatory elements in the cardiac myosin light chain 2 promoter of zebrafish. *Developmental Dynamics*, 228(1), 30–40. <https://doi.org/10.1002/dvdy.10356>
- IARC Handbooks of Cancer Prevention. (1998). *Handbook all-trans-Retinoic acid*. IARC Publications.
- Infante, C. R., Park, S., Mihala, A. G., Kingsley, D. M., & Menke, D. B. (2013). *Pitx1* broadly associates

- with limb enhancers and is enriched on hindlimb cis-regulatory elements. *Developmental Biology*, 374(1), 234–244. <https://doi.org/10.1016/j.ydbio.2012.11.017>
- Inoue, D., & Wittbrodt, J. (2011). One for all—a highly efficient and versatile method for fluorescent immunostaining in fish embryos. *PLoS ONE*, 6(5), 1–7. <https://doi.org/10.1371/journal.pone.0019713>
- Inoue, H., Nojima, H., & Okayama, H. (1990). High efficiency transformation of *Escherichia coli* with plasmids. *Gene*, 96(1), 23–28. [https://doi.org/10.1016/0378-1119\(90\)90336-P](https://doi.org/10.1016/0378-1119(90)90336-P)
- Ivanovski, N. (2016). *Establishment of CRISPR / Cas9 mutagenesis system and the generation of tamoxifen inducible Gal4 driver line for subsequent studies of pelvic fin development in Zebrafish, Final report*. Universität Bayreuth.
- Jao, L. E., Wente, S. R., & Chen, W. (2013). Efficient multiplex biallelic zebrafish genome editing using a CRISPR nuclease system. *Proceedings of the National Academy of Sciences of the United States of America*, 110(34), 13904–13909. <https://doi.org/10.1073/pnas.1308335110>
- Jiang, H., Soprano, D. R., Li, S. W., Soprano, K. J., Penner, J. D., Gyda, M., & Kochhar, D. M. (1995). Modulation of limb bud chondrogenesis by retinoic acid and retinoic acid receptors. *International Journal of Developmental Biology*, 39(4), 617–627. <https://doi.org/10.1387/ijdb.8619960>
- Jinek, M., Chylinski, K., Fonfara, I., Hauer, M., Doudna, J. A., & Charpentier, E. (2012). A Programmable Dual-RNA–Guided DNA Endonuclease in Adaptive Bacterial Immunity, 337, 816–821.
- Jungke, P., Hammer, J., Hans, S., & Brand, M. (2015). Isolation of novel CreERT2-driver lines in zebrafish using an unbiased gene trap approach. *PLoS ONE*, 10(6), 1–24. <https://doi.org/10.1371/journal.pone.0129072>
- Kajita, M., Sugimura, K., Ohoka, A., Burden, J., Suganuma, H., Ikegawa, M., ... Fujita, Y. (2014). Filamin acts as a key regulator in epithelial defence against transformed cells. *Nature Communications*, 5, 1–13. <https://doi.org/10.1038/ncomms5428>
- Kakidani, H., & Ptashne, M. (1988). GAL4 activates gene expression in mammalian cells. *Cell*, 52(lane 1), 161–167.
- Kam, R. K. T., Deng, Y., Chen, Y., & Zhao, H. (2012). Retinoic acid synthesis and functions in early embryonic development. *Cell and Bioscience*, 2(1), 11. <https://doi.org/10.1186/2045-3701-2-11>
- Kawaguchi, R., Yu, J., Honda, J., Hu, J., Whitelegge, J., Ping, P., ... Sun, H. (2007). A Membrane Receptor for Retinol Binding Protein Mediates Cellular Uptake of Vitamin A. *Science*, 315(February), 820–826. <https://doi.org/10.1126/science.1136244>
- Kawaguchi, R., Zhong, M., Kassai, M., Ter-Stepanian, M., & Sun, H. (2015). Vitamin a transport mechanism of the multitransmembrane cell-surface receptor STRA6. *Membranes*, 5(3), 425–453. <https://doi.org/10.3390/membranes5030425>
- Kawakami, K. (2007). Tol2: A versatile gene transfer vector in vertebrates. *Genome Biology*, 8(SUPPL. 1), 1–10. <https://doi.org/10.1186/gb-2007-8-s1-s7>
- Kawakami, K., Koga, A., Hori, H., & Shima, A. (1998). Excision of the Tol2 transposable element of the medaka fish, *Oryzias latipes*, in zebrafish, *Danio rerio*. *Gene*, 225(1–2), 17–22. [https://doi.org/10.1016/S0378-1119\(98\)00537-X](https://doi.org/10.1016/S0378-1119(98)00537-X)
- Kawakami, K., & Shima, A. (1999). Identification of the Tol2 transposase of the medaka fish *Oryzias latipes* that catalyzes excision of a nonautonomous Tol2 element in zebrafish *Danio rerio*. *Gene*, 240(1), 239–244. [https://doi.org/10.1016/S0378-1119\(99\)00444-8](https://doi.org/10.1016/S0378-1119(99)00444-8)
- Kawakami, K., Shima, A., & Kawakami, N. (2000). Identification of a functional transposase of the Tol2 element, an Ac-like element from the Japanese medaka fish, and its transposition in the zebrafish germ lineage. *Proceedings of the National Academy of Sciences of the United States of America*, 97(21), 11403–11408. <https://doi.org/10.1073/pnas.97.21.11403>
- Kawakami, K., Takeda, H., Kawakami, N., Kobayashi, M., Matsuda, N., & Mishina, M. (2004). A transposon-mediated gene trap approach identifies developmentally regulated genes in zebrafish. *Developmental Cell*, 7(1), 133–144. <https://doi.org/10.1016/j.devcel.2004.06.005>
- Kawakami, Y., Capdevila, J., Büscher, D., Itoh, T., Esteban, C. R., & Belmonte, J. C. I. (2001). WNT signals control FGF-dependent limb initiation and AER induction in the chick embryo. *Cell*,

- 104(6), 891–900. [https://doi.org/10.1016/S0092-8674\(01\)00285-9](https://doi.org/10.1016/S0092-8674(01)00285-9)
- Kawakami, Y., Marti, M., Kawakami, H., Itou, J., Quach, T., Johnson, A., ... Belmonte, J. C. I. (2011). Islet1-mediated activation of the  $\beta$ -catenin pathway is necessary for hindlimb initiation in mice. *Development*, 138(20), 4465–4473. <https://doi.org/10.1242/dev.065359>
- Keegan, L., Gill, G., & Ptashne, M. (1986). Separation of DNA binding from the transcription-activating function of a eukaryotic regulatory protein. *Science*, 231(4739), 699–704. <https://doi.org/10.1126/science.3080805>
- Kieft, J. S. (2008). Viral IRES RNA structures and ribosome interactions. *Trends in Biochemical Sciences*, 33(6), 274–283. <https://doi.org/10.1016/j.tibs.2008.04.007>
- Kikuchi, K., Holdway, J. E., Major, R. J., Blum, N., Dahn, R. D., Begemann, G., & Poss, K. D. (2011). Retinoic Acid Production by Endocardium and Epicardium Is an Injury Response Essential for Zebrafish Heart Regeneration. *Developmental Cell*, 20(3), 397–404. <https://doi.org/10.1016/j.devcel.2011.01.010>
- Kim, J. M., Kim, D., Kim, S., & Kim, J.-S. (2014). Genotyping with CRISPR-Cas-derived RNA-guided endonucleases. *Nature Communications*, 5, 1–7. <https://doi.org/10.1038/ncomms4157>
- Kimmel, C. B. (1989). Genetics and early development of zebrafish. *Trends in Genetics*, 5(C), 283–288. [https://doi.org/10.1016/0168-9525\(89\)90103-0](https://doi.org/10.1016/0168-9525(89)90103-0)
- Kimmel, C. B., Ballard, W. W., Kimmel, S. R., Ullmann, B., & Schilling, T. F. (1995). Stages of embryonic development of the zebrafish. *Developmental Dynamics*, 203(3), 253–310. <https://doi.org/10.1002/aja.1002030302>
- Köster, R., & Fraser, S. (2001). Tracing Transgene Expression in Living Zebrafish Embryos. *Developmental Biology*, 346, 329–346.
- Kraft, K., Geuer, S., Will, A. J., Chan, W. L., Paliou, C., Borschiwer, M., ... Andrey, G. (2015). Deletions, inversions, duplications: Engineering of structural variants using CRISPR/Cas in mice. *Cell Reports*, 10(5), 833–839. <https://doi.org/10.1016/j.celrep.2015.01.016>
- Kragestein, B. K., Brancati, F., Digilio, M. C., Mundlos, S., & Spielmann, M. (2019). H2AFY promoter deletion causes PITX1 endoactivation and Liebenberg syndrome. *Journal of Medical Genetics*, 56(4), 246–251. <https://doi.org/10.1136/jmedgenet-2018-105793>
- Kragestein, B. K., Spielmann, M., Paliou, C., Heinrich, V., Schöpflin, R., Esposito, A., ... Andrey, G. (2018). Dynamic 3D chromatin architecture contributes to enhancer specificity and limb morphogenesis. *Nature Genetics*, 50(10), 1463–1473. <https://doi.org/10.1038/s41588-018-0221-x>
- Kudoh, T., Wilson, S. W., & Dawid, I. B. (2002). Distinct roles for Fgf, Wnt and retinoic acid in posteriorizing the neural ectoderm. *Development*, 129(18), 4335–4346.
- Kumar, S., & Duyster, G. (2014). Retinoic acid controls body axis extension by directly repressing Fgf8 transcription. *Development*, 141(15), 2972–2977. <https://doi.org/10.1242/dev.112367>
- Kuratani, S., Martin, J. F., Wawersik, S., Lilly, B., Eichele, G., & Olson, E. N. (1994). The expression pattern of the chick homeobox gene gMHox suggests a role in patterning of the limbs and face and in compartmentalization of somites. *Developmental Biology*. <https://doi.org/10.1006/dbio.1994.1037>
- Labun, K., Montague, T. G., Gagnon, J. A., Thyme, S. B., & Valen, E. (2016). CHOPCHOP v2: a web tool for the next generation of CRISPR genome engineering. *Nucleic Acids Research*, 44(W1), W272–W276. <https://doi.org/10.1093/nar/gkw398>
- Laforest, L., Brown, C. W., Poleo, G., Géraudie, J., Tada, M., Ekker, M., & Akimenko, M. A. (1998). Involvement of the Sonic Hedgehog, patched 1 and bmp2 genes in patterning of the zebrafish dermal fin rays. *Development*, 125(21), 4175–4184.
- Lanctôt, C., Moreau, A., Chamberland, M., Michel L., T., & Drouin, J. (1999). Hindlimb patterning and mandible development require the Ptx1 gene. *Development*, 125, 1805–1810. [https://doi.org/10.1016/S0021-9800\(70\)80080-1](https://doi.org/10.1016/S0021-9800(70)80080-1)
- Laue, K., Jänicke, M., Plaster, N., Sonntag, C., & Hammerschmidt, M. (2008). Restriction of retinoic acid activity by Cyp26b1 is required for proper timing and patterning of osteogenesis during zebrafish development. *Development*, 135(22), 3775–3787. <https://doi.org/10.1242/dev.021238>

- Laurell, T., Nilsson, D., Hofmeister, W., Lindstrand, A., Ahituv, N., Vandermeer, J., ... Nordgren, A. (2014). Identification of three novel fgf16 mutations in x-linked recessive fusion of the fourth and fifth metacarpals and possible correlation with heart disease. *Molecular Genetics and Genomic Medicine*, 2(5), 402–411. <https://doi.org/10.1002/mgg3.81>
- Lawson, N. D., & Weinstein, B. M. (2002). In vivo imaging of embryonic vascular development using transgenic zebrafish. *Developmental Biology*, 248(2), 307–318. <https://doi.org/10.1006/dbio.2002.0711>
- Leussink, B., Brouwer, A., El Khattabi, M., Poelmann, R. E., Gittenberger-de Groot, A. C., & Meijlink, F. (1995). Expression patterns of the paired-related homeobox genes MHox/Prx1 and S8/Prx2 suggest roles in development of the heart and the forebrain. *Mechanisms of Development*, 52(1), 51–64. [https://doi.org/10.1016/0925-4773\(95\)00389-I](https://doi.org/10.1016/0925-4773(95)00389-I)
- Lewandoski, M., Sun, X., & Martin, G. R. (2000). Fgf8 signalling from the AER is essential for normal limb development. *Nature Genetics*, 26(4), 460–463. <https://doi.org/10.1038/82609>
- Lieschke, G. J., Oates, A. C., & Kawakami, K. (2009). *Zebrafish - Methods and Protocols*. (G. J. Lieschke, A. C. Oates, & K. Kawakami, Eds.). New York, USA: Humana Press, Springer Science + Buissnes Media.
- Loehlin, D. W., & Carroll, S. B. (2016). Expression of tandem gene duplicates is often greater than twofold. *Proceedings of the National Academy of Sciences of the United States of America*, 113(21), 5988–5992. <https://doi.org/10.1073/pnas.1605886113>
- Logan, M., & Tabin, C. J. (1999). Role of Pitx1 upstream of Tbx4 in specification of hindlimb identity. *Science*, 283(5408), 1736–1739. <https://doi.org/10.1126/science.283.5408.1736>
- Lu, M.-F., Cheng, H.-T., Lacy, A. R., Kern, M. J., Argao, E. A., Potter, S. S., ... Martin, J. F. (1999). Paired-related homeobox genes cooperate in handplate and hindlimb zeugopod morphogenesis. *Developmental Biology*, 205(1), 145–157. <https://doi.org/10.1006/dbio.1998.9116>
- Lutz, J. D., Dixit, V., Yeung, C. K., Dickmann, L. J., Zelter, A., Thatcher, J. E., ... Isoherranen, N. (2009). Expression and functional characterization of cytochrome P450 26A1, a retinoic acid hydroxylase. *Biochemical Pharmacology*, 77(2), 258–268. <https://doi.org/10.1016/j.bcp.2008.10.012>
- Macdonald, R., & Wilson, S. W. (1997). Distribution of Pax6 protein during eye development suggests discrete roles in proliferative and differentiated visual cells. *Development Genes and Evolution*, 206(6), 363–369. <https://doi.org/10.1007/s004270050065>
- Maden, M., Gale, E., Kostetskii, I., & Zile, M. (1996). Vitamin A-deficient quail embryos have half a hindbrain and other neural defects. *Current Biology*, 6(4), 417–426. [https://doi.org/10.1016/S0960-9822\(02\)00509-2](https://doi.org/10.1016/S0960-9822(02)00509-2)
- Mariani, F. V., Ahn, C. P., & Martin, G. R. (2008). Genetic evidence that FGFs have an instructive role in limb proximal-distal patterning. *Nature*, 453(7193), 401–405. <https://doi.org/10.1038/nature06876>
- Martin, J. F., & Olson, E. N. (2000). Identification of a prx1 limb enhancer. *Genesis*, 26(4), 225–229.
- Marzi, L. (2015). *Vorstudien zur Rolle der Retinsäure in der Bauchflossenentwicklung von Danio rerio anhand transgener Reporterlinien, Masterarbeit*. Universität Bayreuth.
- Masselink, W., Cole, N. J., Fenyes, F., Berger, S., Sonntag, C., Wood, A., ... Currie, P. D. (2016). A somitic contribution to the apical ectodermal ridge is essential for fin formation. *Nature*, 535(7613), 542–546. <https://doi.org/10.1038/nature18953>
- Matzke, M. A., Primig, M., Trnovsky, J., & Matzke, A. J. M. (1989). Reversible methylation and inactivation of marker genes in sequentially transformed tobacco plants. *The EMBO Journal*, 8(3), 643–649. <https://doi.org/10.1002/j.1460-2075.1989.tb03421.x>
- Mayer, A.-M. (2020). *Einfluss von cyp26a1 -Überexpression auf die Bauchflossenentwicklung in Danio rerio, Bachelorarbeit*. Universität Bayreuth.
- McClenahan, P., Troup, M., & Scott, E. K. (2012). Fin-tail coordination during escape and predatory behavior in larval zebrafish. *PLoS ONE*, 7(2), 1–11. <https://doi.org/10.1371/journal.pone.0032295>
- McPherron, A. C., Lawler, A. M., & Lee, S. J. (1999). Regulation of anterior/posterior patterning of the axial skeleton by growth/differentiation factor 11. *Nature Genetics*, 22(3), 260–264.

- <https://doi.org/10.1038/10320>
- Meng, X., Noyes, M. B., Zhu, L. J., Lawson, N. D., & Wolfe, S. A. (2008). Targeted gene inactivation in zebrafish using engineered zinc-finger nucleases. *Nature Biotechnology*, *26*(6), 695–701. <https://doi.org/10.1038/nbt1398>
- Menke, D. B., Guenther, C., & Kingsley, D. M. (2008). Dual hindlimb control elements in the Tbx4 gene and region-specific control of bone size in vertebrate limbs. *Development*, *135*(15), 2543–2553. <https://doi.org/10.1242/dev.017384>
- Merkel, F. (2016). *Towards elucidating the mechanisms of pelvic fin development by forward and reverse genetics*, Master thesis. Universität Bayreuth.
- Meyers, J. R. (2018). Zebrafish: Development of a Vertebrate Model Organism. *Current Protocols in Essential Laboratory Techniques*, e19. <https://doi.org/10.1002/cpet.19>
- Mic, F. A., Haselbeck, R. J., Cuenca, A. E., & Duester, G. (2002). Novel retinoic acid generating activities in the neural tube and heart identified by conditional rescue of Raldh2 null mutant mice. *Development*, *129*(9), 2271–2282.
- Mic, F. A., Molotkov, A., Benbrook, D. M., & Duester, G. (2003). Retinoid activation of retinoic acid receptor but not retinoid X receptor is sufficient to rescue lethal defect in retinoic acid synthesis. *Proceedings of the National Academy of Sciences of the United States of America*, *100*(12), 7135–7140. <https://doi.org/10.1073/pnas.1231422100>
- Mic, F. A., Sirbu, I. O., & Duester, G. (2004). Retinoic acid synthesis controlled by Raldh2 is required early for limb bud initiation and then later as a proximodistal signal during apical ectodermal ridge formation. *Journal of Biological Chemistry*, *279*(25), 26698–26706. <https://doi.org/10.1074/jbc.M401920200>
- Minguillon, C., Del Buono, J., & Logan, M. P. (2005). Tbx5 and Tbx4 are not sufficient to determine limb-specific morphologies but have common roles in initiating limb outgrowth. *Developmental Cell*, *8*(1), 75–84. <https://doi.org/10.1016/j.devcel.2004.11.013>
- Minguillon, C., Nishimoto, S., Wood, S., Vendrell, E., Gibson-Brown, J. J., & Logan, M. P. O. (2012). Hox genes regulate the onset of Tbx5 expression in the forelimb. *Development*, *139*(17), 3180–3188. <https://doi.org/10.1242/dev.084814>
- Mizuguchi, H., Xu, Z., Ishii-Watabe, A., Uchida, E., & Hayakawa, T. (2000). IRES-Dependent Second Gene Expression Is Significantly Lower Than Cap-Dependent First Gene Expression in a Bicistronic Vector. *Molecular Therapy*, *1*(4), 376–382. <https://doi.org/10.1006/mthe.2000.0050>
- Molotkov, A., Fan, X., & Duester, G. (2002). Excessive vitamin A toxicity in mice genetically deficient in either alcohol dehydrogenase Adh1 or Adh3. *European Journal of Biochemistry*, *269*(10), 2607–2612. <https://doi.org/10.1046/j.1432-1033.2002.02935.x>
- Molven, A., Wright, C. V. E., Bremiller, R., De Robertis, E. M., & Kimmel, C. B. (1990). Expression of a homeobox gene product in normal and mutant zebrafish embryos: Evolution of the tetrapod body plan. *Development*, *109*(2), 279–288.
- Montalbano, A., Juergensen, L., Roeth, R., Weiss, B., Fukami, M., Fricke-Otto, S., ... Rappold, G. A. (2016). Retinoic acid catabolizing enzyme CYP26C1 is a genetic modifier in SHOX deficiency. *EMBO Molecular Medicine*, *8*(12), 1455–1469. <https://doi.org/10.15252/emmm.201606623>
- Moon, A. M., & Capecchi, M. R. (2000). Fgf8 is required for outgrowth and patterning of the limbs. *Nature Genetics*, *26*(4), 455–459. <https://doi.org/10.1038/82601>
- Moosajee, M., Gregory-Evans, K., Ellis, C. D., Seabra, M. C., & Gregory-Evans, C. Y. (2008). Translational bypass of nonsense mutations in zebrafish rep1, pax2.1 and lamb1 highlights a viable therapeutic option for untreatable genetic eye disease. *Human Molecular Genetics*, *17*(24), 3987–4000. <https://doi.org/10.1093/hmg/ddn302>
- Moreau, C., Caldarelli, P., Rocancourt, D., Roussel, J., Denans, N., Pourquie, O., & Gros, J. (2019). Timed Collinear Activation of Hox Genes during Gastrulation Controls the Avian Forelimb Position. *Current Biology*, *29*(1), 35-50.e4. <https://doi.org/10.1016/j.cub.2018.11.009>
- Moreno-Mateos, M. A., Vejnar, C. E., Beaudoin, J. D., Fernandez, J. P., Mis, E. K., Khokha, M. K., & Giraldez, A. J. (2015). CRISPRscan: Designing highly efficient sgRNAs for CRISPR-Cas9 targeting in vivo. *Nature Methods*, *12*(10), 982–988. <https://doi.org/10.1038/nmeth.3543>
- Moriyama, Y., Moriyama, Y., Pratiwi, H. M., Ueda, S., Ueda, S., & Tanaka, M. (2019). Localization of  $\beta$ -

- Catenin and islet in the pelvic fin field in Zebrafish. *Zoological Science*, 36(5), 365–371. <https://doi.org/10.2108/zs180185>
- Mosimann, C., Kaufman, C. K., Li, P., Pugach, E. K., Tamplin, O. J., & Zon, L. I. (2011). Ubiquitous transgene expression and Cre-based recombination driven by the ubiquitin promoter in zebrafish. *Development*, 138(1), 169–177. <https://doi.org/10.1242/dev.059345>
- Mruk, K., Ciepla, P., Piza, P. A., Alnaqib, M. A., & Chen, J. K. (2020). Targeted cell ablation in zebrafish using optogenetic transcriptional control. *Development*, 147(12), dev183640. <https://doi.org/10.1242/dev.183640>
- Mück, A. (2018). *Rolle der RA- und Fgf-Signalwege bei der Umformung der Brustflossen-Knorpelscheibe*, Forschungsmodul. Universität Bayreuth.
- Mück, A. (2019). *Manipulation of the RA pathway in zebrafish pelvic fin development using the Gal4/UAS system*, Master thesis. Universität Bayreuth.
- Murata, Y., Tamura, M., Aita, Y., Fujimura, K., Murakami, Y., Okabe, M., ... Tanaka, M. (2010). Allometric growth of the trunk leads to the rostral shift of the pelvic fin in teleost fishes. *Developmental Biology*, 347(1), 236–245. <https://doi.org/10.1016/j.ydbio.2010.07.034>
- Muto, A., Ikeda, S., Lopez-Burks, M. E., Kikuchi, Y., Calof, A. L., Lander, A. D., & Schilling, T. F. (2014). Nipbl and Mediator Cooperatively Regulate Gene Expression to Control Limb Development. *PLoS Genetics*, 10(9). <https://doi.org/10.1371/journal.pgen.1004671>
- Nagayoshi, S., Hayashi, E., Abe, G., Osato, N., Asakawa, K., Urasaki, A., ... Kawakami, K. (2008). Insertional mutagenesis by the Tol2 transposon-mediated enhancer trap approach generated mutations in two developmental genes: *tcf7* and *synembryn-like*. *Development*, 135(1), 159–169. <https://doi.org/10.1242/dev.009050>
- Naiche, L. A., & Papaioannou, V. E. (2003). Loss of *Tbx4* blocks hindlimb development and affects vascularization and fusion of the allantois. *Development*, 130(12), 2681–2693. <https://doi.org/10.1242/dev.00504>
- Naiche, L. A., & Papaioannou, V. E. (2007). *Tbx4* is not required for hindlimb identity or post-bud hindlimb outgrowth. *Development*, 134(1), 93–103. <https://doi.org/10.1242/dev.02712>
- Nakamura, T., Gehrke, A. R., Lemberg, J., Szymaszek, J., & Shubin, N. H. (2016). Digits and fin rays share common developmental histories. *Nature*, 537(7619), 225–228. <https://doi.org/10.1038/nature19322>
- Nardini, N. (2018). *Identification of a transgenic line and hindlimb specific elements for further reverse genetic screens*, Research module. Universität Bayreuth.
- Narita, T., Nishimatsu, S. I., Wada, N., & Nohno, T. (2007). A *Wnt3a* variant participates in chick apical ectodermal ridge formation: Distinct biological activities of *Wnt3a* splice variants in chick limb development. *Development Growth and Differentiation*, 49(6), 493–501. <https://doi.org/10.1111/j.1440-169X.2007.00938.x>
- Narkis, G., Tzchori, I., Cohen, T., Holtz, A., Wier, E., & Westphal, H. (2012). *Isl1* and *Ldb* Co-regulators of transcription are essential early determinants of mouse limb development. *Developmental Dynamics*, 241(4), 787–791. <https://doi.org/10.1002/dvdy.23761>
- Nemec, S., Luxey, M., Jain, D., Huang Sung, A., Pastinen, T., & Drouin, J. (2017). *Pitx1* directly modulates the core limb development program to implement hindlimb identity. *Development*, 144(18), 3325–3335. <https://doi.org/10.1242/dev.154864>
- Ng, J. K., Kawakami, Y., Büscher, D., Raya, Á., Itoh, T., Koth, C. M., ... Belmonte, J. C. I. (2002). The limb identity gene *Tbx5* promotes limb initiation by interacting with *Wnt2b* and *Fgf10*. *Development*, 129(22), 5161–5170.
- Ng, X. J. (2019). *Die Etablierung von Treiber-Linien für die Anwendung des KalTA4 / UAS-Systems in Zebrafischen*, Forschungsmodul. Universität Bayreuth.
- Niederreither, K., & Dollé, P. (2008). Retinoic acid in development: Towards an integrated view. *Nature Reviews Genetics*, 9(7), 541–553. <https://doi.org/10.1038/nrg2340>
- Niederreither, K., Subbarayan, V., Dollé, P., & Chambon, P. (1999). Embryonic retinoic acid synthesis is essential for heart morphogenesis in the mouse. *Nature Genetics*, 21(4), 444–448. <https://doi.org/10.1038/7788>
- Nishimoto, S., & Logan, M. P. O. (2016). Subdivision of the lateral plate mesoderm and specification

- of the forelimb and hindlimb forming domains. *Seminars in Cell and Developmental Biology*, *49*, 102–108. <https://doi.org/10.1016/j.semcdb.2015.11.011>
- Nishimoto, S., Minguillon, C., Wood, S., & Logan, M. P. O. (2014). A Combination of Activation and Repression by a Colinear Hox Code Controls Forelimb-Restricted Expression of Tbx5 and Reveals Hox Protein Specificity. *PLoS Genetics*, *10*(3), 1–13. <https://doi.org/10.1371/journal.pgen.1004245>
- Nishimoto, S., Wilde, S. M., Wood, S., & Logan, M. P. O. (2015). RA Acts in a Coherent Feed-Forward Mechanism with Tbx5 to Control Limb Bud Induction and Initiation. *Cell Reports*, *12*(5), 879–891. <https://doi.org/10.1016/j.celrep.2015.06.068>
- Nomura, R., Kamei, E., Hotta, Y., Konishi, M., Miyake, A., & Itoh, N. (2006). Fgf16 is essential for pectoral fin bud formation in zebrafish. *Biochemical and Biophysical Research Communications*, *347*(1), 340–346.
- Ohuchi, H., Nakagawa, T., Yamamoto, A., Araga, A., Ohata, T., Ishimaru, Y., ... Noji, S. (1997). The mesenchymal factor, FGF10, initiates and maintains the outgrowth of the chick limb bud through interaction with FGF8, an apical ectodermal factor. *Development*, *124*(11), 2235–2244.
- Ondek, B., Shepard, A., & Herr, W. (1987). Discrete elements within the SV40 enhancer region display different cell-specific enhancer activities. *The EMBO Journal*, *6*(4), 1017–1025. <https://doi.org/10.1002/j.1460-2075.1987.tb04854.x>
- Ouimette, J. F., Jolin, M. L., L'honoré, A., Gifuni, A., & Drouin, J. (2010). Divergent transcriptional activities determine limb identity. *Nature Communications*, *1*(4), 1–9. <https://doi.org/10.1038/ncomms1036>
- Pan, X., Wan, H., Chia, W., Tong, Y., & Gong, Z. (2005). Demonstration of site-directed recombination in transgenic zebrafish using the Cre/loxP system. *Transgenic Research*, *14*(2), 217–223. <https://doi.org/10.1007/s11248-004-5790-z>
- Parichy, D. M. (2015). Advancing biology through a deeper understanding of zebrafish ecology and evolution. *eLife*, *4*, 1–11. <https://doi.org/10.7554/eLife.05635>
- Perz-Edwards, A., Hardison, N. L., & Linney, E. (2001). Retinoic acid-mediated gene expression in transgenic reporter zebrafish. *Developmental Biology*, *229*(1), 89–101. <https://doi.org/10.1006/dbio.2000.9979>
- Piedra, M. E., Icardo, J. M., Albajar, M., Rodriguez-Rey, J. C., & Ros, M. A. (1998). Pitx2 participates in the late phase of the pathway controlling left- right asymmetry. *Cell*, *94*(3), 319–324. [https://doi.org/10.1016/S0092-8674\(00\)81475-0](https://doi.org/10.1016/S0092-8674(00)81475-0)
- Pijnappel, W. W. M., Hendriks, H. F. J., Folkers, G. E., van den Brink, C. E., Dekker, E. J., Edelenbosch, C., ... Durston, A. J. (1993). The retinoid ligand 4-oxo-retinoic acid is a highly active modulator of positional specification. *Nature*, *366*(6453), 340–344. <https://doi.org/10.1038/366340a0>
- Poulin, G., Lebel, M., Chamberland, M., Paradis, F. W., & Drouin, J. (2000). Specific Protein-Protein Interaction between Basic Helix-Loop-Helix Transcription Factors and Homeoproteins of the Pitx Family. *Molecular and Cellular Biology*, *20*(13), 4826–4837. <https://doi.org/10.1128/mcb.20.13.4826-4837.2000>
- Pourzadegan, F., Shariati, L., Taghizadeh, R., Khanahmad, H., Mohammadi, Z., & Tabatabaiefar, M. A. (2016). Using intron splicing trick for preferential gene expression in transduced cells: An approach for suicide gene therapy. *Cancer Gene Therapy*, *23*(1), 7–12. <https://doi.org/10.1038/cgt.2015.57>
- Pratt, M. A. C., Kralova, J., & Mcburney, M. W. (1990). A Dominant Negative Mutation of the Alpha Retinoic Acid Receptor Gene in a Retinoic Acid-Nonresponsive Embryonal Carcinoma Cell. *Molecular and Cellular Biology*, *10*(12), 6445–6453.
- Privalsky, M. L. (2004). The role of corepressors in transcriptional regulation by nuclear hormone receptors. *Annual Review of Physiology*, *66*, 315–360. <https://doi.org/10.1146/annurev.physiol.66.032802.155556>
- Purushothaman, S., Elewa, A., & Seifert, A. W. (2019). Fgf-signaling is compartmentalized within the mesenchyme and controls proliferation during salamander limb development. *eLife*, *8*, 1–28. <https://doi.org/10.7554/eLife.48507>
- Rastinejad, F., Wagner, T., Zhao, Q., & Khorasanizadeh, S. (2000). Structure of the RXR-RAR DNA-

- binding complex on the retinoic acid response element DR1. *EMBO Journal*, *19*(5), 1045–1054. <https://doi.org/10.1093/emboj/19.5.1045>
- Reifers, F., Böhli, H., Walsh, E. C., Crossley, P. H., Stainier, D. Y. R., & Brand, M. (1998). Fgf8 is mutated in zebrafish acerebellar (ace) mutants and is required for maintenance of midbrain-hindbrain boundary development and somitogenesis. *Development*, *125*(13), 2381–2395.
- Reijntjes, S., Blentic, A., Gale, E., & Maden, M. (2005). The control of morphogen signalling: Regulation of the synthesis and catabolism of retinoic acid in the developing embryo. *Developmental Biology*, *285*(1), 224–237. <https://doi.org/10.1016/j.ydbio.2005.06.019>
- Rembold, M., Lahiri, K., Foulkes, N. S., & Wittbrodt, J. (2006). Transgenesis in fish: Efficient selection of transgenic fish by co-injection with a fluorescent reporter construct. *Nature Protocols*, *1*(3), 1133–1139. <https://doi.org/10.1038/nprot.2006.165>
- Renaud, J. P., Rochel, N., Ruff, M., Vivat, V., Chambon, P., Gronemeyer, H., & Moras, D. (1995). Crystal structure of the RAR- $\gamma$  ligand-binding domain bound to all-trans retinoic acid. *Nature*, *378*(6558), 681–689. <https://doi.org/10.1038/378681a0>
- Rezsohazy, R., Saurin, A. J., Maurel-Zaffran, C., & Graba, Y. (2015). Cellular and molecular insights into Hox protein action. *Development*, *142*(7), 1212–1227. <https://doi.org/10.1242/dev.109785>
- Rhinn, M., & Dollé, P. (2012). Retinoic acid signalling during development. *Development*, *139*(5), 843–858. <https://doi.org/10.1242/dev.065938>
- Rhinn, M., Schuhbaur, B., Niederreither, K., & Dollé, P. (2011). Involvement of retinol dehydrogenase 10 in embryonic patterning and rescue of its loss of function by maternal retinaldehyde treatment. *Proceedings of the National Academy of Sciences of the United States of America*, *108*(40), 16687–16692. <https://doi.org/10.1073/pnas.1103877108>
- Richter, D., Bayer, K., Toesko, T., & Schuster, S. (2019). ZeBR $\alpha$  a universal, multi-fragment DNA-assembly-system with minimal hands-on time requirement. *Scientific Reports*, *9*(1), 1–16. <https://doi.org/10.1038/s41598-019-39768-0>
- Riddle, R. D., Johnson, R. L., Laufer, E., & Tabin, C. (1993). Sonic hedgehog mediates the polarizing activity of the ZPA. *Cell*, *75*(7), 1401–1416. [https://doi.org/10.1016/0092-8674\(93\)90626-2](https://doi.org/10.1016/0092-8674(93)90626-2)
- Rochette-Egly, C., & Germain, P. (2009). Dynamic and combinatorial control of gene expression by nuclear retinoic acid receptors (RARs). *Nuclear Receptor Signaling*, *7*. <https://doi.org/10.1621/nrs.07005>
- Rosello-Diez, A., Arques, C. G., Delgado, I., Giovinazzo, G., & Torres, M. (2014). Diffusible signals and epigenetic timing cooperate in late proximo-distal limb patterning. *Development*, *141*(7), 1534–1543. <https://doi.org/10.1242/dev.106831>
- Rossi, A., Konarakis, Z., Gerri, C., Nolte, H., Hölper, S., Krüger, M., & Stainier, D. Y. R. (2015). Genetic compensation induced by deleterious mutations but not gene knockdowns. *Nature*, *524*(7564), 230–233. <https://doi.org/10.1038/nature14580>
- Runkle, S., Hill, J., Kantorow, M., Horwitz, J., & Posner, M. (2002). Sequence and spatial expression of zebrafish (*Danio rerio*)  $\alpha$ A-crystallin. *Molecular Vision*, *8*, 45–50.
- Russo, J. E., Hauquitz, D., & Hilton, J. (1988). Inhibition of mouse cytosolic aldehyde dehydrogenase by 4-(diethylamino)benzaldehyde. *Biochemical Pharmacology*, *37*(8), 1639–1642. [https://doi.org/10.1016/0006-2952\(88\)90030-5](https://doi.org/10.1016/0006-2952(88)90030-5)
- Ruvinsky, I., Oates, A. C., Silver, L. M., & Ho, R. K. (2000). The evolution of paired appendages in vertebrates: T-box genes in the zebrafish. *Development Genes and Evolution*, *210*(2), 82–91. <https://doi.org/10.1007/s004270050014>
- Ryan, A. K., Blumberg, B., Rodriguez-Esteban, C., Yonei-Tamura, S., Tamura, K., Tsukui, T., ... Belmonte, J. C. I. (1998). Pitx2 determines left-right asymmetry of internal organs in vertebrates. *Nature*, *394*(6693), 545–551. <https://doi.org/10.1038/29004>
- Sabourin, M., Tuzon, C. T., Fisher, T. S., & Zakian, V. A. (2007). A flexible protein linker improves the function of epitope-tagged proteins in *Saccharomyces cerevisiae*. *Yeast*, *24*(1), 39–45. <https://doi.org/10.1002/yea.1431.A>
- Sadowski, I., Ma, J., Triezenberg, S., & Ptashne, M. (1988). GAL4-VP16 is an unusually potent transcriptional activator. *Nature*, *335*, 563–564.
- Samuel, A., Rubinstein, A. M., Azar, T. T., Ben-Moshe Livne, Z., Kim, S. H., & Inbal, A. (2016). Six3

- regulates optic nerve development via multiple mechanisms. *Scientific Reports*, 6, 1–14. <https://doi.org/10.1038/srep20267>
- Sandell, L. L., Sanderson, B. W., Moiseyev, G., Johnson, T., Mushegian, A., Young, K., ... Trainor, P. A. (2007). RDH10 is essential for synthesis of embryonic retinoic acid and is required for limb, craniofacial, and organ development. *Genes and Development*, 21(9), 1113–1124. <https://doi.org/10.1101/gad.1533407>
- Sander, J. D., & Joung, J. K. (2014). CRISPR-Cas systems for editing, regulating and targeting genomes. *Nature Biotechnology*, 32(4), 347–350. <https://doi.org/10.1038/nbt.2842>
- Sarro, R., Kocher, A. A., Emera, D., Uebbing, S., Dutrow, E. V., Weatherbee, S. D., ... Noonan, J. P. (2018). Disrupting the three-dimensional regulatory topology of the Pitx1 locus results in overtly normal development. *Development*, 145(7). <https://doi.org/10.1242/dev.158550>
- Sato, Y., Ramalanjaona, N., Huet, T., Potier, N., Osz, J., Antony, P., ... Rochel, N. (2010). The “phantom effect” of the rexinoid LG100754: Structural and functional insights. *PLoS ONE*, 5(11). <https://doi.org/10.1371/journal.pone.0015119>
- Sawada, R., Kamei, H., Hakuno, F., Takahashi, S. I., & Shimizu, T. (2015). In vivo loss of function study reveals the short stature homeobox-containing (shox) gene plays indispensable roles in early embryonic growth and bone formation in Zebrafish. *Developmental Dynamics*, 244(2), 146–156. <https://doi.org/10.1002/dvdy.24239>
- Scheer, N., & Campos-Ortega, J. A. (1999). Use of the Gal4-UAS technique for targeted gene expression in the zebrafish. *Mechanisms of Development*, 80, 153–158.
- Schmidt, M. (2017). *Generation of genetic tools to characterize signaling pathways in zebrafish pelvic fin development using the Gal4-UAS and CRISPR-Cas9 systems*, Master thesis. Universität Bayreuth.
- Sekine, K., Ohuchi, H., Fujiwara, M., Yamasaki, M., Yoshizawa, T., Sato, T., ... Kato, S. (1999). Fgf10 is essential for limb and lung formation. *Nature Genetics*, 51(5), 138–141. <https://doi.org/10.1038/s41588-019-0396-9>
- Sekkali, B., Tran, H. T., Crabbe, E., De Beule, C., Van Roy, F., & Vleminckx, K. (2008). Chicken  $\beta$ -globin insulator overcomes variegation of transgenes in *Xenopus* embryos. *The FASEB Journal*, 22(7), 2534–2540. <https://doi.org/10.1096/fj.07-098111>
- Sentmanat, M. F., Peters, S. T., Florian, C. P., Connelly, J. P., & Pruett-Miller, S. M. (2018). A Survey of Validation Strategies for CRISPR-Cas9 Editing. *Scientific Reports*, 8(1), 1–8. <https://doi.org/10.1038/s41598-018-19441-8>
- Shapiro, M. D., Bell, M. A., & Kingsley, D. M. (2006). Parallel genetic origins of pelvic reduction in vertebrates. *Proceedings of the National Academy of Sciences of the United States of America*, 103(37), 13753–13758. <https://doi.org/10.1073/pnas.0604706103>
- Sharpe, C. R., & Goldstone, K. (1997). Retinoid receptors promote primary neurogenesis in *Xenopus*. *Development*, 124(2), 515–523.
- Shoji, W., & Sato-Maeda, M. (2008). Application of heat shock promoter in transgenic zebrafish. *Development Growth and Differentiation*, 50(6), 401–406. <https://doi.org/10.1111/j.1440-169X.2008.01038.x>
- Sinn, R., & Wittbrodt, J. (2013). An eye on eye development. *Mechanisms of Development*, 130(6–8), 347–358. <https://doi.org/10.1016/j.mod.2013.05.001>
- Sirbu, I. O., Gresh, L., Barra, J., & Duester, G. (2005). Shifting boundaries of retinoic acid activity control hindbrain segmental gene expression. *Development*, 132(11), 2611–2622. <https://doi.org/10.1242/dev.01845>
- Snapp, E. (2005). Design and Use of Fluorescent Fusion Proteins in Cell Biology. *Current Protocols in Cell Biology*, 27(1), 21.4.1–21.4.13. <https://doi.org/10.1002/0471143030.cb2104s27>
- Sood, R., Carrington, B., Bishop, K., Jones, M. P., Rissone, A., Candotti, F., ... Liu, P. (2013). Efficient Methods for Targeted Mutagenesis in Zebrafish Using Zinc-Finger Nucleases: Data from Targeting of Nine Genes Using CompoZr or CoDA ZFNs. *PLoS ONE*, 8(2). <https://doi.org/10.1371/journal.pone.0057239>
- Stacker, L. (2018). *Etablierung des CRISPR / Cas9-Systems am Beispiel des knock-outs von Pitx1*, Forschungsmodul. Universität Bayreuth.

- Stacker, L. (2020). *PCR-based identification of CRISPR / Cas9-mediated Pitx1 knockout alleles in zebrafish*, Master thesis. Universität Bayreuth.
- Stafford, D., White, R. J., Kinkel, M. D., Linville, A., Schilling, T. F., & Prince, V. E. (2006). Retinoids signal directly to zebrafish endoderm to specify insulin-expressing  $\beta$ -cells. *Development*, *133*(5), 949–956. <https://doi.org/10.1242/dev.02730>
- Steinmetz, A. C. U., Renaud, J.-P., & Moras, D. (2001). Binding of ligands and activation of transcription by nuclear receptors. *Annu. Rev. Biophys. Biomol. Struct.*, *30*, 329–359. <https://doi.org/10.1002/9783527678679.dg11890>
- Stenkamp, D. L. (2015). Development of the Vertebrate Eye and Retina. *Progress in Molecular Biology and Translational Science*, *134*, 397–414. <https://doi.org/doi:10.1016/bs.pmbts.2015.06.006>.
- Streisinger, G. (1984). Attainment of minimal biological variability and measurements of genotoxicity: production of homozygous diploid zebra fish. *National Cancer Institute Monograph*, *65*, 53–58.
- Streisinger, G., Walker, C., Dower, N., Knauber, D., & Singer, F. (1981). Production of clones of homozygous diploid zebra fish (*Brachydanio rerio*). *Nature*, *291*, 293–296.
- Studer, M., Pöpperl, H., Marshall, H., Kuroiwa, A., & Krumlauf, R. (1994). Role of a Conserved Retinoic Acid Response Element in Rhombomere Restriction of Hoxb-1. *Science*, *265*(5179), 1728–1732.
- Sturdee, A., & Connock, M. (1975). The Embryonic Limb Bud of the Urodele: Morphological Studies of the Apex. *Differentiation*, *3*(1–3), 43–49. <https://doi.org/10.1111/j.1432-0436.1975.tb00844.x>
- Sun, X., Lewandoski, M., Meyers, E. N., Liu, Y. H., Maxson, R. E., & Martin, G. R. (2000). Conditional inactivation of Fgf4 reveals complexity of signalling during limb bud development. *Nature Genetics*, *25*(1), 83–86. <https://doi.org/10.1038/75644>
- Suster, M. L., Abe, G., Schouw, A., & Kawakami, K. (2011). Transposon-mediated BAC transgenesis in zebrafish. *Nature Protocols*, *6*(12), 1998–2021. <https://doi.org/10.1038/nprot.2011.416>
- Suster, M. L., Sumiyama, K., & Kawakami, K. (2009). Transposon-mediated BAC transgenesis in zebrafish and mice. *BMC Genomics*, *10*, 477. <https://doi.org/10.1186/1471-2164-10-477>
- Szeto, D. P., Rodriguez-Esteban, C., Ryan, A. K., O'Connell, S. M., Liu, F., Kioussi, C., ... Rosenfeld, M. G. (1999). Role of the Bicoid-related homeodomain factor Pitx1 in specifying hindlimb morphogenesis and pituitary development. *Genes and Development*, *13*(4), 484–494. <https://doi.org/10.1101/gad.13.4.484>
- Taher, L., Collette, N. M., Muruges, D., Maxwell, E., Ovcharenko, I., & Loots, G. G. (2011). Global gene expression analysis of murine limb development. *PLoS ONE*, *6*(12). <https://doi.org/10.1371/journal.pone.0028358>
- Takeuchi, J. K., Koshiba-Takeuchi, K., Suzuki, T., Kamimura, M., Ogura, K., & Ogura, T. (2003). Tbx5 and Tbx4 trigger limb initiation through activation of the Wnt/Fgf signaling cascade. *Development*, *130*(12), 2729–2739. <https://doi.org/10.1242/dev.00474>
- Tamura, K., Yonei-Tamura, S., & Belmonte, J. C. I. (1999). Differential expression of Tbx4 and Tbx5 in Zebrafish Fin buds. *Mechanisms of Development*, *87*(1–2), 181–184. [https://doi.org/10.1016/S0925-4773\(99\)00126-4](https://doi.org/10.1016/S0925-4773(99)00126-4)
- Tanaka, M. (2013). Molecular and evolutionary basis of limb field specification and limb initiation. *Development Growth and Differentiation*, *55*(1), 149–163. <https://doi.org/10.1111/dgd.12017>
- Tanaka, M., Hale, L. A., Amores, A., Yan, Y. L., Cresko, W. A., Suzuki, T., & Postlethwait, J. H. (2005). Developmental genetic basis for the evolution of pelvic fin loss in the pufferfish *Takifugu rubripes*. *Developmental Biology*, *281*(2), 227–239. <https://doi.org/10.1016/j.ydbio.2005.02.016>
- Tank, P. W., Carlson, B. M., & Connelly, T. G. (1977). A scanning electron microscopic comparison of the development of embryonic and regenerating limbs in the axolotl. *Journal of Experimental Zoology*, *201*(3), 417–429. <https://doi.org/10.1002/jez.1402010308>
- Thaller, C., & Eichele, G. (1987). Identification and spatial distribution of retinoids in the developing chick limb bud. *Nature*, *329*, 855–857.
- Thermes, V., Grabher, C., Ristoratore, F., Bourrat, F., Choulika, A., Wittbrodt, J., & Joly, J. S. (2002). I-SceI meganuclease mediates highly efficient transgenesis in fish. *Mechanisms of Development*, *118*(1–2), 91–98. [https://doi.org/10.1016/S0925-4773\(02\)00218-6](https://doi.org/10.1016/S0925-4773(02)00218-6)
- Thisse, B., Heyer, V., Lux, A., Alunni, V., Degraeve, A., Seiliez, I., ... Thisse, C. (2004). Spatial and temporal expression of the zebrafish genome by large-scale in situ hybridization screening.

- Methods Cell Biol*, 77, 505–519.
- Thisse, B., Obrecht-Pflumio, S., Fürthauer, M., Loppin, B., Heyer, V., Degraeve, A., ... Thisse, C. (2001). *Expression of the zebrafish genome during embryogenesis*. ZFIN Direct Data Submission.
- Thompson, A. C., Capellini, T. D., Guenther, C. A., Chan, Y. F., Infante, C. R., Menke, D. B., & Kingsley, D. M. (2018). A novel enhancer near the *pitx1* gene influences development and evolution of pelvic appendages in vertebrates. *ELife*, 7, 1–21. <https://doi.org/10.7554/eLife.38555>
- Thyme, S. B., Akhmetova, L., Montague, T. G., Valen, E., & Schier, A. F. (2016). Internal guide RNA interactions interfere with Cas9-mediated cleavage. *Nature Communications*, 7, 1–7. <https://doi.org/10.1038/ncomms11750>
- Tickle, C., & Towers, M. (2017). Sonic hedgehog signaling in limb development. *Frontiers in Cell and Developmental Biology*, 5(FEB), 1–19. <https://doi.org/10.3389/fcell.2017.00014>
- Tsuji, T., & Niida, Y. (2008). Development of a simple and highly sensitive mutation screening system by enzyme mismatch cleavage with optimized conditions for standard laboratories. *Electrophoresis*, 29(7), 1473–1483. <https://doi.org/10.1002/elps.200700729>
- Urasaki, A., Morvan, G., & Kawakami, K. (2006). Functional dissection of the Tol2 transposable element identified the minimal cis-sequence and a highly repetitive sequence in the subterminal region essential for transposition. *Genetics*, 174(2), 639–649. <https://doi.org/10.1534/genetics.106.060244>
- Usdin, K. (2008). The biological effects of simple tandem repeats: Lessons from the repeat expansion diseases. *Genome Research*, 18(7), 1011–1019. <https://doi.org/10.1101/gr.070409.107>
- van Eeden, F. J. M., Granato, M., Schach, U., Brand, M., Furutani-Seiki, M., Haffter, P., ... Nüsslein-Volhard, C. (1996). Genetic analysis of fin formation in the zebrafish, *Danio rerio*. *Development*, 123(Table 1), 255–262.
- Varga, M. (2018). The doctor of delayed publications: The remarkable life of George Streisinger (1927-1984). *Zebrafish*, 15(3), 314–319. <https://doi.org/10.1089/zeb.2017.1531>
- Varshney, G. K., Carrington, B., Pei, W., Bishop, K., Chen, Z., Fan, C., ... Burgess, S. M. (2016). A high-throughput functional genomics workflow based on CRISPR/Cas9-mediated targeted mutagenesis in zebrafish. *Nature Protocols*, 11(12), 2357–2375. <https://doi.org/10.1038/nprot.2016.141>
- Varshney, G. K., Pei, W., Lafave, M. C., Idol, J., Xu, L., Gallardo, V., ... Burgess, S. M. (2015). High-throughput gene targeting and phenotyping in zebrafish using CRISPR/Cas9. *Genome Research*, 25(7), 1030–1042. <https://doi.org/10.1101/gr.186379.114>
- Vauti, F., Stegemann, L. A., Vögele, V., & Köster, R. W. (2020). All-age whole mount in situ hybridization to reveal larval and juvenile expression patterns in zebrafish. *PLoS ONE*, 15(8 August), 1–17. <https://doi.org/10.1371/journal.pone.0237167>
- Walker, M. B., & Kimmel, C. B. (2007). A two-color acid-free cartilage and bone stain for zebrafish larvae. *Biotechnic and Histochemistry*, 82(1), 23–28. <https://doi.org/10.1080/10520290701333558>
- Wan, H., He, J., Ju, B., Yan, T., Lam, T. J., & Gong, Z. (2002). Generation of two-color transgenic zebrafish using the green and red fluorescent protein reporter genes *gfp* and *rfp*. *Marine Biotechnology*, 4(2), 146–154. <https://doi.org/10.1007/s10126-001-0085-3>
- Wang, J. S., Infante, C. R., Park, S., & Menke, D. B. (2018). PITX1 promotes chondrogenesis and myogenesis in mouse hindlimbs through conserved regulatory targets. *Developmental Biology*, 434(1), 186–195. <https://doi.org/10.1016/j.ydbio.2017.12.013>
- Wang, X., Chen, X., & Yang, Y. (2012). Spatiotemporal control of gene expression by a light-switchable transgene system. *Nature Methods*, 9(3), 266–269. <https://doi.org/10.1038/nmeth.1892>
- Wang, Y., Li, X., Liu, Z., Zhang, T., Chen, B., Hou, G., ... Du, S. (2014). All-trans-retinoid acid (ATRA) may have inhibited chondrogenesis of primary hind limb bud mesenchymal cells by downregulating *Pitx1* expression. *Toxicology Letters*, 224(2), 282–289. <https://doi.org/10.1016/j.toxlet.2013.06.220>
- Weber, S. (2020). *Expression patterns of selected genes during early pelvic fin development and their dependency on retinoic acid signaling*, Bachelor thesis. Universität Bayreuth.
- Webster, N., Jin, J. R., Green, S., Hollis, M., & Chambon, P. (1988). The yeast UASG is a transcriptional

- enhancer in human HeLa cells in the presence of the GAL4 trans-activator. *Cell*, 52(2), 169–178. [https://doi.org/10.1016/0092-8674\(88\)90505-3](https://doi.org/10.1016/0092-8674(88)90505-3)
- Welte, C. (2011). *Retinoic acid during zebrafish paired fin development*, Bachelor thesis. Konstanz University.
- Wendt, K. S., Yoshida, K., Itoh, T., Bando, M., Koch, B., Schirghuber, E., ... Peters, J. M. (2008). Cohesin mediates transcriptional insulation by CCCTC-binding factor. *Nature*, 451(7180), 796–801. <https://doi.org/10.1038/nature06634>
- Westerfield, M. (2000). *The zebrafish book, A guide for the laboratory use of zebrafish Danio (Brachydanio) rerio* (4th ed.). Eugene: University of Oregon Press.
- White, R. M., Sessa, A., Burke, C., Bowman, T., LeBlanc, J., Ceol, C., ... Zon, L. I. (2008). Transparent Adult Zebrafish as a Tool for In Vivo Transplantation Analysis. *Cell Stem Cell*, 2(2), 183–189. <https://doi.org/10.1016/j.stem.2007.11.002>
- Wilson, J. G., Roth, C. B., & Warkany, J. (1953). An analysis of the syndrome of malformations induced by maternal vitamin a deficiency. Effects of restoration of vitamin a at various times during gestation. *American Journal of Anatomy*, 92(2), 189–217. <https://doi.org/10.1002/aja.1000920202>
- Xie, K. T., Wang, G., Thompson, A. C., Wucherpennig, J. I., Reimchen, T. E., MacColl, A. D. C., ... Kingsley, D. M. (2019). DNA fragility in the parallel evolution of pelvic reduction in stickleback fish. *Science*, 363, 81–84.
- Xu, H., Xiao, T., Chen, C.-H., Li, W., Meyer, C. A., Wu, Q., ... Liu, X. S. (2015). Sequence determinants of improved CRISPR sgRNA design. *Genome Research*, 25(8), 1147–1157. <https://doi.org/10.1101/gr.191452.115>
- Xu, X., Weinstein, M., Li, C., Naski, M., Cohen, R. I., Ornitz, D. M., ... Deng, C. (1998). Fibroblast growth factor receptor 2 (FGFR2)-mediated reciprocal regulation loop between FGF8 and FGF10 is essential for limb induction. *Development*, 125(4), 753–765.
- Yang, L., Cai, C. L., Lin, L., Qyang, Y., Chung, C., Monteiro, R. M., ... Evans, S. (2006). Isl1 Cre reveals a common Bmp pathway in heart and limb development. *Development*, 133(8), 1575–1585. <https://doi.org/10.1242/dev.02322>
- Yano, T., Abe, G., Yokoyama, H., Kawakami, K., Tamura, K., Yano, T., ... Tamura, K. (2012). Mechanism of pectoral fin outgrowth in zebrafish development. *Development*, 139(22), 4291. <https://doi.org/10.1242/dev.090324>
- Yashiro, K., Zhao, X., Uehara, M., Yamashita, K., Nishijima, M., Nishino, J., ... Hamada, H. (2004). Regulation of retinoic acid distribution is required for proximodistal patterning and outgrowth of the developing mouse limb. *Developmental Cell*, 6(3), 411–422. [https://doi.org/10.1016/S1534-5807\(04\)00062-0](https://doi.org/10.1016/S1534-5807(04)00062-0)
- Ye, F., & Signer, E. R. (1996). RIGS (repeat-induced gene silencing) in Arabidopsis is transcriptional and alters chromatin configuration. *Proceedings of the National Academy of Sciences of the United States of America*, 93(20), 10881–10886. <https://doi.org/10.1073/pnas.93.20.10881>
- Yonei-Tamura, S., Abe, G., Tanaka, Y., Anno, H., Noro, M., Ide, H., ... Tamura, K. (2008). Competent stripes for diverse positions of limbs/fins in gnathostome embryos. *Evolution and Development*, 10(6), 737–745. <https://doi.org/10.1111/j.1525-142X.2008.00288.x>
- Zhao, X., Sirbu, I. O., Mic, F. A., Molotkova, N., Molotkov, A., Kumar, S., & Duester, G. (2009). Retinoic Acid Promotes Limb Induction through Effects on Body Axis Extension but Is Unnecessary for Limb Patterning. *Current Biology*, 19(12), 1050–1057. <https://doi.org/10.1016/j.cub.2009.04.059>
- Zoltowski, B. D., Schwerdtfeger, C., Widom, J., Loros, J. J., Bilwes, A. M., Dunlap, J. C., & Crane, B. R. (2007). Conformational switching in the fungal light sensor Vivid. *Science*, 316, 1054–1057.

## 6 List of abbreviations

aa	Amino acid(s)
ace	Acerebellar
AD	Transactivation domain
Adh	Alcohol dehydrogenases
AER	Apical ectodermal ridge
af	Anal fin
Aldh	Retinaldehyde dehydrogenase
ap	Anterior process
Arg	Arginine
ATP	Adenosine triphosphate
BAC	Bacterial artificial chromosome
bp	Base pares
BCIP	5-Bromo-4-chloro-3-indolyl phosphate
BT	Bayreuth
°C	Degree celsius
ca.	Circa
Cas	CRISPR associated
ccd	Control of cell division or death
cDNA	Coding DNA
cf	Caudal fin
cmlc2	Cardiac myosin light chain 2
CNS	Conserved non-coding sequence
Col2a1	Collagen type II alpha 1 chain
Crbp	Cellular retinoid binding protein
Cre	Causes recombination
CRISPR	Clustered regularly interspaced short palindromic repeats
CRISPR-STAT	CRISPR somatic tissue activity test
crRNA	CRISPR RNA
CTP	Cytidine triphosphate
Cyp26	Cytochrome p450 family 26
Cys	Cysteine
DEAB	4-Diethylaminobenzaldehyde
DEPC	Diethyl pyrocarbonate
dATP	Deoxyadenosine triphosphate
dCTP	Deoxycytidine triphosphate
df	Dorsal fin
dGTP	Deoxyguanosine triphosphate
dNTP	Deoxynucleoside triphosphate
dpf	Days post fertilization
DBD	DNA binding domain
DIG	Digoxigenin

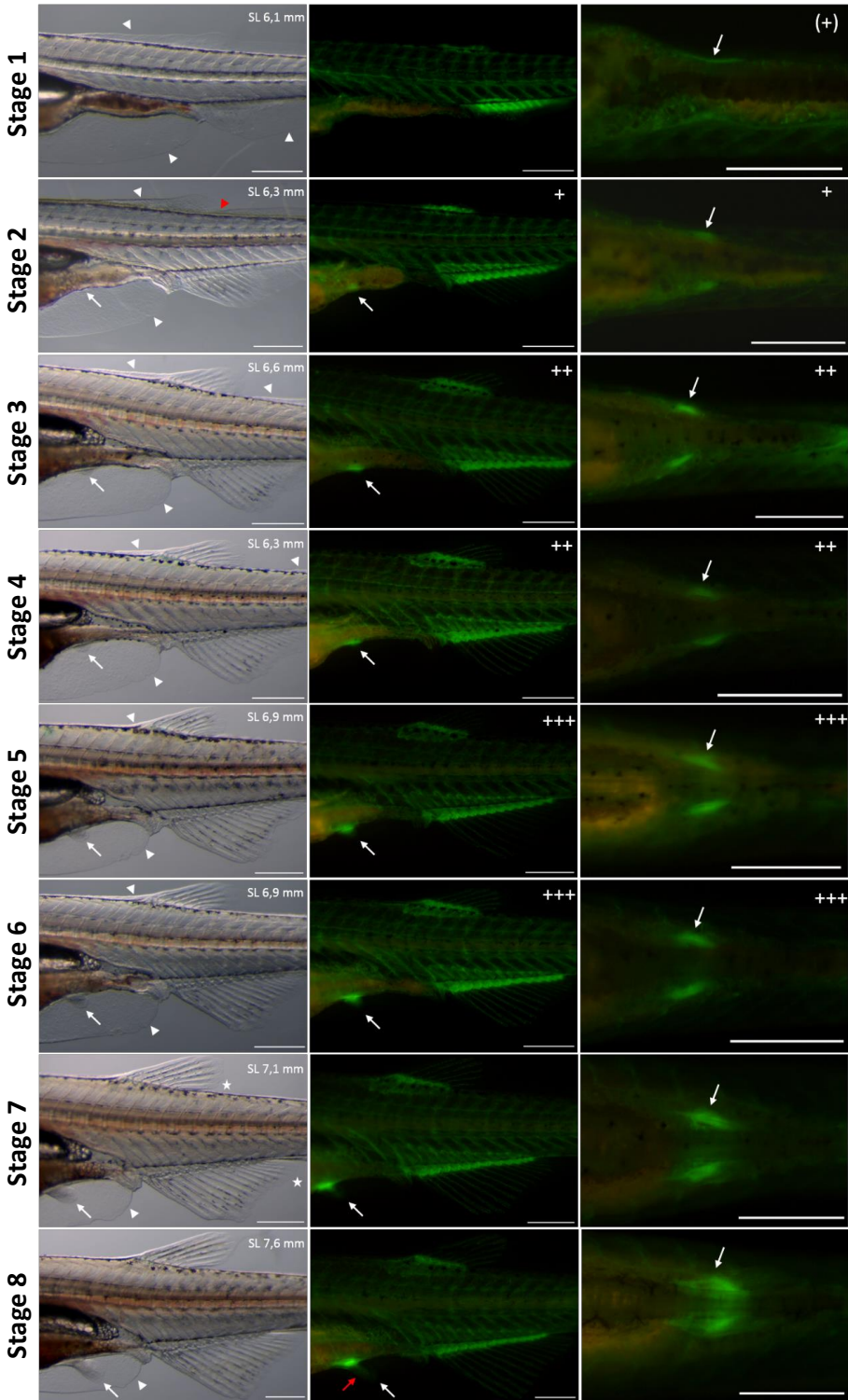
DMSO	Dimethyl sulfoxide
dn	Dominant negative
DNA	Deoxyribonucleic acid
dol	Dolphin
DSB	Double-strand break
dTTP	Deoxythymidine triphosphate
E. coli	Escherichia coli
EDTA	Ethylenediaminetetraacetic acid
eGFP	Enhanced green fluorescent protein
EMCV	Encephalomyocarditis virus
Eng1	Engrailed homeobox 1
Epha4a	Ephrin Receptor A4a
ERT2	Estrogen receptor 2
et al.	Et alia (and others)
EtOH	Ethanol
FAM	Fluorescein amidite
fb	Fin base
ff	Fin fold
Fgf	Fibroblast growth factor
Fgfr	Fibroblast growth factor receptor
Fig	Figure
FL	Fin (bud) length
Fli	Friend leukemia integration
FM1-3	Fin malformation class 1-3
FP	Fluorescing protein
Gal4	Galactose metabolic gene 4
Gdf	Growth differentiation factor
GFP	Green fluorescent protein
GI	$\beta$ -globin intron
Gly	Glycine
GTP	Guanosine triphosphate
H	Helix
h	Hour
HDR	Homology directed repair
His	Histidine
HLEA/B	Hind limb enhancer A/B
Hox	Homeobox
hpf	Hours post fertilization
Hsp70l	Heat-shock promoter 70 like
Ile	Isoleucine
indel	Insertion or deletion
ika	Ikarus
IRES	Internal ribosomal entry site
kb	Kilo bases

KN	Konstanz
l	Litre
LB	Lysogeny broth
LBD	Ligand-binding domain
LBP	Ligand-binding pocket
LED	Light-emitting diode
Leu	Leucine
lep	Lepidotrich
lig	Ligament
LOV	Light-oxygen-voltage
loxP	Locus of X-over P1
LPM	Lateral plate mesoderm
Met	Methionine
min	Minute
µg	Microgram
mg	Milligram
µl	Microlitre
ml	Millilitre
µm	Micrometre
µM	Micromolar
mm	Millimetre
mM	Millimolar
mr	Marginal ray
mRNA	Messenger ribonucleic acid
MyoD	Myoblast determination protein 1
n	Number
NBT	4-nitro blue tetrazolium chloride
N-CoR	Nuclear receptor corepressor
NEB	New England Biolabs
ng	Nanogram
NHEJ	Non-homologous end joining
nls	Neckless
NLS	Nuclear localisation signal
nm	Nanometre
nof	No fin
nr	Non-repetitive
nt	Nucleotide
NTP	Nucleoside triphosphate
4-OHT	4-hydroxy-tamoxifen
p	Plasmid
PAM	Protospacer adjacent motif
Pax2a/6a	Paired box 2a/6a
PBS	Phosphate buffered saline
PBTw	Phosphate buffered saline + Tween 20

PBTx	Phosphate buffered saline + Triton X-100
PCR	Polymerase chain reaction
pec fin	Pectoral fin
PelA/B	Pelvic enhancer A/B
PEG	Polyethylene glycol
Pen	Pan-limb enhancer
PFA	Paraformaldehyde
pfl	Pelvic finless
pg	Picogram
Phe	Phenylalanine
Pitx1	Paired-like homeodomain 1
pp	Posterior process
PPE1/2	Putative Pitx1 enhancer 1/2
Pro	Proline
Prrx1	Paired-related homeobox 1
qPCR	quantitative polymerase chain reaction
r	Radial
RA	All- <i>trans</i> -retinoic acid
RAI	Retinoic acid inhibitor
RAL	Retinaldehyde
Raldh	Retinaldehyde dehydrogenase
Rar	Retinoic acid receptor
RARE	Retinoic acid response element
Rbp	Retinol binding protein
Rdh	Retinol dehydrogenase
RFP	Red fluorescent protein
RNA	Ribonucleic acid
ROL	Retinol
rpm	Rounds per minute
RT	Room temperature
Rxr	Retinoid X receptor
S1-14	Pelvic fin developmental stages 1-14
SALR	Salmon river
sec	Second
Ser	Serine
sgRNA	Single-guided RNA
Shh	Sonic hedgehog
Shox	Short stature homeobox
Six3	Sine oculis homeobox homolog 3
SL	Standard length
SM0-5	Skeletal malformation class 0-5
SMRT	Silencing mediator of retinoic acid and thyroid hormone receptor
SOC	Super optimal broth with catabolite repression
som	Somite

Sox9	SRY-Box transcription factor 9
Sp8	Specifying protein 8
SSC	Saline-sodium citrate
T1,5,19,50	Target 1,5,19,50
T7E1	T7 endonuclease 1
TAE	Tris acetate EDTA
TALEN	Transcription activator-like effector nucleases
Tbx	T-box transcription factor
Tcf/Lef	Transcription factor/lymphoid enhancer binding factor
TE	Tris EDTA
TF	Transcription factor
Tg	Transgene
Tgf	Transforming growth factor
TIDE	Tracking of indels by decomposition
TL	Total length of the pelvic girdle
Tol2	Transposable element 2
tracrRNA	Transactivating CRISPR RNA
tRNA	Transfer ribonucleic acid
TSS	Transcriptional start site
TTP	Thymidine triphosphate
TTR	Transthyretin
TW	Total width of the pelvic girdle
Tyr	Tyrosinase
U	Unit
UAS	Upstream activating sequences
ubi	Ubiquitin
UV	Ultraviolet
V	Volt
VAD	Vitamin A deficiency
VP16	Herpes simplex virus protein vmw65
v/v	Volume per volume
vvd	Vivid
WISH	Whole-mount <i>in situ</i> hybridisation
Wnt	Wingless-related integration site
wpf	Weeks post fertilization
WT	Wild type
w/v	Weight per volume
zf	Zebrafish
ZFN	Zinc-finger nucleases
ZPA	Zone of polarizing activity

# 7 Supplementary data



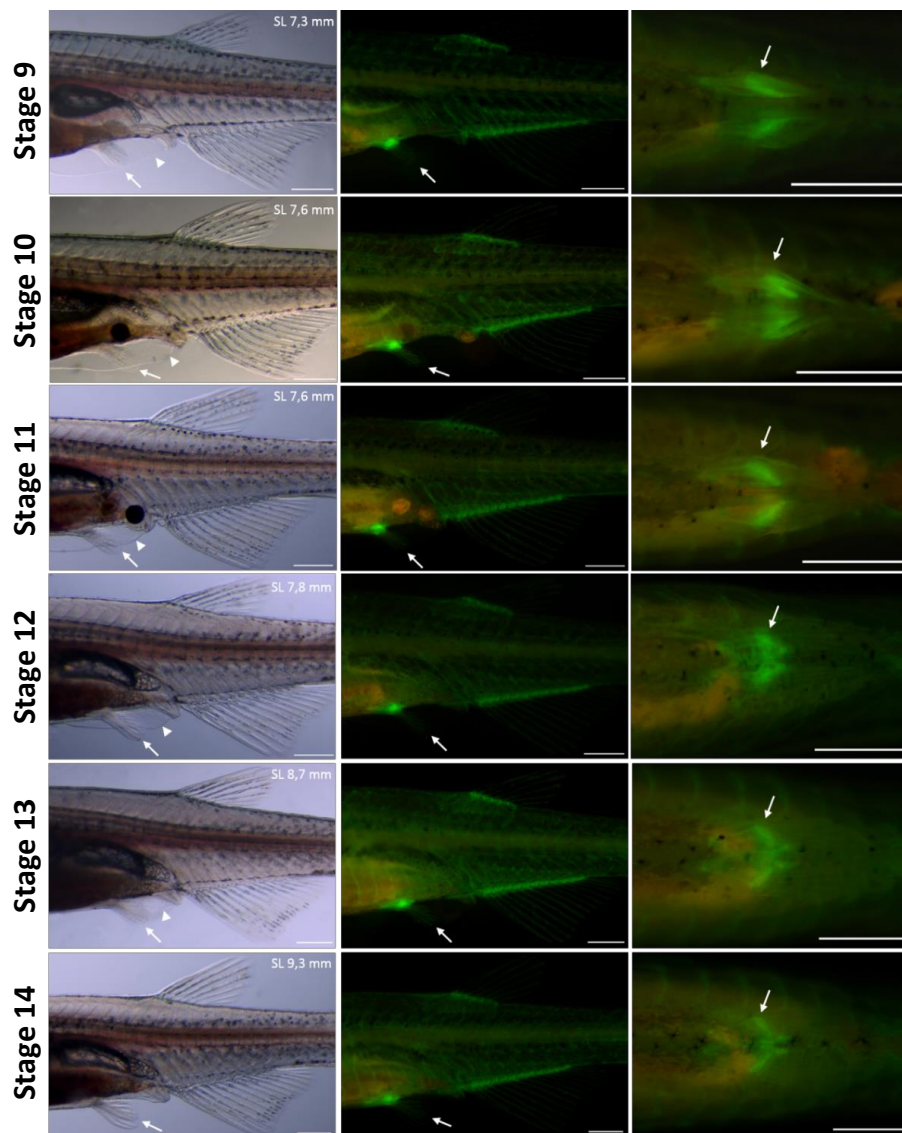


**Fig. S1 Definition of the stages of pelvic fin development.** To classify the developmental stages, the size of the growing pelvic fin was set in relation to the decrease of the distal border of the minor lobe. The anal and dorsal radials that formed at the same time were counted in relation to this. **A,B:** Lateral representation of the pelvic fins. **C:** Ventral representation of the pelvic fin region. Increasing fluorescence strength ventrally: (+), +, ++, +++. Arrows: ventral fin bud / ventral fin. Red arrows: first pelvic ray. Arrowheads: larval fin edge decline. Red arrowhead: posterior notch of the dorsal fin. Asterisks: dorsal / anal fin separated by the fin edge. Continuous increase in standard length (SL). Lateral and ventral images with cranial to the left. Scale bars: 500  $\mu$ m. 14 stages. **Stage 1:** no pelvic fin bud. **Stage 2:** lateral pelvic fin bud. **Stage 3:** pelvic fin bud occupying 1/8 of the minor lobe. **Stage 4:** pelvic fin bud occupying 1/6 of the minor lobe. **Stage 5:** pelvic fin bud occupying 1/4 of the minor lobe. **Stage 6:** pelvic fin bud occupying 1/3 of the minor lobe. **Stage 7:** pelvic fin bud occupying 1/2 of the minor lobe. **Stage 8:** pelvic fin bud occupying 2/3 of the minor lobe. **Stage 9:** distal border of the minor lobe and pelvic fin at the same level. **Stage 10:** minor lobe occupying 3/4 of the pelvic fin. **Stage 11:** minor lobe occupying 2/3 of the pelvic fin. **Stage 12:** minor lobe occupying 1/2 of the pelvic fin. **Stage 13:** minor lobe occupying 1/4 of the pelvic fin. **Stage 14:** ventral fin without a fin border. Figure taken without modifications from Marzi, 2015. Caption translated from Marzi, 2015.





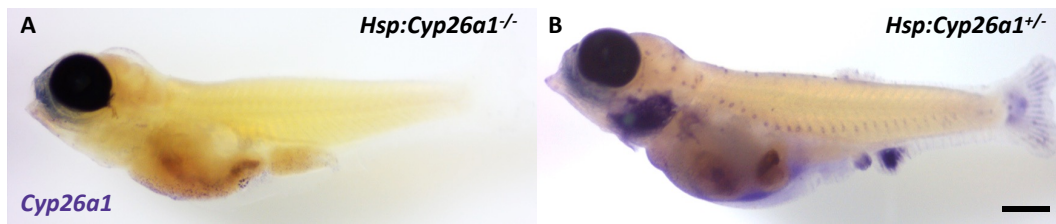


**Fig. S4 Expression of *Cyp26a1*** in *Hsp70l:Cyp26a1<sup>-/-</sup>;fli:eGFP<sup>+/-</sup>;col2a1:mCherry<sup>+/-</sup>* (A) and *Hsp70l:Cyp26a1<sup>+/-</sup>;fli:eGFP<sup>+/-</sup>;col2a1:mCherry<sup>+/-</sup>* (B) larvae at an age of 3 - 4 wpf following one single heat-shock treatment at 38.5 °C for 1.5 h. Larvae were fixed in 4 % PFA 48 h after the heat-shock and WISH against *Cyp26a1* was performed. Intense purple WISH staining was found in several surface exposed body parts of *Hsp70l:Cyp26a1<sup>-/-</sup>* fish, including all fin types, the gills and the lateral line, indicating effective *Cyp26a1* overexpression. Scale bar: 500  $\mu$ m.

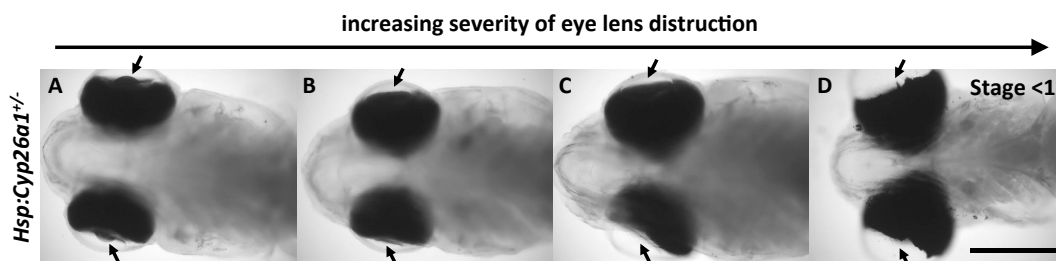


**Fig. S5 *Cyp26a1* overexpression destroys eye lens structure.** Following long-term heat-shock treatment, diverse severities of eye lens destruction were observed in *Hsp70l:Cyp26a1<sup>+/-</sup>;fli:eGFP<sup>+/-</sup>;col2a1:mCherry<sup>+/-</sup>* juveniles. All shown individuals were treated for approximately 4 weeks beginning from pelvic fin developmental Stage <1 **A:** In mild phenotypes, the lens was small, but still visible (arrow). **B,C:** Intermediate phenotypes were characterized by the absence of the eye lenses (arrows). **D:** The most severe phenotype exhibited a completely destroyed eye structure, affecting not only the lens, but the entire organ (arrow). Scale bar: 500  $\mu$ m.

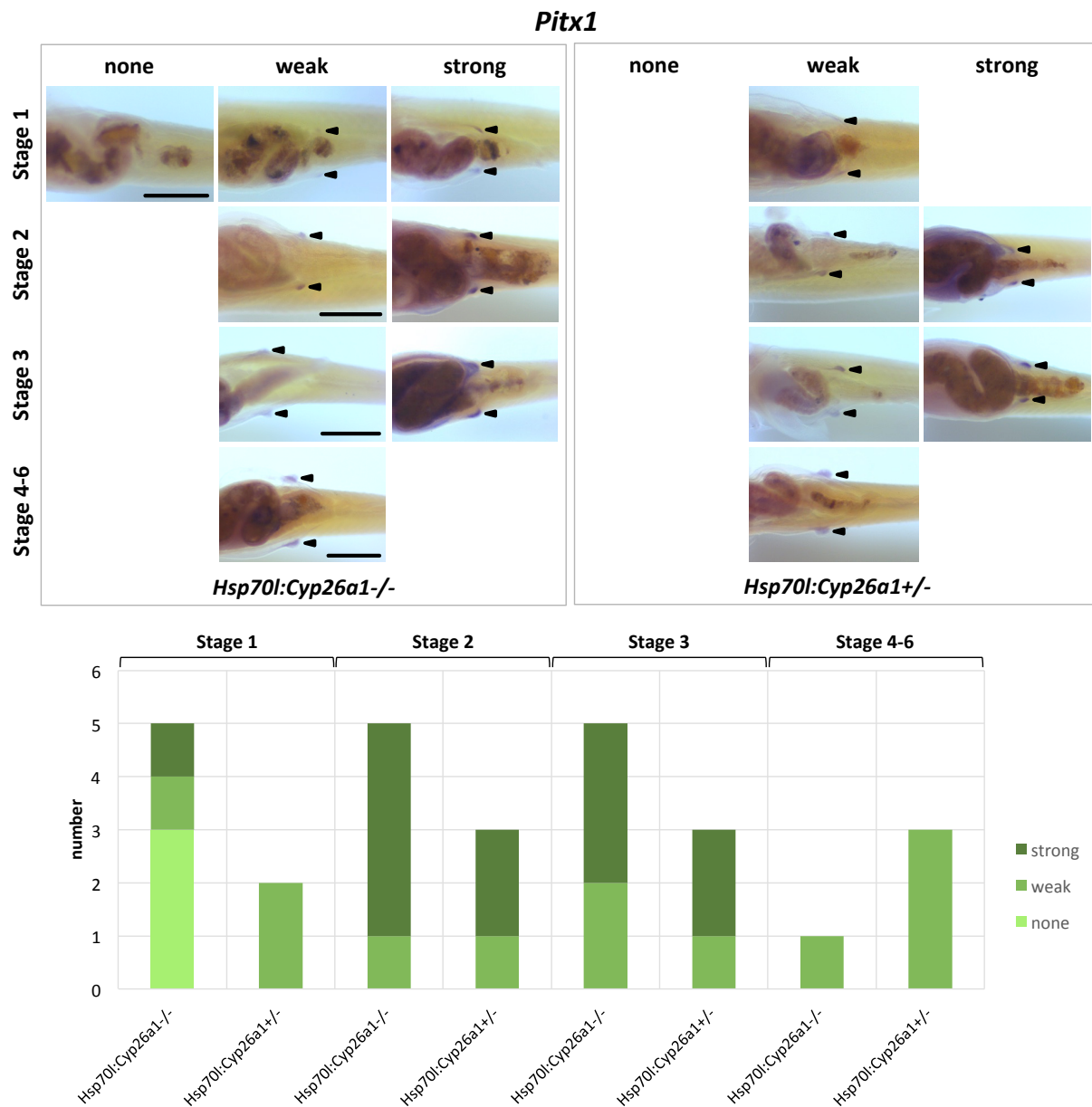


**Fig. S6 Expression of *Pitx1* in dependency of reduced RA signalling.** *Hsp70l:Cyp26a1<sup>-/-</sup>;fli:eGFP<sup>+/-</sup>;col2a1:mCherry<sup>+/-</sup>* and *Hsp70l:Cyp26a1<sup>+/-</sup>;fli:eGFP<sup>+/-</sup>;col2a1:mCherry<sup>+/-</sup>* larvae were sorted according to their pelvic fin developmental stage at an age of 3 - 4 wpf (Stages 4, 5 and 6 were pooled). Afterwards, a single heat-shock at 38.5 °C for 1.5 h was performed. 24 h after the heat-shock, larvae were fixed in 4 % PFA and *Pitx1* transcripts were detected by means of whole-mount *in situ* hybridisation (WISH). According to their intensity of WISH staining in pelvic fin buds, the larvae were sorted in three categories: strong expression, weak and none. Exemplary pictures for each category and developmental stage are presented. The pelvic fin region of the larvae is shown from ventral view; anterior is to the left; stained pelvic fin buds are marked with arrowheads. Scale bar: 500 µm. The graphical representation shows distribution of the different staining categories on the developmental stages and genotypes. Pictures and graph by Sophia Weber, taken and modified from Weber, 2020.

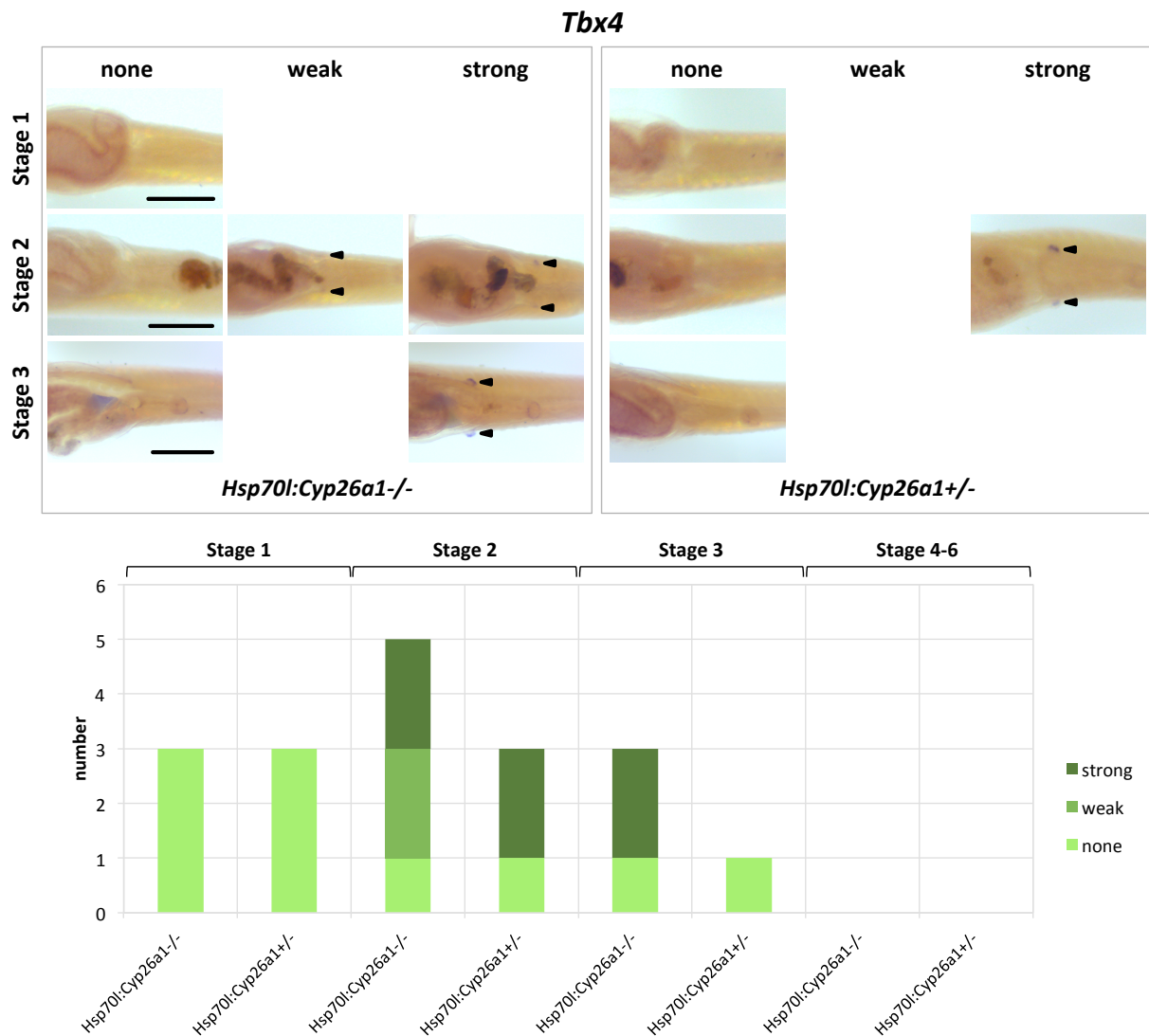


**Fig. S7 Expression of *Tbx4* in dependency of reduced RA signalling.** *Hsp70l:Cyp26a1*<sup>-/-</sup>;*fli:eGFP*<sup>+/-</sup>;*col2a1:mCherry*<sup>+/-</sup> and *Hsp70l:Cyp26a1*<sup>+/-</sup>;*fli:eGFP*<sup>+/-</sup>;*col2a1:mCherry*<sup>+/-</sup> larvae were sorted according to their pelvic fin developmental stage at an age of 3 - 4 wpf (Stages 4, 5 and 6 were pooled). Afterwards, a single heat-shock at 38.5 °C for 1.5 h was performed. 24 h after the heat-shock, larvae were fixed in 4 % PFA and *Tbx4* transcripts were detected by means of whole-mount *in situ* hybridisation (WISH). According to their intensity of WISH staining in pelvic fin buds, the larvae were sorted in three categories: strong expression, weak and none. Exemplary pictures for each category and developmental stage are presented. The pelvic fin region of the larvae is shown from ventral view; anterior is to the left; stained pelvic fin buds are marked with arrowheads. Scale bar: 500  $\mu$ m. The graphical representation shows distribution of the different staining categories on the developmental stages and genotypes. Larvae in the group S4 - S6 did not exhibit WISH staining, why no further analysis took place. Pictures and graph by Sophia Weber, taken and modified from Weber, 2020.

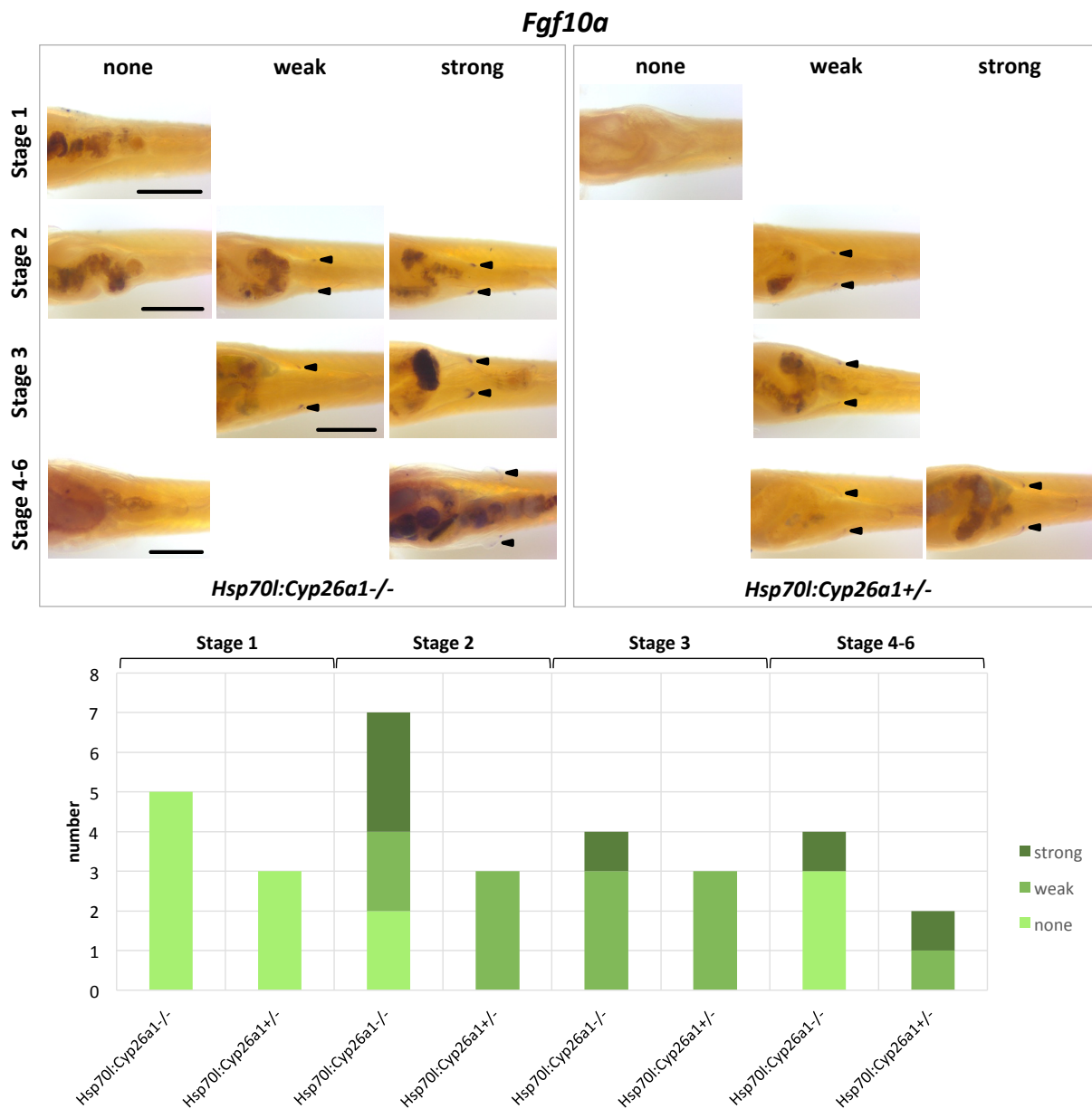


**Fig. S8 Expression of *Fgf10a* in dependency of reduced RA signalling.** *Hsp70l:Cyp26a1<sup>-/-</sup>;fli:eGFP<sup>+/-</sup>;col2a1:mCherry<sup>+/-</sup>* and *Hsp70l:Cyp26a1<sup>+/-</sup>;fli:eGFP<sup>+/-</sup>;col2a1:mCherry<sup>+/-</sup>* larvae were sorted according to their pelvic fin developmental stage at an age of 3 - 4 wpf (Stages 4, 5 and 6 were pooled). Afterwards, a single heat-shock at 38.5 °C for 1.5 h was performed. 24 h after the heat-shock, larvae were fixed in 4 % PFA and *Fgf10a* transcripts were detected by means of whole-mount *in situ* hybridisation (WISH). According to their intensity of WISH staining in pelvic fin buds, the larvae were sorted in three categories: strong expression, weak and none. Exemplary pictures for each category and developmental stage are presented. The pelvic fin region of the larvae is shown from ventral view; anterior is to the left; stained pelvic fin buds are marked with arrowheads. Scale bar: 500 µm. The graphical representation shows distribution of the different staining categories on the developmental stages and genotypes. Pictures and graph by Sophia Weber, taken and modified from Weber, 2020.

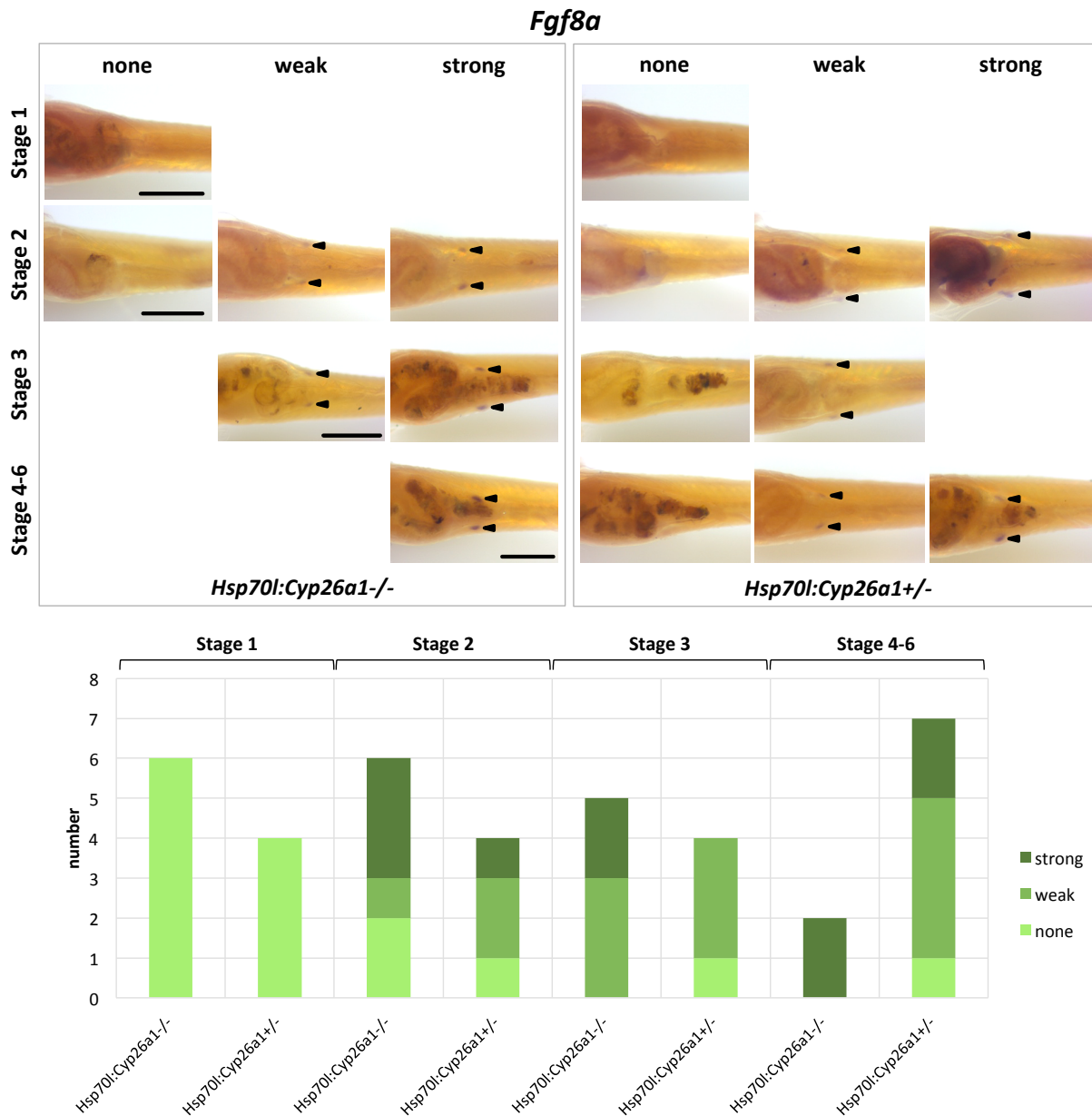


**Fig. S9 Expression of *Fgf8a* in dependency of reduced RA signalling.** *Hsp70l:Cyp26a1<sup>-/-</sup>;fli:eGFP<sup>+/-</sup>;col2a1:mCherry<sup>+/-</sup>* and *Hsp70l:Cyp26a1<sup>+/-</sup>;fli:eGFP<sup>+/-</sup>;col2a1:mCherry<sup>+/-</sup>* larvae were sorted according to their pelvic fin developmental stage at an age of 3 - 4 wpf (Stages 4, 5 and 6 were pooled). Afterwards, a single heat-shock at 38.5 °C for 1.5 h was performed. 24 h after the heat-shock, larvae were fixed in 4 % PFA and *Fgf8a* transcripts were detected by means of whole-mount *in situ* hybridisation (WISH). According to their intensity of WISH staining in pelvic fin buds, the larvae were sorted in three categories: strong expression, weak and none. Exemplary pictures for each category and developmental stage are presented. The pelvic fin region of the larvae is shown from ventral view; anterior is to the left; stained pelvic fin buds are marked with arrowheads. Scale bar: 500  $\mu$ m. The graphical representation shows distribution of the different staining categories on the developmental stages and genotypes. Pictures and graph by Sophia Weber, taken and modified from Weber, 2020.



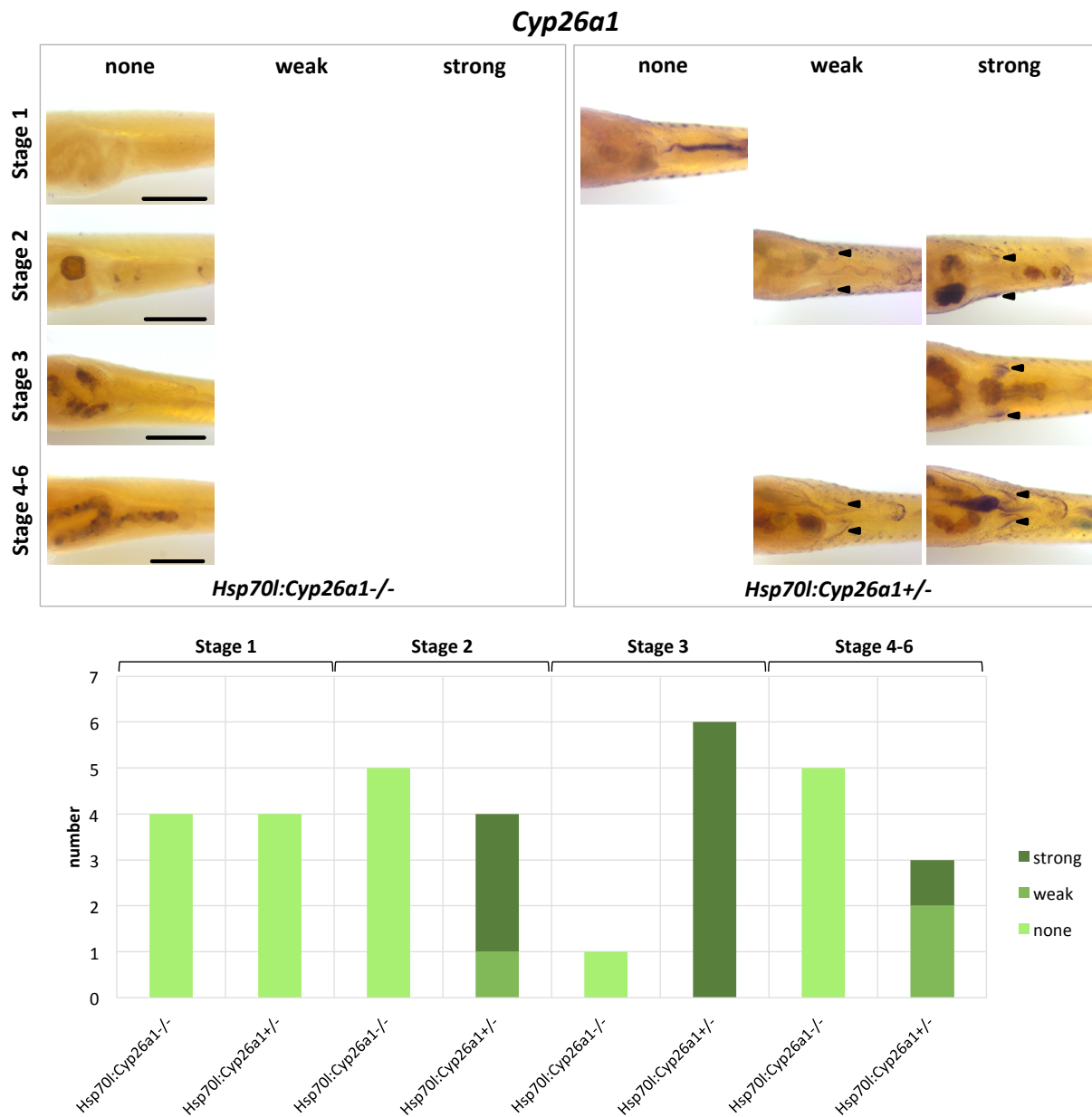


**Fig. S11 Expression of *Cyp26a1* in *Hsp70l:Cyp26a1<sup>-/-</sup>;fli:eGFP<sup>+/-</sup>;col2a1:mCherry<sup>+/-</sup>* and *Hsp70l:Cyp26a1<sup>+/-</sup>;fli:eGFP<sup>+/-</sup>;col2a1:mCherry<sup>+/-</sup>* larvae following heat-shock treatment.** Larvae were sorted according to their pelvic fin developmental stage at an age of 3 - 4 wpf (Stages 4, 5 and 6 were pooled). Afterwards, a single heat-shock at 38.5 °C for 1.5 h was performed. 24 h after the heat-shock, larvae were fixed in 4 % PFA and *Cyp26a1* transcripts were detected by means of whole-mount *in situ* hybridisation (WISH). According to their intensity of WISH staining in pelvic fin buds, the larvae were sorted in three categories: strong expression, weak and none. Exemplary pictures for each category and developmental stage are presented. The pelvic fin region of the larvae is shown from ventral view; anterior is to the left; stained pelvic fin buds are marked with arrowheads. Scale bar: 500  $\mu$ m. The graphical representation shows distribution of the different staining categories on the developmental stages and genotypes. Pictures and graph by Sophia Weber, taken and modified from Weber, 2020.

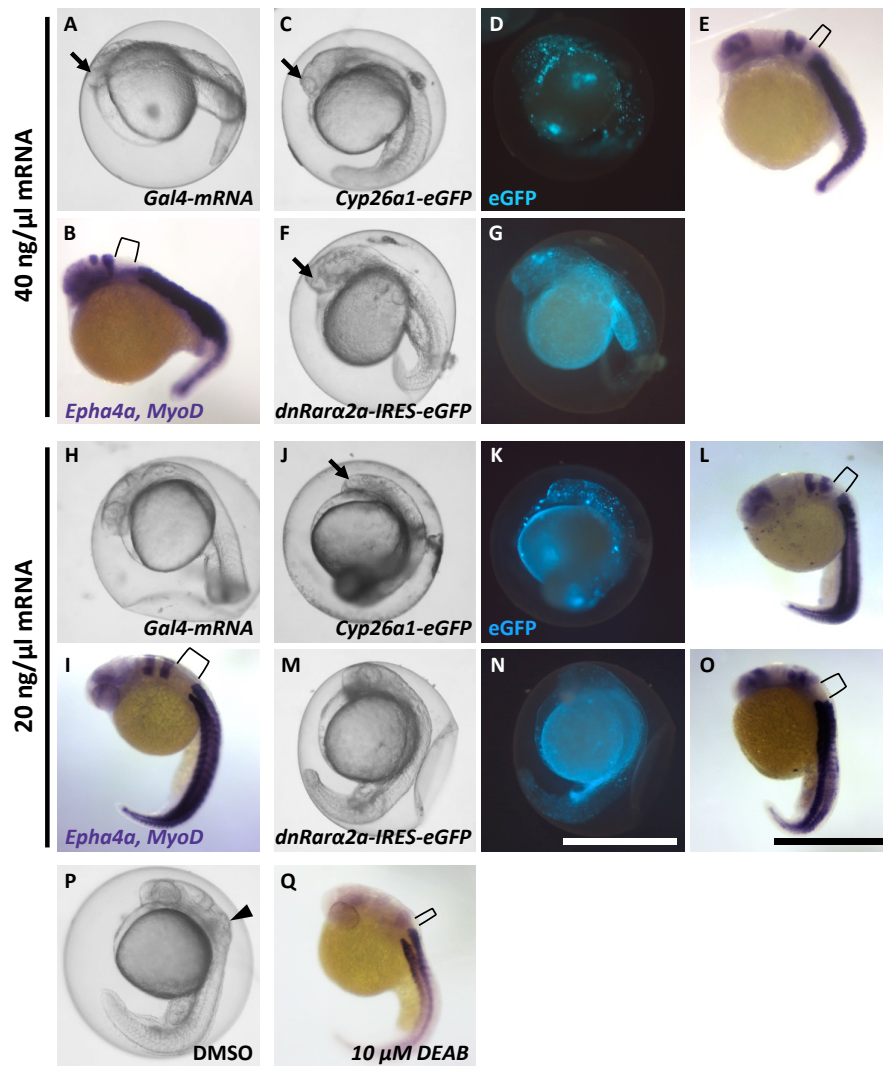


**Fig. S12 Gal4 activates transgene expression upon co-injection of *Gal4* mRNA with 5xUAS effector plasmids.** The plasmids *pTol2\_5xUAS:Cyp26a1-eGFP* or *pTol2\_5xUAS:dnRara2a-IRES-eGFP* were co-injected with *Gal4-VP16* mRNA in the one-cell stage of zebrafish embryos of the *Casper* strain. Control embryos were injected only with *Gal4-VP16* mRNA. **A-G:** A concentration of 40 ng/ $\mu$ l was used for both, plasmid and mRNA. At 24 hpf co-injected embryos showed mosaic-like eGFP fluorescence throughout the entire body (**D,G**). Whole-mount *in situ* hybridisation against *Epha4a* and *MyoD* mRNA revealed a truncation of the anteroposterior axis anterior to the somites (**E**), also in control embryos (**B**). The distance between rhombomere 5 and somite 1 is indicated with brackets (**E,B**). Missing or reduced eyes (arrows) together with other malformation like truncated tails or misshaped heads were observed frequently (**C,F**), also in control embryos (**A**). **H-O:** Concentrations of 40 ng/ $\mu$ l (plasmid) and 20 ng/ $\mu$ l (mRNA) were used. At 24 hpf co-injected embryos showed mosaic-like eGFP fluorescence throughout the entire body (**K,N**). Whole-mount *in situ* hybridisation against *Epha4a* and *MyoD* mRNA revealed a truncation of the anteroposterior axis anterior to the somites (**L,O**), that was not seen in control embryos (**I**). Missing or reduced eyes (arrows) together with other malformation like truncated tails or misshaped heads were observed frequently in co-injected embryos (**J**), but not in control embryos (**H**). **P-Q:** As a positive control for the RA-deficiency phenotype, embryos of the *Casper* strain were treated with 10  $\mu$ M DEAB or an equivalent amount of pure DMSO from 50 % epiboly onwards. At 24 hpf DEAB-treated individuals show the characteristic bulge in the 'neck' of the RA-deficiency-phenotype (**P**, arrowhead) and a shortening of the distance between rhombomere 5 and somite 1 (brackets) (**Q**). All embryos are shown in lateral view with anterior to the left. Scale bars: 500  $\mu$ m. Pictures by Jean Eberlein; taken and modified from Eberlein, 2018b.

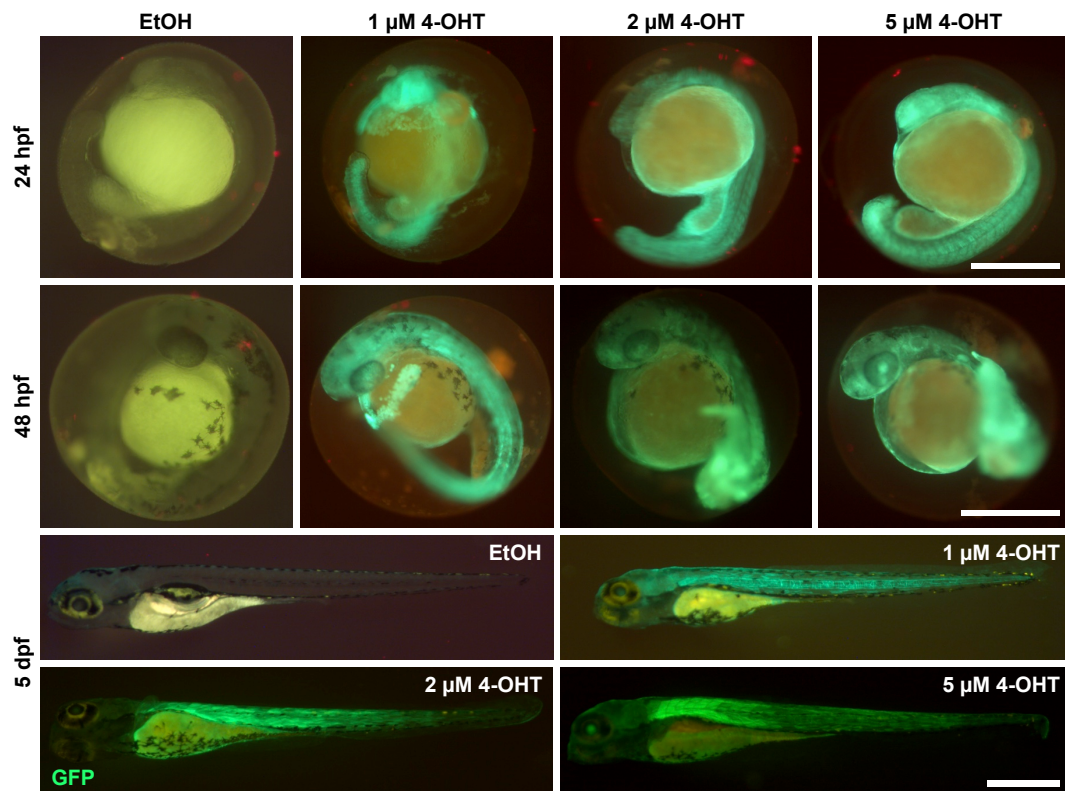


**Fig. S13 ERT2-Gal4-VP16 activates transgene expression in *UAS:GFP* zebrafish line.** *ERT2-Gal4-VP16* mRNA (50 ng/μl) was injected in eggs of the *UAS:GFP* zebrafish line at the one-cell stage and subsequently induced with the indicated concentrations of 4-hydroxy-tamoxifen (4-OHT). The control group was treated with an equivalent amount of pure EtOH. Intense GFP fluorescence was observed for all 4-OHT concentrations and documented up to 5 dpf. Control embryos did not exhibit any fluorescence. Embryos and larvae are shown in lateral view with anterior to the left. Scale bars: 500 μm.

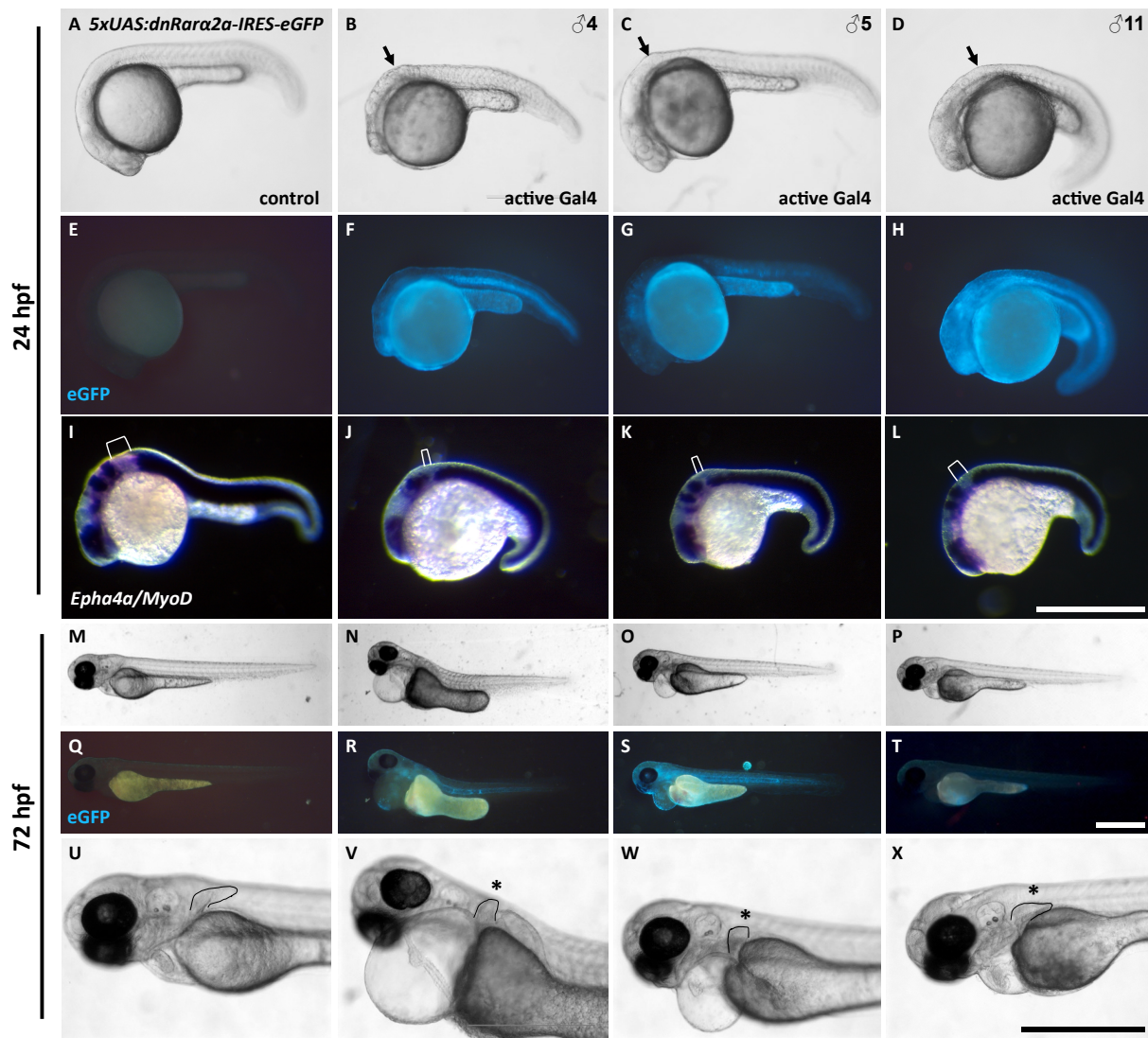


**Fig. S14 Active Gal4 causes a RA-deficiency phenotype in the *5xUAS:dnRara2a-IRES-eGFP* effector line.** *ERT2-Gal4-VP16* mRNA (40 ng/ $\mu$ l) was injected in zebrafish eggs of the *5xUAS:dnRara2a-IRES-eGFP* effector line (F2 generation) at the one-cell stage and the embryos were subsequently treated with 2  $\mu$ M 4-OHT or EtOH (control) at 50 % epiboly. The results of the lines founded by  $\sigma$ 4,  $\sigma$ 5 and  $\sigma$ 11 are shown. At 24 hpf only induced embryos show the characteristic bulge in the 'neck' of the RA-deficiency-phenotype (arrows, **A-D**). Intense eGFP fluorescence is visible in these embryos throughout the whole body (**E-H**). Whole-mount *in situ* hybridisation against *Epha4a* and *MyoD* mRNA shows a truncation of the anteroposterior axis anterior to the somites. The distance between rhombomere 5 and somite 1 is indicated with brackets (**I-L**). At 72 hpf eGFP fluorescence is visible only in induced larvae throughout the whole body (**Q-T**). **U-X**: magnifications of the anterior body half of larvae shown in **M-P**. Reduction of pectoral fin size indicates the RA deficiency phenotype (asterisks). Black lines in **U-X** highlight outlines of pectoral fins. Other severe side effects are frequently observed, like pericardial edema (**V,W**). All embryos are shown in lateral view with anterior to the left. Scale bars: 500  $\mu$ m. Pictures by Jean Eberlein; taken and modified from (Eberlein, 2018a).

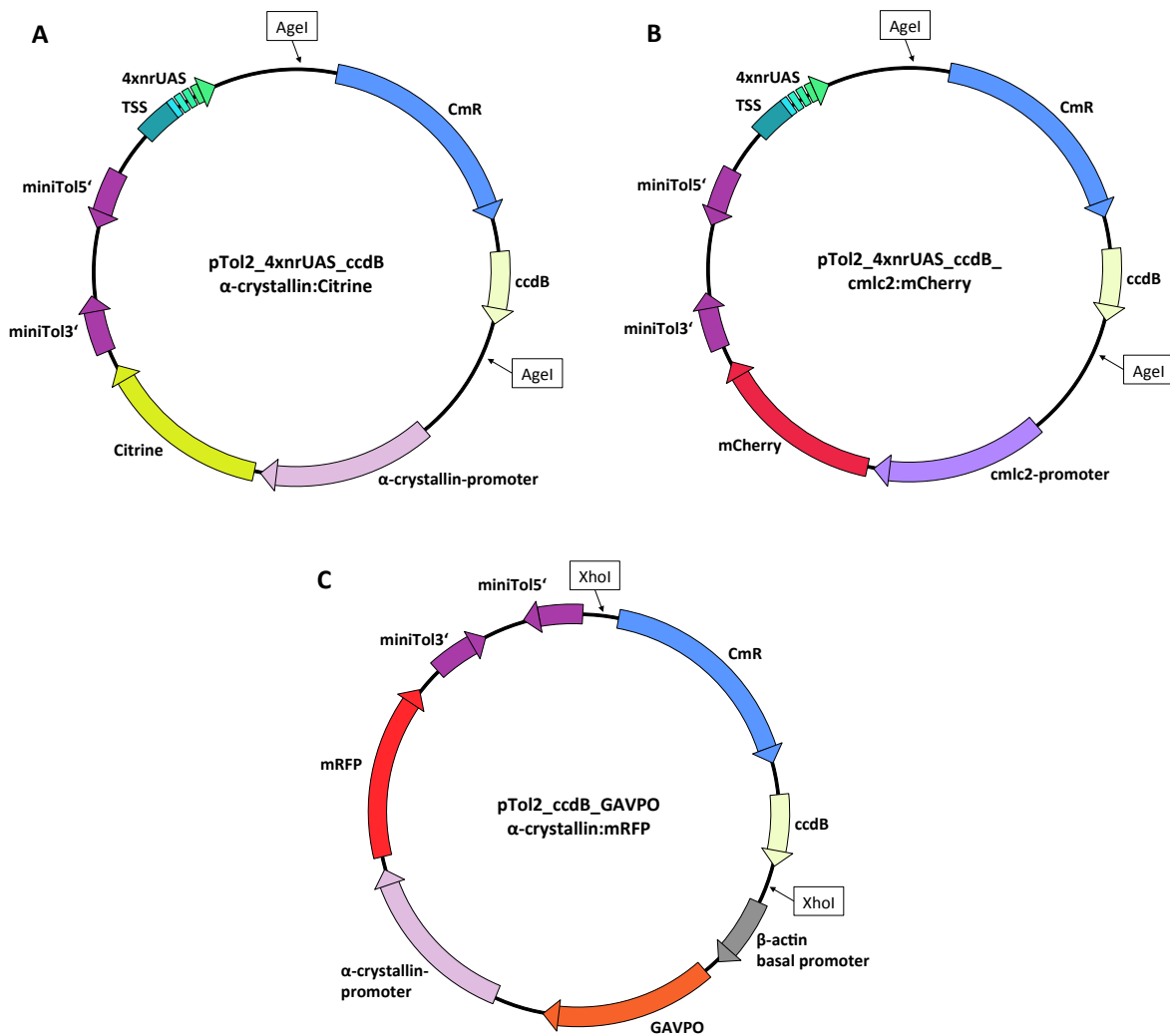


**Fig. S15 Schematic representation of 'zero background' Tol2 vectors.** The vectors contain minimal Tol2 *cis* sequences flanking the entire expression cassette to enable random integration into the genome by Tol2 transposase activity. The 'zero-background' feature is based on the toxic gene *ccdB*. This is combined with a Chloramphenicol resistance (*CmR*) gene to facilitate a positive selection in the *ccdB*-resistant *E. coli* strain DB3.1. For various cloning strategies, the entire *CmR-ccdB*-cassette can be removed by restriction digest with the DNA endonucleases *Agel* or *XhoI*. The identification of transgenes is facilitated either by an  $\alpha$ -crystallin-promoter connected to *Citrine* (**A**) or *mRFP* (**C**) or a *cmlc2*-promoter in combination with *mCherry* (**B**), mediating green or red fluorescence in the eye lenses or red fluorescence of the myocardium, respectively. **A/B**: 4xnrUAS effector constructs. The vectors further contain a transcriptional start site (TSS) and four non-repetitive upstream activating sequences (4xnrUAS) **C**: GAVPO driver construct. The vector further contains a  $\beta$ -actin basal promoter upstream of the *Gal4*-derived gene *GAVPO*. Both *pTol2\_4xnrUAS-ccdB* vectors were designed and assembled by David Richter (University of Bayreuth); the *pTol2\_ccdB-GAVPO* vector was designed in cooperation with David Richter.

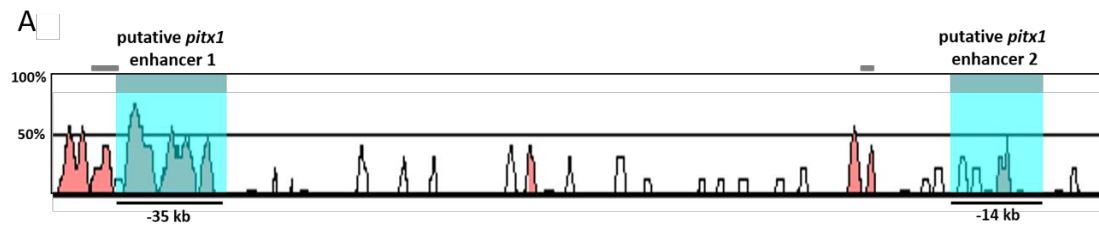


**Fig. S16 Identification of putative zebrafish *Pitx1* enhancers.** Two putative *Pitx1* enhancers (light blue) were identified by comparing a published *Pitx1* enhancer of stickleback with the region 45 kb upstream of *Pitx1* in zebrafish. Putative *Pitx1* enhancer 1 (PPE1) is located 35 kb upstream of *Pitx1* and putative *Pitx1* enhancer 2 (PPE2) 14 kb, also upstream. Plot was generated with mVista. Grey bars indicate repetitive sequences. The y-axis shows percentage sequence identity, pink shading indicates regions of 20 bp or more that are  $\geq 70\%$  identical. Graph and caption taken with minor modifications from Merkel, 2016.

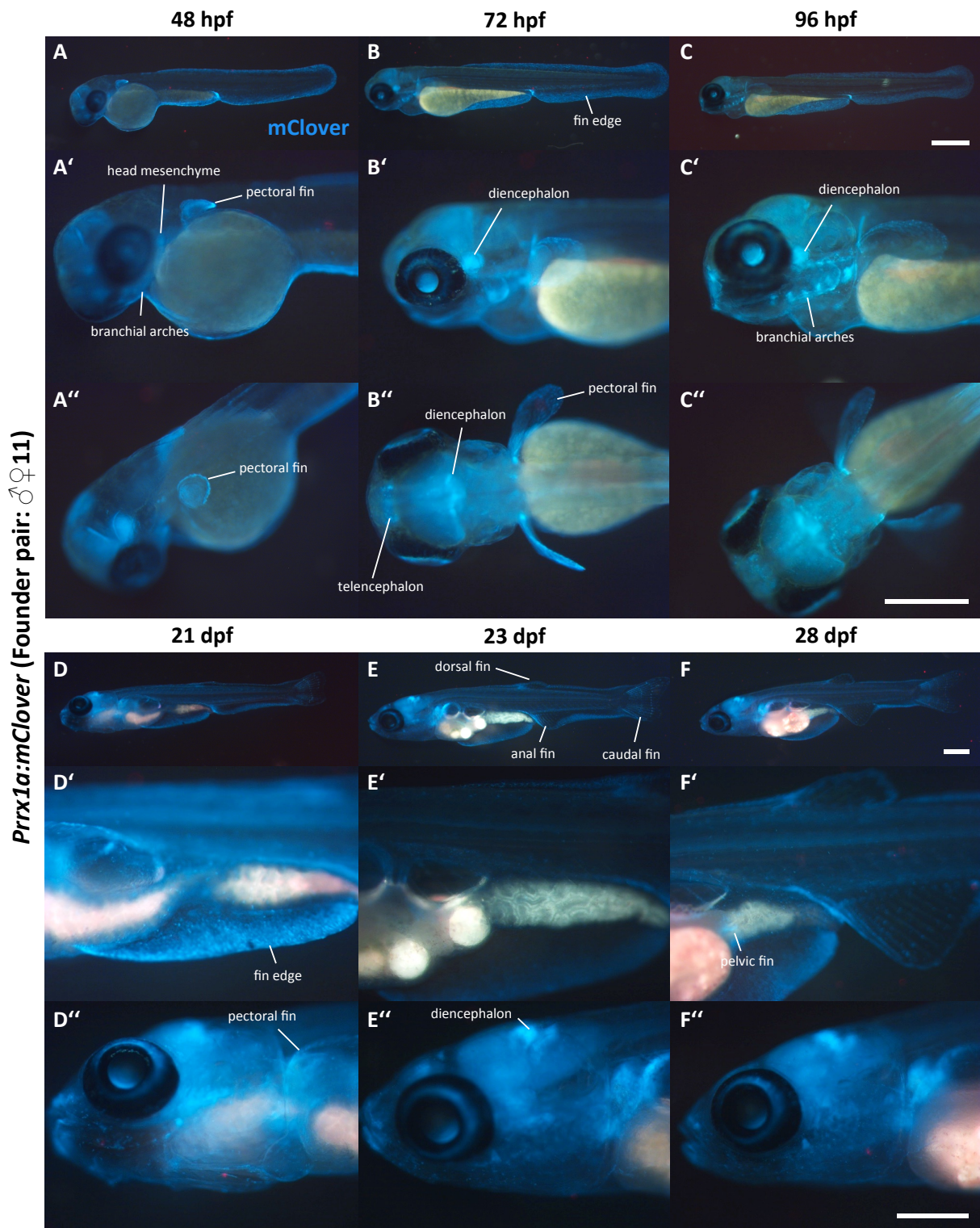


**Fig. S17** Transgene expression in the F3 generation of the *Prrx1a:mClover* zebrafish line from founder pair ♂11 and ♀11. mClover fluorescence was visualized at ages of 48 hpf (A-A''), 72 hpf (B-B''), 96 hpf (C-C''), 21 dpf (D-D''), 23 dpf (E-E'') and 28 dpf (F-F''). Striking expression locations are designated. Embryos and larvae are shown in lateral or dorsolateral view with anterior to the left. Scale bars: 500  $\mu$ m.

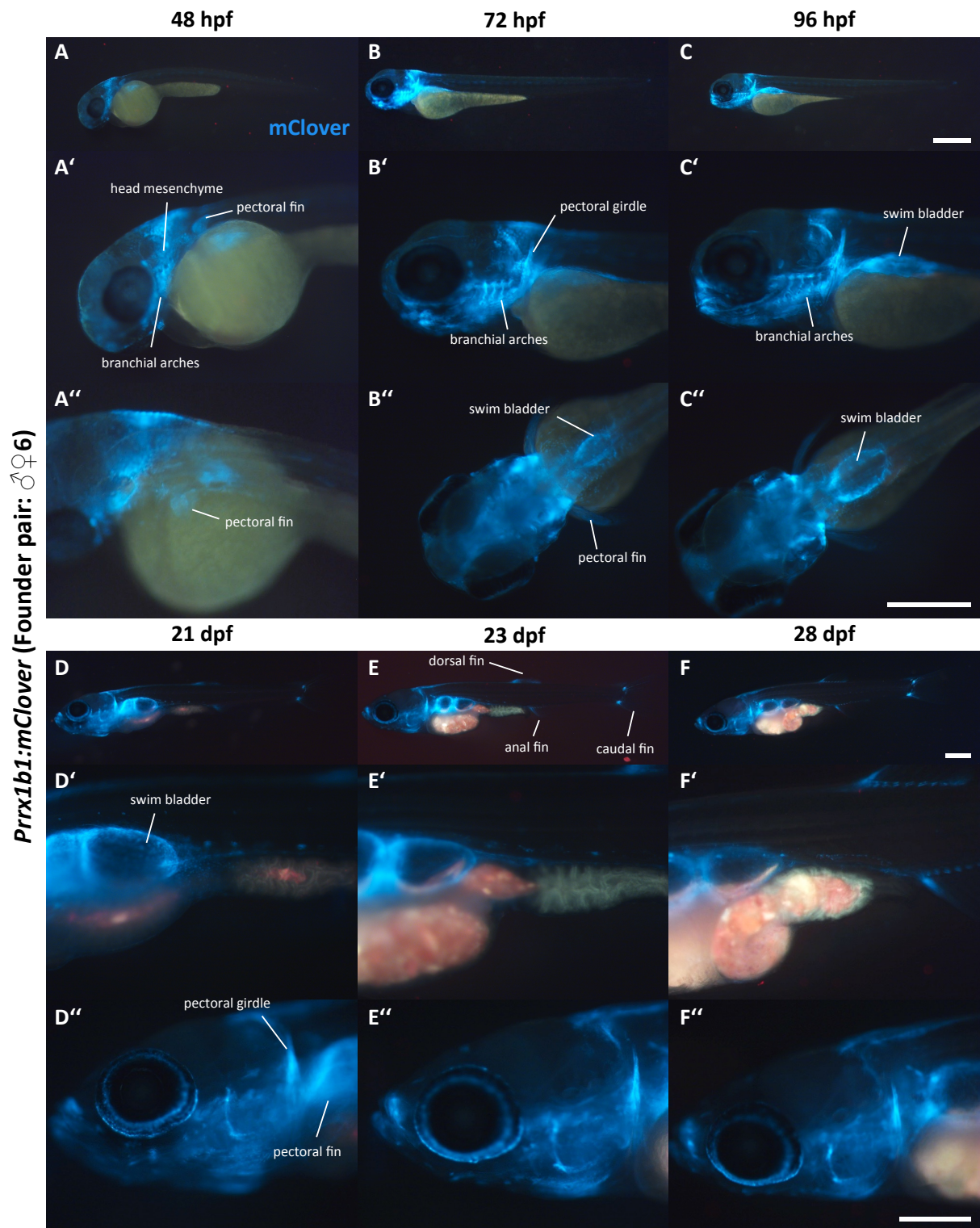


**Fig. S18** Transgene expression in the F3 generation of the *Prrx1a:mClover* zebrafish line from founder pair ♂6 and ♀6. mClover fluorescence was visualized at ages of 48 hpf (A-A''), 72 hpf (B-B''), 96 hpf (C-C''), 21 dpf (D-D''), 23 dpf (E-E'') and 28 dpf (F-F''). Striking expression locations are designated. Embryos and larvae are shown in lateral or dorsolateral view with anterior to the left. Scale bars: 500  $\mu$ m.

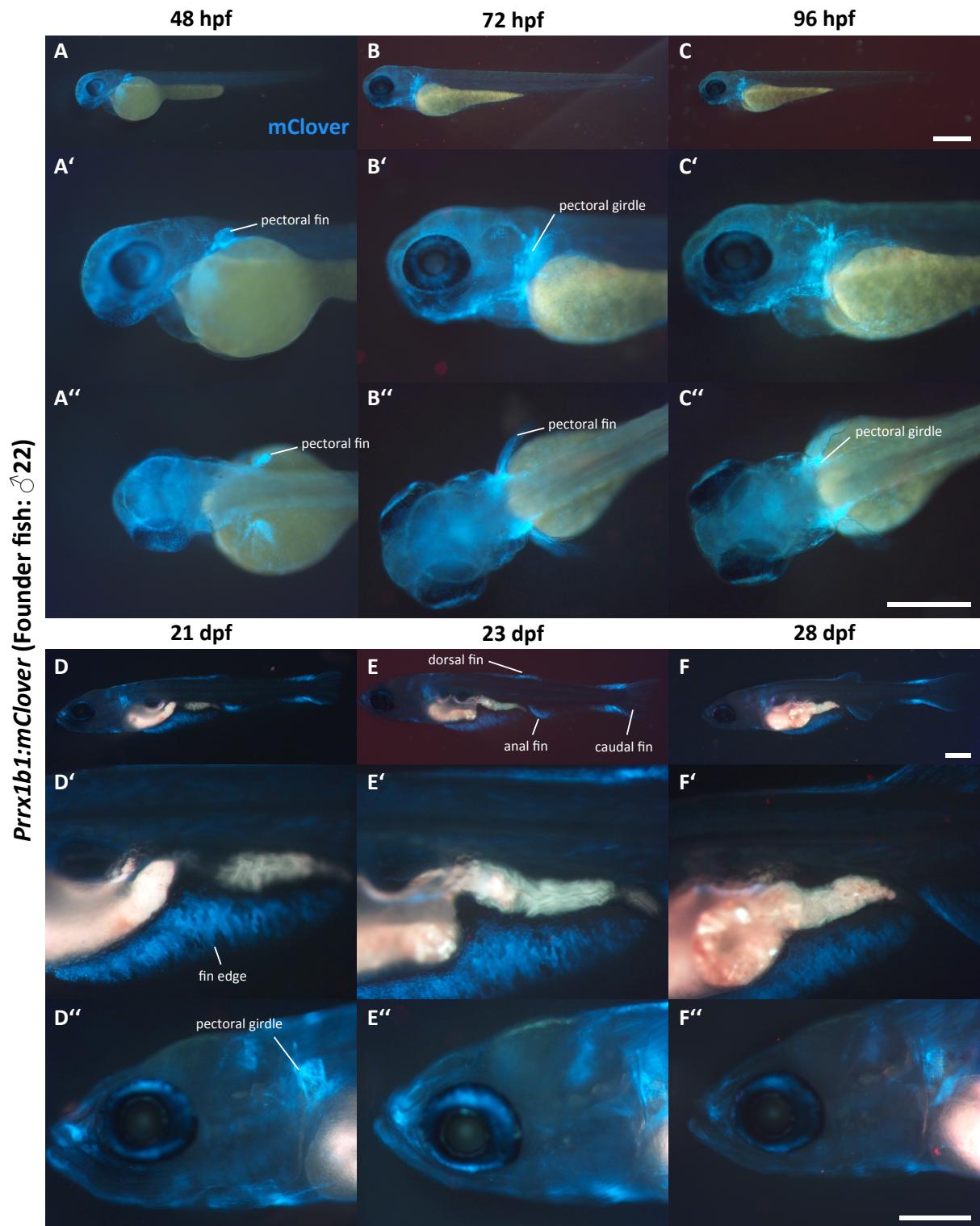


**Fig. S19** Transgene expression in the F3 generation of the *Prrx1a:mClover* zebrafish line from founder fish ♂22. mClover fluorescence was visualized at ages of 48 hpf (A-A''), 72 hpf (B-B''), 96 hpf (C-C''), 21 dpf (D-D''), 23 dpf (E-E'') and 28 dpf (F-F''). Striking expression locations are designated. Embryos and larvae are shown in lateral or dorsolateral view with anterior to the left. Scale bars: 500  $\mu$ m.

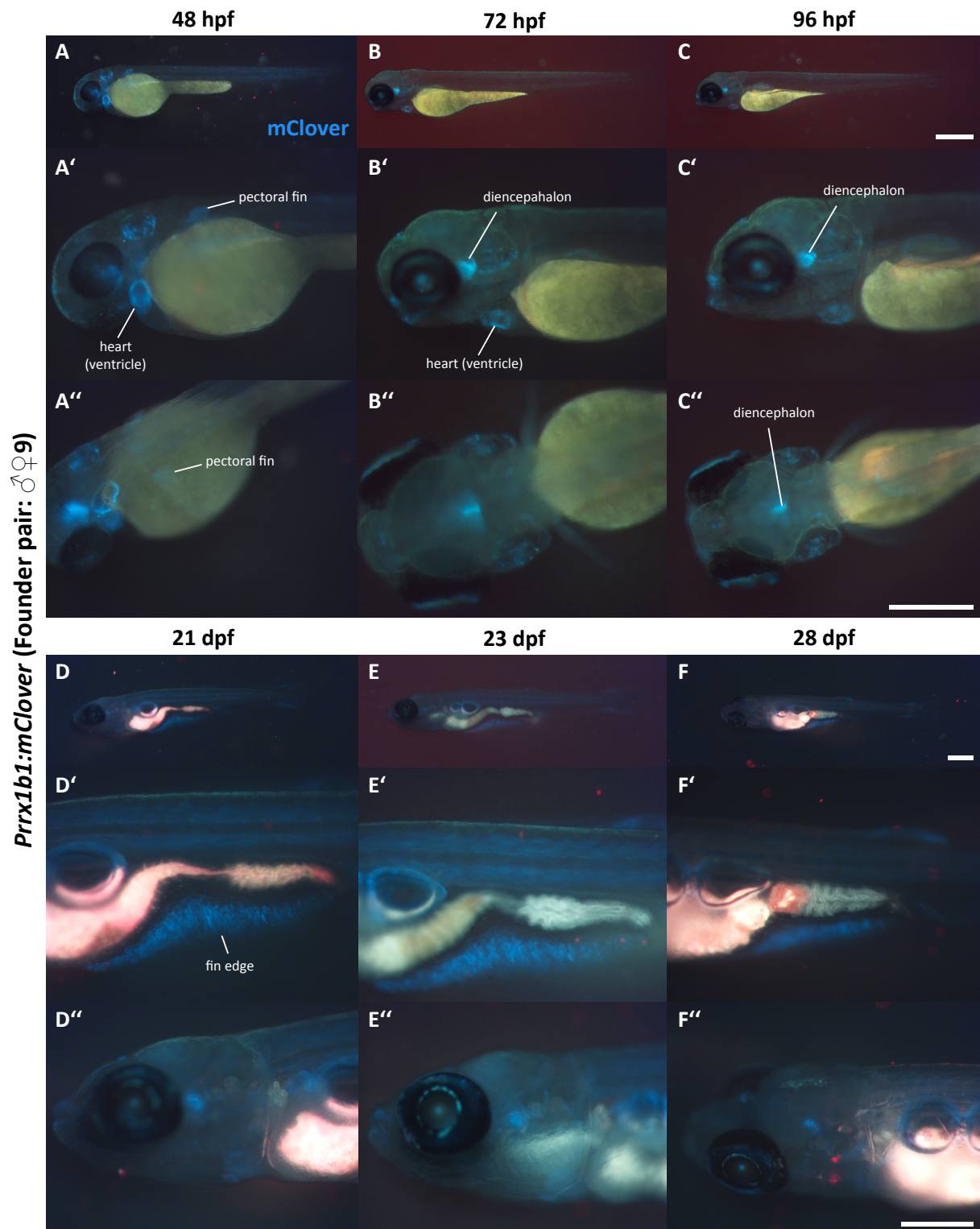


**Fig. S20** Transgene expression in the F3 generation of the *Prrx1a:mClover* zebrafish line from founder pair ♂9 and ♀9. mClover fluorescence was visualized at ages of 48 hpf (A-A''), 72 hpf (B-B''), 96 hpf (C-C''), 21 dpf (D-D''), 23 dpf (E-E'') and 28 dpf (F-F''). Striking expression locations are designated. Embryos and larvae are shown in lateral or dorsolateral view with anterior to the left. Scale bars: 500  $\mu$ m.

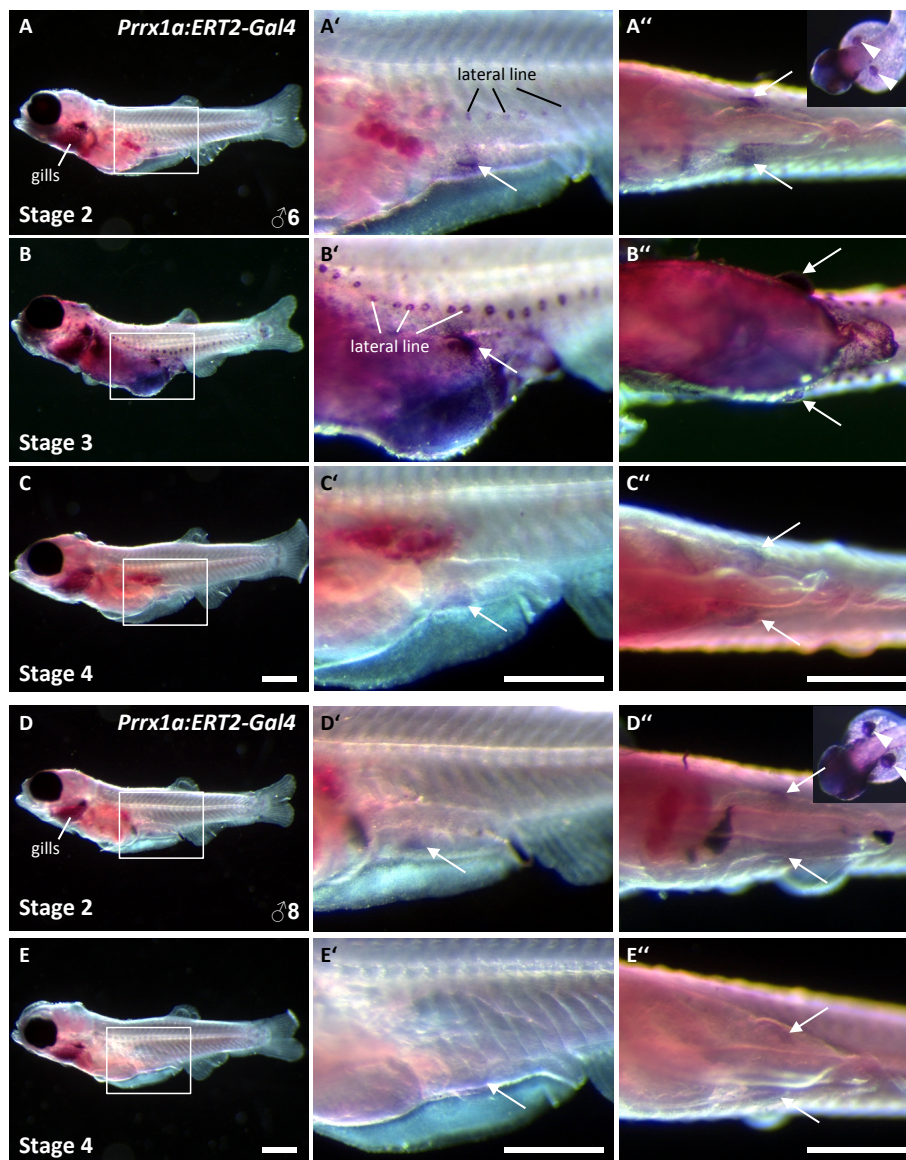


**Fig. S21** Expression of *ERT2-Gal4-VP16-GI* in *Prrx1a:ERT2-Gal4-VP16-GI* F2 larvae from founder fish ♂ 6 (A-C) and ♂ 8 (D-E) at pelvic fin developmental stages between 2 - 4 (approximately 28 dpf) determined by whole-mount *in situ* hybridisation against *Gal4 DBD*. Framed areas are shown in higher magnification in the middle column of the panel (A'-E'). Specific WISH staining is visible in the pelvic fin buds in all stages (highlighted by white arrows). Additionally, *ERT2-Gal4-VP16* expression was detected in the gills and partly in the lateral line. Larvae are shown with anterior to the left in lateral or ventral view (A''-E''). Insets in A'' and D'' show an embryo at 48 hpf in dorsal view demonstrating *ERT2-Gal4-VP16* expression in the pectoral fin bud (arrowheads). Scale bars: 500  $\mu$ m.

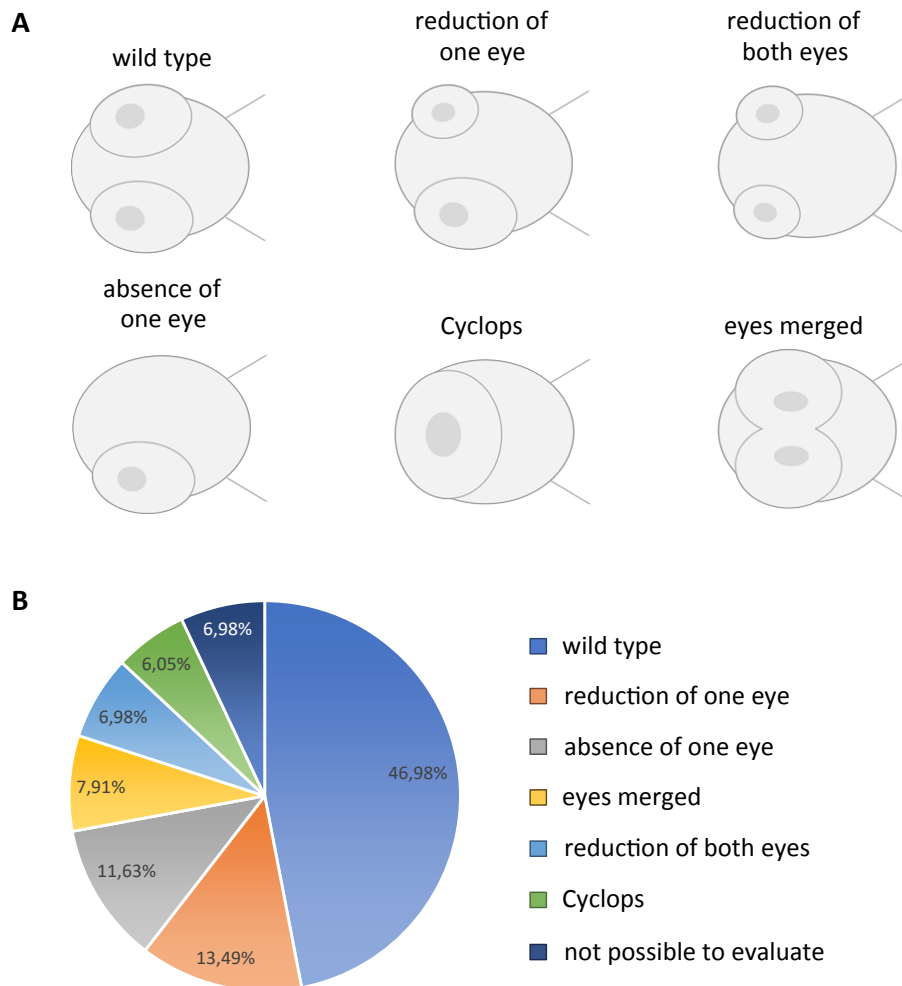
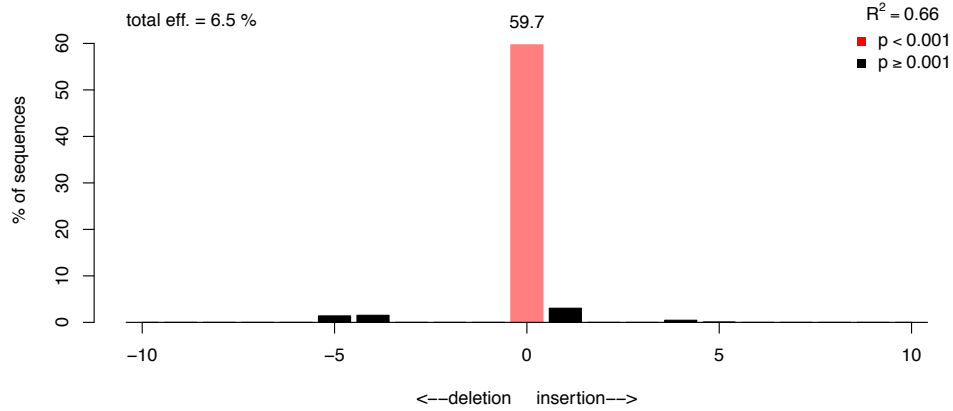
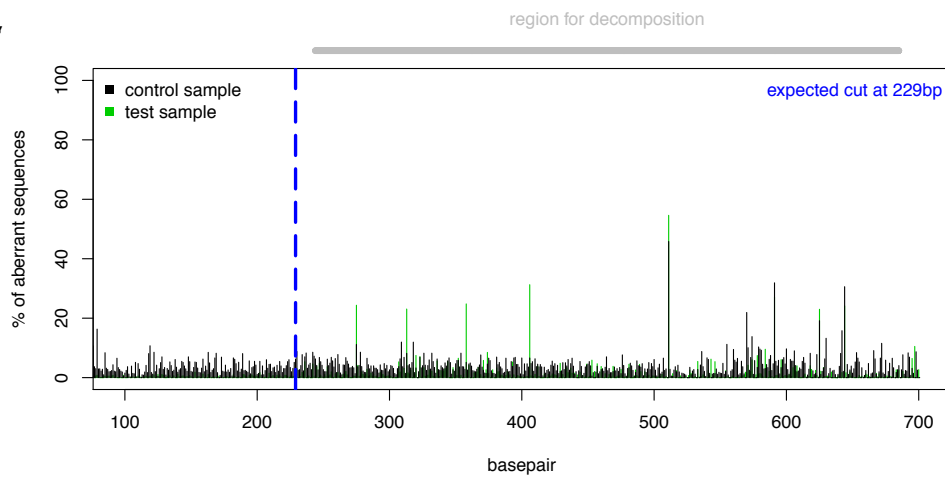


**Fig. S22 Eye defects occurring in zebrafish embryos following manipulation of the RA pathway.** Injection of *dnRara2a* mRNA (250 - 350 ng/ $\mu$ l) in the one-cell stage of zebrafish eggs of the *Casper* strain results in various malformations of the eyes at 24 hpf. Schematic representations of the heads of zebrafish embryos illustrate the different phenotypes **(A)**. A pie chart represents the frequencies of the respective phenotypes **(B)**. Illustrations and graphs by Antonia Bule, taken and modified from Bule, 2019.

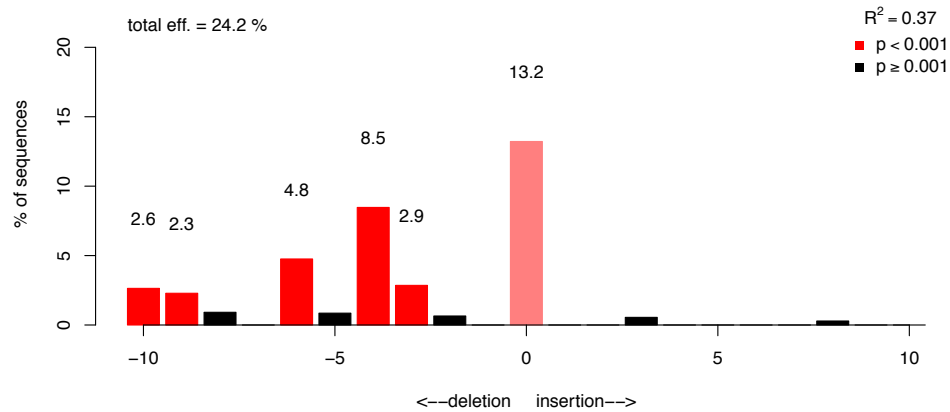
**A Pitx1 T5 sgRNA**



**A'**



**B Pitx1 T50 sgRNA**



**B'**

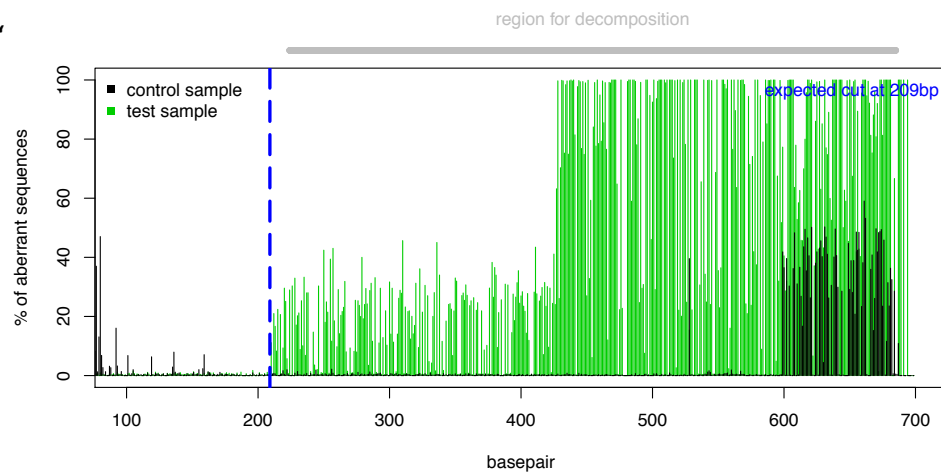


**Fig. S23 TIDE to estimate spectrum and frequency of CRISPR/Cas9 mediated indel mutation.** *Pitx1* T5 or *Pitx1* T50 sgRNA (50 pg) were co-injected with *Cas9* mRNA (300 pg) in zebrafish embryos of the *Casper* strain at the one-cell stage. Genomic DNA was isolated of a pool of 15 injected (test sample) or uninjected embryos (control sample) at 24 hpf. The targeted region was amplified via PCR and sequenced using Sanger sequencing. The aberrant signals of control and test samples are visualized for *Pitx1* T5 and T50 in **A'** and **B'**, respectively. For *Pitx1* T5 sgRNA a total efficiency of 6.5 % is predicted (**A**). *Pitx1* T50 sgRNA is rated with an efficiency of 24.2 % with a wide spectrum of induced indel mutations ranging from -10 to -2 base pairs (**B**). Graphs created with TIDE webtool (Brinkman et al., 2014). Taken and modified from Borrero Malo, 2018.

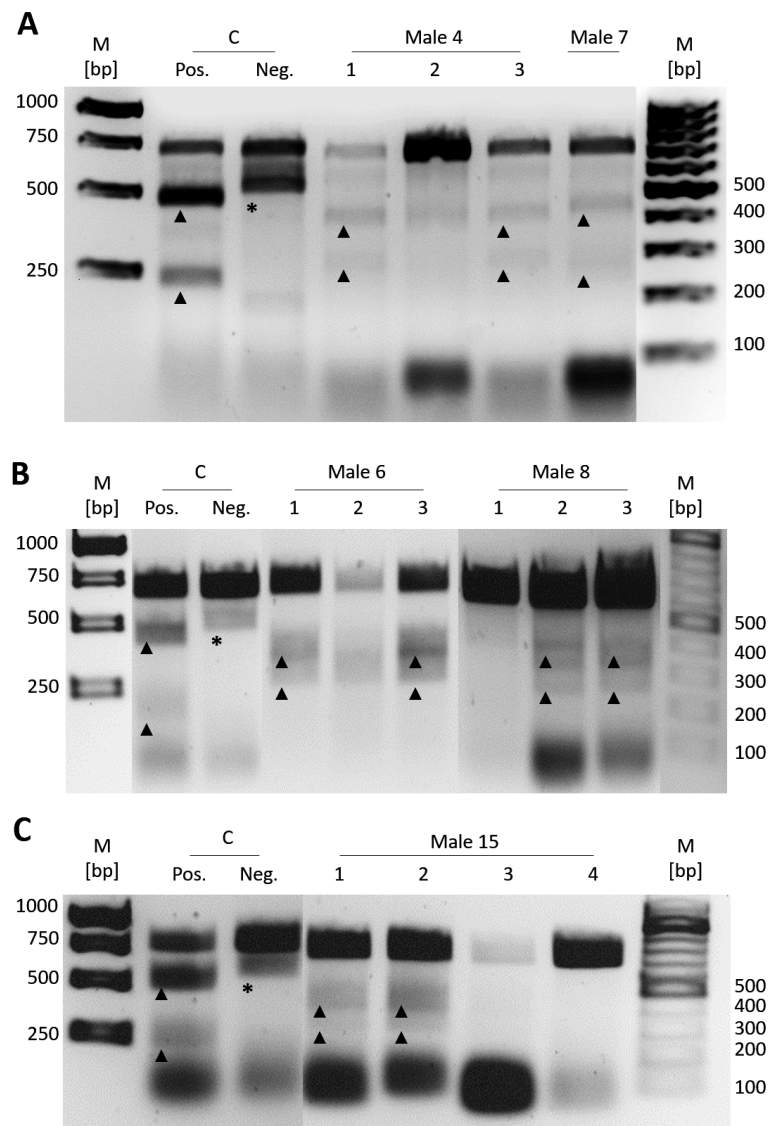


**Fig. S24 Identification of germline founders using T7E1 assay.** Exemplary T7E1 assays for germline founders  $\sigma$  4 and  $\sigma$  7 (**A**),  $\sigma$  6 and  $\sigma$  8 (**B**) and  $\sigma$  15 (**C**). Analysis took place using a 1.5 % agarose gel. The uncleaved PCR product is about 750 bp in length. Arrowheads point to smaller fragments resulting from T7E1 cleavage; asterisks indicate the presence of false positive bands in the Tyr T1 control. C: control; Pos: positive; Neg: negative. Numbers indicate different offspring samples from the same parent. Experiments performed by Lina Stacker. Figure and caption taken with minor modification from Stacker, 2020.

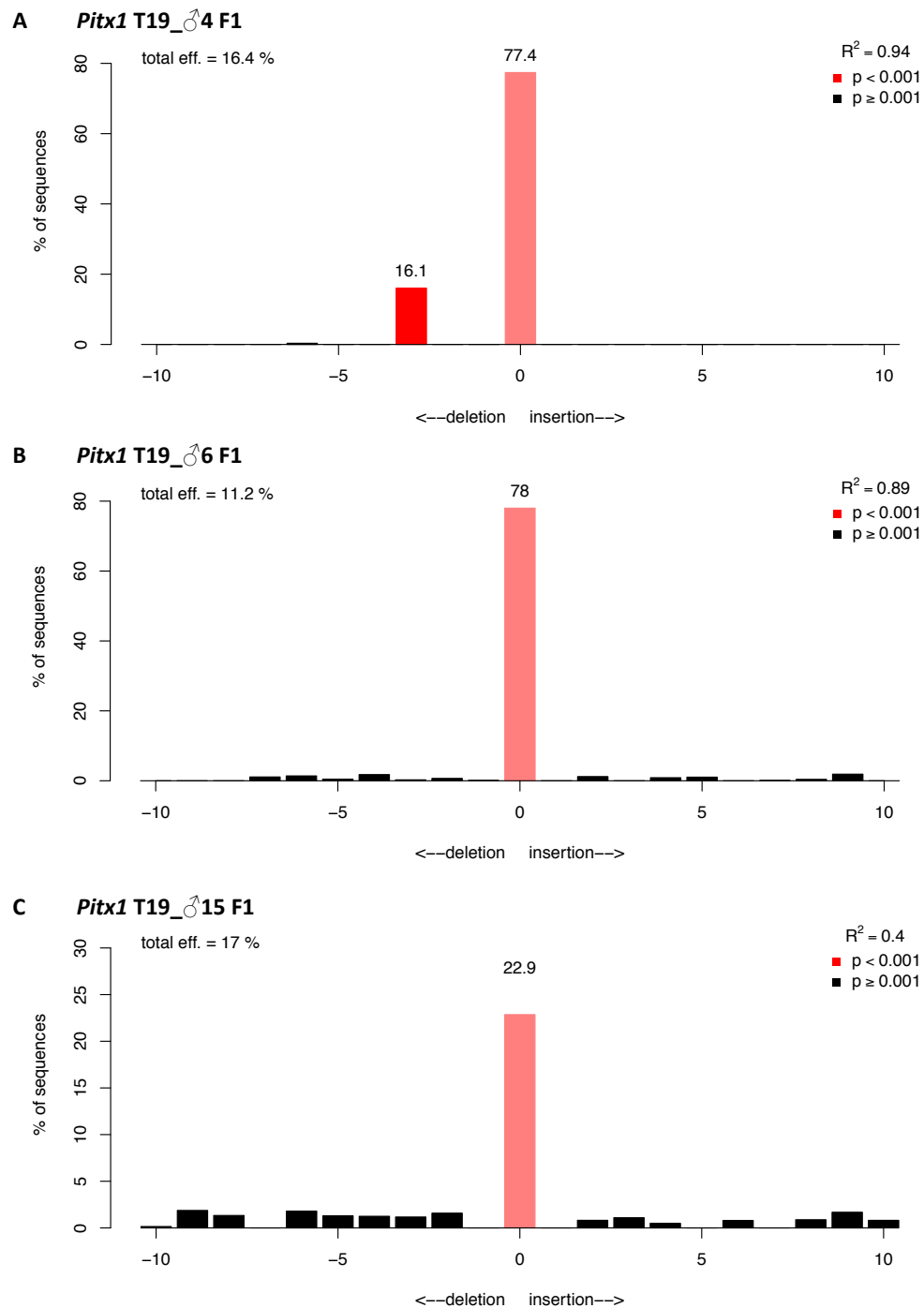


**Fig. S25 TIDE to predict CRISPR/Cas9 mediated indel mutation in heterozygous F1 fish.** *Pitx1* T19 sgRNA (50 pg) was first co-injected with *Cas9* mRNA (300 pg) in zebrafish embryos at the one-cell stage (F0). Adult F0 fish were outcrossed to wild type fish of the *Casper* strain. The offspring (F1 generation) were raised to adulthood. Genomic DNA was isolated from fin tissue of adult F1 fish. The targeted region was amplified via PCR and sequenced using Sanger sequencing. For heterozygous individuals derived by founder fish ♂4 (**A**), ♂6 (**B**) and ♂15 (**C**) mutational frequencies of 16.4 %, 11.2 % and 17 % were calculated. An indel mutation with a significant level was predicted only for F1 fish derived from founder ♂4, being a deletion of 3 base pairs (-3). Graphs created with TIDE webtool (Brinkman et al., 2014).



**C** *Pitx1* T19\_ ♂ 15 F2

**Fig. S26 Sequence information of homozygous *Pitx1* T19 F2 fish.** Genomic DNA was isolated from F2 larvae derived by founder fish ♀4, ♂8 and ♂15. Sanger sequencing revealed genotype of homozygous fish carrying indel mutations. **A:** In descendants from ♀4 a total of seven base pairs were deleted and four new ones added, resulting in the overall deletion of three base pairs. The consequence was the exchange of Pro(12) and Arg(13) with Phe (framed in red). **B:** In descendants from ♂8 six base pairs were deleted. The consequence was the lack of Phe(9) and His(10) (framed in red). **C:** In descendants from ♂15 a total of 18 base pairs were deleted and nine new ones added, resulting in the overall deletion of nine base pairs. The consequence was the exchange of Ser(8), Phe(9), His(10), Leu(11), Pro(12) with Met and Cys (framed in red). However, the quality of the sequencing reaction was not optimal and showed numerous overlays of nucleotides downstream of the mutation site. The exchange of Ser(14) with Ile due to a point mutation can therefore most likely be attributed to sequencing mistakes. Sanger sequencing carried out by eurofins.com. Alignment performed with SnapGene.

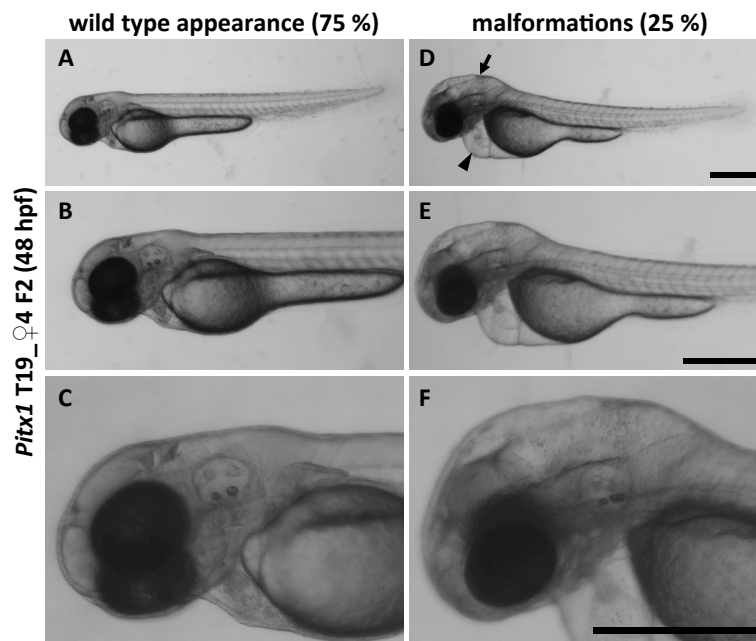


**Fig. S27 Phenotype of *Pitx1* T19 F2 generation from founder fish ♀4.** At 48 hpf approximately 25 % of the F2 generation derived from founder ♀4 exhibited severe malformations. This included an enlarged and misshaped head (arrow) and a pronounced pericardial edema (arrowhead) (D-F). The remaining 75 % showed a wild type-like appearance (A-C). Sequencing revealed that the phenotype occurs independently of the mutant *Pitx1* allele. Scale bars: 500  $\mu$ m.

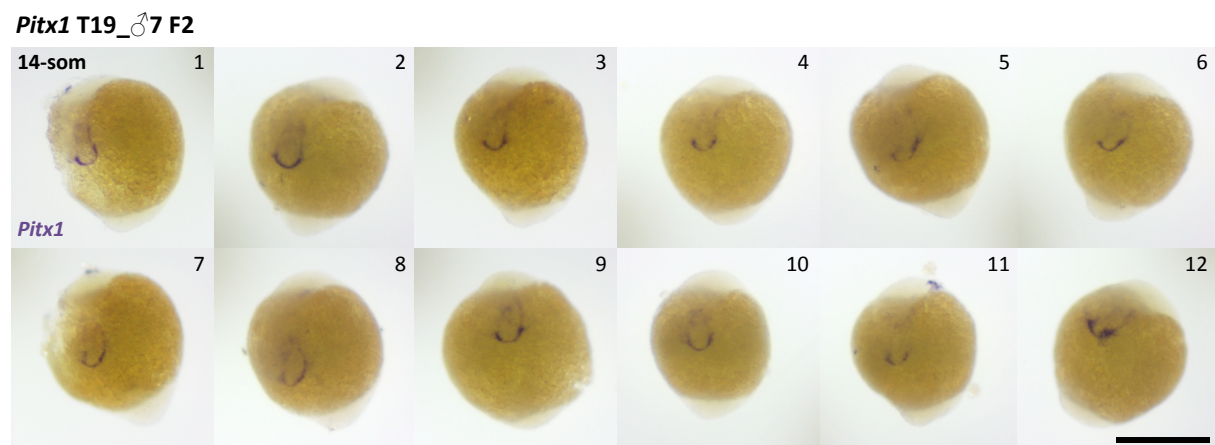


**Fig. S28 *Pitx1* expression in *Pitx1* T19 F2 generation from founder fish ♂7.** Expression of *Pitx1* in the pituitary gland was detected by whole-mount *in situ* hybridisation (WISH) at the 14-somite stage. Intense WISH staining was found in all embryos derived from an incross of adult F1 fish that were heterozygous for the mutated *Pitx1* allele. The figure shows exemplary pictures of 12 individuals. The pituitary gland appeared normally developed in terms of shape and size. The genotype of the individual embryos was not determined. Anterior is to the front. Scale bar: 500  $\mu$ m.

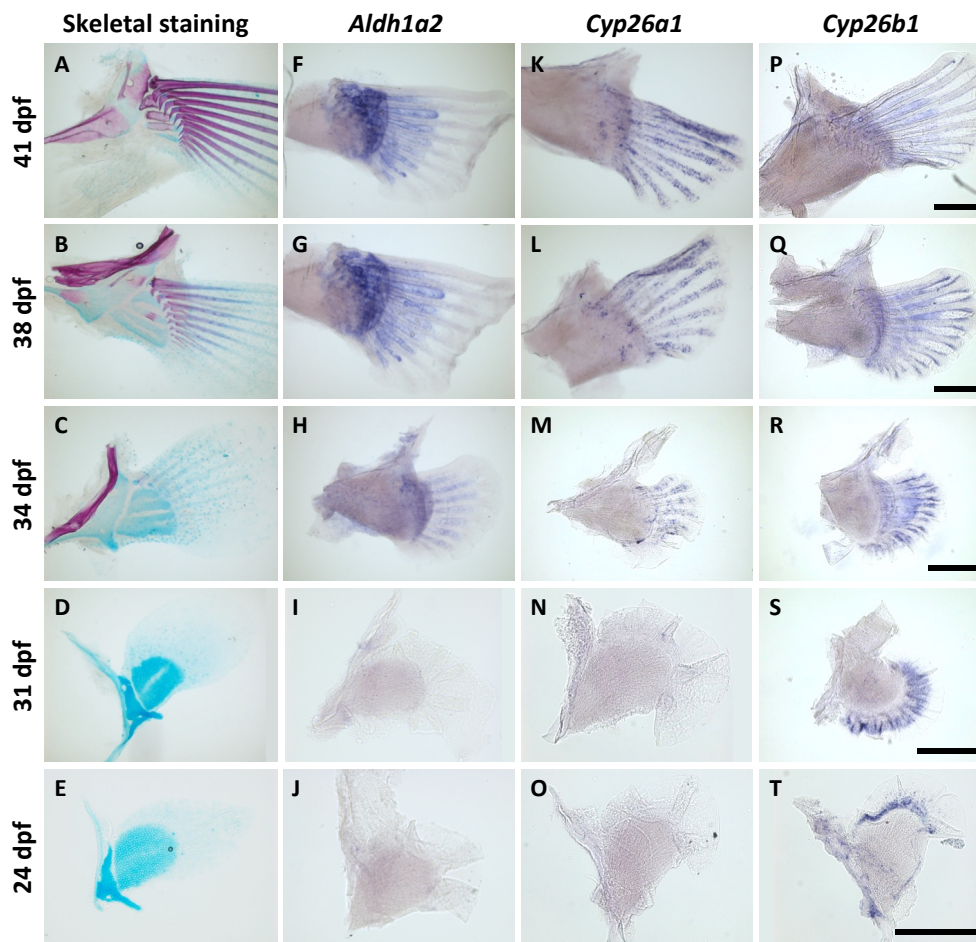


**Fig. S29 Expression of genes of the RA pathway during pectoral fin morphogenesis.** Dissected pectoral fins during various stages of pectoral fin morphogenesis from the larval to the adult form (Dewit et al., 2011; Grandel & Schulte-Merker, 1998). **A-E:** Skeletal staining with Alcian blue and Alizarin Red labelling cartilage and bone elements, respectively. **F-T:** Whole-mount *in situ* hybridisation against *Aldh1a2*, *Cyp26a1* and *Cyp26b1*. **F-J:** Expression of *Aldh1a2*. WISH staining was detected from 34 dpf onwards. The WISH staining was particularly intense around the base of the lepidotrichs and between the lepidotrichs, up to half of the length. **K-O:** Expression of *Cyp26a1*. Transcripts were detected from 34 dpf onwards in a punctiform pattern along the lepidotrichs. **P-T:** Expression of *Cyp26b1*. Intense WISH staining was detected from 24 hpf onwards. The WISH staining was first located in the fin fold, extending along the edge to the endoskeletal disk. At 31 dpf the expression domain expanded distally. At 34 dpf the expression domain was located along the lateral borders of the lepidotrichs and at their bases. Anterior is left, posterior is right. Scale bars: 200  $\mu$ m. Pictures by Amelie Mück, taken and modified from Mück, 2018.

## 8 Acknowledgements

First of all, thanks to my supervisor and mentor Prof. Dr. Gerrit Begemann for giving me the opportunity to work on this project. I learned a lot during my years here, was able to develop personally and will remember our collaboration for a long time. Thank you also for organizing the annual excursions and Christmas dinners, which have brought us together as a team.

Thank you to Prof. Dr. Stefan Schuster and Prof. Dr. Stefan Heidmann for assisting me as mentors. Thank you for your advice, support and for useful discussions.

Thank you to the Deutsche Forschungsgemeinschaft (DfG) for providing the funding for this research project. Thank you also to all the researchers, who provided the plasmids and other materials, without whom much of this work would not have been possible.

Thank you to all the lovely members of the Animal Physiology and the Developmental Biology working group for letting me be part of this team. Thank you for your support and help and for all the friendly encounters and nice conversations.

A special thank to Stephanie Höfner and Sabine Bartel and all other animal keepers for loving care of all the zebrafish and who thus played an essential role in all experiments carried out. Another special thank to our technicians Sandra Boser and Carmen Kunert for ensuring that we never ran out of buffers, reagents or plastic ware and thus made everyday life in the laboratory much easier. Thank you also to David Richter and Thomas Toesko for sharing enzymes, plasmids and competent cells and for good collaboration and useful discussions.

Another special thank to Marlene Schmidt (Master thesis 2017), Mike Breu (Master thesis 2017), Fabian Merkel (Master thesis 2016) and Lisa Marzi (Master thesis 2015) for your great work, which made the start of this entire project a lot easier for me.

Many excellent students contributed to this work by absolving their Master or Bachelor thesis or their research module under my supervision. Without your help this project would not have been possible on this scale. A very special thank therefore goes to:

Jean Eberlein (research module 2018, Master thesis 2018), Amelie Mück (research module 2018, Master thesis 2019), Lina Stacker (research module 2018, master thesis 2020), José A. Borrero Malo (Bachelor thesis 2018), Antonia Bule (Bachelor thesis 2019), Anna-Maria Mayer (Bachelor thesis 2020), Sophia Weber (Bachelor thesis 2020), Niels Nardini (research module 2018) and Xuen J. Ng (research module 2019).

It was a pleasure to work with each of you! Thank you Jean for being a great friend and for teaching me about beetles, bugs and naked mole-rats. Thank you Amelie for bringing positive energy to the lab every single day and for baking the most delicious plucked cake. Thank you Lina for all the fun we had and for making me familiar with all those memes. Thank you José for disappearing and reappearing all the time, Antonia for cooking the most delicious summer roles for us, Anna for baking the best chocolate cookies in the world, Sophia for inspiring me, Niels for designing a team logo and for being the first to buy the large pack of polymerase and Xuen for being the coolest guy ever. We were great together as 'Team Heidrun'!

A very special thank to Thomas 'Toni' Liebenstein and again to Stephi Höfner for being great colleagues and friends. Thank you for accompanying me during this entire work. Without you two, the daily work would not have been the same. Thank you Stephi for our hiking excursions and for so many conversations about hobbies and husbands. Thank you Toni for your support in every respect and for your everlasting good mood. Thank you also for regularly supplying us with Ruby bananas and this way sweeten up even the most frustrating Mondays.

Thank you also to all the lovely people who worked in our group as part of 'Team Toni'. We had such a great time together that I wouldn't want to miss. A special thank in this context goes to Laura Löhner for bringing happiness to the lab with your catching laugh.

Finally, thank you to my whole family for your endless support. A very special thank to my parents Irmgard and Norbert Quoika, for your unconditional support in every possible way. Thank you for believing in me, encouraging me and telling me that I can do more!

Thank you to my husband Thomas for being a part of me for over thirteen years now. You are my refuge after a stressful day when everything goes wrong. Thank you for your endless love, your everlasting support and for simply being you and being there for me, every day forever.

## 9 (Eidesstattliche) Versicherung und Erklärung

(§ 9 Satz 2 Nr. 3 PromO BayNAT)

*Hiermit versichere ich eidesstattlich, dass ich die Arbeit selbstständig verfasst und keine anderen als die von mir angegebenen Quellen und Hilfsmittel benutzt habe (vgl. Art. 64 Abs. 1 Satz 6 BayHSchG).*

(§ 9 Satz 2 Nr. 3 PromO BayNAT)

*Hiermit erkläre ich, dass ich die Dissertation nicht bereits zur Erlangung eines akademischen Grades eingereicht habe und dass ich nicht bereits diese oder eine gleichartige Doktorprüfung endgültig nicht bestanden habe.*

(§ 9 Satz 2 Nr. 4 PromO BayNAT)

*Hiermit erkläre ich, dass ich Hilfe von gewerblichen Promotionsberatern bzw. -vermittlern oder ähnlichen Dienstleistern weder bisher in Anspruch genommen habe noch künftig in Anspruch nehmen werde.*

(§ 9 Satz 2 Nr. 7 PromO BayNAT)

*Hiermit erkläre ich mein Einverständnis, dass die elektronische Fassung meiner Dissertation unter Wahrung meiner Urheberrechte und des Datenschutzes einer gesonderten Überprüfung unterzogen werden kann.*

(§ 9 Satz 2 Nr. 8 PromO BayNAT)

*Hiermit erkläre ich mein Einverständnis, dass bei Verdacht wissenschaftlichen Fehlverhaltens Ermittlungen durch universitätsinterne Organe der wissenschaftlichen Selbstkontrolle stattfinden können.*

.....  
Ort, Datum, Unterschrift